



**UNIVERSITY OF NAPLES FEDERICO II**

Department of Chemistry

**PhD Thesis in  
Chemical Sciences  
24<sup>th</sup> cycle**

**Industrial catalytic processes intensification  
through the use of microreactors**

*Rosa Turco*

Tutor: prof. Elio Santacesaria  
Supervisor: prof. Luciano Santoro  
PhD Coordinator: prof. Lucio Previtiera

# Table of Content

---

<b>Chapter 1 Introduction .....</b>	<b>1</b>
1.1 Background .....	2
1.2 Research Scope .....	3
<b>Chapter 2 A summary of Process Intensification Status of Art .....</b>	<b>4</b>
2.1 History and definitions.....	5
2.2 Advantages of Process Intensification .....	7
2.3 Components of Process Intensification .....	8
2.3.1 Process intensifying equipment.....	10
2.3.1.1 Static mixers .....	10
2.3.1.2 Microreactors .....	11
2.3.1.3 Monolithic Catalysts .....	14
2.3.2 Process intensifying methods.....	15
2.3.2.1 Multifunctional Reactors .....	15
2.3.1.2 Membrane Reactors .....	16
2.3.2.3 Use of alternative forms and sources of energy .....	17
References .....	19
<b>Part A: Vegetable oils Epoxidation Reaction.....</b>	<b>20</b>
<b>Chapter 3 Vegetable Oils Epoxidation Process: General Aspects .....</b>	<b>21</b>
3.1 Epoxidized Oils: Uses and Market .....	22
3.2 Epoxidation Methods.....	22
3.3 Soybean Oil with Performic acid: The Chemicals Reactions.....	23
3.4 Soybean Oil with Performic acid: Industrial Process .....	25
3.5 Intensification of Soybean Oil Epoxidation Process.....	27
References .....	30

<b>Chapter 4 Vegetable Oils Epoxidation reaction with Performic acid in batch reactor:</b>	
<b>Kinetic Aspects .....</b>	<b>31</b>
4.1 Introduction .....	32
4.2 Experimental Section .....	33
4.2.1 Description of Kinetic Runs.....	33
4.3 Discussion and Results.....	39
4.3.1 Epoxidation Kinetic Runs.....	39
4.4 Theoretical approach for the development of the kinetic model .....	43
4.4.1 Description of the reaction scheme and of the kinetic rate laws .....	43
4.4.2 Theoretical approach for the estimation of partition coefficients, mass transfer rates and overall heat exchange .....	45
4.4.3 Mass and Energy balances .....	49
4.4.3.1 Mass balance .....	49
4.4.3.2 Energy balance .....	50
4.4.4 Determination of the model parameters, runs simulation and discussion .....	51
4.5 Conclusions .....	57
References.....	59
Nomenclature.....	60
<b>Chapter 5 Oxirane Ring Opening Reaction studied in Independent Way .....</b>	<b>61</b>
5.1 Introduction .....	62
5.2 Experimental Section .....	64
5.2.1 Apparatus .....	64
5.2.2 Methods .....	64
5.3 Discussion and Results .....	65
5.3.1 Description of Kinetic runs .....	65
5.3.2 Mathematical Model .....	68
5.4 Conclusion .....	70
References.....	71
Nomenclature.....	72
<b>Chapter 6 Vegetable Oils Epoxidation reaction with Performic acid in Continuous reactor:</b>	
<b>Kinetic Aspects.....</b>	<b>73</b>
6.1 Introduction .....	74

6.2 Experimental Section .....	74
6.2.1 Apparatus .....	74
6.2.2 Methods .....	76
6.3 Discussion and Results .....	76
6.3.1 Description Kinetic Runs .....	76
6.3.2 Kinetic Modelling .....	77
6.3.2.1 Modelling of the epoxidation reaction: theoretical approach .....	77
6.3.2.2 Mass and Energy balances .....	79
6.3.2.3 Kinetic Model Results .....	80
6.4 Conclusions .....	85
References .....	86
Nomenclature .....	87
 <b>Chapter 7 Alternatives to the Prileschajew type reaction in soybean oil epoxidation .....</b>	<b>89</b>
7.1 Introduction .....	90
7.1.1 Heterogenization of Prileschajew type epoxidation reaction .....	90
7.1.2 Metal-Catalyzed Epoxidation .....	91
7.1.2.1 Titanium Catalysts .....	92
7.1.2.2 Tungsten Catalysts .....	93
7.1.2.3 Molybdenum Catalysts .....	94
7.1.2.4 Niobium Catalysts .....	94
7.1.3 Non Metal-Catalyzed Epoxidation using Hydrogen Peroxide .....	94
7.1.3.1 Alumina .....	95
7.2 Evaluation of Nb <sub>2</sub> O <sub>5</sub> -SiO <sub>2</sub> catalysts in Soybean Oil Epoxidation .....	96
7.2.1 Introduction .....	96
7.2.2 Experimental Section .....	96
7.2.2.1 Synthesis of Catalysts .....	96
7.2.2.2 Structural Characterization .....	97
7.2.2.3 Epoxidation Tests .....	97
7.2.2.4 Transesterification/Esterification Tests .....	97
7.2.3 Discussion and Results .....	98
7.2.3.2 Soybean Oil Epoxidation .....	98



7.2.3.2 Transesterification/Esterification Reactions .....	101
7.2.4 Conclusions .....	102
7.3 Alumina as heterogeneous catalysts for Soybean Oil Epoxidation .....	102
7.3.1 Introduction .....	102
7.3.2 Experimental .....	102
7.3.2.1 Catalysts Characterization .....	102
7.3.2.2 Epoxidation/ Solvent Effect Tests .....	103
7.3.3 Discussion and Results .....	103
7.3.3.1 Soybean Oil Epoxidation .....	103
7.3.3.2 Solvent Effect .....	106
7.3.4 Conclusions .....	107
References .....	108
<b>Part B: Vegetable Oils Transesterification Process for Biodiesel Production.....</b>	<b>110</b>
<b>Chapter 8 Vegetable Oils Transesterification Reaction for Biodiesel Production: General Aspects .....</b>	<b>111</b>
8.1 Background .....	112
8.2 Transesterification Reaction .....	115
8.3 Conventional Biodiesel production process .....	117
8.4 Intensification of Biodiesel Production Process .....	118
References .....	121
<b>Chapter 9 Use of Corrugated Plates Heat Exchanger Reactor for Biodiesel Production.....</b>	<b>122</b>
9.1 Introduction .....	123
9.2 Experimental Section .....	125
9.2.1 Apparatus .....	125
9.2.2 Reactor Fluid Dynamic Characterization Runs.....	126
9.2.3 Soybean Oil Transesterification Runs.....	126
9.3 Results and discussion .....	128
9.3.1 Reactor fluid dynamic characterization .....	128
9.3.2 Reactor Performances .....	130
9.3.3 The kinetic approach and the comparison with other reactors .....	132
9.4 Possibilities of a More General Use of the CP-HEX Reactors for Other Reactions.....	136

<i>References</i> .....	137
<i>Nomenclature</i> .....	138
<b>Chapter 10 <i>Biodiesel Process Intensification using Static Mixer Tubular Reactors</i></b> .....	<b>139</b>
10.1 Introduction .....	140
10.2 Experimental Section .....	145
10.2.1 Reactor Setup .....	145
10.2.2 Fluid Dynamic Characterization Tests .....	147
10.2.3 Methanol-soybean oil transesterification runs .....	148
10. 3 Results and discussion .....	148
10.3.1 Results of the fluid dynamic tests .....	148
10.3.2 Methanol-soybean oil transesterification runs performed in the described packed bed reactors .....	152
10.3.1.1 Methanol-soybean oil transesterification runs performed TRR .....	152
10.3.1.2 Methanol-soybean oil transesterification runs performed TP1.....	153
10.3.1.3 Methanol-soybean oil transesterification runs performed TP21.....	154
10.3.1.4 Methanol-soybean oil transesterification runs performed TP22.....	155
10.3.1.5 Methanol-soybean oil transesterification runs performed RWTR.....	157
10.3.3 Methanol-soybean oil transesterification, a comparison of the runs performed in different packed bed tubular reactors (TRR, RP1, RP21, RP22, RWTR).....	159
10. 4 Results and discussion .....	160
<i>References</i> .....	161
<b>Chapter 11 <i>A biphasic model describing vegetable oil transesterification with methanol in batch and continuous reactors</i></b> .....	<b>162</b>
11.1 Introduction .....	163
11.2 Mechanism of the methanol-soybean oil transesterification reaction .....	164
11.3 Description of the biphasic kinetic model and application to batch runs taken by the literature .....	168
11.4 Biphasic kinetic model applied to continuous runs .....	174
11.5 Conclusions .....	178
<i>References</i> .....	179
<i>Nomenclature</i> .....	180

<b>Chapter 12 Conclusions .....</b>	<b>181</b>
<b>Appendix.....</b>	<b>185</b>
A.1 Properties of Epoxidized Soybean Oil and Soybean oil .....	185
A.1.1 Epoxidized Soybean Oil .....	185
A.2.2 Soybean Oil .....	186
A.2 Analysis of epoxidation reaction mixtures .....	187
A.2.1 Determination of Iodine Number .....	188
A.2.2 Determination of Oxirane Number .....	189
A.3 Determination of Residual Hydrogen Peroxide .....	189
A.4 Analysis of transesterification reaction mixtures .....	190
A.4.1 NMR analysis .....	190
A.4.2 Gas-cromatographic analysis .....	190
<i>References .....</i>	<i>191</i>
<b>Publications.....</b>	<b>192</b>

# Chapter 1

## *Introduction*

“By seeking and blundering we learn”

**Johann Wolfgang Von Goethe**

(1749-1832, German Poet, Dramatist, Novelist)

## 1.1 Background

Nowadays, chemical industry must respond several needs in order to satisfy both the increasing market requirements for specific properties requires by the customer, and the social, and the raw material and energy savings, and environmental constraints of the industrial-scale process.

Process Intensification (PI) commonly mentioned as one of the most promising development paths for these requirements.

The PI concepts was the first proposed in the 1980's by Ramshaw. He defined it as the strategy to make dramatic changes in plant size by several orders of magnitude.

The size reductions in chemical plant may be results from decreased size of processing units or a decreased number of processing units.

The definitions of PI was extended by Stankiewicz and Molijn. They defined the PI as novel equipment, processing techniques and development of new methods in order to have substantial improvements in chemical processing in terms of energy consumption waste generation, plant size and safety.

The new design philosophy of PI has also the aim to improve the mass and heat transfer characteristics, by generating a better contacting between fluids, in order to give possible a process which has chemical kinetics as its only limitations. This means that all other processing limitations due to the mass and heat transfer are eliminated, resulting in an increase of productivity and safety.

Moreover by reducing the equipment size, the main plant cost should be reduced, with a reduction of capital cost. In addition to cost saving, PI can offer other benefits such as smaller items which would have lower residence time and thus easier controllability and intrinsically safer units in plants. Furthermore, PI can reduce the environmental impact of a plant because the unit hardware size are drastically reduced, the restrictions would be met and a complete plant can be built and put together on a small area.

Thus process intensification leads to more or less complex technologies that replace large, expensive, energy intensive equipment or processes with ones that are smaller, less costly, more efficiently plants, minimizing environmental impact, increasing safety and improving control and automation, or that combine multiple operation into as single or fewer apparatus.

Microtechnologies developed, especially in Germany, (for example, IMM, Mainz and Forschungszentrum, Karlsruhe) and in USA (MIT and DuPont) lead to microreactors, micromixers, micro heat exchanger, making accurate control of reaction conditions possible with respect to mixing, quenching, and temperature profile. The high heat and mass transfer rates possible in microfluidic systems allows reactions aggressive conditions with higher yields than conventional reactors.

## 1.2 Research scope

The research proposed in this thesis has as aim the intensification of two interesting industrial processes:

1. Biodiesel production;
2. Epoxidized Vegetable oils production.

Common elements between two above mentioned processes are: (i) the raw materials, which are vegetable oil, therefore renewable, non toxic and biodegradable; (ii) the presence of reactants in immiscible liquids phases.

Biodiesel is a renewable fuel, which is mainly produced by transesterification of vegetable oils with alcohol in the presence of base or acid catalysts. The reaction takes place in a liquid-liquid two phase system and its reaction rate is limited by mass transfer due to immiscibility of oils and alcohol. The efficiency of the contact between the feed oil and the alcohol/catalyst reaction mixture is crucial to achieving a high rate of reaction and achievement of an economic reactor size.

The epoxidized oils are important chemicals, normally used as plasticizers and stabilizers for PVC resins. The epoxidation of vegetable oils is industrially carried out reacting the double bonds of oils with a percarboxylic acid (peracetic or performic), latter generated in situ, for safety reasons, by reaction of concentrated hydrogen peroxide and correspondent carboxylic acid in presence of a mineral acid. For this process, a part from the immiscibility of reactants (oil and hydrogen peroxide) that slows down the mass transfer, there are also problems related to high exothermicity of reaction. In view of this, process intensification technologies can be applied to enhance liquid-liquid contacting, increase mass transfer rate during both processes and heat transfer for the epoxidation reaction with a quick removal heat released.

The feasibility of the intensification of two processes mentioned above is explored in the two parts of this dissertation:

1. Vegetable oils Epoxidation Production (**Part A**)
2. Vegetable oils Transesterification for Biodiesel Production (**Part B**)

First a brief summary of state of art of PI is presented in the chapter 2, where some novel process intensification technologies, that include novel reactors and mixer devices, are analyzed.

# Chapter 2

## A summary of Process Intensification Status of art

*The first step to knowledge is to know that we are ignorant*

**Socrates**

(470 – 399 B.C., philosopher)

## 2. 1 History and definitions

Process intensification (PI) is presently receiving considerable interest in the chemical engineering community [1].



**Figure 2.1:** 16th century technology for retrieving gold from ore [3].

Several international conferences, smaller symposia/workshops every year, and a number of dedicated issues of professional journals are clear proof of it.

But how did it all begin?

According to *Miriam-Webster's Collegiate Dictionary*, the word *intensive* has probably its origins somewhere in 15th century [2]. And it was not many years later, in the 16th century, when Georgius Agricola published his famous book *De Re Metallica* [3], the book that is commonly regarded as the first comprehensive textbook on the engineering of mining and metallurgy.

*De Re Metallica* is richly illustrated and shows equipments and processing methods used in the times of Agricola. In many of those pictures clear elements of process intensification can be found. One example is

shown in Figure 2.1, which illustrates the process of retrieving gold.

The resemblance between some of the devices shown in the picture (for instance, the stirred vessels *O* and the stirrers *S*) and the equipment of today's chemical process industries is striking.

But, what actually *is* process intensification?

Several definitions of PI have been proposed in the last decade (table 2.1) [1], that are quite different in nature. In the first definitions of PI the plant miniaturization was often emphasized. It's clear that the miniaturization was and remains the hallmark of PI. The definition was change over the years, how it is evident in table 2.1.

Ramshaw was the first to define the processes intensification (PI) in his papers published in 1983 by [4, 5], he describes PI as strategy for making dramatic reduction in the sizes of a chemical plant so as to reach a given production objective.



**Table 2.1:** Selected Definitions of Process Intensification over the Last decades.

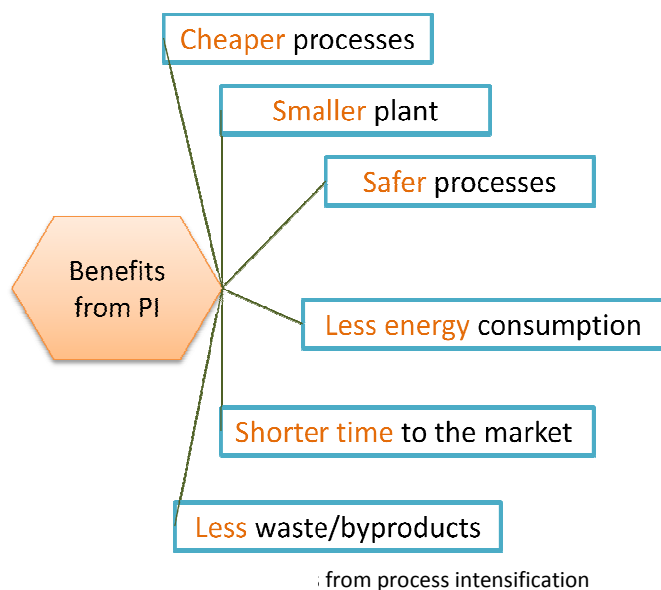
Process Intensification...	Reference (year)
"[is the] devising exceedingly compact plant which reduce both the 'main plant item' and the installations costs."	Ramshaw (1983)[4]
"[is the] strategy of reducing the size of chemical plant needed to achieve a given production objective."	Cross and Ramshaw [5](1986)
"[is the] development of innovative apparatuses and techniques that offer drastic improvements in chemical manufacturing and processing, substantially decreasing equipment volume, energy consumption, or waste formation, and ultimately leading to cheaper, safer, sustainable technologies."	Stankiewicz and Moulijn [6](2000)
refers to technologies that replace large, expensive, energy-intensive equipment or process with ones that are smaller, less costly, more efficient or that combine multiple operations into fewer devices (or a single apparatus)."	Tsouris and Porcelli [7](2003)
"provides radically innovative principles ('paradigm shift') in process and equipment design which can benefit (often with more than a factor two) process and chain efficiency, capital and operating expenses, quality, wastes, process safety and more."	ERPI [8](2008)
"stands for an integrated approach for process and product innovation in chemical research and development, and chemical engineering in order to sustain profitability even in the presence of increasing uncertainties."	Becht et al. [9](2008)12

Ramshaw's definition is quite restrictive because describing process intensification exclusively in terms of the reduction in plant or equipment size. In fact, this is one of several possible desired effects. Clearly, a dramatic increase in the production capacity within a given equipment volume, a step decrease in energy consumption per ton of product, or even a marked cut in wastes or byproducts formation also qualify as process intensification. The last aspects need changes in operations and development of novel methods and equipment. In this way the definition of process intensification has changed accordingly. It is no longer exclusively regarded as drastically smaller equipment/plants, but PI comprises *novel equipment, process techniques, and processes development methods that, compared to conventional ones, offer substantial improvements in chemical manufacturing and processing.*

## 2. 2 Advantages of Process Intensification

The Process Intensification (PI) is defined as a strategy to achieve substantial benefits in various production processes, according to an approach that aims at a reduction (miniaturization) of the volume of equipment, thanks to the use of microsystems.

The intensification process has now become synonymous with increased security, reduced energy consumption, minimizing waste by-products. This strategy is



summarized in two basic principles, "Smaller is safer" (a decrease in the size of the equipment in use in the chemical industry would significantly reduce the consequences of a possible crash) and "Producing much more with less" (target prefixed with an effort of reaching for a maximization of a process). This results in obvious potential benefits that would result from implementation of miniaturization provided by a PI, such as the reduction of process

costs, by preventing runaway reactions, a better transfer of matter, heat and momentum, with a consequent improvement in safety and productivity of the process.

The process intensification leads to cheaper process due a reduction of:

- *investment costs*, resulting from compact equipment(reducing piping, integrated processing units),
- *raw materials*, due to high yields/selectivities
- *utilities*, due to higher energy efficiency,
- *waste processing*, due to less waste generated in process-intensive plants.

Given the anticipated plant volume reductions, the toxic and flammable inventories of intensified plant are correspondingly reduced, thereby making a major contribution to intrinsic safety. It is obvious that smaller is safer. Considering the more severe chemical disasters of the past century, such as Seveso 1976 with 7-ton inventory and 3 tons escaped or Bhopal with 41 tons released, the disastrous consequences may arise from large inventories when something goes wrong. Furthermore, using smaller equipment there are better possibilities to keeping processes under control, for instance, via

extremely efficient heat removal from exothermic reactions or via controlled gas liquid flow in structured catalyst that prevents liquid maldistribution and hot spot formation. The most telling environmental influence of PI could well be in the development of new reactor designs which give high selectivity. Improved performance of PI technologies could achieve high energy efficiency and decrease in energy consumption by enhancement of transport rates and combination of reaction and separation.

## 2.3 Components of process intensification

Process intensification is driven by four generic principles:

1. Maximize the effectiveness of intra and intermolecular events.
2. Give each molecule the same processing experience.
3. Optimize the driving forces on every scale and maximize the specific areas to which those forces apply.
4. Maximize the synergistic effects from events and partial processes.

Four main domains, which constitute the pillars of PI scientific approach, may be identified [10]:

1. Structure (spatial domain).
2. Energy (thermodynamic domain).
3. Synergy (functional domain).
4. Time (temporal domain).

Figure 2.3 presents the most relevant issues addressed by PI in each of these areas.

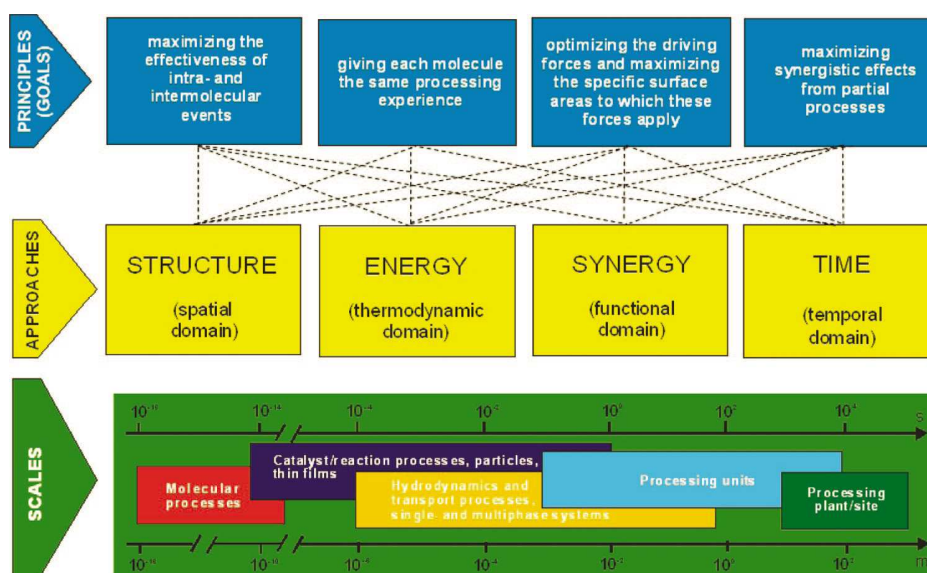


Figure 2.3: Fundamental view on process intensification.

According to Stankiewicz, A. and Moulijn [2] the process intensification concept generally can be divided into two areas (Figure 2.4):

- **process-intensifying equipment**, such as novel reactors, and intensive mixing, heat-transfer and mass transfer devices;
- **process-intensifying methods**, such as new or hybrid separations, integration of reaction and separation, heat exchange, or phase transition (in so-called multifunctional reactors), techniques using alternative energy sources (light, ultrasound, etc.), and new process-control methods (like intentional unsteady-state operation).

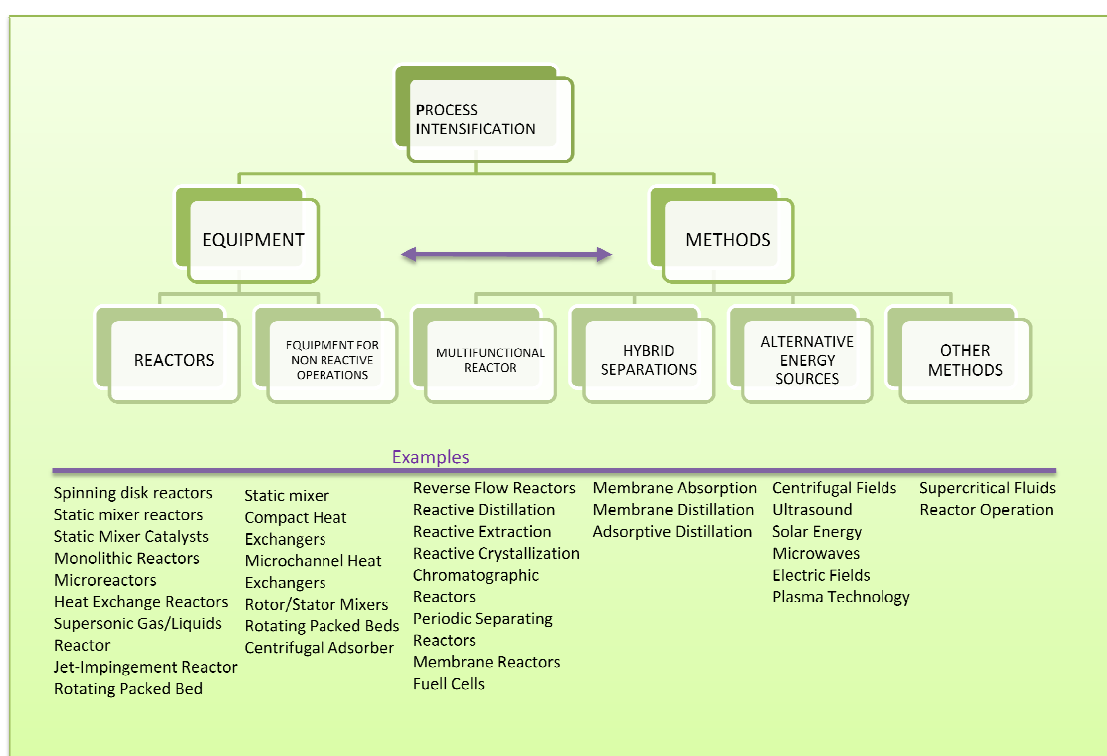


Figure 2.4: Process intensification and its component.

Obviously, there can be some overlap. New methods may require novel types of equipment to be developed and *vice versa*, while novel apparatuses already developed sometimes make use of new, unconventional processing methods.

### 2.3.1 Process Intensifying Equipment

Relevant examples of Process Intensifying Equipment are briefly discussed below.

#### 2.3.1.1 Static Mixers

Static mixers are fine examples of process-intensifying equipment. Fig 2.5 shows an example of a static mixer. Static mixers are motionless mixers, comprise of geometric mixing elements fixed within a pipe, which use the energy of flow stream to create mixing between two or more fluids [11].

The elements of the static mixer divert the flow radially towards the pipe walls regardless of the velocity. As a consequence the products are continuously intermixed to eliminate radial gradients of temperature, velocity and composition.

Geometries of these elements are various and sometimes patented [11].

Static-mixers perform a series of mechanism to mix reactants, namely dividing, rotating, channeling, or diverting the flow, before recombining it.

These static mixers have many properties and functions [12, 13]. The first of them is of course the mixing of miscible components regardless of the volume, density, viscosity and properties of the

fluids. It is also interesting to use them as contactor of liquids with gases. It creates high mass transfer and high rates of absorption, reaction, vaporization and condensation.

But static mixers can also be used in shell and tube heat exchangers [12]. Heat is efficiently supplied or removed (3–10 times greater transfer rates than empty tubes [14]) can successfully be applied in processes in which simultaneous mixing and intensive heat removal or supply are necessary (e.g. nitration, neutralization reaction, etc.) (Sulzer SMXL, SMX, SMR Mixers [13]). Static mixers can also be inserted in reactors. Such reactors behave like plug flow reactors even at low Reynolds number with high residence times without the traditionally required increase of the reactor volume or decrease of flow velocity. Results showed good heat transfer characteristics high conversion, high product yields and very low impurity levels (Sulzer SMVMixers). However, at high flow rate, conversion is lower than in batch reactors. So, increasing residence time, through enhancing reactor length, would be expected while paying attention to pressure drops.



Figure 2.5: Example of Static Mixers

One of disadvantages of SMRs is their sensitivity to clogging by solids, making their utility for reactions involving a slurry catalysts limited.

### 2.3.1.2 Microreactors

Microreactors are defined as miniaturized reaction system fabricated by using, at least partially, methods of microtechnology and precision engineering [15]. The term “microreactor” is the name that is generally used to describe a great number of devices that have small dimensions and designed for chemical engineering purpose such as reactions, heat and mass transfer. As a result of active research and development in the field, microscale processing units such as micromixers, microheat exchangers and reactions modules are commercially available.

Microreactors consist of multiple parallel channel where the reactions occur. As it can be inferred from the prefix micro, the channels inside the reactor have diameters in the scale of several micrometers, mostly over 10 micrometers but, however, less than 1 millimeter as stated above [16].

The small size of a microreactor is illustrated in Figure 2.6.A. Small channels can be seen in Figure 2.6.B.

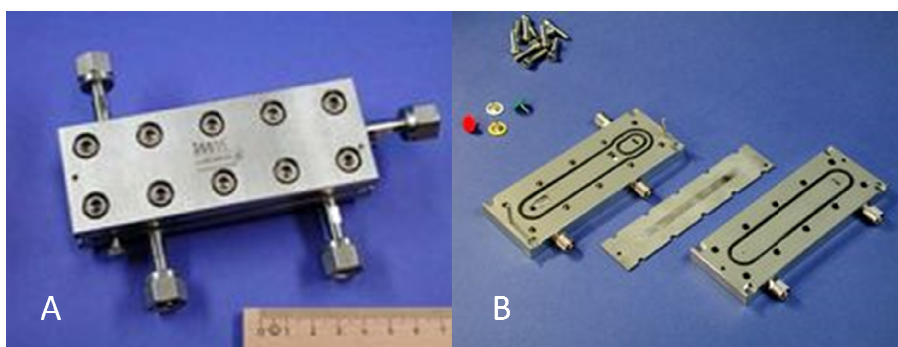


**Figure 1.6:** Example of Microreactors furnished by IMM (Institut für Mikrotechnik Mainz GmbH, [17]). A) Liquid/Liquid-Microstructured Reactor LLMR – MIX; B) Opened Liquid/Liquid-Microstructured Reactor LLMR – MIX.

Microreactor technology (MRT) is rather a novel subject in the field of chemical process engineering compared with conventional macro-scale chemical reaction engineering. Nevertheless, according to Kothare [18], the first reports on micro-scale chemical handling have first occurred in the mid 1930's at an annual meeting of the American Chemical Society. According to Ehrfeld et al. [19], the discipline proper of MRT originated several decades later in the late 1980s in Europe and the USA. Later on, process and reaction miniaturization have created more and more interest within chemical process engineering.

Various emerging applications and technologies have been driving the trend of miniaturization during the last two decades [20].

A variety of materials and methods are now available for construction of microreactors and microprocesses components. In general, the fabrication methods depend on the composition of a specific material of construction.

A review of materials and fabrication is provided in several dedicated monographs and journal publication [15, 21-24].

Forschungszentrum Karlsruhe and Institute for Microtechnology Mainz (IMM) have been the primary drivers of the multichannel microreactors, micromixers and micro-heat exchanger in metal by use of lithography, electroplating and molding [15]. Coating the interior surface of these channels with a catalytic active material turns mixers and heat exchanger into reactors. Microreactors have been developed and applied for liquid, liquid-liquid, gas gas-gas, gas-liquid and gas-liquid-solid phase process. They are applied for example for partial oxidation of a vitamin intermediate, an addition reaction for fine chemical production and polymer synthesis.

One of the most important fundamental advantages is the decrease of the physical size of a reactor. For a given difference in a physical property, decrease of linear dimensions leads to an increase of the gradient of the processing parameters (such as temperature, concentration, density or pressure) [15]. Accordingly, the mass transfer, heat transfer, and diffusional flux are enhanced. In these small devices, a high specific surface area in the range of 10,000-50,000 m<sup>2</sup> m<sup>-3</sup> is achieved, which enables an effective mass and heat transfer compared to traditional chemical reactors [25].

As result, heat transfer coefficients measured in microreactors goes up to 25000 W/m<sup>2</sup>K. This exceeds heat transfer coefficient of conventional exchanger by at least one order of magnitude [15].

The excellent heat transfer properties in microreactors avoid the risk of potential significant industrial accidents caused by thermal runaway [15]. As a consequence, very exothermic reactions, such as hydrogenation of nitrobenzene, nitration can be performed at isothermal conditions.

Due to the small channel dimensions, in all microreactors a laminar flow regime predominates. By rearrangement of Fick's law the dependence of the mixing time ( $t_{mixing}$ ) on the width of the lamellae ( $d$ ) is revealed by the following equation , where it can be seen the positive effect of miniaturization of characteristic structures on mixing

$$t_{mixing} \propto \frac{d_l^2}{D}$$

D is the diffusion coefficient and  $d_l^2$  is lamellae width [15].



Consequently, a rather rapid diffusion mixing is promoted in microreactors compared with the turbulence and chaotic mixing in conventional reactors, *i.e.* mixing time scale in microseconds in microreactors[26] vs. seconds or longer in classical reactors [15].

The decreased reaction volume also enhances process safety and, due to the shorter residence time, improves selectivity of certain reactions [15]. The smaller devices provide easy transportation which enables a distributed point-of-use production of highly reactive toxic chemicals [27] and low cost of construction materials and energy used for chemical production.

Another advantage of microreactor systems is so called “numbering up” (Figure 2.7), which means to connect microreactors of same dimensions in parallel or in series in order to build up a compact microplant with higher capacities [28]. The numbering up avoids the traditional approach for the scaling-up. Indeed in traditional approach, the increase of the size of conventional reactors requires plant designers to increase the size of each reactor unit. This makes scale up expensive, time-consuming and sometimes extremely difficult. In contrast, the microreactors can be shop-fabricated, and the Microchannel based plants can be constructed more quickly and easily with guarantees that desired features of basic unit will remain unchanged when increasing total system capacity. Besides that, in microplant continuous operation is uninterrupted with the replacement of the failed microreactor, while the other parallel units continue production [15].

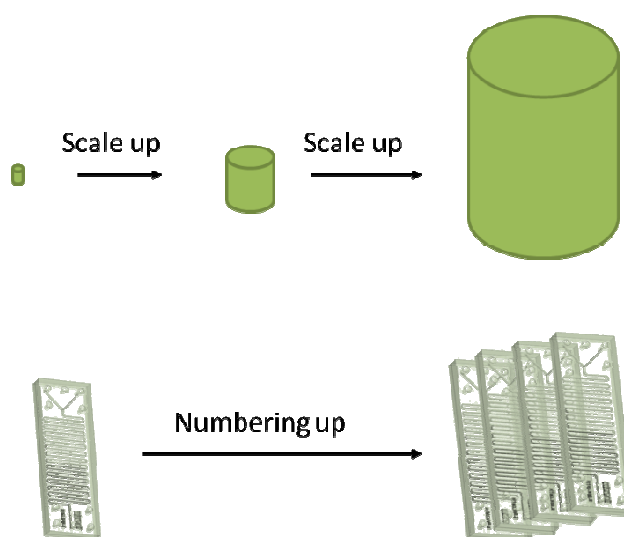


**Figure 2.7:** Comparison of scale-up methodology in macroreactor and microreactor system.



The most significant drawback of microreactors is the challenge related to economic aspects. At least in general, more companies with added capital are needed in the field of MRT to participate in developing the technology in order to find more useful and potential applications and to improve those which are already found. In addition to cost issues, the other demerits of MSR include the aforementioned numbering up as well as the potential clogging of channel tubes [20].

**Table 2.2:** The advantages and disadvantages of microreactors when compared to conventional reactors.

Advantages	Disadvantages
Enhanced safety	Cost issues
High surface-to-volume ratio	Challenges in numbering up
Improved mass and heat transfer rates	Clogged tubes
Mitigation of runaway reactions	
A narrow RTD	
Faster system response	
Better process control	
High product yields	
Compactness	
Light weight	
Lower material and energy consumption	
Distributed production	
Quick start-up and shutdown	
Increased conversion and selectivity	
Easier scale-up	
Short residence time	
Accelerated laboratory process development	

### 2.3.1.3 Monolithic catalysts

The monolithic substrates are metallic or non metallic bodies with a honeycomb structure (defined uniform cross-sectional shape). They are widely used as catalysts or

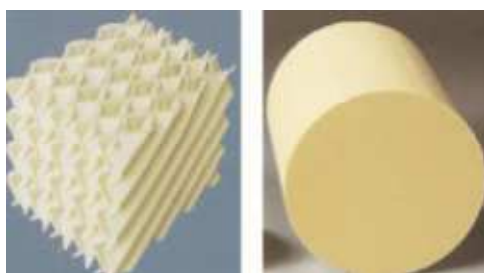


**Figure 2.8:** Example of Monolithic Catalysts

catalysts support for gas treatment applications as well as for performing three-phase catalytic reactions. For the latter application, particular interest has been focused on catalytic reactions such as hydrogenation, oxidation and bioreactions.

To ensure sufficient porosity and enhance the catalytically active surface, the inner walls of the monolith channels usually are covered with a thin layer of washcoat, which acts as the support for the catalytically active species.

The most important features of the monoliths are :

- very low pressure drop in single or two phase flow;

- high specific surface area;
- high catalytic efficiency due to very short diffusion path;
- good performance in process in which selectivity is influenced by mass transfer resistances.

One of problems in monolith reactors, especially for gas-phase catalytic processes, is difficult heat removal due to the absence of radial dispersion. For the highly exothermic gas-phase reactions, so called HEX reactors developed by BHR group, Ltd (Cranfield, U.K.) [29]. In these reactors, one side of a compact heat exchanger is made catalytically active, either by washcoating or by introducing catalytically active elements. One of this reactor is developed by Corning Inc. (Corning, NY), [30].

### 2.3.2 Process Intensifying Methods

As shown in figure 2.4, most process intensifying methods fall into following principal areas:

1. integration of reaction and one or more unit operations into so-called multifunctional reactors;
2. development of new hybrid separations;
3. use of alternative forms and source of energy for processing.

#### 2.3.2.1 Multifunctional Reactors

The term 'multifunctional reactor' can be defined as reaction equipment in which performance is synergistically enhanced by means of integrating one or more additional process functions (usually unit operation) that conventionally would be separate piece of equipment [31]. A widely known example of integrating reaction and heat transfer in a

multifunctional unit is the reverse flow reactor [32]. In these reactors the periodic flow reversal allows perfect utilisation of heat of exothermic reactions by keeping it within the catalysts bed and, after reversion of the flow direction, using it to preheating the cold reactant inlet gases.

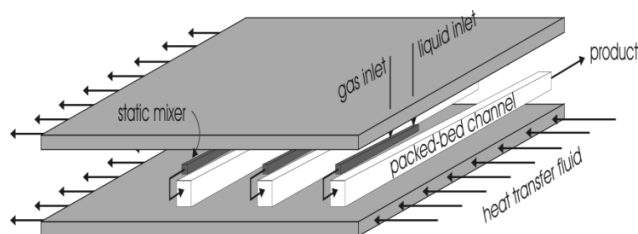


**Figure 2.9:** Design of a compact multifunctional reactor for selective oxidation of alcohols by molecular oxygen.

Another widely adopted multifunctional reactor is the combined reactor/ heat exchanger for fast exothermic chemical reactions, aimed at improving product selectivity and reducing the risk of explosions [33]. An example of such is the 'sandwich reactor'; it consists in three zones- a catalyst bed between two beds of packing in a heat exchanger: in this way the three-phase compact reactor integrating the functionalities of static

mixing, reaction and heat transfer in a single monolithic block; figure 2.9 shows a schematic representation [34].

Reactive distillation is the better example of integrating reaction and separation in a continuous apparatus [35]. A reactive distillation column consists of three sections: (i) the reactive section, in which the reactants are converted into products, and where, by means of distillation, the products are separated out of the reactive zone; the tasks of rectifying (ii) and stripping (iii) sections depend on the boiling points of the reactants and products.

The advantages of catalytic distillation units, besides the continuous removal of reactions products and higher yields due to the equilibrium shift, consist mainly of reduced energy requirements and lower capital investments. The incorporation of internally monoliths into multifunctional reactors for catalytic distillation combines both areas of process intensification.

The other examples of combined reactions and separations process are:

- reactive extraction;
- reactive crystallization;
- reactive sorption, i.e. chromatographic reactors and pneumatic transport reactors;

In all these processes, the incorporation of a separation unit shifts equilibrium towards product formation.

### 2.3.2.2 Membrane Reactors

Membrane reactors are used for a wide variety of applications including biochemical, chemical, environmental and petrochemical systems [36].

Membranes perform a wide variety of functions often more than one function in a given context. They can be employed to:

- introduce/separate/purify reactants and products;
- provide the surface for a reaction;
- provide a structure for the reaction medium;
- Retain specific catalysts.

Within these broad contexts, the membranes can be catalytic/non-catalytic, polymeric/inorganic, and ionic/non-ionic and have different physical/chemical structures and geometries.

The scientific literature on catalytic membrane reactors is rich, and includes many very interesting ideas (such as heat- and mass-integrated combination of hydrogenation and dehydrogenation process in a single membrane unit). Large scale applications haven't yet been reported due to many factors such as high price of membrane units, low permeability and thermal/mechanical fragility.

### 2.3.2.3 Use of alternative forms and sources of energy

Different alternative sources and forms of energy can be applied to intensify the chemical process.

The most important resumed in table:

**Table 2.3** : The most important alternative forms and sources of energy.

Energy Source	Intensified Element	Degree of Possible Intensification	Sustainable Effect
Electric Field	Interfacial Area	500x	Energy
	Heat Transfer	10x	
Microwaves	Reaction Time	1250x	Energy, material efficiency
	Distillation Time	20x	
Light	Product yield/selectivity	Improved selectivity	Material efficiency waste reduction, safety
		25x	
Ultrasounds	Reaction Time	5x	Energy, material efficiency
	Gas-Liquid mass transfer	20x	
	Liquid-solid mass transfer		
Supersonic Shockwave	Gas-liquid mass transfer	10x	Energy, material efficiency

Among all, three alternative energy forms have particularly attracted research interest: microwaves, light and ultrasounds. Microwaves frequencies ranges from 300 to about 3000000 MHz polar molecules subjected to microwave irradiation exhibit dipole rotation, trying to align with rapidly changing electric field of the microwave. The rotational motion of the molecule results in a transfer of energy. Additionally, in substances where free ions or ionic species are present, the energy is also transferred by the ionic motion in an oscillating microwave field. As a result of both these mechanisms the substances is heated directly and almost evenly. Heating with microwaves is therefore fundamentally different from conventional heating by conduction. Microwaves accelerate chemical reactions, often by factors of hundreds, and in many cases significantly better product yields are reported. A relevant challenge to amplify the effect of microwaves is to couple with microreactor technology. This coupling offers a great opportunity to increase process selectivity by an instantaneous heating of the reactants and a fast quenching of the reaction products.

The formation of micro bubbles (cavities) in the liquid reaction medium as a result of *ultrasound waves* has opened new possibilities for chemical syntheses. These cavities can be thought of as high energy microreactors. Bubble collapse in liquids results in an enormous concentration of energy from the conversion of the kinetic energy of the liquid motion into heating of the contents of the bubble. The high local temperatures and pressures, combined with extraordinarily rapid cooling, provide a unique means for

driving chemical reactions under extreme conditions. A diverse set of applications of ultrasound to enhance chemical reactivity has been explored with important uses.

Solar energy also may play a role in chemistry processing. A novel high temperature reactor in which solar energy is absorbed by a cloud of reacting particles to supply heat directly to the reaction site has been studied [37].

Studies describe, for example, the cycloaddition reaction of a carbonyl compound to an olefin carried out in a solar furnace reactor [38] or oxidation of 4-chlorophenol in a solar-powered fiber-optic cable reactor [39].

## References

- [1] T. Van Gergen, A Stankiewicz., *Ind. Eng. Chem. Res.* 48 (2009) 2465.
- [2] A. Stankiewicz, J.A. Moulijn, *Re-Engineering the Chemical Processing Plant*, CRC Press 2003, DOI: 10.1201/9780203913291.ch1
- [3] G. Agricola, *De Re Metallica Libri XII*. Basel: J. Froben & N. Episopus, (1556)
- [4] C. Ramshaw, Higee, *Chem. Eng. London* 389(1983) 13.
- [5] W.T. Cross, C.Ramshaw, *Chem. Eng. Res. Des.*, 64 (1986), 293.
- [6] A. Stankiewicz, J.A. Moulijn, *Chem. Eng. Progr.* 96 (1) (2000), 22.
- [7] C. Tsouris, J.V.Porcelli, *Chem. Eng. Progr.*, 99 (10) (2003), 50.
- [8] European Roadmap for Process Intensification. Creative Energy - Energy Transition. [www.creative-energy.org](http://www.creative-energy.org).
- [9] S.Becht, R.Franke , A. Geisselman, H. Hahn, *Chem. Eng. Process.*,48 (2009) 329.
- [10] T. Van Gerven, A. Stankiewicz, *Ind. Eng. Chem. Res.*, 48 (2009) 2465.
- [11] R.K. Thakuri, Vial Ch., K.D.P. Nigam, E.B.Nauman, G. Djšselveh , *Trans I ChemE*, 81(A) (2003) 787.
- [12] Fluitec (CH), CSE-XR mixer heat-exchanger for highly viscous polymer melts,Fluitec doc. N°11.119 Rev.1.
- [13] Sulzer Chemtech (CH), Mixing and reaction technology, Sulzer brochure 23.27.06.40-100, 1997.
- [14] Chemineer Inc. (US), Kenics mixing technology — Bulletin 800.  
[www.chemineer.com/images/pdf/bulletin\\_800](http://www.chemineer.com/images/pdf/bulletin_800.pdf) . pdf.
- [15] W. Erhfeld, V. Hessel, H. Löwe, *Microreactors: New Technology for Modern Chemistry*, Wiley-VCH, Weinheim, 2005, 1-69.
- [16] L. Kiwi-Minsker, A. Renken, *Catal. Today*, 110 (2005)2.
- [17] IMM, Catalogue Chemical Process Technology 5/2009, [www.imm-main.de/519.htm](http://www.imm-main.de/519.htm)
- [18] M.V. Kothare, *Computers & Chem. Eng.*, 30 (10–12) (2006) 1725.
- [19] W. Ehrfeld, V. Hessel, V. Haverkamp , *Micro reactors*. Ullmann's Encyclopedia of Industrial Chemistry. (2002) Wiley-VCH Verlag GmbH.
- [20]P.L. Mills, D.L. Quiram, J.F. Ryley, *Chem. Eng. Sci.*, 62 (2007) 6992.
- [21] J.J. Allan, *Micro Electric Mechanical System Design*. (2005) CRC Press, Boca Raton, F.L,
- [22] M.J. Madou, *Fundamentals of Microfabrication- The Science of Miniaturization*. (2002)CRC Press Boca Raton, F.L.,
- [23] V. Hessel, H. Lowe, *Chem. Eng. Technol.*, 26 (4) (2003b) 391.
- [24] T.R. Dietrich, A. Freitag, R. Scholz , *Chem. Eng. Technol.* 28 (4) (2005), 477.
- [25] A. Renken, V. Hessel, P. Lob, R. Miszczuk, M. Uerdinggen, L. Kiwi- Minsker, *Chem. Eng. Proc.* 46(9) (2007) 840.
- [26] B.P. Mason, K.E. Price, J.L. Steinbacher, A.R. Bogdan, D.T. CMcQuade, *Chem. Rev.*, 107(6) (2007) 2300.
- [27] J.C. Charpentier, *Chem. Eng. Technol.*, 28(3) (2005) 255.
- [28] R. Schenk, V. Hessel, C. Hofmann, H. Löwe, F. Schönfeld, *Chem. Eng. Technol.*, 26 (2003) 1271.
- [29] C.H. Philipps, G. Lauschke, Peerhossaini, *Appl. Therm. Eng.*, 17 (8-10) (1997), 809.
- [30] T. Ketcham, D.J.St. Jullien, Method of Making a Cross-Flow Hiney-comb Structure, U.S. Patent 5,660,778.
- [31] D.W. Agar, *Chem. Eng. Sci.*, 54 (1999) 1299.
- [32] Yu.Sh. Matros, G.A. Bunimovich, *Catal. Review—Sci. and Eng.*, 38 (1996) 1.
- [33] E.V. Rebrov, M.M.M. de Croon, J.C. Schouten, *Catal. Today*, 69 (2001) 183.
- [34] Yu.Sh. Matros, G.A. Bunimovich, *Ind. Eng. Chem. Res.*, 50 (9) (2011) 5448.
- [35] J.L. DeGarmo, V.N. Parulekar, V. Pinjala, *Chem. Eng. Progress*, 88(3) (1992) 43.
- [36] K.K. Sirkar, P. Shanbhag, S. Kovvali, *Ind. Eng. Chem. Res.*, (1999) 3715.
- [37] A. Meier, J. Ganz, A. Steinfeld, *Chem. Eng. Sci.*, 51 (11) (1996) 3181.
- [38] B. Pohlmann, H.D. Scharf, U. Jarolimek, P. Maurmann, *Solar Energy*, 61(3) (1997)159.
- [39] N.J. Peill, M.R. Hoffmann , *J. Solar Energy Eng.*, 119(3) (1997)229.

# Chapter 3

## *Vegetable Oils Epoxidation Process: General Aspects*

*Research is to see what everybody else see and to think what nobody else has thought*

**A. Szent-Gorgyi**

(Hungarian Biochemist, 1937 Nobel Prize for Medicine)

### 3.1. Epoxidized Oils: Uses and Market

Epoxidation occurs when a cyclic ether is formed at sites of ethylenic unsaturation (C=C) located along the fatty acid (FA) chains by the addition of an oxygen atom. This epoxy group has the general structure shown in figure 3.1.

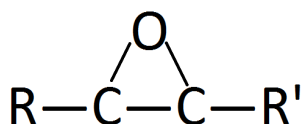


**Figure 3.1:** Epoxy Group structure, where R and R' represent the continuation of fatty acid chain either side of the epoxy group.

The Bond angles are about 60°, making the ring highly strained and highly reactive[1]. Today, one of the most important epoxidized oil is soybean oil (ESO), and its worldwide production is about 200,0000 t/year (European Market ~9000 t/year), but will further increase is approximately 7% for next year.

Fatty Epoxides are used directly as plasticizers which are compatible with polyvinylchloride (PVC), and as stabilizers (HCl scavenger) for PVC resins to improve flexibility, elasticity and to impart the stability of polymers towards heat and UV radiation. The efficiency of these epoxides is directly related to the amount of epoxy group present in the molecule oil, expressed with Oxirane Number [Appendix].

Epoxidized oils are natural, non toxic, non corrosive and biodegradable and for this can be good substitutes of phthalates, other plasticizers derived by petroleum, banned by EU in many countries due to their toxicity [2].

Due to high reactivity of the oxirane ring epoxides also act as raw materials for a variety of chemicals, such as alcohols, glycols, alkanolamines, carbonyl compounds, olefinic compounds, and polymers like polyesters, polyurethane (PU), and epoxy resins.

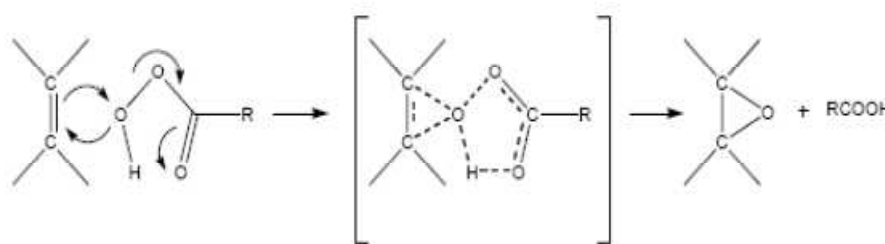
The modified soy-based vegetable oil polyoils could be incorporated as a replacement for conventional polyoils to produce flexible PU foams, elastomers and coating [3].

### 3.2. Epoxidation Methods

There are basically four known technologies to produce epoxides from olefins:

- a) Epoxidation with percarboxylic acids [4] (Prileschajew), the most widely used in industry. The percarboxylic acid is formed in situ by the reaction of carboxylic acid and hydrogen peroxide, catalyzed by acids or by enzymes [5]. The general accepted reaction mechanism is shown in scheme :





Scheme 3.1

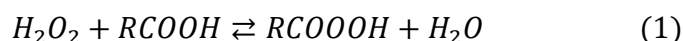
- b) Epoxidation with organic and inorganic hydroperoxides, which includes hydrogen peroxide epoxidation as well transition metal-catalyzed epoxidation [6].
- c) Epoxidation with halohydrins, using hypohalous acids (HOX) and their salts as reagents for the epoxidation of olefin with electron-deficient double bonds [7];
- d) Epoxidation with molecular oxygen [7].

Among the ways of the epoxidation methods, the available technologies that needs to be explored are only the a) and b) as described above, which are clean and efficient. These technologies can be rendered cleaner by using heterogeneous catalysts replacing traditional homogenous ones.

### 3.3 Soybean oil epoxidation with Percarboxylic acid: the chemical reactions

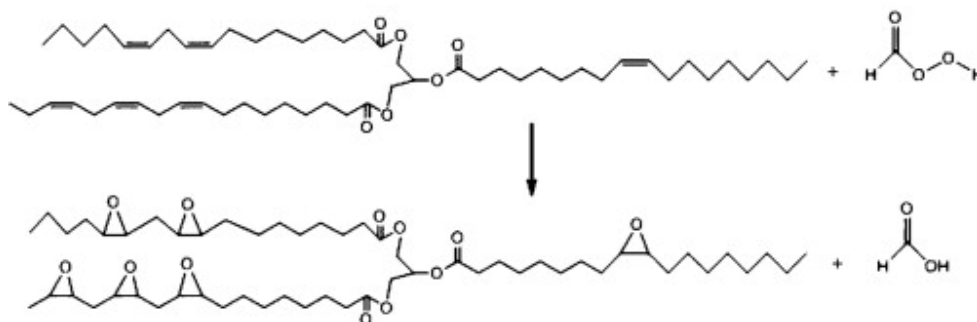
Epoxidized vegetable oils are commercially produced via the Prileschajew epoxidation by using peracids. In this way the unsaturated oils react with peracids generated in situ, for safety reasons, through the acid-catalyzed peroxidation of the respective organic acids with hydrogen peroxide.

The peracid formation occurs in the aqueous phase according to the following reaction:



Soluble mineral acids, most commonly sulphuric or phosphoric acid, are used as catalyst for this reaction. Industrially, various peroxyacids are possible, such as performic, peracetic, perbenzoic, m-chloroperbenzoic, from which performic and peracetic are preferred due their easy availability, lower prices, high epoxidation efficiency and reasonable stability at ordinary temperature [8].

Subsequently, performic acid obtained migrates into the oil immiscible phase giving to the reaction (2).



Scheme 3.2

Peracetic acid spontaneously reacts with double bonds of oil forming epoxide groups, this at last returns to the aqueous phase and reaction cycle restarts.

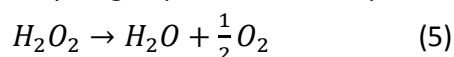
However it was found that while the rate of the formation of epoxide was higher with formic acid [9], using acetic acid resulted in 10% conversion of ethylenic unsaturation (EU) to epoxides [1] and lower amount of undesirable byproducts were formed. An explanation for this is that due to the very high activity of the formic acid, the hydrogen peroxide is rapidly decomposed leaving the batch oxygen depleted [10].

Other reactions can occur, these are the epoxide ring opening, occurring in two steps (3, 4) in which the first one is rate determining, due the presence of mineral acid used for the preparation of peracids. Ring opening takes place through cleavage of one of the carbon-oxygen bonds.

In acid catalyzed ring opening, the nucleophile attacks the protonated epoxide ring from the side opposite the epoxide group (see scheme 3.3). The carbon being attacked undergoes an inversion of configuration. The new C-O bond is always formed from the side opposite that of the original epoxide ring because the ring-opening reaction is an  $S_N2$  reaction.

Acid catalysis assists epoxide ring-opening by providing a better leaving group (an alcohol) at the carbon undergoing nucleophilic attack. In this way, the yield of the epoxidation reaction is largely conditioned and selectivity is lower too.

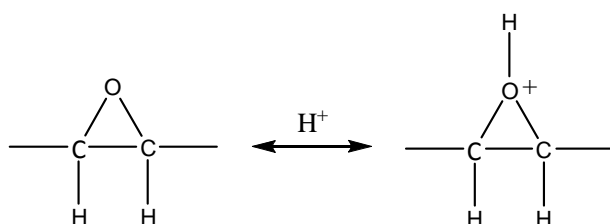
Another important reaction involved in epoxidation processes is related to hydrogen peroxide decomposition the hydrogen peroxide decomposition (5):



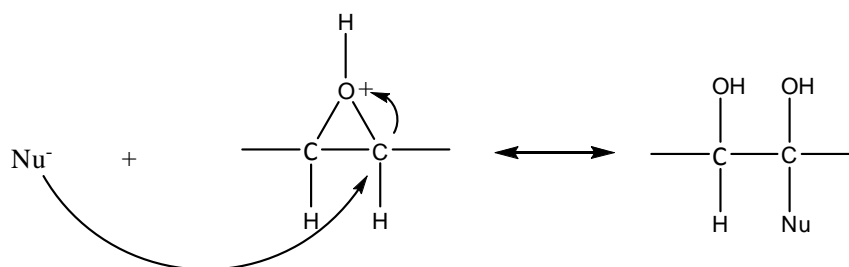
This reaction is important for two reasons:

1. It is promoted by the metal walls the industrial reactors are usually built.
2. As it is usually used in large excess, at the end of the epoxidation process it necessary to decompose it.

## Epoxidation Activation



## Nucleophilic attack



Scheme 3.3

**3.4 Soybean oil epoxidation with Percarboxylic acid: Industrial Process**

On Industrial scale, the soybean oil epoxidation takes place in a pulse fed batch reactor at the reaction temperature in the range of 65-70°C. (see Figure 3.2 and 3.3).



Figure 3.2 : Epoxidation Batch Reactor, by courtesy of MYTHEN SPA.

The reactor is normally filled with oil and catalyst ( $\text{H}_2\text{SO}_4$  or  $\text{H}_3\text{PO}_4$ ), the oxidant mixture (Hydrogen peroxide and Formic Acid) are added in limited amount in order to prevent an excessive increase of temperature. The addition operation is repeated ten times by using an excess of  $\text{H}_2\text{O}_2$  (from 1.2-1.5) and by keeping the temperature in the range of 60-70 °C. This step is called as “Adding Period”. The time required for any additional step clearly depends on the efficiency of heat exchanger. After each added amount of the oxidant reagents the temperature goes up. A heat exchanger cools the reaction mixture avoiding that the temperature goes above 70-75°C. It is known, in fact, that higher temperatures promote the secondary ring opening reactions, therefore reducing the selectivity. This aspect is enhanced by the long residence times required by the mentioned reactor.

A simplified scheme of the actual epoxidation industrial plant is reported in Figure 3.3. At last, a digestion period of 2-3 hours is necessary to complete the reaction and to obtain a product with market target properties (Appendix). The reaction, normally, requires totally about 6-8 hours.

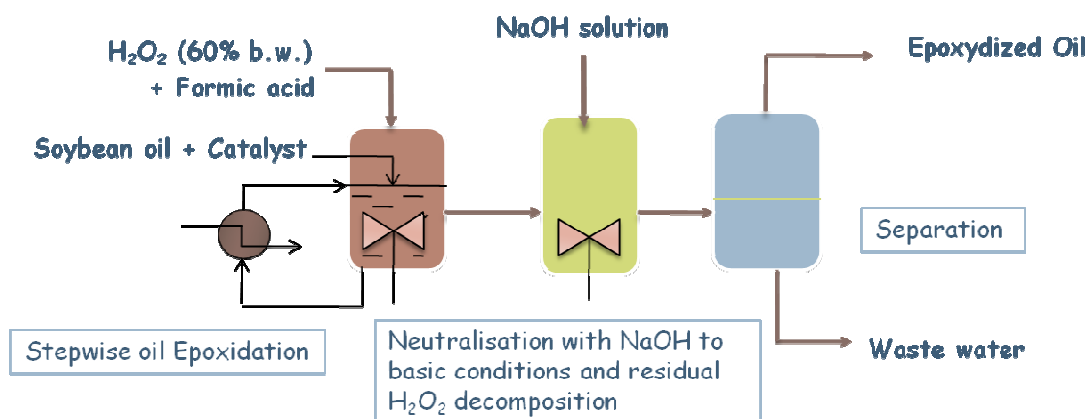


Figure 3.3: Simple scheme of Soybean Oil Epoxidation Process.

The epoxidation reaction is followed by the hydrogen peroxide decomposition using sodium hydroxide (normally used in a moderate excess of 20-30% with respect to the stoichiometric need and neutralization step, creating a basic environment. Afterwards, the aqueous phase is separated and product is washed and at least filtered.

### 3.5 Intensification of Soybean Oil Epoxidation Process

Current technology of production of epoxidized oils, based on batch reactors, has several limitations (what has emerged from the analysis up to this point) that can be related to:

1. Exothermicity of the reactions involved ( $\Delta H = -55$  kcal/mol)
2. Immiscibility of the reagents
3. Low productivity
4. Slow operation (About 10 hours)
5. Use of Homogenous Acid catalyst (low selectivity and corrosion and disposal salt problems)
6. Hydrogen peroxide Decomposition (this reaction is catalyzed by the metal walls of the reactor).

These limitations could be overcome with an intensification of process, that should occur with:

A) The transfer from Pulse Fed Batch to continuous reactor able to efficiently mix the immiscible liquid reactants (oil and oxidant) and remove the heat released in the reaction. Taking into account the features of epoxidation reaction, the use of a microreactor seems to be the best solution. In fact, the high dispersion capabilities of micromixer might take the improvements in the mass transfer, in the reaction rate, in the selectivity and in the yield of process, as well as in the process work up. While the tight control over temperature and residence time connected with microstructured reactor, characterized by high heat transfer properties, is expected to result in a better management of unwanted consecutive reaction. Therefore, the possible effects of an intensification process through microreactors use might be:

- Speed-up of the reaction due to the mass transfer increase;
- Selectivity increase due to the better defined concentrations (through mass transfer) and temperature (through heat removal) fields, suppressing the side and consecutive reactions;
- Selectivity increase due to just providing the time for the reaction intrinsically need and not providing more which could promote consecutive reactions with short residence times.

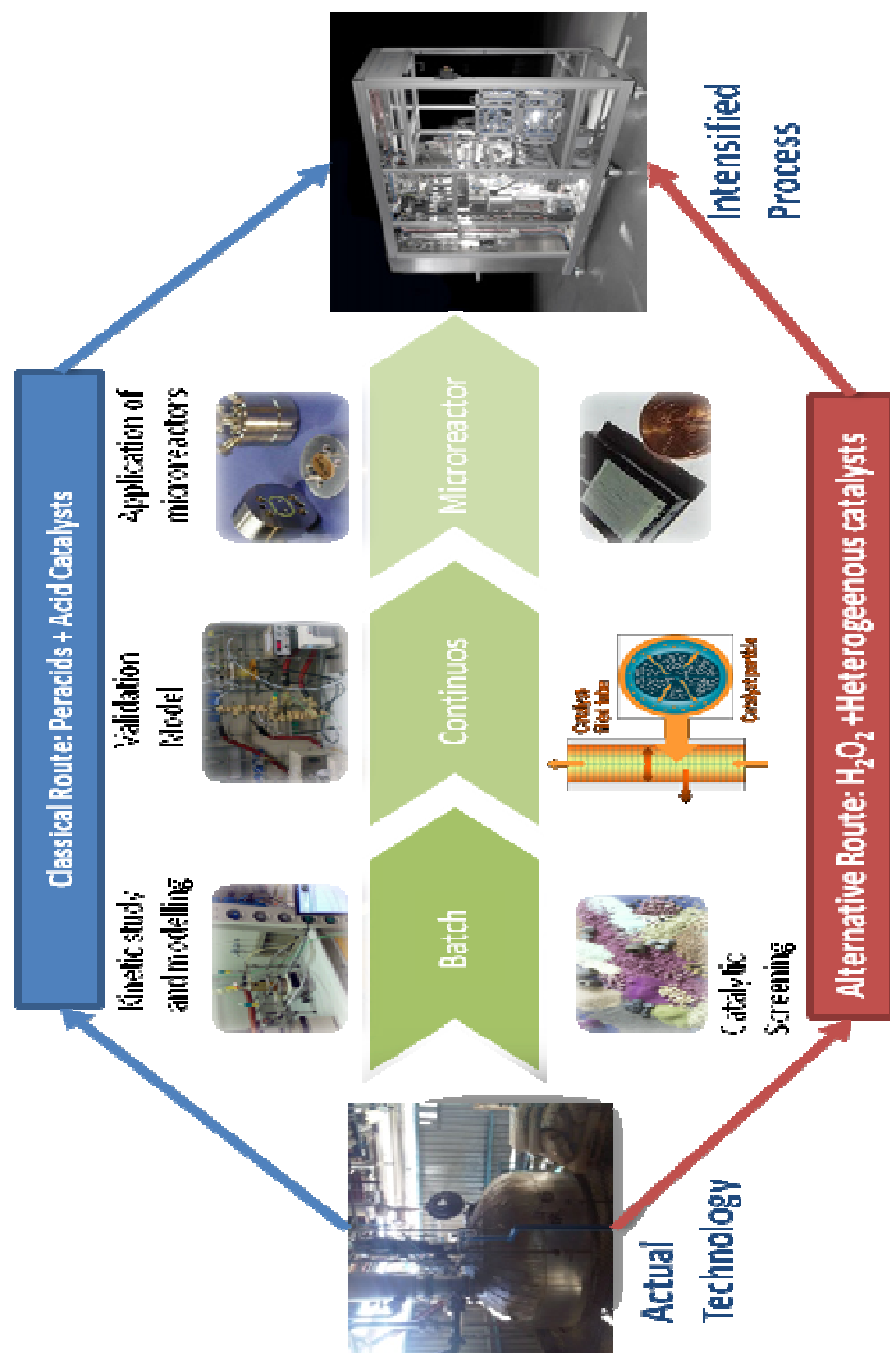
This task (A) requires a detailed investigation, that allows to get a full kinetic picture including the side reactions for biphasic and to define the desired reaction performance (yields). In order to do this, it is very important to develop a biphasic kinetic model considering both the kinetic laws of all involved reactions and partition of all components between the polar and non-polar phases occurring (Chapter 4, 5 and 6).

B)Heterogeneous Catalysts use for epoxidation with peracids, avoiding the use soluble mineral acid ( $\text{H}_2\text{SO}_4$  AND  $\text{H}_3\text{PO}_4$ ) for peracid formation, in order to suppress the ring opening reactions. A hydrophilic solid would be a better catalyst for this reaction and zeolites would be ideal because the formation of performic would be promoted by the acid sites inside the zeolitic pores that could not be reached by the soybean oil bulky molecules. A preliminary epoxidation run performed by using an acid zeolite has shown a relatively low activity but a very encouraging selectivity.

C)Heterogeneous Catalysts use for epoxidation with hydrogen peroxide, avoiding the use of peracids. The benefits related to the use of hydrogen peroxide respect than the peracids are clear: it is environmentally benign, it can be handled and stored safely, it produces water as the only byproducts. (Chapter 7).

D)Development of continuous operation also for decomposition residual hydrogen peroxide, after the epoxidation reaction. This operation is now days performed in industry simply adding an excess of sodium hydroxide to the aqueous solution, creating a basic environment. In alkaline conditions, hydrogen peroxide is unstable and promptly decompose with an exothermic reaction (98kJ/mol). It is clear that in a continuous plant it would be easier to promote this reaction in the presence of a heterogeneous solid catalysts. It has been found, for example, that stainless steel promotes the hydrogen peroxide decomposition, also in neutral or moderately acids conditions [11]. However, many other heterogeneous catalysts have been found which are much more active than stainless steel. Research is still in progress to evaluate the best one which can be coated on the walls of a microreactor with the aim of intensifying the operation.

The experimental research evolution related to intensification of soybean oil epoxidation can be summarized in the following scheme:



**References**

- [1] R. Mungroo, N.C. Pradhan, V.V. Goud, A.K. Dalai, *J. Am. Chem Soc.* 85(9) (2008), 887.
- [2] S. Biedrman-Brem, M. Biedrmann, S. Pfenninger, M. Bauer, W. Altkofer, U. Hauri, C. Droz, K. Grob, *Cromatographia*, 68,(2008), 227-234.
- [3] I. Javni, Z.S. Petrovic, A. Guo, R. Fuller, *J. App. Polym. Sci.*, 77 (2000) 1723.
- [4] N. Prileschajew, *Berichte der deutschen chemischen Gesellschaft*, 42 (1909) 4811.
- [5] S. Warwel, M. Rüschen, Klaas, *J. Mol. Cat. B: Enzym.*, 1 (1995) 29-35
- [6] I.W.C.E. Arends, R.A Sheldon, *Topics Catal.*, 19(1) (2002) 133.
- [7] M. Bartok, K.L. Lang, "Oxiranes" in: S. Patai, *The chemistry of ethers, crown ethers, hydroxyl groups and their sulfur analogues*, J. Wiley & Sons, New York, Part 2, Chapter 14, (1980), 609-879.
- [8] V. Vaibhan, V.V. Gound, A.V. Patwardhan, N.C. Pradhan, *Ind. Eng. Chem. Res.* 46 (2007) 3078.
- [9] S. Dinda, A.V. Patwardhan, V.V. Gound, N.C. Pradhan, *Bioresour. Technol.*, 99(9) (2008) 3737.
- [10] Z.S. Petrovic, A. Zlatanovic, C.C. Lava, S. Sinadinovic-Fiser, *Eur. J. of Lip. Sci. Technol.* 104(5) (2002) 725.
- [11] E. Santacesaria, M. Di Serio, R. Tesser, V. Russo, R. Turco, *Ind. Eng. Chem. Res.* 50 (2011) 2569.



# Chapter 4

## Vegetable Oils Epoxidation Reaction with Performic acid batch reactor: Kinetic Aspects

*"Real is what can be measured"*

**Max Planck**

(1858-1947, German physicist)

#### 4. 1 Introduction

As discussed in part A of this thesis, an intensification of soybean oil epoxidation process requires a detailed study about both the kinetics of the occurring reactions and the effects of heat and mass transfer. This study corresponds to the objective of this chapter.

In the last decade, some papers have been published concerning the kinetics of the epoxidation of vegetable oil [1], [2] and [3]. Normally, all these papers have considered, for the purposes of simplification, the reaction occurring in a monophasic system (pseudo-homogeneous models). Rangarajan et al. [4] are the first to propose a two-phase model, considering a local phase concentration in order to calculate the reaction rate and the mass transfer effect. Campanella et al. [5] and [6] have studied the degradation of the oxirane rings of epoxidized vegetable oils by hydrolysis and by  $\text{H}_2\text{O}_2$  attack. Moreover, Campanella et al. [1], also reported a study on the kinetics of both epoxidation and oxirane rings opening reaction, taking into account the presence of two reacting immiscible liquids. The monophasic approach is clearly oversimplified, while, the few biphasic approaches, reported by the literature, need confirmation of the effectiveness of the adopted models and related parameters. Finally, all of the kinetic studies previously proposed, did not consider the hydrogen peroxide decomposition that, according to our experimental observations, is enhanced by the stainless steel surface of the industrial reactors [7]. In the present chapter, the kinetics of the soybean oil epoxidation by peroxyformic acid (PFA), generated in situ, by reacting concentrated  $\text{H}_2\text{O}_2$  (60 wt.%) with formic acid, in the presence of sulphuric or phosphoric acid as catalysts, has been studied in a fed-batch reactor. In particular, in this kinetic study we have considered:

- (i) the partition between the phases of reagents and products;
- (ii) the kinetics of the reactions occurring in the two different phases;
- (iii) the degradation of the oxirane rings with related reactions;
- (iv) the hydrogen peroxide decomposition;
- (v) any effect of mass transfer in limiting the reaction rates;
- (vi) the three occurring thermal contributions related, respectively to the heat released by reactions, the heat removed by exchange with the thermostating fluid and the heat dispersed with the external environment. As it is difficult to maintain isothermal conditions with a so extreme exothermic reaction, kinetic runs have been performed in thermal dynamic conditions. Some kinetic runs have been made in pulse-fed-batch conditions by adding the oxidant reagents in different subsequent steps, other have been performed in fed-batch conditions by adding a continuous flow rate of the oxidant reagent. Knowing the amount of heat generated by the reaction, the heat exchanged with the re-circulating fluid and the heat dispersed, it is possible to relate the thermal

profile directly to the double bond conversion. An effort has also been made to estimate the partition coefficients of reagents and products in the two reacting phases using the SPARC method [8].

The main scopes of this work are: (i) to verify the kinetic laws of all the involved reactions and to evaluate the related parameters on the basis of our experimental runs, (ii) to evaluate the role of heat and mass transfer in the reaction and (iii) to develop a model useful for modeling a continuous reactor operating in safe conditions.

## 3.2 Experimental section

### 3.2.1 Description of kinetic runs

Epoxidation of soybean oil was carried out with peroxyformic acid generated in situ by reacting  $\text{H}_2\text{O}_2$  (60 wt.%) and formic acid (95 wt.%) in the presence of sulphuric (98 wt.%) or phosphoric acid (86 wt.%) as catalysts. The main adopted reaction conditions are resumed in Table 4.1.

**Table 4.1:** List of the performed runs and relative reaction conditions.

Run	Oil (g)	$\text{H}_2\text{O}_2$ (g) (60 wt.%)	Formic Acid (g) (95 wt.%)	Catalyst	Mass of catalyst (g)	Operating Modality
1	100	36.7	5.38	$\text{H}_2\text{SO}_4$	0.64	Pulse-Fed-Batch
2	100	36.7	5.38	$\text{H}_2\text{SO}_4$	0.64	Fed-Batch
3	100	42.0	10.76	$\text{H}_2\text{SO}_4$	0.84	Fed-Batch
4	100	33.4	2.69	$\text{H}_2\text{SO}_4$	0.57	Fed-Batch
5	100	36.7	5.38	$\text{H}_2\text{SO}_4$	0.64	Pulse-Fed-Batch
6	100	36.7	5.38	$\text{H}_2\text{SO}_4$	0.32	Pulse-Fed-Batch
7	100	36.7	5.38	$\text{H}_2\text{SO}_4$	0.64	Pulse-Fed-Batch
8	100	36.7	5.38	$\text{H}_2\text{SO}_4$	1.28	Pulse-Fed-Batch
9	100	36.7	5.38	$\text{H}_3\text{PO}_4$	0.98	Pseudo-Fed-Batch
10	80	29.5	4.41	$\text{H}_3\text{PO}_4$	0.78	Pulse-Fed-Batch

Two typical procedures were followed, differing in the modality of the oxidizing aqueous phase addition, i.e., a semi-continuous fed-batch in the first case and a pulse-fed-batch in the second. Fed-batch runs (runs 2-4 of Table 4.1) are characterized by a continuous flow rate of  $0.3 \text{ cm}^3/\text{minute}$  of an oxidizing mixture of hydrogen peroxide and formic acid, the composition of which is reported in Table 4.1. The oil was kept at about  $65^\circ\text{C}$ , while, the oxidizing mixture was fed at room temperature. As the reaction is strongly exothermic, the temperature in the reactor increased, reaching a value oscillating between  $68$  and  $72^\circ\text{C}$ . However, the temperature profile, over time, was continuously monitored and registered. The temperature of the thermostating fluid was changed to obtain an approximately constant reaction temperature. Small samples were taken at different times for the analysis of the iodine number (for determining double bonds

conversion) and epoxide number (for evaluating selectivity and yield), as reported in Appendix. Thermal profiles obtained for the runs 2-4 are reported in Figure 4.1. These runs were performed with the scope of estimating the role of formic acid concentration and evaluating the kinetic constants for a given temperature.

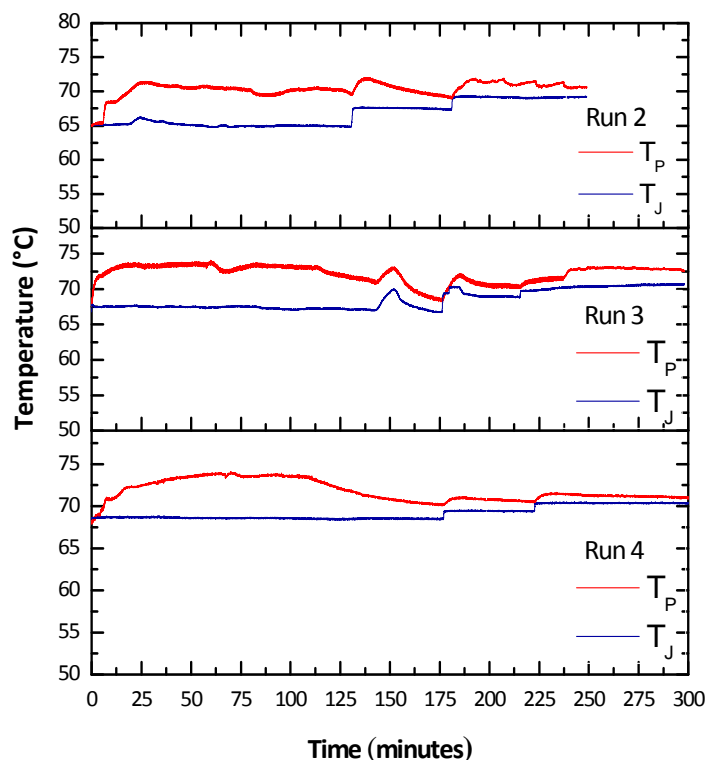


**Figure 4.1:** Thermal profiles of runs 2, 3 and 4 of Table 4.1.  $T_p$  and  $T_j$  refer, respectively, to the reaction environment and jacket temperature.

For the pulse fed batch procedure: 100 g of soybean oil (0.504 moles of double bonds unsaturation) were loaded in the glass reactor and heated under constant magnetic stirring (750 r.p.m.), at 55°C. At this temperature, the catalyst was added and the heating was continued. At about 60°C, a mixture of hydrogen peroxide and formic acid, the composition of which is reported in Table 4.1, was added in a limited amount. The increase of the temperature of the reacting mixture was continuously recorded by a data acquisition system. The water re-circulating in the reactor jacket cools the reaction mixture until the initial starting temperature or other higher predetermined temperature is reached. At this point, another limited amount of hydrogen peroxide/formic acid mixture was added to the oil/catalyst mixture and again the temperature progressively increased for the epoxidation reaction and decreased due to the cooling effect of the re-circulating thermostatted water. The described sequence

was repeated several times (in general 7-10 additions) and Figure 4.2 reports the thermal effect registered related to run 1 of Table 4.1.

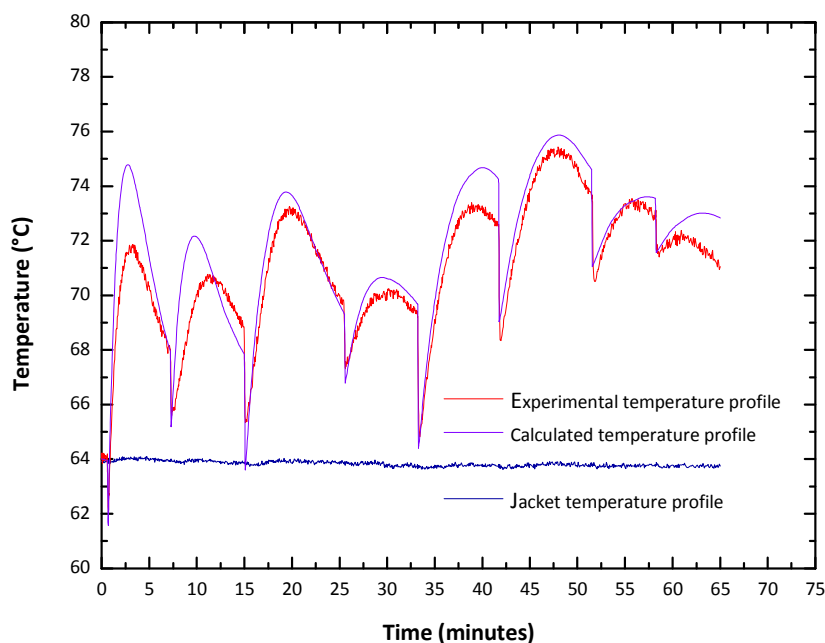
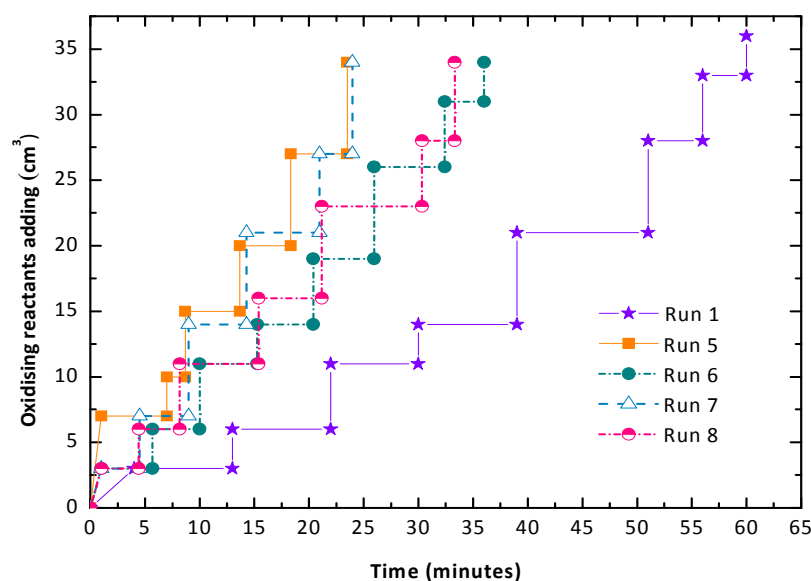


Figure 4.2 : Thermal behaviour of the run 1 of Table 4.1.

The sequence and modality of the reactant additions was consistently changed for each pulse fed batch run, listed in Table 4.1, with the scope of evaluating the effect of increasing or decreasing the amount of reactants added in each step. The added amounts were also changed within a single run starting, normally, with smaller amounts for the first steps and increasing the amounts in the subsequent steps. The pulse-fed-batch reactants adding modalities for run 1, 5-8 of Table 4.1, are reported in Figure 4.3 (catalyst sulphuric acid). In run 1, samples to be analyzed were taken, after each pulse addition, to evaluate activities and selectivities achieved during the oxidizing additions. In this case, after each addition we waited the time necessary for lowering the temperature to a predetermined value before a further pulse addition. With this modality, the entire operation had duration of about one hour. This run was performed with the scope of determining the overall heat transfer coefficient  $U$  and validating the kinetic model and related parameters.

In the other pulse-fed-batch runs (5-8) we have to distinguish two different reaction periods, i.e., the addition period that had a duration of 24-36 minutes (see Figure 4.3) and a digestion period in which the reaction continued for about 2-3 hours without any further addition of the oxidizing reagents. Also in these cases thermal profiles were carefully monitored and registered. Examples of such profiles related to run 5 and 6 are reported in Figure 4.4.



**Figure 4.3:** Reactants mixture successive additions ( $\text{H}_2\text{O}_2$  and formic acid in the ratio reported in Table 4.1) for epoxidation reaction runs with  $\text{H}_2\text{SO}_4$  as catalyst.

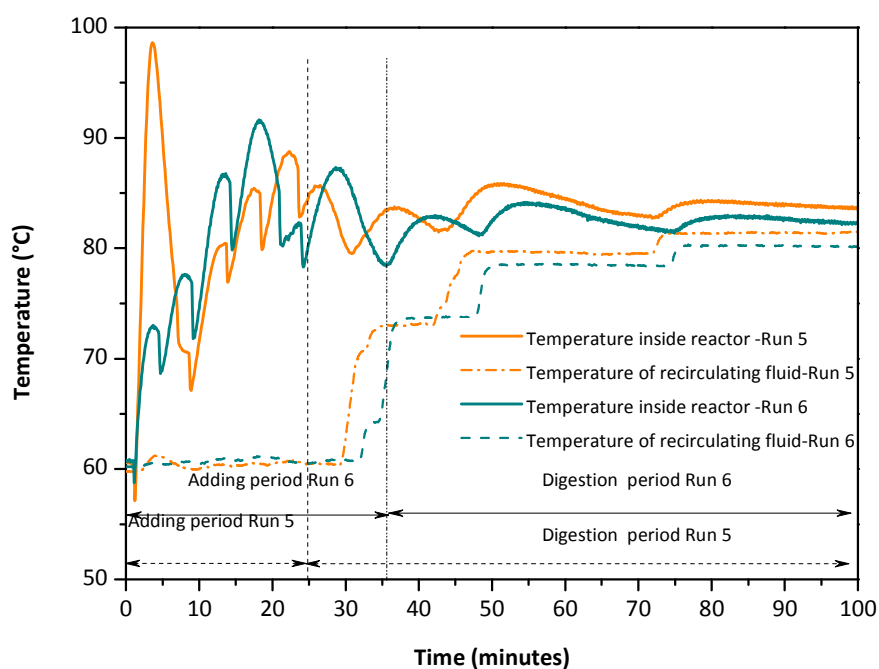


**Figure 4.4:** Thermal profiles obtained in the epoxidation of soybean oil by following different adding times and modalities (see Table 4.1, run 5, run 6 and Figure 4.3).

As can be seen from this figure, the addition of 7 mL of reactants (first adding of run 5) caused a more significant increase in the temperature than when using 3 mL (first

adding in run 6). The thermal profiles reported in Figure 4.4 suggest that in the first part (adding period) the epoxidation reaction rate is much faster, as the observed increase in the temperature would appear to show. This behaviour can be related to the dilution of both the catalyst and the  $\text{H}_2\text{O}_2$ , occurring during the reaction, also as a consequence of the large amount of water formed in the epoxidation reaction, in the ring opening reactions and in the  $\text{H}_2\text{O}_2$  decomposition. The temperature peaks observed after the adding time were due to our intervention in heating the reaction mixture to investigate the behaviour of the reaction during the digestion period at higher temperatures in order to better estimate the ring opening reaction rates. In these runs (runs 5-8 of Table 4.1) the first sample for the analyses was taken at the end of the addition period. Other samples were then taken at different times during the digestion period with the aim of better evaluating the contribution of the epoxide ring opening reactions in lowering the selectivity to the desired product. These runs were also performed with the scope of determining the activation energies considering the significant temperature increases obtained during these type of runs.

Other examples of pulse fed-batch runs, related to phosphoric acid (runs 9,10) are reported in Figure 4.5.

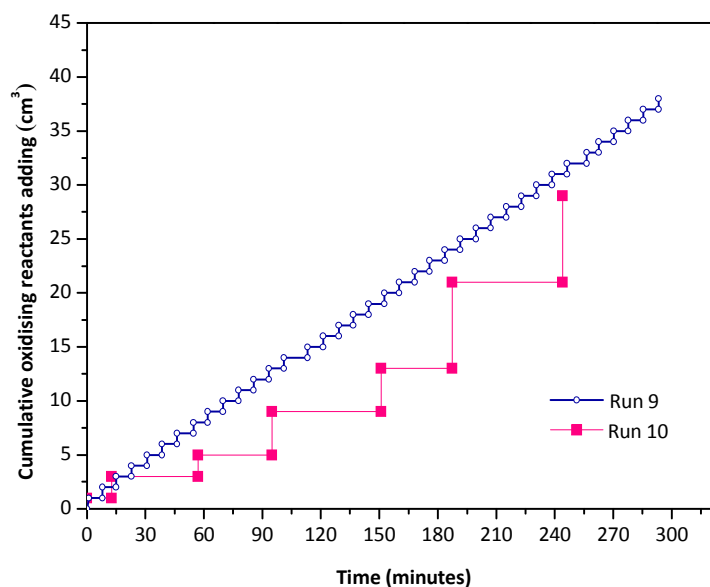


**Figure 4.5:** Reactants mixture successive additions ( $\text{H}_2\text{O}_2$  and formic acid in the ratio reported in Table 4.1 for epoxidation reaction runs with  $\text{H}_3\text{PO}_4$  as catalyst (runs 9 and 10 of Table 4.1).

As can be seen in Figure 4.5, run 9 was performed by adding very small amounts of the reactants thus approaching a fed batch behaviour. The corresponding thermal behaviour for such run is reported in Figure 4.6A, while, the thermal profile for run 10 is reported in Figure 4.6B.

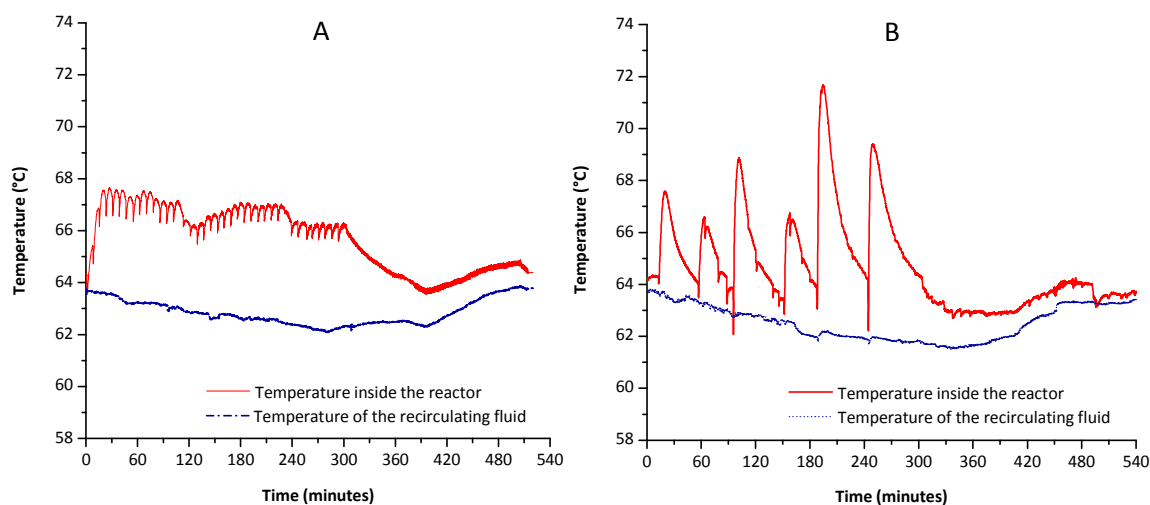


**Figure 4.6:** Thermal behaviour of runs 9 of Table 4.1 (reported in A) characterised by a pseudo-continuous addition of the oxidizing reactants ( $\text{H}_2\text{O}_2$  and formic acid in the ratio reported in Table 4.1) and of the pulse-fed-batch run 10 of Table 4.1 (reported in B).

As already mentioned for the runs 5-8 and 10, when the reactants addition steps were completed, the reaction was continued for several hours at a constant temperature.

In order to study the heat exchange of the used reactor, several runs were carried out by heating or cooling, using the re-circulating thermostatted water, a known amount of soybean oil put in the reactor. The observed changes in temperature of the oil and of the heating/cooling water, at respectively the inlet and the outlet of the reactor jacket, were recorded and registered using the data acquisition system. These temperatures data allow an estimation of both the heat exchange rate and the overall heat exchange coefficient in the used device.



### 4.3 Discussion and Results

#### 4.3.1 Epoxidation kinetic runs

The experimental runs with, respectively,  $\text{H}_2\text{SO}_4$  and  $\text{H}_3\text{PO}_4$  as catalysts, showed that the two catalysts have different activities: sulphuric acid being much more active than phosphoric acid. This fact is evident in Figure 4.7, where the thermal profiles, obtained by adding an equal amount of the oxidant mixture, in the presence of respectively  $\text{H}_2\text{SO}_4$  and  $\text{H}_3\text{PO}_4$ , are reported. As can be seen, using  $\text{H}_2\text{SO}_4$  an increase of the temperature of more than  $60^\circ\text{C}$  was observed, while, with  $\text{H}_3\text{PO}_4$  the increase was only  $13^\circ\text{C}$ . The epoxidation performed in the presence of  $\text{H}_2\text{SO}_4$  is faster than that in the presence of  $\text{H}_3\text{PO}_4$ .

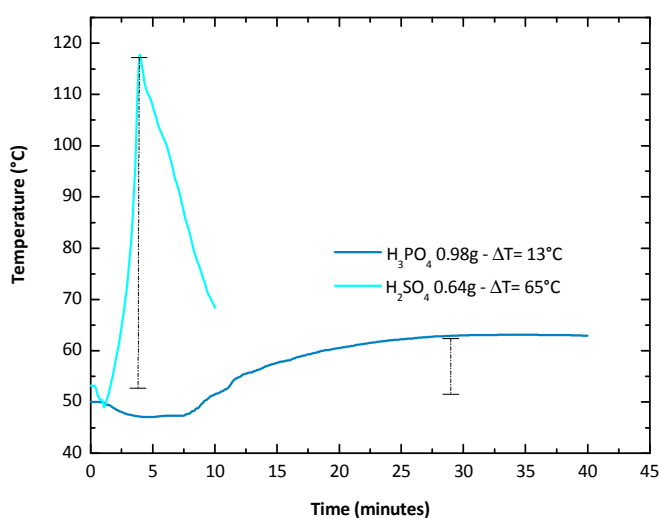


**Figure 4.7:** Thermal profiles related to the first addition of 17 mL of the oxidizing reactants (solution of  $\text{H}_2\text{O}_2$  and formic acid) by using respectively  $\text{H}_2\text{SO}_4$  (run 5 of Table 4.1) and  $\text{H}_3\text{PO}_4$  (run 9), as catalysts.

As a consequence, the stepwise reactants addition periods of pulse-fed-batch modality can consistently be shortened, maintaining a satisfactory level of the Oxirane Number. For this reason, we have focused our work mainly on the description of the runs performed with  $\text{H}_2\text{SO}_4$ . The epoxidation reaction rate, seems to depend linearly on the sulphuric acid concentration, as can be seen by observing the initial temperature profiles reported in Figure 4.8, obtained in the presence of different amounts of catalyst, but maintaining constant the ratio between the reagents and the volume of added oxidant. As reported in Table 4.1, 10 different kinetic runs were performed. In Table 4.2, data collected for the isothermal runs (2-4) are reported.

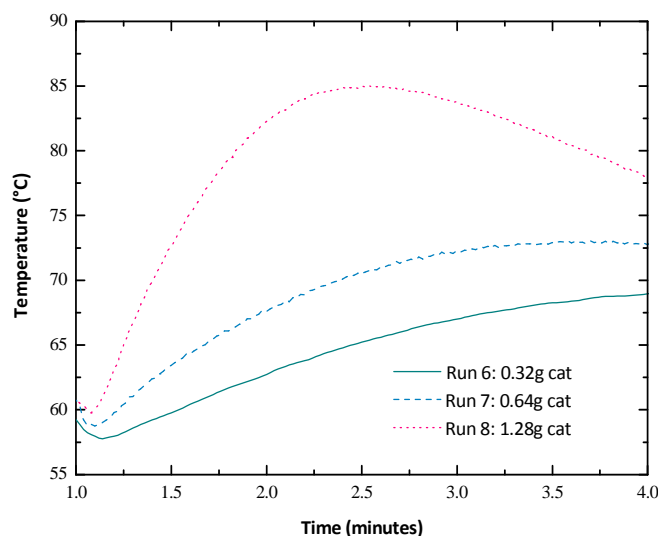


**Figure 4.8:** Experimental thermal profile of the first reactants addition in epoxidation of soybean oil at different catalyst concentration (see Table 4.1, run 6, 7 and 8).

These runs have been performed in the presence of different amounts of formic acid maintaining approximately constant the concentrations of the other components (hydrogen peroxide and catalyst) to evaluate the influence of this factor on the reaction rate. In Figure 4.9 it is possible to observe that despite a great change in formic acid concentration the reaction rate (decrease of Iodine Number) is poorly affected.

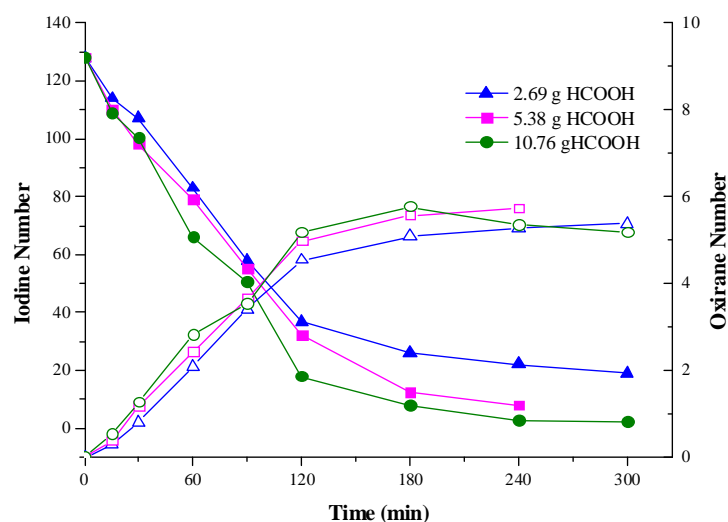


**Figure 4.9:** Effect of formic acid concentration (runs 2, 3, 4) on the rate of Iodine Number decrease.

**Table 4.2:** Kinetic data related to the runs performed in isothermal conditions (runs 2-4 of Table 4.1). The mean volume of each withdrawn sample was about 4 cm<sup>3</sup>.

Run	Time (min)	Epoxide Number		Iodine Number		Conversion (%)	Yield (%)	Selectivity (%)	
		<i>Exp</i>	<i>Calc</i>	<i>Exp</i>	<i>Calc</i>			<i>Exp</i>	<i>Calc</i>
2	15	0.37	0.42	110.0	111.0	14.1	4.6	32.6	34.0
	30	1.17	1.37	98.0	98.2	23.4	14.5	62.0	63.0
	60	2.42	3.00	79.0	68.1	38.3	30.0	78.3	81.0
	90	3.66	3.69	55.0	43.6	57.0	45.4	79.6	82.7
	120	4.97	5.30	32.0	26.1	75.0	61.6	82.1	82.6
	180	5.57	5.78	12.0	11.7	90.6	69.1	76.3	78.9
	240	5.72	5.65	7.8	7.0	94.0	70.9	75.4	74.0
3	15	0.52	0.53	108.6	110.0	15.1	6.4	42.4	50.0
	30	1.26	1.42	100.2	96.8	21.7	15.6	71.4	72.3
	60	2.81	3.10	66.1	66.0	48.3	34.8	72.0	79.3
	90	3.54	4.46	50.6	40.0	60.4	43.9	72.0	80.4
	120	5.17	5.38	17.8	21.0	86.1	64.1	74.4	80.0
	180	5.77	5.85	7.8	5.0	93.9	71.6	76.2	75.4
	240	5.35	5.48	2.5	1.6	98.0	66.3	67.6	68.8
	300	2.00	4.8	2.0	0.6	98.4	64.2	65.0	62.2
4	15	0.29	0.34	114.0	115.0	10.9	3.6	32.9	44.0
	30	0.80	1.07	107.0	103.0	16.4	9.9	60.5	69.8
	60	2.09	2.54	83.0	79.5	35.2	25.9	73.7	75.8
	90	3.41	3.73	58.0	56.4	54.7	42.3	77.3	80.6
	120	4.54	4.47	37.0	40.3	71.1	56.3	79.2	81.0
	180	5.08	4.95	26.0	29.7	79.7	63.0	79.1	79.9
	240	5.28	4.95	22.0	23.4	82.8	65.5	79.1	75.6
	300	5.38	4.80	19.0	20.1	85.2	66.7	78.4	71.0

It is interesting to observe that at low conversions the selectivities and yields are unexpectedly low, as it can be appreciated in Figure 4.10 that is related to run 2 of Table 4.1.

This means that the ring opening reaction contribution, in the initial part of the reaction, is very high and this aspect must be taken into account in the kinetic model. This behavior can be explained considering, according to the literature [9], the epoxidation reaction occurs with rates that could be different for respectively trienes, dienes or monoenes. In particular, it seems that one bond of trienes (5% of double bonds) is much

more active than all the other bonds It seems that also the ring opening reaction follows the same trend.

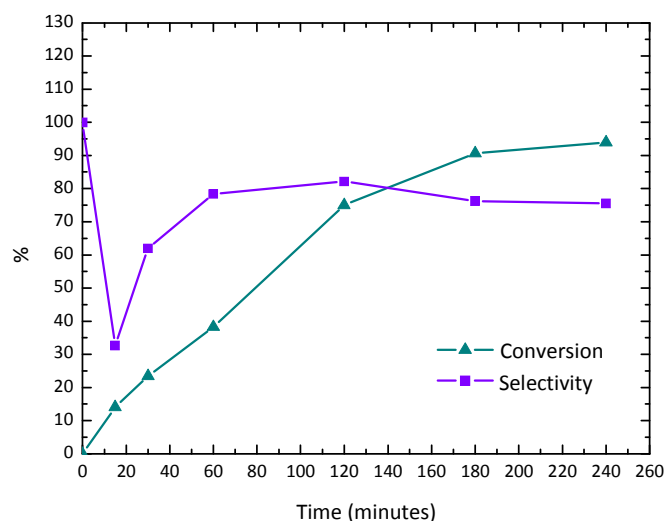


**Figure 4.10:** An example of the kinetic behavior of one of the quasi-isothermal runs (run 2).

This result is further confirmed by observing the data reported in Table 4.3, related to run 1 of Table 4.1.

**Table 3.3:** Kinetic data related to run 1 of Table 3.1. The mean volume of each withdrawn sample was about 2.3 cm<sup>3</sup>.

Time (min)	Epoxide Number		Iodine Number		Conversion (%)	Yield (%)	Selectivity (%)	
	Exp	Calc	Exp	Calc			Exp	Calc
4.0	0.37	0.24	109.5	120.0	14.5	4.6	31.7	47.9
13.0	0.78	0.77	103.8	108.0	18.9	9.7	51.3	61.4
22.0	1.45	1.60	91.2	93.1	28.7	18.0	62.6	72.7
30.0	1.92	2.08	82.4	83.6	35.6	23.8	66.8	74.2
39.0	2.63	2.80	68.6	70.0	46.4	32.6	70.2	76.7
51.0	3.70	3.92	51.2	49.3	60.0	45.9	76.5	79.1
56.0	4.23	4.24	40.3	43.1	68.5	52.5	76.6	79.2
61.0	4.46	4.51	37.5	37.7	70.7	55.3	78.2	79.1

#### 4.4 Theoretical approach for the development of the kinetic model

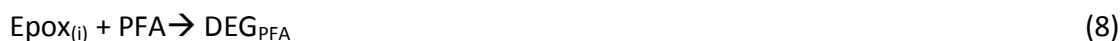
##### 4.4.1 Description of the reaction scheme and of the kinetic rate laws

As mentioned in a previous section, the epoxidation reaction occurs in two successive steps: one, promoted by an acid catalyst, occurring in the aqueous solution between formic acid and hydrogen peroxide to give performic acid, and the other occurring in the organic phase between performic acid and the double bonds contained in the soybean oil molecules. Obviously, the second reaction can occur only if performic acid partially migrates from the aqueous to the organic phase. This implies, for a correct interpretation of the experimental data, the knowledge of performic and formic acids partition coefficients and of the related mass transfer coefficients. Then, it is necessary to take into account that other parasitic reactions can occur, opening the epoxide ring. On the basis of the suggestions coming from the literature [1-6] a complete scheme of all the possible occurring reactions can be written as it follows:

##### *Aqueous phase:*

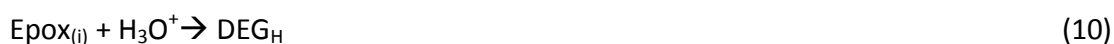


##### *Organic phase:*



Then, it must be pointed out that reaction (5), corresponding to the reaction between the double bonds and performic acid, to give the epoxidized desired product, according to La Scala and Wool [9], occurs with rates that are different for, respectively, trienes, dienes or monoenes. In particular, La Scala and Wool [9] demonstrated that trienes are much more reactive than dienes and monoenes, and perhaps also that the ring opening reaction rate would be susceptible to the characteristics of the molecular structure. This will be ascertained through our experimental runs and we have taken into account these aspects in our kinetic model. According to the reported scheme (3-9) there are four reactions concurring in lowering the yield by opening the oxirane rings. For this purpose, it is opportune to point out that the only works describing the kinetics of these

reactions [5, 6, 10], show that the pH of the aqueous solution is determinant in promoting all these reactions. Moreover, according to the same authors the ring opening reactions mainly occur at the water-oil interphase [5, 6, 10]. In this case, the reaction scheme can be simplified by considering only one ring opening reaction promoted by the protonic attack of the epoxide rings at the interphase followed by the formation of a carbocation that can promptly react with hydrogen peroxide, water, formic and performic acids. If the ring opening to carbocation step is rate determining, the kinetic law in this case can simply be described by the product of the aqueous protonic concentration multiplied by the oxirane group concentration at the interphase that we have assumed proportional to that of bulk concentration. On the other hand:



In this work we have considered both the hypothesis of four independent ring opening reactions, each with its own kinetic law, and a single acid promoted ring opening reaction obtaining comparable results in the runs simulations.

On the basis of both our observations and the information taken from the literature, the following kinetic expressions have been adopted, all expressed in  $[\text{mol L}^{-1} \text{min}^{-1}]$ :

**Aqueous phase:**

$$r_b^{aq} = k_b \cdot [\text{H}_3\text{O}^+] \cdot \left\{ [\text{H}_2\text{O}_2]_{aq} \cdot [\text{FA}]_{aq} - \frac{1}{K_{eq}} \cdot [\text{PFA}]_{aq} \cdot [\text{H}_2\text{O}]_{aq} \right\} \quad (11)$$

$$r_a^{aq} = k_a \cdot [\text{H}_2\text{O}_2]_{aq}^{2.5} \quad (12)$$

**Organic phase:**

$$r_c^{org}(i) = k_c(i) \cdot [\text{DB}(i)]_{org} \cdot [\text{PFA}]_{org} \quad (13)$$

**Liquid-liquid interphase**

$$r_d^{org}(i) = k_d(i) \cdot [\text{Epox}(i)]_{org} \cdot [\text{H}_3\text{O}^+]_{aq} \quad (14)$$

The index (i) is related to the possibility of a different reactivity of the double bonds respectively present in trienes, dienes and monoenes fatty acid chains.

The kinetic expression related to the hydrogen peroxide decomposition considers a 2.5 order as our previous researches have demonstrated [7].

The kinetic law used to describe the peroxyacid formation (equation 11) is taken from the literature. As a matter of fact, De Filippis and Scarsella [11] have deeply studied the kinetics of this reaction in the presence of a soft acid environment (formic acid) obtaining, in those conditions, an activation energy of 10.40 Kcal/mol and an

equilibrium constant, at 25°C, of 0.8. The kinetic parameters found by De Filippis and Scarsella have been adopted by us as first attempt parameters for submitting our experimental data to mathematical regression analysis.

#### 4.4.2 Theoretical approach for the estimation of partition coefficients, mass transfer rates and overall heat exchange

As mentioned before, epoxidation reaction requires that performic acid, formed in the aqueous phase, migrates in the organic phase (see reaction 5). In the meantime, reaction (5) gives formic acid that returns back to the aqueous phase. Partition equilibria for these two compounds allow the development of both the reactions (3) and (5), provided that the interface surface area is large enough to warrant a mass transfer faster than the reaction demand. A picture of what occurs in the two phases and across the interface water-oil is shown in Figure 4.11.

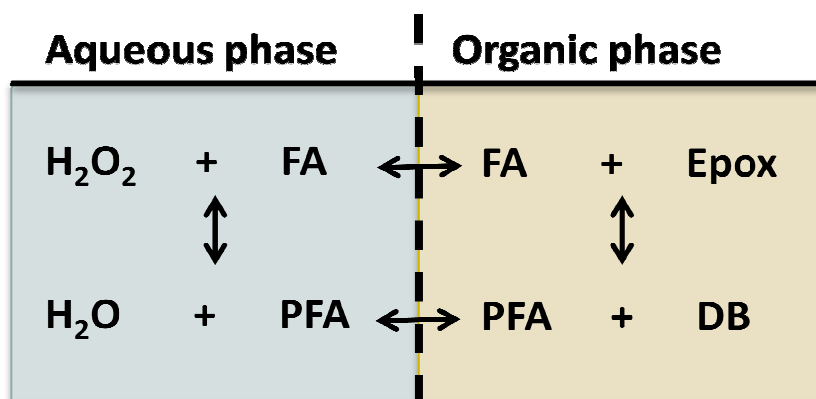


**Figure 4.11:** Simplified scheme of both the partition equilibria and the reactions involved in the two phases aqueous and organic.

For a rigorous kinetic approach, it is necessary to consider together the partition and mass transfer phenomena related to both formic and performic acids. Moreover, water and hydrogen peroxide are also partitioned even though their solubilities are very low. Concerning mass transfer rates, we adopted the Whitman's two films theory [12] in which the gradients are confined into the boundary layers of the two liquids sides. In this case, we can write for a generic  $j$  specie the following mass balance equations:

$$J_{FA}^{aq} = \beta_{FA}^{aq} \cdot ([FA]_{aq} - H_{FA} \cdot [FA]_{org}^*) \quad (15)$$

$$J_{FA}^{org} = \beta_{FA}^{org} \cdot ([FA]_{org}^* - [FA]_{org}) \quad (16)$$

$$J_{PFA}^{aq} = \beta_{PFA}^{aq} \cdot ([PFA]_{aq} - H_{PFA} \cdot [PFA]_{org}^*) \quad (17)$$

$$J_{PA}^{org} = \beta_{PFA}^{org} \cdot ([PFA]_{org}^* - [PFA]_{org}) \quad (18)$$

$$J_{H_2O_2}^{aq} = \beta_{H_2O_2}^{aq} \cdot ([H_2O_2]_{aq} - H_{H_2O_2} \cdot [H_2O_2]_{org}^*) \quad (19)$$

$$J_{H_2O_2}^{org} = \beta_{H_2O_2}^{org} \cdot ([H_2O_2]_{org}^* - [H_2O_2]_{org}) \quad (20)$$

Where  $H_j$  are the partition coefficients defined as  $[C]_j^{aq*}/[C]_j^{org*}$ . In order to calculate the partition coefficients, useful for describing the studied system, some authors have applied, on the basis of experimental measurements on soybean oil/acetic acid/water or epoxidized soybean oil/acetic acid/water systems, the UNIQUAC approach, matching the experimental data [20-21]. Unfortunately, there is not enough experimental data available related to the binary parameters for percarboxylic acids, in particular performic acid. For this reason, both UNIQUAC or UNIFAC cannot be confidently applied to describe the partition of all the chemical species constituting the reactive system. Concerning the partition of formic-performic acid, this aspect has been tackled only by Campanella et al. [1] using UNIFAC, but the groups' contributions for performic are not reported in the current literature and Campanella et al. don't explain how they estimated these values. For this reason, in the present work, the partition coefficients have been calculated using the SPARC on-line calculator [8]; the following equations represent the obtained values and related dependence on the temperature.

$$1/H_{FA} = 9.0E - 07 \cdot T_p^2 - 5.0E - 05 \cdot T_p + 0.0046, \quad R^2 = 0.9782 \quad (21)$$

$$1/H_{PFA} = 4.0E - 06 \cdot T_p^2 - 4.0E - 05 \cdot T_p + 0.0402, \quad R^2 = 0.9899 \quad (22)$$

$$1/H_{H_2O_2} = 9.0E - 08 \cdot T_p^2 - 6.0E - 06 \cdot T_p + 0.0005, \quad R^2 = 0.9592 \quad (23)$$

In Figure 4.12, a plot of the oil/water partition coefficients for, respectively, formic, performic acids and hydrogen peroxide are reported as a function of the temperature. As water is always present in great excess, its concentration in oil can be considered constant and equal to an average value of 0.28 g of water for 100 g of oil, at 70 °C. From the data reported in Figure 4.12 we can observe that solubility are in the order  $PFA > FA > H_2O_2$ .



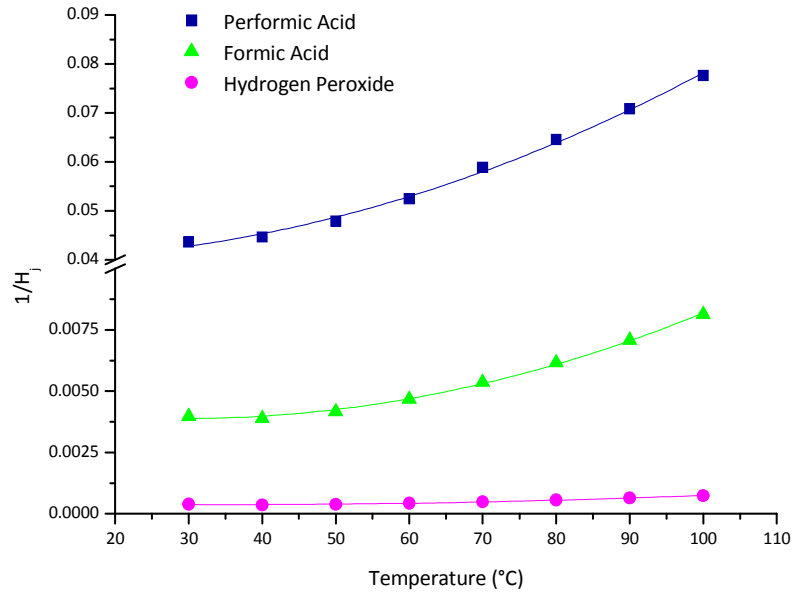


**Figure 4.12 :** Oil/water partition coefficients for formic, performic acids and hydrogen peroxide, as a function of the temperature. The coefficients have been obtained by using the SPARC on-line calculator.

Concerning  $\beta_J^i$ , this parameter represents the product between the mass transfer coefficient and the interfacial surface area for the component J in the phase i. In particular, we have adopted, as a first approximation, that this parameter is constant for the aqueous phase ( $\beta_J^{aq}$ ). In fact, as the liquid volume ( $V^{aq}$ ) increases during the experimental runs, the generated absolute interface area (S) increases too, so the ratio between these two parameters, that represents the specific interfacial area for the liquid phase ( $a^{aq}$ ), can be considered roughly constant ( $a^{aq}=S/V^{aq}$ ). On the contrary, considering the organic phase, the interfacial area increases with the aqueous volume. Therefore, it is possible to obtain  $\beta_J^{org}$  from the following expression:

$$\beta_J^{org} = k_L \cdot a^{org} = k_L \cdot a^{aq} \cdot \frac{V^{aq}}{V^{org}} = \beta_J^{aq} \cdot \frac{V^{aq}}{V^{org}} \quad (24)$$

We have assumed that  $\beta_J^{aq}$  is the same for all the involved components.

Starting from expressions (21-24), it is possible to calculate the concentrations of all the mentioned compounds at the interface, by stating that in steady-state conditions, the following balance is always valid:

$$J_J^{aq} \cdot V_{aq} = J_J^{org} \cdot V_{org} \quad (25)$$

As a consequence the following expressions for calculating the interphase concentrations, can be derived:

$$[FA]_{org}^* = \frac{V_{aq} \cdot \beta_{FA}^{aq} \cdot [FA]_{aq} + V_{org} \cdot \beta_{FA}^{org} \cdot [FA]_{org}}{V_{org} \cdot \beta_{FA}^{org} + V_{aq} \cdot \beta_{FA}^{aq} \cdot H_{FA}} \quad (26)$$

$$[PFA]_{org}^* = \frac{V_{aq} \cdot \beta_{PFA}^{aq} \cdot [PFA]_{aq} + V_{org} \cdot \beta_{PFA}^{org} \cdot [PFA]_{org}}{V_{org} \cdot \beta_{PFA}^{org} + V_{aq} \cdot \beta_{PFA}^{aq} \cdot H_{PFA}} \quad (27)$$

$$[H_2O_2]_{org}^* = \frac{V_{aq} \cdot \beta_{H_2O_2}^{aq} \cdot [H_2O_2]_{aq} + V_{org} \cdot \beta_{H_2O_2}^{org} \cdot [H_2O_2]_{org}}{V_{org} \cdot \beta_{H_2O_2}^{org} + V_{aq} \cdot \beta_{H_2O_2}^{aq} \cdot H_{H_2O_2}} \quad (28)$$

Temperature profiles obtained by heating or cooling soybean oil in the absence of the reaction, have been interpreted using the following heat balance equation:

$$\frac{dT_P}{dt} = \frac{U \cdot A \cdot (T_j - T_P)}{c_{P_{oil}} \cdot W_{oil}} \quad [^{\circ}C \text{ min}^{-1}] \quad (29)$$

where  $T_P$  is the temperature of the oil inside the reactor and  $T_j$  is the temperature of water flowing in the external jacket. In order to apply this equation it is necessary to find an expression for the specific heat capacity of the oil. For this purpose, it is possible to find in the literature [15] the following relationship:

$$c_{P_{oil}} = 4.777 \cdot 10^{-4} \cdot T_P + 0.4688 \text{ [cal g}^{-1} \text{ }^{\circ}C^{-1}] \quad (30)$$

From all the data collected, in different experimental conditions, we have estimated for the overall heat exchange coefficient ( $U$ ), in the range of 60-75 $^{\circ}C$  (temperature range of the reaction), a value falling in the range of 2550-3000  $\text{cal m}^{-2} \text{ min}^{-1} \text{ }^{\circ}C^{-1}$ .

It must be considered that as a consequence of the epoxidation reaction the oil phase composition changes over a period of time. As a matter of fact, epoxidized soybean oil is much more viscous than the unreacted substrate (respectively 450 Cp for epoxidized soybean oil and 110 Cp for soybean oil at 25 $^{\circ}C$ ) and we can foresee that the overall heat exchange coefficient  $U$  will change with the conversion degree. Therefore, the values estimated with independent runs in the absence of the reaction and of the aqueous solution can only be considered first attempt values. A more precise parameter can be obtained by regression analysis on the kinetic runs by considering the difference between the temperature of the thermostating fluid flowing in the jacket and the reaction temperature inside the reactor. (see Figure 4.2, 4.3, 4.5, 4.8A, B).

However, an approximated linear dependence of U with the conversion has been found:

$$U = U_0 + \alpha \cdot X_{DB} \quad (31)$$

#### 4.4.3 Mass and Energy balances

##### 4.4.3.1 Mass balance

The mass balance has been written as follows:

$$\text{accumulation} = \text{inlet} + \text{reacted} [=] \text{mol} \cdot \text{min}^{-1} \quad (32)$$

The inlet term represents the adding of the reactive mixture of  $\text{H}_2\text{O}_2$  and formic acid; for this purpose, in the case of pulse fed batch runs, it is necessary to introduce a square pulse function to simulate the additions. This function can be written as the sum of each adding volume divided by the time necessary for the adding itself. It is then possible to write the mole balance equation for each component in ( $\text{mol min}^{-1}$ ).

##### **Aqueous phase:**

$$\frac{dn_{\text{H}_2\text{O}_2}^{aq}}{dt} = F_{\text{H}_2\text{O}_2} + (-r_a - r_b - J_{\text{H}_2\text{O}_2}^{aq}) \cdot V_{aq} \quad (33)$$

$$\frac{dn_{\text{H}_2\text{O}}^{aq}}{dt} = F_{\text{H}_2\text{O}} + (r_a + r_b) \cdot V_{aq} \quad (34)$$

$$\frac{dn_{\text{FA}}^{aq}}{dt} = F_{\text{FA}} + (-r_b - J_{\text{FA}}^{aq}) \cdot V_{aq} \quad (35)$$

$$\frac{dn_{\text{PFA}}^{aq}}{dt} = F_{\text{PFA}} + (+r_b - J_{\text{PFA}}^{aq}) \cdot V_{aq} \quad (36)$$

##### **Organic phase:**

$$\frac{dn_{\text{H}_2\text{O}_2}^{org}}{dt} = (+J_{\text{H}_2\text{O}_2}^{org}) \cdot V_{org} \quad (37)$$

$$\frac{dn_{\text{FA}}^{org}}{dt} = (+r_c(i) + J_{\text{FA}}^{org}) \cdot V_{org} \quad (38)$$

$$\frac{dn_{\text{PFA}}^{org}}{dt} = (-r_c(i) + J_{\text{PFA}}^{org}) \cdot V_{org} \quad (39)$$

$$\frac{dn_{\text{DB}}^{org(i)}}{dt} = -r_c(i) \cdot V_{org} \quad (40)$$

$$\frac{dn_{\text{EpoX}}^{org(i)}}{dt} = (+r_c(i) - r_d(i)) \cdot V_{org} \quad (41)$$

$$\frac{dn_{\text{DEGH}}^{org(i)}}{dt} = +r_d(i) \cdot V_{org} \quad (42)$$

In order to integrate these equations the following initial conditions have been considered.

First of all, the total number of the double bonds present in the oil is given by the following expression:

$$n_{\text{DB}}^{\text{TOT},0} = \frac{N_{\text{iodine}}^0 \cdot \text{Moil}}{\text{PM}_{\text{I}_2} \cdot 100} \quad \text{where } N_{\text{iodine}}^0 = 128 \text{ (g I}_2 \text{ in 100g of substrate)} \quad (43)$$

Moreover, as it has been seen, it is important to consider separately the double bonds in fatty acid chains of, respectively, monoenes, dienes and trienes. The initial values of the mentioned double bonds are calculated starting from the molar fraction of each kind of double bond present in the soybean oil  $\Phi_i$ . In this way, the initial value of each double bond is calculated as follows:

$$n_{DB}(i)^0 = \Phi_i \cdot n_{DB}^{TOT,0} \quad (44)$$

The other initial concentrations are zero before adding the oxidizing reagents.

### 3.4.3.2 Energy balance

The second step of the experimental data elaboration regards the simulation of the thermal profiles using an opportune enthalpy balance. As a first approximation, we have considered that the heat released by the reactions is instantaneously distributed on the entire mass of the reaction.

Therefore, the heat balance can be interpreted with the following relation:

$$q_{accumulation} = q_{inlet} + q_{reaction} - q_{exchange} [=] \text{ cal} \cdot \text{mol}^{-1} \quad (45)$$

and the terms of the heat balance can be written as follows:

$$q_{accumulation} = \bar{c}_p \cdot M_{tot} \cdot \frac{dT_P}{dt} \quad (46)$$

$$q_{inlet} = (W_{H_2O_2} \cdot cp_{H_2O_2} + W_A \cdot cp_A + W_{H_2O} \cdot cp_{H_2O}) \cdot (T_{add} - T_P) \quad (47)$$

$$q_{reaction} = [\Delta H_r \cdot (-r_c(i)) + \Delta H_{deg} \cdot (-r_d(i))] \cdot V_{org} + [\Delta H_{ox} \cdot (-r_a)] \cdot V_{aq} \quad (48)$$

$$q_{exchange} = U \cdot A \cdot (T_P - T_J) \quad (49)$$

The overall thermal exchange coefficient (U) and its dependence on double bond conversion, has been evaluated by regression analysis. All the densities, specific heats and enthalpy change values necessary for the calculation are reported in Table 4.4.

**Table 4.4** : Average values of density, specific heat and reaction enthalpy

Density (g cm <sup>-3</sup> )	Specific heats (cal g <sup>-1</sup> °C <sup>-1</sup> )	Enthalpy (cal mol <sup>-1</sup> )
$\rho_{H_2O_2} = 1.44$	$cp_{H_2O_2} = 0.622$	$\Delta H_r = -55000$ [4]
$\rho_{oil} = 0.89$	$cp_{oil} = 0.50$	$\Delta H_{ox} = -23440$ [16]
$\rho_A = 1.16$	$cp_A = 0.531$	$\Delta H_{deg} = -21000$ [17]
$\rho_{H_2O} = 0.985$	$cp_{H_2O} = 1$	

**4.4.4 Determination of the model parameters, runs simulation and discussion**

Each kinetic run, reported in Table 4.1, is characterised by a number of 6-8 samples taken at different times. Three different analyses have been carried out on these samples to determine the Iodine Number (to evaluate the double bonds conversion), the Oxirane Number (to evaluate the epoxidation reaction yields) and the residual hydrogen peroxide after the epoxidation reaction and eventual decomposition. Finally, the evolution of the temperature over a period of time in each run has been monitored by a data acquisition system for each second of reaction time, that is, for the temperature we have thousands experimental points. All of this experimental data has been subjected to mathematical regression analysis and the best fittings have been obtained with the parameters reported in Table 4.5.

**Table 4.5:** Kinetic constants values determined at the reference temperature of 70°C by mathematical regression analysis on the experimental data and numerical value of other parameters of the model.

Parameter	Value	Unit
$k_a$	$1.04\text{E-}03 \pm 1.6\text{E-}0.4$	$\text{L}^{1.5,\text{aq}} \text{mol}^{-1.5} \text{min}^{-1}$
$k_b$	$6.56\text{E-}01 \pm 2.0\text{E-}02$	$\text{L}^{2,\text{org}} \text{mol}^{-2} \text{min}^{-1}$
$K_{\text{eq}}$	$5.17 \pm 0.8$	-
$k_c^{\text{mono,a}}$	$2.72 \pm 0.5$	$\text{L}^{\text{org}} \text{mol}^{-1} \text{min}^{-1}$
$k_c^{\text{mono,b}}$	$2.00 \pm 0.4$	$\text{L}^{\text{org}} \text{mol}^{-1} \text{min}^{-1}$
$k_c^{\text{tri}}$	$133.9 \pm 9.8$	$\text{L}^{\text{org}} \text{mol}^{-1} \text{min}^{-1}$
$k_d^{\text{mono,a}}$	$2.94\text{E-}03 \pm 4.6\text{E-}04$	$\text{L}^{\text{aq}} \text{mol}^{-1} \text{min}^{-1}$
$k_d^{\text{mono,b}}$	$7.97\text{E-}04 \pm 5.7\text{E-}05$	$\text{L}^{\text{aq}} \text{mol}^{-1} \text{min}^{-1}$
$k_d^{\text{tri}}$	$0.40 \pm 0.05$	$\text{L}^{\text{aq}} \text{mol}^{-1} \text{min}^{-1}$
$\beta^{\text{aq}}$	$250 \pm 20$	$\text{min}^{-1}$
$E_{a_b}$	$11.39 \pm 0.6$	$\text{Kcal mol}^{-1}$
$E_{a_c}$	$24.89 \pm 0.2$	$\text{Kcal mol}^{-1}$
$E_{a_d}$	$8.86 \pm 0.4$	$\text{Kcal mol}^{-1}$
$U_0$	$4571 \pm 10$	$\text{cal m}^{-2} \text{min}^{-1} \text{ } ^\circ\text{C}^{-1}$
$\alpha$	$-32.39 \pm 0.2$	$\text{cal m}^{-2} \text{min}^{-1} \text{ } ^\circ\text{C}^{-1}$

a)Parameters valid for the runs performed with  $\text{H}_2\text{SO}_4$ .

b)Parameters valid for the runs performed with  $\text{H}_3\text{PO}_4$ .

The dependence of the kinetic constants with the temperature has been described with the following relationship:

$$k_i = k_i^{\text{ref}} \exp \left[ \frac{E_{ai}}{R} \left( \frac{1}{T^{\text{ref}}} - \frac{1}{T_p} \right) \right] \quad (50)$$

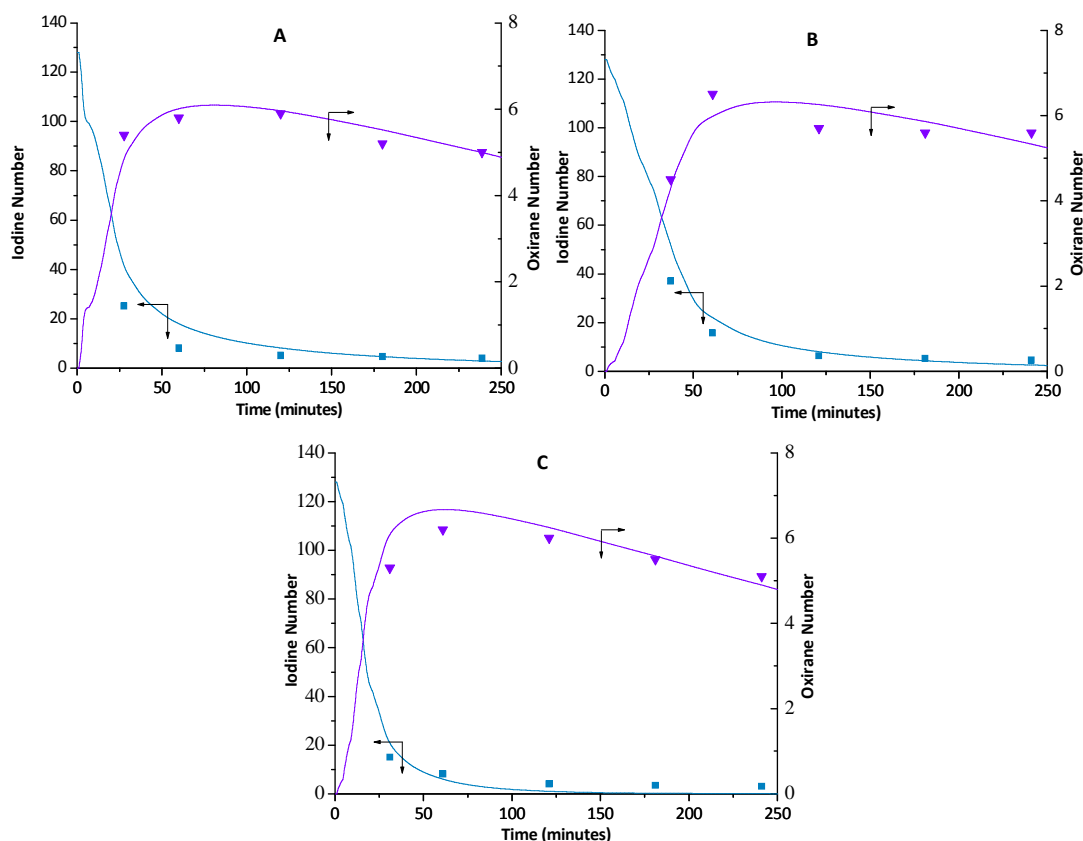
$k_i^{\text{ref}}$  being the kinetic constant chosen at a fixed temperature (here 70°C). The activation energies values, when known, have been taken, as a first approximation, by

the literature [4-6, 13, 15]. According to our preliminary study, the hydrogen peroxide decomposition reaction, in the examined temperature range, is not very sensitive to the temperature. As reported in the previous section 4.4.1, and in agreement with the literature findings [9] trienes are more reactive than dienes and monoenes in the epoxidation reaction. Our experimental results also suggest that the ring opening reaction rate is higher for trienes and the selectivity at low conversions is much lower as a consequence. Hence, in order to simulate the experimental data it would be necessary to introduce different rates and related parameters for trienes, dienes and monoenes. As a matter of fact, we observed that in order to obtain a satisfactory agreement it is enough to distinguish only the greater activities in both the reactions (epoxidation and ring opening) for only one double bond of the trienes (about 5% of the total double bonds in soybean oil). All of the other double bonds have approximately the same reactivity in both the reactions. In conclusion, we have two kinds of double bonds, one extremely reactive in both the reactions (5% of the total), and less reactive ones. For each type of double bond we have two different equations to integrate (epoxidation and ring opening rates) and the related parameters are reported in Table 4.5. We have obtained a reactivity ratio between the most reactive double bonds and the others of approximately 50 compared to the value of 4 that can be estimated from the work of La Scala and Wool [9] but these authors have obtained their results operating at a lower temperature (19°C) in the absence of sulphuric acid catalyst and interpreted their results with a monophasic model. The presence of sulphuric acid probably favours the double bonds shifting, increasing the formation of more reactive conjugated double bonds.

The agreements obtained with the described model for the isothermal runs 2-4 can be appreciated in Table 4.2, where, experimental and calculated Epoxide Numbers, Iodine Numbers and selectivities are reported for comparison. As can be seen in Figure 4.1, these runs have shown an increase in the temperature in the reactor of about 5-6°C as a consequence of the reaction. This aspect has been considered and the values of  $U$  (see relation 31), the overall thermal exchange coefficient, that can be calculated with the parameters reported in Table 4.5, effectively reproduce the observed thermal gradients. The agreement obtained in describing run 1 can be appreciated in Table 4.3 concerning Iodine Numbers, Epoxide Numbers and Selectivities and in Figure 4.2 for the thermal profile. Also in this case the gradient between the temperature of the reaction and that of the thermostating fluid, flowing in the reactor jacket, is well simulated as can be seen in Figure 4.2.

The model developed in this work is able to simulate, with satisfactory agreement, all of the kinetic runs performed. For this purpose, Figures 4.13 (A-C) show the experimental

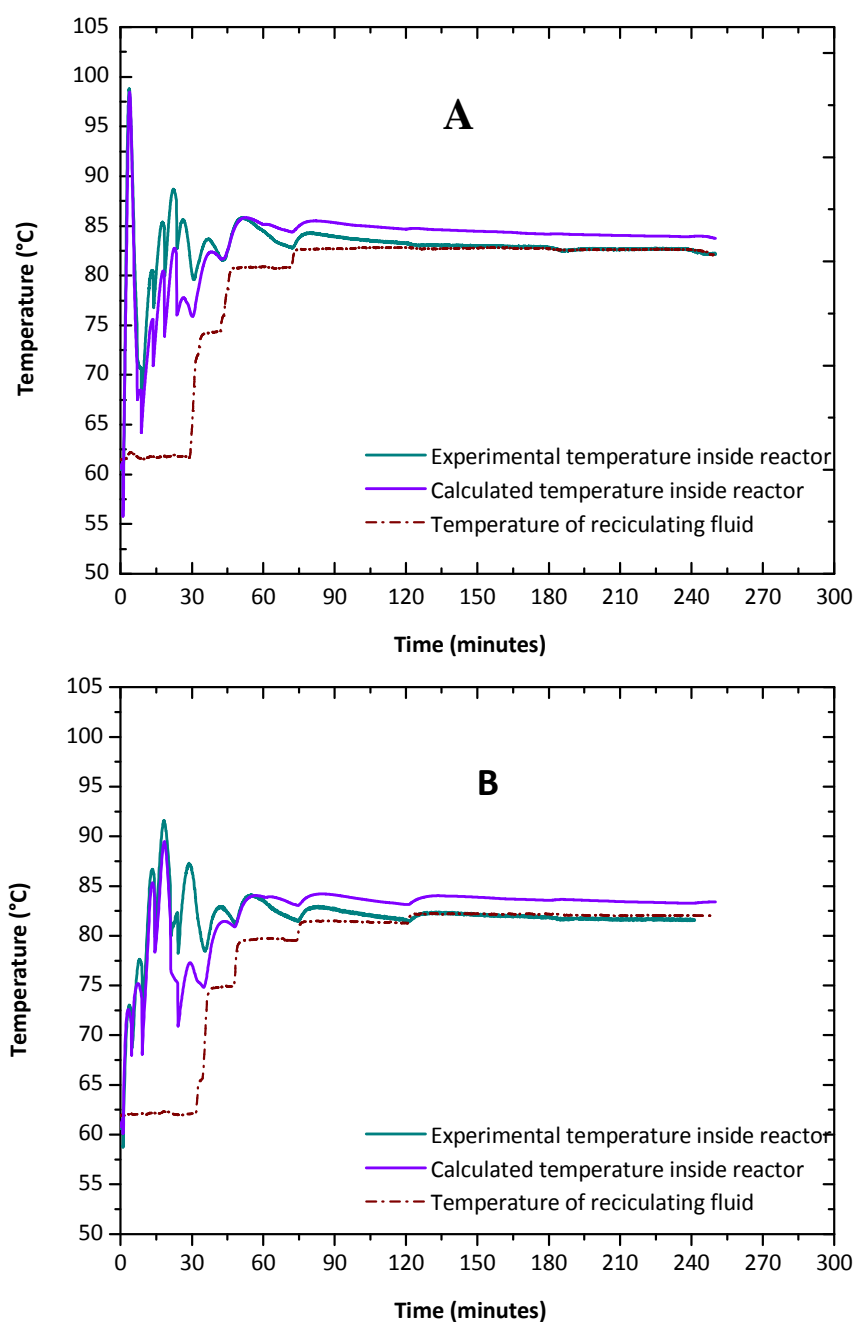
data and related simulations for the runs 5-7 of Table 4.1, performed in the presence of sulphuric acid, as a catalyst.



**Figure 4.13** :Experimental and simulated Iodine and Oxirane Numbers against the epoxidation reaction time reaction. Dots are experimental data, curves correspond to model prediction. Plot in (A)-(C) correspond to runs 5-7 of Table 4.1. The mean volume of each withdrawn sample was about 9.2 cm<sup>3</sup>.

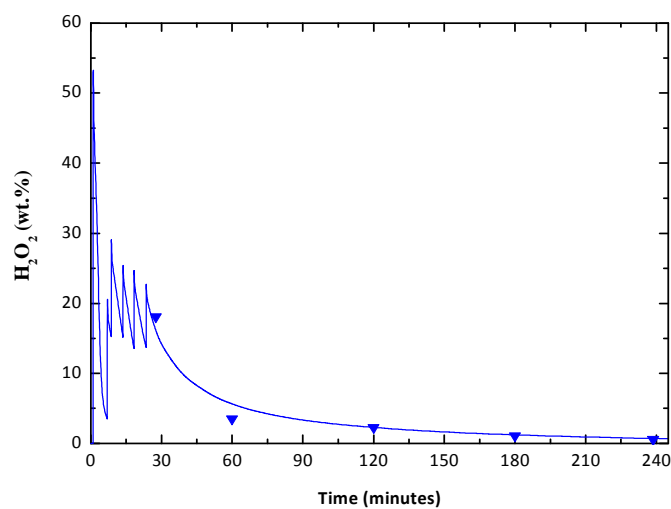
The simulation of the thermal profiles for the runs 5 and 7 are reported, as examples, in Figure 4.14 (A and C). The model is also able to simulate the hydrogen peroxide consumption during the time (for both the reactions of epoxidation and decomposition), see Figure 4.15 as an example, corresponding to run 5 of Table 4.1.

Figure 4.16 (A, B) on the contrary, show the experimental data and related simulations for the runs 9, 10 of Table 4.1, performed in the presence of H<sub>3</sub>PO<sub>4</sub>, as a catalyst, while, Figure 4.17 (A, B), shows thermal profiles related to runs 9 and 10. It is interesting to observe that the kinetic constants of the epoxidation reaction for, respectively, phosphoric and sulphuric acid, are comparable, but the ring opening kinetic constants are different even considering the difference in the acidity for the two different systems.



**Figure 4.14** Experimental and simulated temperature of the reacting system for the run 5 (graph A) and 7 (graph B) of Table 4.1. Continuous curve is related to experimental data, dotted curve correspond to the model prediction.





**Figure 4.15:** Experimental and simulated  $\text{H}_2\text{O}_2$  (wt.%) residual against the reaction time. Dots are experimental data, continuous curve is model prediction for run 5 of Table 4.1.

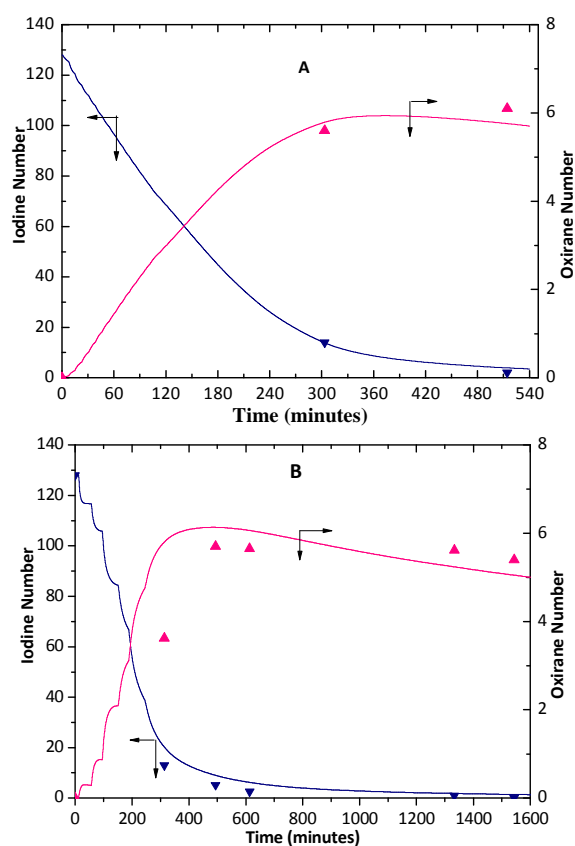


**Figure 4.16:** Experimental and simulated Iodine and Oxirane Numbers against the epoxidation time reaction. Dots are experimental data, curves are model prediction. Plot in (A) and (B) correspond to run 9 and 10 of Table 4.1. The mean volume of each withdrawn sample was about  $8 \text{ cm}^3$ .

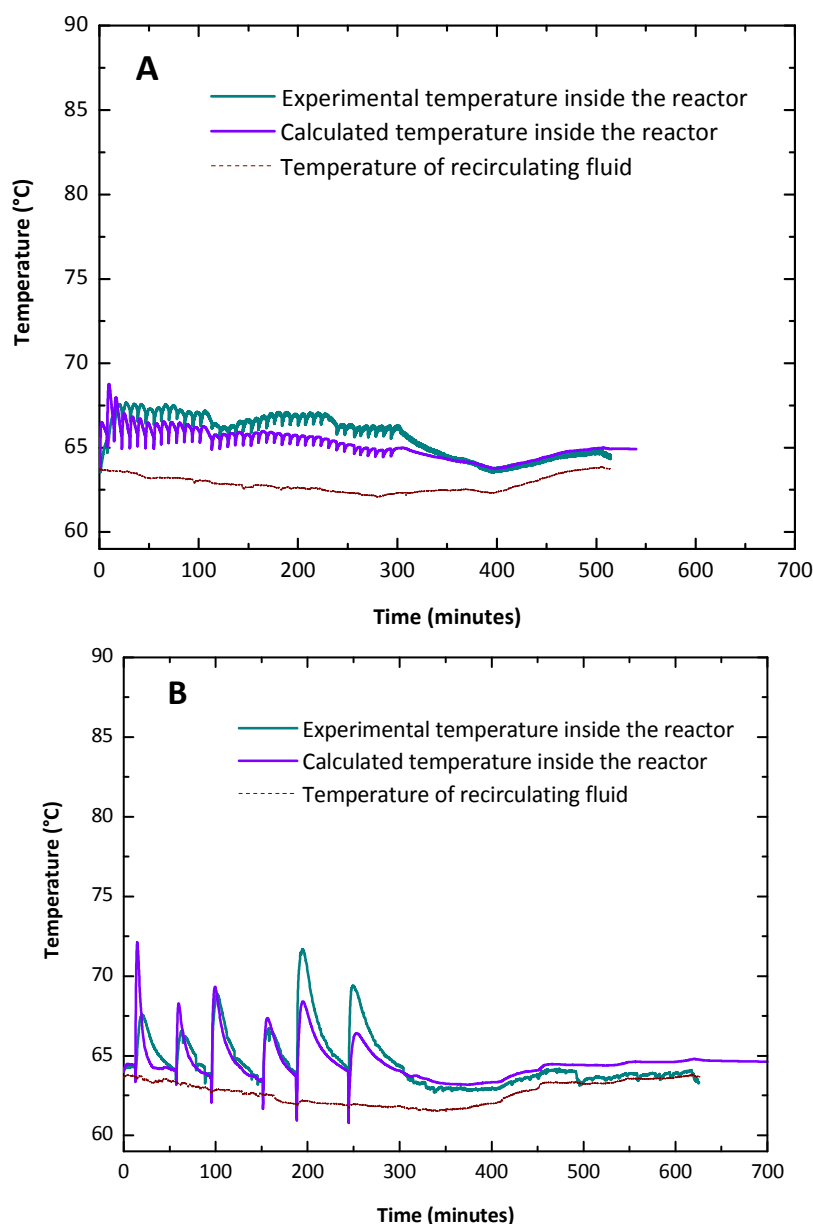


**Figure 4.17:** Experimental and simulated temperature of the reacting system for the run 5 (graph A) and 7 (graph B) of Table 4.1. Continuous curve is related to experimental data, dotted curve correspond to the model prediction.

On the contrary, the activation energies found by regression analysis for both the catalysts and reactions are very similar and an average value is reported in Table 4.5. In the examined runs we have changed the temperature, the adding oxidant solution modality, the type and catalyst concentration and the concentration of formic acid. The hydrogen peroxide concentration and iodine and epoxide number change with time during each run. Therefore, we have all of the possible factors that can affect the reaction under control. It must be pointed out that, normally, mass transfer does not affect

epoxidation rate in the adopted conditions with the exception of those runs in which very high temperatures are reached.

Another observation is related to the identification of the rate determining step (rds). By plotting the ratio between the epoxidation and the performic acid formation rates  $r_c^{org}(i)/r_b^{aq}$  it is possible to observe a value less than 1. The greatest value obtained for monoenes is approximately 0.2. This means that that epoxidation reaction in the oil phase is rds in disagreement with the assumption generally made in the previous literature. On the other hand it is known that the formation of performic acid occurs faster than the formation of other peracids [18]. Another observation, deriving from the previous one is that despite the fact that formic acid intervenes with a first order kinetic law in the performic acid formation rate the influence of its concentration on the overall epoxidation rate is quite low as can be appreciated by comparing the data reported in Table 4.2. As can be seen, the evolution of the conversion for the three runs over a period of time is quite similar.

#### 4.5 Conclusions

The epoxidation of soybean oil with hydrogen peroxide (60 wt.%) has been studied in the presence of, respectively, sulphuric and phosphoric acid, as catalysts. We observed, in agreement with other authors, that the reaction is strongly affected mainly by the temperature and, in the initial steps, also by the catalyst concentration. As it is very difficult to keep the temperature of the reacting mixture constant due to the strong exothermicity of the main reaction, we have studied simultaneously the kinetics of all the involved reactions (main and side reactions) in a thermal dynamic way, by measuring accurately the evolution of the temperature gradient between the thermostating fluid flowing in the reactor jacket and the liquid bulk inside the reactor over a period of time. A biphasic kinetic model considering all the reactions occurring respectively in the aqueous phase (oxidation of formic to performic acid and hydrogen peroxide decomposition), in the oil phase (epoxidation) and at the water/oil interphase (epoxide ring opening reaction) has been developed. The partition equilibria of reactants and products, between the two phases, have been estimated using the SPARC method, because there is no experimental data available for the involved substances. The model also considers the possibility of mass transfer limitation for the diffusion of a reactant, for example performic acid, from the aqueous to the oil phase or formic acid, formed in the oil phase diffusing from oil to water. Kinetic laws have been identified for each reaction with the help of the information found in the literature. All of the kinetic runs have been subjected to regression analysis, thus determining all of the parameters of the model. The model leads to a very satisfactory agreement. Some relevant aspects, never observed before, have been identified. For example, in contrast with the current

literature on the subject, which asserts that performic acid formation is rate determining step in the epoxidation, we have demonstrated that the epoxidation occurring in the oil phase is approximately five times slower than the oxidation of formic to performic acid. Another observation arising from the analysis of our experimental data is that some double bonds (about 5% of the total) are more reactive in both epoxidation and ring opening reaction. As a consequence, the selectivity to epoxide is low (35-40%) at low conversion (10-15%) then increases for higher conversions reaching a maximum value of 75-80% and then decreases again for the intervention of the ring opening reaction. This last reaction has been considered in our model as a single reaction whose rate determining step is the protonic attack to the epoxide ring followed by the formation of a carbocation that can readily react with hydrogen peroxide, formic and performic acids, or water. This assumption strongly reduces the number of parameters of the model without decreasing the fitting agreement. As water is always present in excess, the acid catalysed hydrolysis of the epoxide rings is probably the most favoured reaction. This model has been developed with the aim of simulating the behaviour of the industrial reactors currently working in pulse fed-batch conditions but in perspective for modelling and simulating continuous reactors, this being the basis for the process intensification.

**References**

- [1] A. Campanella, C. Fontanini, M.A. Baltanas, *Chem. Eng. J.*, 144 (2008) 466.
- [2] L.H. Gan, S.H. Goh, K.S. Ooi, *J. Amer. Oil Chem. Soc.* 69 (1992) 347.
- [3] S. Sinadinovic-Fiser, M. Jankovic, Z.S. Petrovic, *J. Amer. Oil Chem. Soc.* 78 (2001) 725.
- [4] B. Rangarajan, A. Havey, E.A. Grulke, P.D. Culnan, *J. Amer. Oil Chem. Soc.* 72 (1995) 1161.
- [5] A. Campanella, M.A. Baltanas, *Latin Amer. App. Res.*, 35 (2005) 205.
- [6] A. Campanella, M.A. Baltanas, *Latin Amer. App. Res.*, 35 (2005) 211.
- [7] E. Santacesaria, M. Di Serio, R. Tesser, V. Russo, R. Turco, *Ind. Eng. Chem. Res.*, 50 (2011) 2569.
- [8] L.A. Carreira, S. Hilal, S.W. Karickhoff, *Theoretical and Computational Chemistry, Quantitative Treatment of Solute/Solvent Interactions*, Eds. P. Politzer and J. S. Murray, Elsevier Publishers, 1994.; <http://sparc.chem.uga.edu/sparc/>
- [9] J. La Scala, R.P. Wool, *J. Amer. Oil Chem. Soc.*, 79 (2002) 373.
- [10] F.A. Zaher, M. H El Mallah, M.M. El Hefnawy, *J. Amer. Oil Chem. Soc.* 66 (5) (1989) 668.
- [11] P. De Filippis, M. Scarsella, N. Verdone, *Ind. Eng. Chem. Res.* 48(3)(2009) 1372.
- [12] W. G. Whitman, *Chem. Metall. Eng.* 29 (1923) 146.
- [13] M Jankovic, S. Sinadinovic-Fiser, M. Lamshoeft; *J. Am. Oil Chem. Soc.* DOI: 10.1007/S11746-009-1531-Z (2009)
- [14] S. Sinadinovic-Fiser, M. Jankovic; *J. Am. Oil Chem. Soc.*, 84 (2007) 669.
- [15] N. A. Morad, A.A. Mustafa Kamal, F. Panau, T.W. Yew, *J. Amer. Oil Chem. Soc.*, 77(9) (2000) 1001.
- [16] C. W. Jones, *Applications of Hydrogen Peroxide and Derivatives*; ( Series Ed.), RSC Clean Technology Monographs, Cambridge (1999) pp. 14
- [17] Information from: <http://www.ethyleneoxide.com>
- [18] S. Leveneur, PhD dissertation under the supervision of D.Y. Murzin, T. Salmi, L. Estel of the Abo Akademi University (INSA) 2009

**Nomenclature**

C=C	Unsaturated group (Double bond)
FA	Formic Acid
PFA	Performic Acid
Epox	Epoxide group
DEG <sub>i</sub>	Decomposed oxirane group by i=H <sub>2</sub> O <sub>2</sub> , FA, PFA, H <sub>2</sub> O, H (proton)
$r_i$	Reaction rate [mol L <sup>-1</sup> min <sup>-1</sup> ]
$k_i$	Kinetic constant (the units depends on the reaction)
$J_j^i$	Mass transfer rate for the component j in the phase i [mol L <sup>-1</sup> min <sup>-1</sup> ]
$\beta_j^i$	Product between the mass transfer coefficient and the interfacial surface area for the component j in the phase i
$a^i$	Specific interfacial area for the phase i [dm <sup>2</sup> /dm <sup>3</sup> ]
$H_j$	Partition coefficients defined as $[C]_{aq}^*/[C]_{org}^*$
S	Absolute interfacial area for the liquid phase [dm <sup>2</sup> ]
U	Global thermal exchange coefficient [cal m <sup>-2</sup> min <sup>-1</sup> °C <sup>-1</sup> ]
A	Exchange area [m <sup>2</sup> ]
$V^i$	Reaction Volume referred to the phase i [L]
$F_i$	Molar flow-rate of the compound i [mol min <sup>-1</sup> ]
$n_i$	moles of i-th compound [mol]
$C_{p,i}$	Specific heat capacity at constant pressure of the specie i [cal g <sup>-1</sup> °C <sup>-1</sup> ]
$T_i$	Temperature of the fluid i [°C]
$T_j$	Temperature of the jacket [°C]
$PM_i$	Molecular weight of the i-th compound [g mol <sup>-1</sup> ]
q	Heat flow [cal min <sup>-1</sup> ]
$\Delta H_i$	Enthalpy of the i-th reaction [cal mol <sup>-1</sup> ]

**Subscripts and superscripts**

H	Proton
DB	Double Bond
FA	Formic Acid
PFA	Performic Acid
Epox	Epoxide Group
aq	Aqueous phase
org	Organic phase
0	Initial value
J	Jacket
P	Process
r	Epoxidation reaction
ox	H <sub>2</sub> O <sub>2</sub> decomposition
deg	Ring Opening reaction (degradation)
add	adding

# Chapter 5

## *Oxirane Ring Opening Reaction Studied in Independent Way*

*“What is research but a blind date with knowledge?”*

**Will Harvey**

(Silicon Valley entrepreneur)

### 5. 1 Introduction

Besides the main reaction (the formation of the oxirane ring by reaction of the unsaturations of hydrocarbon chains of vegetable oils with peracids) several other side reactions occur in the epoxidation process. They all imply the oxirane losses via ring-opening reactions (Figure 5.1), so they must be minimized in order to achieve high selectivities in epoxidation reaction.

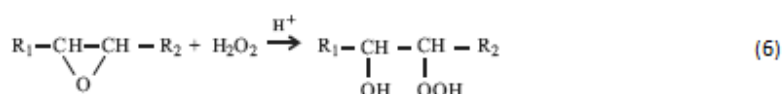
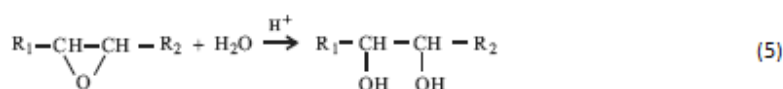
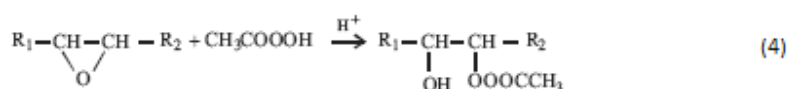
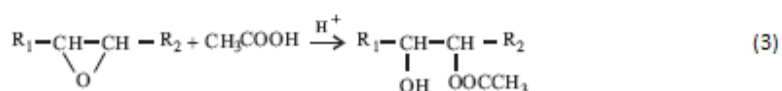
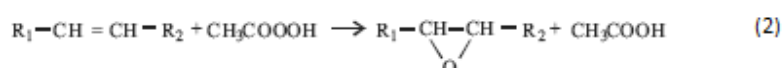
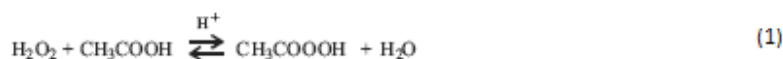


**Figure 5.1:** Epoxidation and ring opening reactions of the double bonds of vegetable oils (unsaturated triglycerides).

These oxirane cleavage reaction can occur in series with the epoxidation reaction (2) and are almost promoted by an acid environment. In particular, being the formic to performic acid formation (1) catalyzed by strong Brønsted acids, such as sulfuric or phosphoric acid, the same catalysts promote also the side ring opening reaction. It is important to point out that the peracid formation reaction (1) occurs in the aqueous phase, where the mineral acid is dissolved, while, epoxide rings are dissolved in the oil phase. It is reasonable, therefore, to assume the ring opening reactions occur at the water/oil interface.

Taking account the deleterious effect of ring opening reaction in order to reach high yield and selectivity a detailed study with kinetic of degradation reaction can be useful to find the optimal operative conditions to minimize its influence. The last is the object of this chapter.



Under realistic processes conditions, the hydrolysis of epoxide occurs through a mechanism that implied a nucleophilic substitution [1]. The type of nucleophile and pH has an impact on the type of substitution that the system undergoes (SN1 or SN2). Several papers have specifically studied the hydrolysis of epoxidized vegetable oils, focused on the effect of pH, the temperature and reaction mixture composition on degradation reaction rate [2-5].

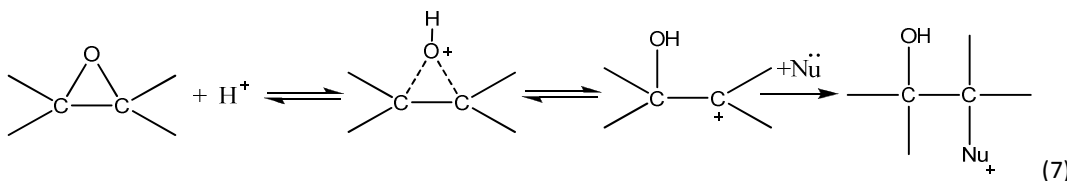
The following rate expression was proposed for the degradation of epoxidized soybean oil:

$$\text{Rate of degradation (mol}_{\text{Epoxide}}\text{L}^{-1}\text{min}^{-1}) = k_d[\text{Epox}][\text{Nu}]^2$$

The second order with respect to nucleophilic compound, proposed in literature [6], was only in agreement with experimental information on epoxide ring opening of long chain unsaturated reaction upon attack with formic /acetic acid [6], but didn't justify the proposed mechanism.

Another very important observation comes out from the literature analysis, that is, the pH of the reaction environment is a key feature in promoting the oxirane ring opening reaction. Moreover, according to the already mentioned authors [2-4] the ring opening reaction mainly occurs at the water-oil interface.

Starting from these observations, the reaction scheme can be simplified as following:



Scheme 5.1

In this way, the formation of carbocation by proton attack was assumed as determining step.

The relative reaction rate expression is then the product of the aqueous protonic concentration and the oxirane group concentration at the interphase, that can be assumed proportional to the related bulk concentrations. Starting from these assumption, in this work the effect of some operative variables, such as temperature, stirring rate and the catalyst concentration on the ring opening reaction rate has been investigated.

## 5.2 Experimental Section

### 5.2.1 Apparatus

The kinetic runs have been carried out in a cylindrical jacketed glass reactor of 2 L, equipped with a thermocouple for the reaction temperature control. The reacting mixture was stirred by mechanical stirring, while the temperature control was made by using a recirculating thermostat, that flows water in the reactor jacket. The adopted experimental device is shown in Figure 5.2.



**Figure 5.2:** Experimental device adopted for ring opening runs. 1. Reactor; 2. Recirculating thermostat; 3. Mechanical stirrer.

### 5.2.2 Methods

The ring opening reactions were carried out by working with aqueous solution of  $\text{H}_2\text{O}_2$ , water and formic acid in the presence of sulphuric acid. In particular, a classical experimental procedure is described as it follows: a mixture containing 36.7 g of hydrogen peroxide (20 wt.%), 5.38 g of formic acid (95 wt.%) and 0.64 g of sulfuric acid (98 wt.%), was added to 100g of well mixed epoxidized soybean oil (ESBO), heated at a desired temperature. As soon as the substrate reached the established temperature, the aqueous mixture was fed to the reactor ( $t=0$ ) and samples have been periodically withdrawn during the 4 hours of reaction. The samples have been cooled, a solution of NaCl in water was added to neutralize the residual acidity and then magnesium sulfate anhydrous to remove the water. The withdrawn samples were then analyzed for determining the oxirane number, according to the analytical methods reported in appendix of this thesis.

## 5.3 Discussion and Results

### 5.3.1 Description of Kinetic runs

To fully take into account the effect of the main process variables on ring opening reaction, several runs were performed at different stirring speeds, values of concentration of acid catalyst (sulphuric acid) and temperature. A list of all the performed experimental runs are resumed in Table 5.1

**Table 5.1** : List of the ring opening experimental runs performed.

Run	W <sub>ESBO</sub> (g)	Temperature (°C)	Stirring Rate (rpm)	W <sub>sulphuric acid</sub> (g)	W <sub>H2O2</sub> (g)	W <sub>Formic acid</sub> (g)
1	100	70	250	0.64	36.7	5.38
2	100	70	500	0.64	36.7	5.38
3	100	70	750	0.64	36.7	5.38
4	100	70	1000	0.64	36.7	5.38
5	100	70	750	0.32	36.7	5.38
6	100	70	750	1.28	36.7	5.38
7	100	80	750	0.64	36.7	5.38
8	100	90	750	0.64	36.7	5.38

As the ring opening reactions occur at interphase, where the protons stay, it's clear that the dispersion of the organic phase in water one and mixing degree are very important. At this purpose, the runs 1-4 were performed changing only the stirring speed and keeping constant the rest of process variables (T=70°C; catalyst mass=0.64g). In Figure 5.3 the profiles of residual oxirane (percentage) found for runs 1-4 are reported.

At 250 rpm the ring opening rate is very low and increase with the stirring speed. It is evident that increasing the stirring speed the interfacial area increases and in this way the degradation rate too. The figure 5.3 shows also the presence of an induction time in very case, that can be related to the need of enough active area-to-volume ratio in the system, after which a “break point” is reached, and ring opening reaction can occur.

The behavior of degradation reaction with the mixing degree represents an important aspect that have to be taken in account in designing a continuous reactor with purpose of the epoxidation process intensification: while the epoxidation reaction (2) need a high interfacial area to promote the mass transfer of formed peracid, a very high value of area is detrimental for the occurrence of ring opening reactions.

Furthermore, reactors like microreactors, static mixers reactors are characterized by a very efficient mixing degree can affect negatively on the yield of the epoxidation reaction.

Clearly, a compromise between these two contradictory constraints is opportune.

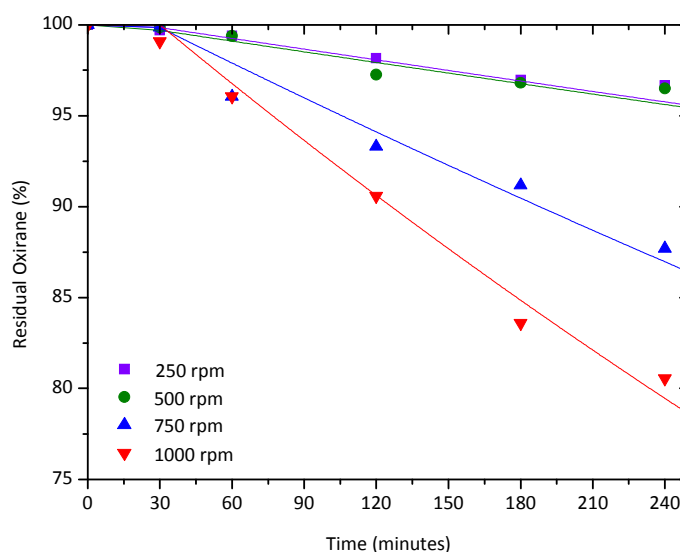


**Figure 5.3:** Effect of stirring speed in the oxirane ring opening of epoxidized soybean oil. Temperature and the catalysts mass were respectively 70 °C and 0.64g. Symbols represent the experimental data, while lines the simulations.

The effect of acidity of media was evaluated in the runs 3, 5, 6, where different amounts of acid catalyst were used. Figure 5.4 shows the results obtained for these runs.

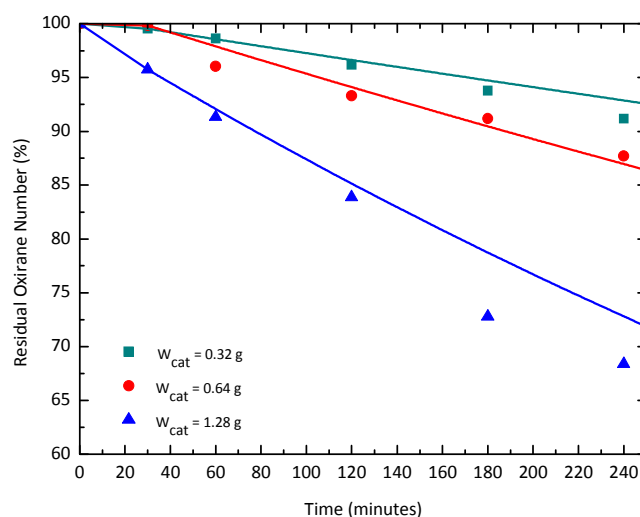
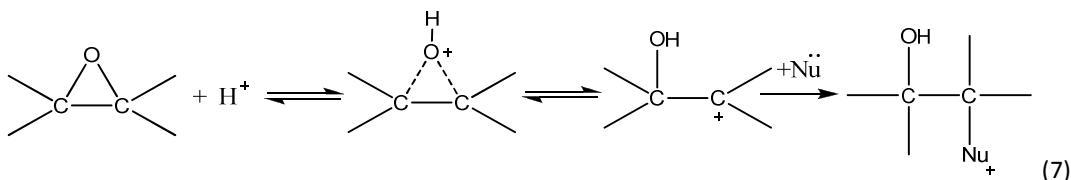
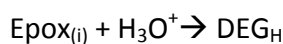


**Figure 5.4:** Experimental residual oxirane profile as a function of the reaction time, at different catalyst concentrations. Temperature and the stirring rate were respectively 70 °C and 750 rpm. Symbols represent the experimental data, while lines the simulations.

It is evident that the degradation of oxirane ring increase with the proton concentration, justifying in this way the assumption made for the mechanisms proposed that the protonic attack with the formation of carbocation is the rate determining step.



Therefore, the degradation reaction rate depends exclusively on protonic concentration and not nucleophilic one:



This second aspect has to be also taken in account when choosing the best operative conditions for the epoxidation of soybean oil reaction: in fact sulphuric acid catalyzes the formic to performic acid oxidation and promotes the ring opening reaction too.

At last, the effect of temperature was studied at 70°C, 80°C and 90°C (Runs 3, 7, 8 in Table 5.1 and Figure 5.5).

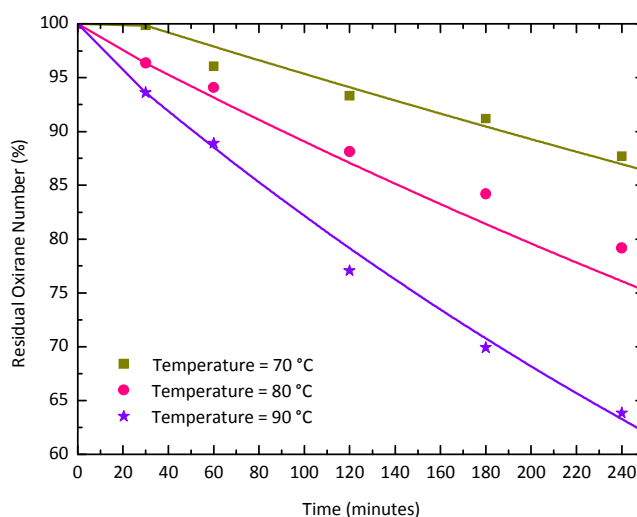


**Figure 5.5:** Experimental residual oxirane profile as a function of the reaction time, at different temperatures. Stirring rate and catalyst mass were respectively 750 rpm and 0.64 g. Symbols represent the experimental data, while lines the simulations.

As it is possible to observe, an increase in temperature corresponds to a higher ring opening rate.

### 5.3.2 Mathematical Model

A kinetic rate expression, in according to mechanism proposed, suitable for describing the oxirane ring opening is given, all expressed in  $[\text{mol L}^{-1} \text{min}^{-1}]$ :

$$r_d = k_d \cdot [\text{EpoX}]_{org} \cdot [\text{H}_3\text{O}^+]_{aq} \quad (1)$$

The mass balance has been written as follows:

$$\text{accumulation} = \text{reacted} [=] \text{mol} \cdot \text{min}^{-1} \quad (2)$$

It is possible to write the mole balance equation for each component in  $(\text{molmin}^{-1})$ :

$$\frac{dn_{\text{EpoX}^{org}}}{dt} = -r_d \cdot V_{org} \quad (3)$$

$$\frac{dn_{\text{Deg}^{org}}}{dt} = +r_d \cdot V_{org} \quad (4)$$

In order to integrate these equations the following initial conditions have been considered. First of all, the total number of the oxirane rings present in the epoxidized soybean oil is given by the following expression:

$$n_{\text{EpoX}}^0 = \frac{N_{\text{epox}}^0 \cdot M_{oil}}{PMO \cdot 100} \text{ where } N_{\text{oxirane}}^0 = 6.58 \text{ (g O}_2 \text{ in 100g of substrate)} \quad (5)$$

The dependence of the kinetic constants with the temperature has been described with the following relationship:

$$k_d = k_d^{ref} \exp \left[ \frac{E_{a,d}}{R} \left( \frac{1}{T^{ref}} - \frac{1}{T_P} \right) \right] \quad (6)$$

Being  $k_d^{ref}$  the kinetic constant chosen at a fixed temperature (here 70°C). All the performed kinetic runs have been submitted to mathematical regression analysis. For example, in Figure 5.6 the trend of the ring opening kinetic constant, as a function of the stirring rate, is shown. As it can be seen, there is a linear dependence of the ring opening activity with the stirring rate. The kinetic constants found for the different stirring rates are reported in Table 5.2.

**Table 5.2:** List of the ring opening kinetic constant at different stirring rates.

Run	kd [Laq/(mol·min)]	Stirring rate (rpm)
1	5.96 E-04	250
2	5.96 E-04	500
3	1.97 E-03	750
4	3.28 E-03	1000

Then, it must be reminded that:

$$k_d = k_d^{true} \cdot a_{sq} \cdot K_{eq} \quad (7)$$

Where,  $k_d^{true}$  is the real kinetic constant,  $a_{sp}$  the specific interfacial area and  $K_{eq}$  the equilibrium constant of the first reaction in (7).

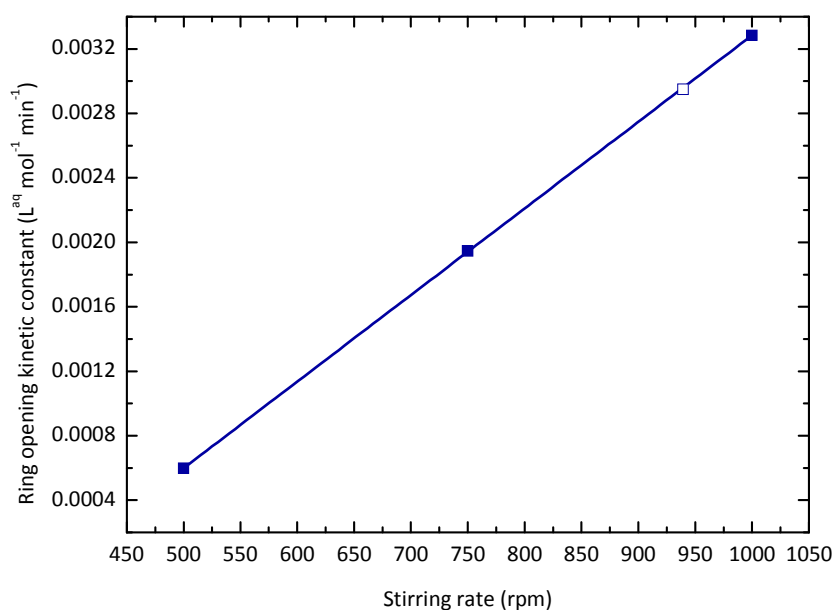


**Figure 5.6:** Trend of the ring opening kinetic constant as a function of the stirring rate. The full dot correspond to the experimental runs related to the ring opening reactions; the empty dot correspond to the kinetic constant regressed on the epoxidation experimental runs, reported in previous chapter 4.

For what concerns the catalyst dependence on the reaction rate, in Figure 5.4, both the experimental data and the simulated profiles are reported. As the reaction rate resulted linearly dependent on the protonic concentration, the calculated profiles already include the catalyst concentration. Therefore, it is possible to use only one kinetic

constant equal to  $1.97 \times 10^{-3} \text{ L}^{\text{aq}} \text{ mol}^{-1} \text{ min}^{-1}$  to describe all the three runs. The satisfactory fitting is a clear evidence of the validity of the adopted mechanism and related kinetic expression.

At last, the investigation of the effect of the temperature on the ring opening reaction has been performed. The three runs performed at different temperatures have furnished an activation energy value of 12.9 kcal/mol. The corresponding obtained agreements can be appreciated in Figure 5.5.

As it is possible to observe, the described kinetic model is able to simulate properly all the performed experimental runs.

#### 5.4 Conclusions

A new kinetic approach, based on a reliable mechanism, has been developed in order to properly describe the epoxide ring opening reaction. The model is based on the assumption that the rate determining step of the reaction network is the carbocation formation, that would be a superficial reaction occurring between the oxirane ring (dissolved in oil phase) and protons (dissolved in aqueous phase). This model is able to describe properly all the experimental data, that have been collected in a wide range of experimental conditions.



**References**

- [1] Y. Pocker, B.P Roland, K.W. Anderson, *J. Am. Chem. Soc.*, 110 (1998) 6492.
- [2] A. Campanella, M.A. Baltanas, *Latin Am. App. Res.*, 35(2005) 205.
- [3] A. Campanella, M.A. Baltanas, *Latin Am. App. Res.*, 35 (2005) 211.
- [4] L.H. Gan, S.H. Goh, K.S. Ooi, *J. Am. Oil Chem. Soc.* , 69 (1992) 347.
- [5] B. Rangarajan, A. Havey, E.A. Grulke, P.D. Culnan, *J. Am. Oil Chem. Soc.*, 72 (1995) 1161.
- [6] F.A. Zaher, M.H. El-Shami, *Gracias y Aceites*, 41 (1990) 361.

**Nomenclature**

Epox	Epoxide group
DEG <sub>i</sub>	Decomposed oxirane
$r_d$	Reaction rate [ $\text{mol L}^{-1}\text{min}^{-1}$ ]
$k_d$	Kinetic constant (the units depends on the reaction)
$n_i$	Moles of the i-th compound [mol]
$V^i$	Reaction volume referred to the phase i [L]
$PM_i$	Molecular weight of the i-th compound [ $\text{g mol}^{-1}$ ]

**Subscripts and superscripts**

$\text{H}^+$	Proton
Epox	Epoxide group
0	Initial value

# Chapter 6

## *Vegetable Oils Epoxidation Reaction with Performic Acid in Continuous Reactor*

“Science is but an image of the truth.”

**Francis Bacon**

(1561-1626, English philosopher)

## **6. 1 Introduction**

An intensification of soybean oil epoxidation process, in order to increase the productivity of industrial process and reduce the potential for explosion danger through enhanced control, could be possible through the transfer from fed-batch reactors (current technology) to continuous ones. To design continuous process that works in safe conditions, detailed information about the kinetic of occurring reactions and heat and mass transfer are needed.

For this purpose, a detailed kinetic study on soybean oil epoxidation with performic acid has been performed and reported in Chapter 4, and all the kinetic runs have been interpreted with a biphasic kinetic model taking into account: (i) the kinetic laws of all the reactions occurring in the two immiscible phases; (ii) the partition of all the components involved in the reactions; (iii) the mass transfer from one phase to the other; (iv) the heat transfer affecting the reactor temperature.

Moreover a detailed study on ring opening reaction has been showed in Chapter 5, where it was found that a very high interfacial area, need to promote the mass transfer of peracid, is deleterious to reach high selectivity for the occurrence of the ring opening reaction.

Object of this chapter is to validate the biphasic model developed and described in Chapter 4, on continuous kinetic runs, verifying the rate law equations and related parameters, taking in account what found in Chapter 5.

As continuous reactor a tubular packed bed reactor was used. The reactor packing is constituted of small sphere of stainless steel with the scope to act as static mixer for favouring the local micro-mixing. The partition coefficients of the reagents and products, in the two reacting phases, have been estimated with the SPARC method, like in Chapter 4.

The developed model is clearly a useful base for modelling, optimizing and intensifying the epoxidation reaction in continuous reactors.

## **6.2 Experimental Section**

### **6.2.1 Apparatus**

The kinetic runs were carried out in two jacketed glass tubular reactors of different sizes, completely filled with spheres of stainless steel (AISI 316) of 2.2 mm of diameter (Figure 6.3). Reactor 1 was a tube of 1.0 cm of diameter and 27 cm of length, the volume of the empty reactor was 22cm<sup>3</sup>, while, the void volume of the reactor filled with the mentioned spheres was 8.3 cm<sup>3</sup> (void fraction = 0.37). Reactor 2 was a tube of 1 cm of diameter and 46 cm of length, the volume of the empty reactor was 38 cm<sup>3</sup>, while, the void volume of the reactor filled with the mentioned spheres was 14 cm<sup>3</sup>

(void fraction = 0.37). A scheme of the used laboratory plant is reported in Figure 6.1. and 6.2.

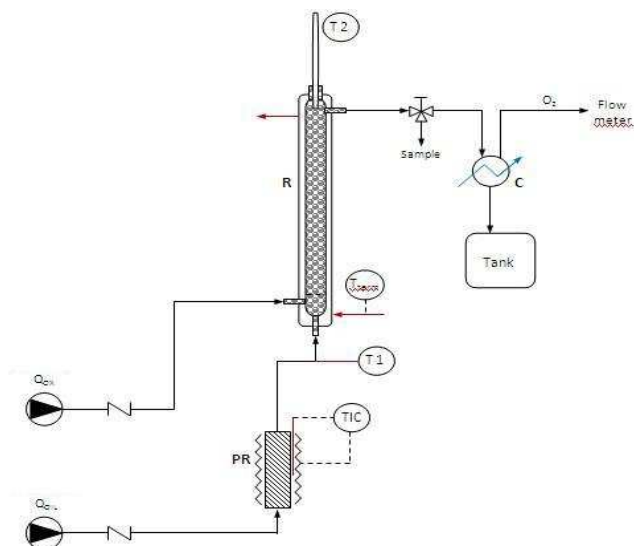


**Figure 6.1:** Scheme of the used laboratory plant. T1 and T2 are respectively the temperatures at the inlet and at the outlet of the tubular reactor, R is the reactor, C is a cooler, TIC is a temperature controller.

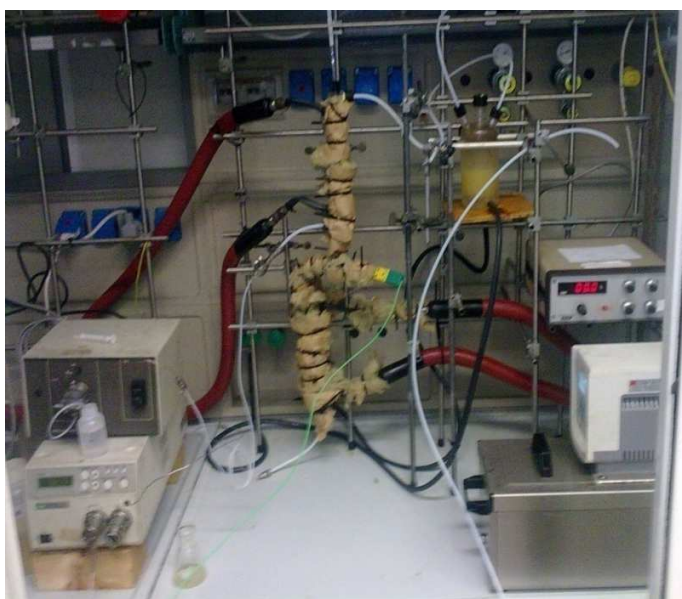


**Figure 6.2:** A picture of Continuous laboratory plant used for kinetic runs.



**Figure 6.3:** Tubular packed reactor

## 6.2.2 Methods

A preheated stream of oil was fed to the reactor, while, a mixture of hydrogen peroxide, formic and sulphuric acid, taken at room temperature, was mixed with the hot oil at the inlet of the continuous reactor. Periodically, samples were withdrawn at the reactor outlet and quickly cooled; then the oil phase was separated from the aqueous one, by centrifugation at 3500 rpm, for 30 min in 50 mL vials. The organic phase was dissolved in ethyl acetate and washed with a solution of sodium bicarbonate in water (5 wt.%) and then, with a solution of NaCl (5 wt.%), until the complete elimination of the acidity is achieved. The final product was then dried in a rotary evaporator. The conversion and yield of the withdrawn samples was monitored through the determination of, respectively, the iodine and the oxirane numbers, according to the analytical methods reported in Appendix.

## 6.3 Results and discussion

### 6.3.1 Description of the kinetic runs

Epoxidation of soybean oil was carried out in continuous tubular packed reactor with peroxyformic acid generated in situ by reacting  $\text{H}_2\text{O}_2$  (60 wt%) and formic acid (95 wt%) in presence of sulphuric acid (98 wt%) as catalyst. The main adopted reaction conditions for the kinetic runs are reported in table 6.1.

**Table 6.1:** List of performed runs performed in reactor 1 (runs 1-5) and Reactor 2 (runs 6-17), reaction conditions.

Run	$Q_{\text{oil}}/Q_{\text{ox}}$	$\tau$ (min)	$T_j$ (°C)	$T_{\text{IN}}$ (°C)	$T_{\text{OUT}}$ (°C)
1	4/1	1.66	70.0	66.0	70.0
2	4/1	1.66	77.0	78.0	77.0
3	4/1	1.66	93.0	83.0	93.0
4	3/2	1.66	67.0	66.0	67.0
5	3/2	1.66	78.0	78.0	78.0
6	8/2	1.40	72.5	71.0	74.0
7	8/2	1.40	82.5	80.3	93.0
8	9/1	1.40	72.5	70.4	76.0
9	9/1	1.40	82.5	80.2	87.0
10	4/1	2.80	72.5	70.4	79.0
11	14/1	0.93	72.5	70.2	75.0
12	14/1	0.93	82.5	80.5	84.0
13	14/1	0.93	92.5	90.0	97.5
14	28/1	0.47	92.5	90.4	92.5
15	29/1	0.47	92.5	90.3	94.0
16	26/4	0.47	72.5	70.0	76.5
17	24/6	0.47	72.5	70.0	78.0

### 6.3.2 Kinetic Modelling

#### 6.3.2.1 Modelling of the epoxidation reaction: theoretical approach

A complete scheme of all the occurring reactions involved in soybean oil epoxidation process, that are considered for the kinetic model, is reported in table 6.2.

**Table 6.2:** Scheme of reaction occurring in epoxidation process.

Reactions Scheme	Kinetic Laws
<p><i>Aqueous phase</i></p> $H_2O_2 + HCOOH \leftrightarrow HCOOOH + H_2O$ $H_2O_2 \rightarrow H_2O + \frac{1}{2}O_2$	$r_b^{aq} = k_b \cdot [H_3O^+] \cdot \left\{ [H_2O_2]_{aq} \cdot [FA]_{aq} - \frac{1}{K_{eq}} \cdot [PFA]_{aq} \cdot [H_2O]_{aq} \right\}$ $r_a^{aq} = k_a \cdot [H_2O_2]_{aq}^{2.5}$
<p><i>Organic phase</i></p> $HCOOOH + C = C_{(i)} \rightarrow Epox_{(i)} + HCOOH$	$r_c^{org(i)} = k_c(i) \cdot [DB(i)]_{org} \cdot [PFA]_{org}$
<p><i>Liquid–Liquid interphase</i></p> $Epox_{(i)} + H^+ \rightarrow DEG_{(i)}$	$r_d^{org(i)} = k_d(i) \cdot a_{sp}^{aq} \cdot [Epox(i)]_{org} \cdot [H_3O^+]_{aq}$

The index (i) is related to the possibility of a different reactivity of the double bonds contained in the oil as respectively trienes, dienes and monoenes, according to the findings by La Scala et al. [1] and our previous experimental observations.

Concerning to mass transfer rates, we adopted the Whitman's two films theory [2], that considers the gradients are confined into the boundary layers of the two liquids sides, like described in previous chapter. In this case, following mass transfer equations are derived:

$$J_{FA}^{aq} = \beta_{FA}^{aq} \cdot ([FA]_{aq} - H_{FA} \cdot [FA]_{org}^*) \quad (1)$$

$$J_{FA}^{org} = \beta_{FA}^{org} \cdot ([FA]_{org}^* - [FA]_{org}) \quad (2)$$

$$J_{PFA}^{aq} = \beta_{PFA}^{aq} \cdot ([PFA]_{aq} - H_{PFA} \cdot [PFA]_{org}^*) \quad (3)$$

$$J_{PFA}^{org} = \beta_{PFA}^{org} \cdot ([PFA]_{org}^* - [PFA]_{org}) \quad (4)$$

Mass transfer related to hydrogen peroxide and water have been neglected, because, these components are poorly soluble in oil and are always in excess with respect to formic and performic acids.

$H_j$  are the partition coefficients defined as  $[C]_{aq}^*/[C]_{org}^*$  and calculated by using the SPARC on-line calculator [3].

Concerning to  $\beta_k^i$ , this parameter represents the product between the mass transfer coefficient and the interfacial surface area for the component k in the phase i. At this purpose, on the basis of experimental evidences, the  $\beta$  values are separated in two

different contributions ( $k_L$  and  $a_{sp}$ ), by considering a dependence of the specific interfacial area on both the overall volumetric flow-rate and the ratio between the oxidizing mixture and oil according to a polynomial correlation of the type:

$$a_{sp}^{aq} = \delta_1 \cdot \left( \frac{Q_{aq}}{Q_{org}} \cdot \frac{Q_{tot}}{Q_{tot}^{ref}} \right) + \delta_2 \cdot \left( \frac{Q_{aq}}{Q_{org}} \cdot \frac{Q_{tot}}{Q_{tot}^{ref}} \right)^2 + \delta_3 \cdot \left( \frac{Q_{aq}}{Q_{org}} \cdot \frac{Q_{tot}}{Q_{tot}^{ref}} \right)^3 \quad (5)$$

$Q_{tot}^{ref}$  is equal to 1 cm<sup>3</sup>/minute.

Concerning the specific area, the most important effect influencing both the conversion and the oxirane selectivity is related to the overall volumetric flow-rate was observed. Applying relation (5) it was observed that  $\delta_2$  and  $\delta_3$  were not influent.

Since the specific interfacial area corresponds to the ratio between the interphase and the volume of the relative phase, the specific areas of respectively aqueous and organic phase were correlated as it follows:

$$\frac{a_{sp}^{aq}}{a_{sp}^{org}} = \frac{Q_{org}}{Q_{aq}} \rightarrow a_{sp}^{org} = \frac{Q_{aq}}{Q_{org}} \cdot a_{sp}^{aq} \quad (6)$$

Moreover, the  $k_L$  values for the two phases can be roughly estimated by using the Wilke and Chang correlation [4]. Starting from their expression it is possible to write the ratio between the two mass transfer coefficients as it follows:

$$\frac{k_{L,aq}}{k_{L,org}} = \sigma \cdot \sqrt{\frac{\varphi_{aq} \cdot PM_{aq}}{\varphi_{org} \cdot PM_{org}}} \cdot \frac{\mu_{org}}{\mu_{aq}} \quad (7)$$

Where,  $\varphi_{aq}=2.6$  for water,  $\varphi_{org}=1$  for oil,  $\mu$  is the viscosity and  $\sigma$  is a correction coefficient determined from the experimental results.

The Wilke-Chang relation is useful to estimate in a first approximation the mass transfer coefficients of the components in respectively the aqueous and the oil phase. The evaluation of this ratio clearly reduces the number of adjustable parameters being the mass transfer in water related to the one in oil for the same substance. The correction coefficient  $\sigma$  has been introduced, because, in this approach we considered a pseudo-binary mixture. On the contrary, the reaction mixture is not composed by oil and water but is much more complex. A constant value of  $\sigma$  along the reactor was assumed even if it was known that the viscosity of the epoxidized soybean oil is much greater than the one of the fresh oil. Last approximation is reasonable because conversion and yields were relatively low. All chemical and physical properties were considered at an average temperature as a reasonable approximation. However, it was checked that this



approximation does not significantly affect the agreement between calculated and experimental results.

Starting from expressions (1-6), it is possible to calculate the concentrations of all the mentioned compounds at the interface, by imposing that in steady-state conditions, the following balance is always valid:

$$J_k^{aq} \cdot Q_{aq} = J_k^{org} \cdot Q_{org} \quad (8)$$

As a consequence the following expressions for calculating the interphase concentrations, can be derived:

$$[FA]_{org}^* = \frac{Q_{aq} \cdot \beta_{FA}^{aq} \cdot [FA]_{aq} + Q_{org} \cdot \beta_{FA}^{org} \cdot [FA]_{org}}{Q_{org} \cdot \beta_{FA}^{org} + Q_{aq} \cdot \beta_{FA}^{aq} \cdot H_{FA}} \quad (9)$$

$$[PFA]_{org}^* = \frac{Q_{aq} \cdot \beta_{PFA}^{aq} \cdot [PFA]_{aq} + Q_{org} \cdot \beta_{PFA}^{org} \cdot [PFA]_{org}}{Q_{org} \cdot \beta_{PFA}^{org} + Q_{aq} \cdot \beta_{PFA}^{aq} \cdot H_{PFA}} \quad (10)$$

Concerning the heat transfer, it must be considered that as a consequence of the epoxidation reaction, the oil phase composition changes along the reactor's axis. As a matter of fact, epoxidized soybean oil is much more viscous than the unreacted substrate (respectively 450 Cp for epoxidized soybean oil and 110 Cp for soybean oil at 25°C) and we can foresee that the overall heat exchange coefficient  $U$  will change with the conversion degree, considering an approximated linear dependence of  $U$  with the conversion:

$$U = U_0 + \alpha \cdot X_{DB} \quad (11)$$

### 6.3.2.2 Mass and Energy balances

The balance equations for each component can be written as it follows:

*Aqueous phase:*

$$\frac{d[H_2O_2]^{aq}}{dV} = \frac{-r_a - r_b}{Q^{tot}} \quad (12)$$

$$\frac{d[H_2O]^{aq}}{dV} = \frac{+r_a + r_b}{Q^{tot}} \quad (13)$$

$$\frac{d[FA]^{aq}}{dV} = \frac{-r_b - J_{FA}^{aq}}{Q^{tot}} \quad (14)$$

$$\frac{d[PFA]^{aq}}{dV} = \frac{+r_b - J_{PFA}^{aq}}{Q^{tot}} \quad (15)$$

Organic phase:

$$\frac{d[FA]^{org}}{dV} = \frac{+r_c(i) + J_{FA}^{org}}{Q^{tot}} \quad (16)$$

$$\frac{d[PFA]^{org}}{dV} = \frac{-r_c(i) + J_{PFA}^{org}}{Q^{tot}} \quad (17)$$

$$\frac{d[DB]^{org}(i)}{dV} = \frac{-r_c(i)}{Q^{tot}} \quad (18)$$

$$\frac{d[Epoxy]^{org}(i)}{dV} = \frac{+r_c(i) - r_d(i)}{Q^{tot}} \quad (19)$$

$$\frac{d[DEG_H]^{org}(i)}{dV} = \frac{+r_d(i)}{Q^{tot}} \quad (20)$$

Concerning the energy balance, we have considered, as a first approximation, that the heat released by reaction is instantaneously distributed on all the mass of the reaction. Therefore, the heat balance can be interpreted with the following relation:

$$q_{accumulation} = +q_{reaction} - q_{exchange} [=] \text{ cal} \cdot \text{L}^{-1} \text{ min}^{-1} \quad (21)$$

and the terms of the heat balance can be written as it follows:

$$q_{accumulation} = \bar{c}_p \cdot W_{tot} \cdot \frac{dT_P}{dV} \quad (22)$$

$$q_{reaction} = [\Delta H_r \cdot (-r_c(i)) + \Delta H_{deg} \cdot (-r_d(i))] + [\Delta H_{ox} \cdot (-r_a)] \quad (23)$$

$$q_{exchange} = U \cdot \frac{A}{V} \cdot (T_P - T_J) \quad (24)$$

The thermodynamic properties of the different components the reaction are reported in Table 6.3.

**Table 6.3** :Average values of density, specific heat and reaction enthalpy

Density (g cm <sup>-3</sup> )	Specific heats (cal g <sup>-1</sup> °C <sup>-1</sup> )	Enthalpy (cal mol <sup>-1</sup> )
$\rho_{H_2O_2} = 1.44$	$cp_{H_2O_2} = 0.622$	$\Delta H_r = - 55000$ [5]
$\rho_{oil} = 0.89$	$cp_{oil} = 0.50$	$\Delta H_{ox} = - 23440$ [6]
$\rho_A = 1.16$	$cp_A = 0.531$	$\Delta H_{deg} = - 21000$ [7]
$\rho_{H_2O} = 0.985$	$cp_{H_2O} = 1$	

### 6.3.2.3 Kinetic Modelling Results

The kinetic runs, reported in Table 6.2, have been simulated with the described model using the same kinetic parameters determined in a previous chapter for describing fed-batch and pulse-fed-batch runs. Those parameters are reported in Table 6.4.

**Table 6.4 :** Kinetic constants values determined in previous chapter 4 from runs performed in fed-batch conditions .

Parameter	Value $\pm$ Confidence interval	Unit
$k_a$	$1.04\text{E-}03 \pm 1.6\text{E-}0.4$	$\text{L}^{1.5,\text{aq}} \text{mol}^{-1.5} \text{min}^{-1}$
$k_b$	$6.56\text{E-}01 \pm 2.0\text{E-}02$	$\text{L}^{2,\text{org}} \text{mol}^{-2} \text{min}^{-1}$
$K_{\text{eq}}$	$5.17 \pm 0.8$	-
$k_c^{\text{mono}}$	$2.72 \pm 0.5$	$\text{L}^{\text{org}} \text{mol}^{-1} \text{min}^{-1}$
$k_c^{\text{tri}}$	$133.9 \pm 9.8$	$\text{L}^{\text{org}} \text{mol}^{-1} \text{min}^{-1}$
$E_{a_b}$	$11.39 \pm 0.6$	$\text{Kcal mol}^{-1}$
$E_{a_c}$	$24.89 \pm 0.2$	$\text{Kcal mol}^{-1}$
$E_{a_d}$	$8.86 \pm 0.4$	$\text{Kcal mol}^{-1}$

The adjustable parameters of the model are only: the mass and heat transfer coefficients ( $k_L$ ,  $\sigma$  and  $U_0$ ) these being dependent on the adopted fluid dynamic conditions, as well as the interfacial area. The mathematical regression have been performed on three experimental points for each run that are Iodine, Oxirane Numbers and the outlet temperature of the reaction mixture.

These parameters are reported in Table 6.5.

**Table 6.5:** Adjustable parameters for describing continuous runs.

Parameter	Reactor 1	Reactor 2	Unit
$U_0$	9900	6000	$\text{cal}/(\text{m}^2 \text{min } ^\circ\text{C})$
$\alpha$	-32.00	-32.00	$\text{cal}/(\text{m}^2 \text{min } ^\circ\text{C})$
$\delta_1$	580	641	$\text{cm}^2/\text{cm}^3$
$\sigma$	3.06	3.06	-
$k_{L,\text{aq}}$	0.32	0.32	$\text{cm}/\text{min}$
$k_{L,\text{org}}$	0.14	0.14	$\text{cm}/\text{min}$
$k_d^{\text{mono}}$	$2.42\text{E-}05$	$2.42\text{E-}05$	$(1/1000) \cdot \text{L}^{2,\text{aq}} \cdot \text{mol}^{-1} \cdot \text{cm}^{-2} \cdot \text{min}^{-1}$
$k_d^{\text{tri}}$	$3.35\text{E-}03$	$3.35\text{E-}03$	$(1/1000) \cdot \text{L}^{2,\text{aq}} \cdot \text{mol}^{-1} \cdot \text{cm}^{-2} \cdot \text{min}^{-1}$

A resume of experimental and calculated values of both Iodine and Oxirane Numbers is reported in table 6.6.

**Table 6.6:** Experimental results and simulations related to the continuous epoxidation runs performed in Reactor 1 (entries 1-5) and Reactor 2 (entries 6-17). The composition of the oxidant mixture has been kept constant corresponding to: 85.9 wt.% of  $H_2O_2$  (with concentration of 60 wt.%), 12.6 wt.% of formic acid (with concentration of 6 wt.%) and 1.5 wt.% of sulphuric acid (with concentration 97 wt.%).

Run	$Q_{oil}/Q_{ox}$	$\tau$ (min)	$T^{OUT}$ (°C)		Iodine Number		Oxirane Number	
			EXP	SIM	EXP	SIM	EXP	SIM
1	4/1	1.66	70.0	72.1	125.0	121.0	0.18	0.40
2	4/1	1.66	77.0	79.3	117.0	119.0	0.65	0.51
3	4/1	1.66	93.0	95.6	118.0	114.9	0.54	0.71
4	3/2	1.66	67.0	69.4	113.6	116.3	0.88	0.61
5	3/2	1.66	78.0	81.4	102.4	102.4	1.58	1.38
6	8/2	1.40	74.0	75.3	116.0	113.5	0.55	0.65
7	8/2	1.40	93.0	86.2	101.1	101.1	1.10	1.34
8	9/1	1.40	76.0	73.9	119.2	121.6	0.44	0.33
9	9/1	1.40	87.0	83.9	117.6	119.3	0.42	0.42
10	4/1	2.80	79.0	73.5	108.8	110.2	1.01	0.85
11	14/1	0.93	75.0	73.8	121.9	125.1	0.26	0.16
12	14/1	0.93	84.0	84.2	121.3	124.2	0.25	0.19
13	14/1	0.93	97.5	93.8	121.0	123.5	0.18	0.22
14	28/1	0.47	92.5	95.7	123.7	123.7	0.20	0.21
15	29/1	0.47	94.0	94.1	125.9	126.9	0.08	0.06
16	26/4	0.47	76.5	77.1	115.6	121.6	0.66	0.30
17	24/6	0.47	78.0	78.7	110.4	118.9	0.98	0.37

As it can be seen, the agreement is satisfactory. Therefore, the proposed biphasic kinetic model has been validated and the determined parameters may be considered reliable. In figure 6.4, an example of the profiles calculated along the reactor for respectively the oxirane and iodine numbers and of the temperature has been reported. This example is referred to the run 7 of Table 6.1 that is the run with the highest reached conversion.

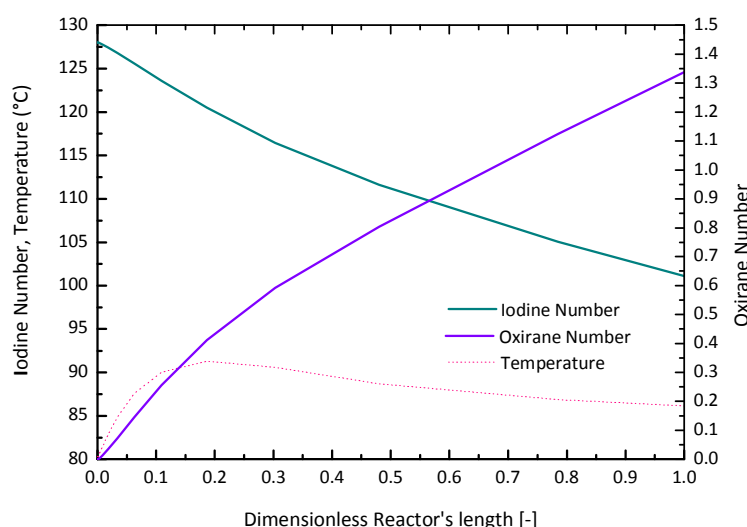
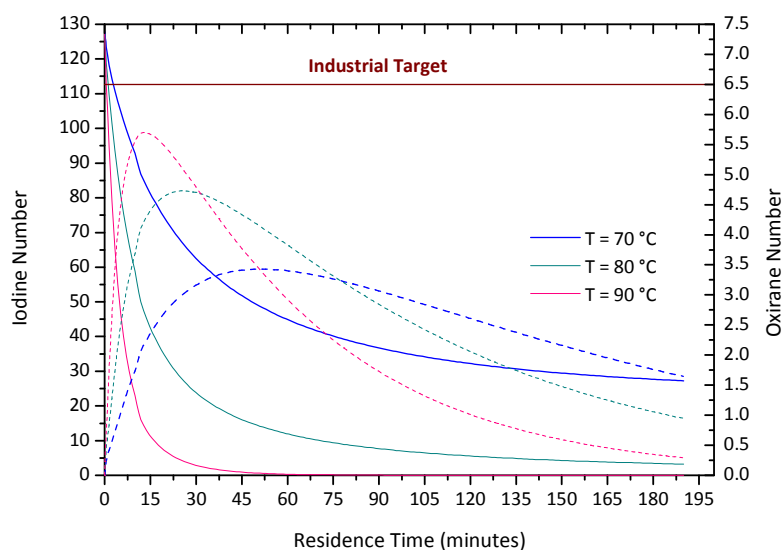


Figure 6.4: Simulation of both aqueous and oil phase compositions for Run 7 of Table 6.1.

The performed continuous runs have validated the kinetic model developed in a previous section for describing many different fed batch kinetic experimental runs. We have shown that continuous runs can be described by using the same rate laws and kinetic parameters with the exception of : (i) the mass and heat transfer coefficient that must be adapted to the new fluid dynamic conditions and (ii) the ring opening reaction which rate depends on the interfacial area that is relatively high in the described tubular reactors containing small stainless steel spheres as static mixer elements. This last point is very important, because, to increase very much the interfacial area is positive for the initial conversion, giving place to a very fast epoxidation reaction, but in the meantime the ring opening reaction rate being strongly increased, by increasing the interfacial area, the oxirane number is limited for a prolonged residence time. This behaviour is clearly shown in Figure 6.5, where the simulations for respectively the oxirane and iodine numbers at different temperatures (70, 80, 90 °C) are reported, by assuming the oil/oxidant volumetric ratio equal 8:2.5, by assuming isothermal conditions. As it can be seen, by operating with the described packed bed tubular reactor (reactor 2) the target values required by the industrial operation are never reached. This occurs because the ring opening reaction rate is too high and lowers the oxirane yields. Another observation is that at higher temperature the epoxidation yields are higher at low residence time. Therefore, in order to obtain the best performances it is necessary to lower the ring opening reaction rate by limiting the available interfacial area. Hence, a two step reaction can be adopted using two different reactors, one characterized by a high interface area and another with a lower interface area using, in this last case, a less efficient static mixer.



**Figure 6.5:** Simulation of continuous reactors working at different temperature, imposing the same  $\beta$  value found in the experimental runs and a oil/oxidant flow-rate ratio of 8/2.5.

In Figure 6.6, it is reported the simulation of two reactors in serie in which the first reactor is similar to the previously described reactor 2 but imposing 10 minutes of residence time, plus another reactor having an interfacial area of 1/10 with respect to the first one, both operating at 90°C.

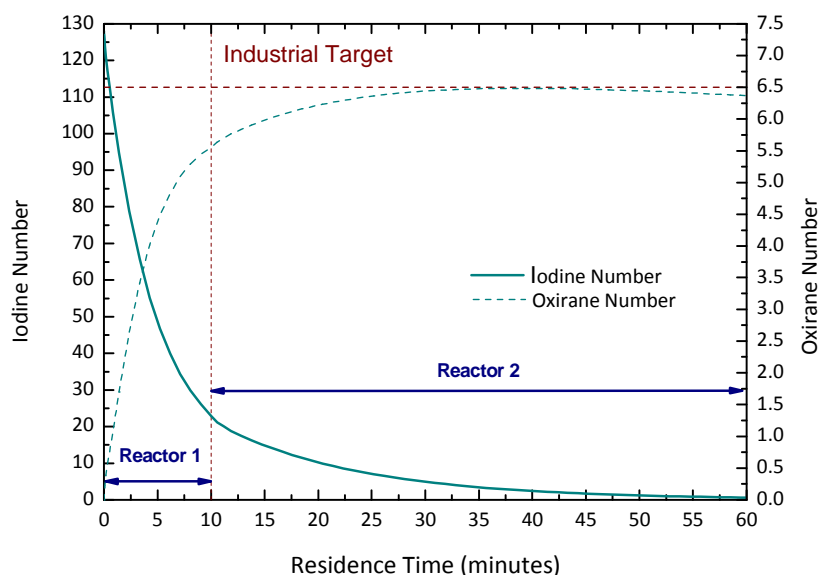


**Figure 6.6:** Simulation of two continuous reactors put in series. The first reactor works imposing a residence time of 10 minutes and the same  $\beta$  value found in the experimental runs, while the second reactor works with a  $\beta$  value of 10 % respect to the first reactor. Both the reactors work with a oil/oxidant flow-rate ratio of 8/2.5 and a temperature of 90°C.

In this case, as it can be seen, the industrial target values are reached for both oxirane number ( $\approx 6.5$ ) and iodine number ( $\leq 2.0$ ) in about 45 minutes instead of 6-8 hours, the time required in industry for the fed batch operation.

#### **6.4 Conclusions**

In the present work a biphasic kinetic model, with related parameters, developed for describing the soybean oil epoxidation reaction, performed in fed-batch reactors, has been validated by applying it to describe also the kinetic runs performed in a continuous tubular reactor packed with stainless steel spheres, used as static mixer, at the scope of favouring local micromixing. This model could be used for modelling continuous reactors and would be the base for promoting the process intensification.

### **References**

- [1] J. La Scala, R.P. Wool, *J. Amer. Oil Chem. Soc.*, 79 (2002) 373.
- [2] W.G. Whitman, *Chem. Metall. Eng.* 29 (1923) 146.
- [3] L.A. Carreira, S. Hilal, S.W. Karickhoff, Theoretical and Computational Chemistry, Quantitative Treatment of Solute/Solvent Interactions. Eds. P. Politzer and J. S. Murray, Elsevier Publishers, 1994.  
<http://sparc.chem.uga.edu/sparc/>
- [4] C.R. Wilke, P. Chang, *A.I.Ch.E. Journal*, 1 (1955) 264.
- [5] B. Rangarajan, A. Havey, E.A. Grulke, P.D. Culnan, *J. Amer. Oil Chem. Soc.*, 72 (1995) 1161.
- [6] Jones, C. W.; Applications of Hydrogen Peroxide and Derivatives. Series Ed., RSC Clean Technology Monographs, Cambridgepp. 14, 1999.
- [7] Information from: <http://www.ethyleneoxide.com>



### Nomenclature

C=C/DB	Unsaturated group (Double bond)
FA	Formic Acid
PFA	Performic Acid
Epox	Epoxide group
DEG <sub>H</sub>	Decomposed oxirane group by H (proton)
Nu	Nucleophilic molecule
$r_i$	Reaction rate [ $\text{mol L}^{-1} \text{min}^{-1}$ ]
$k_i$	Kinetic constant (the units depends on the reaction)
$J_k^i$	Mass transfer rate for the component k in the phase i [ $\text{mol L}^{-1} \text{min}^{-1}$ ]
$\beta_k^i$	Product between the mass transfer coefficient and the interfacial surface area for the component k in the phase i
$a_{sp}^i$	Specific interfacial area for the phase i [ $\text{cm}^2/\text{cm}^3$ ]
$\delta$	Polynomial parameter for the specific interfacial area [ $\text{cm}^2/\text{cm}^3$ ]
$k_{L,i}$	Mass transfer coefficient for the phase i [ $\text{cm}/\text{min}$ ]
$H_j$	Partition coefficients defined as $[C]_{aq}^*/[C]_{org}^*$
$\sigma$	Wilke and Chang correction parameter [-]
U	Global thermal exchange coefficient [ $\text{cal m}^{-2} \text{min}^{-1} \text{°C}^{-1}$ ]
Uo, $\alpha$	Parameters that express the dependence of the global thermal exchange coefficient with the double bonds conversion degree [ $\text{cal m}^{-2} \text{min}^{-1} \text{°C}^{-1}$ ]
A	Exchange area [ $\text{m}^2$ ]
V	Reactor's volume [L]
$Q_i$	Volumetric flow-rate: aq=aqueous phase, org=organic phase, tot=overall [ $\text{cm}^3 \text{min}^{-1}$ ]
$Q_{tot}^{ref}$	Reference overall flow-rate imposed equal to $1 \text{ cm}^3 \text{min}^{-1}$
$W_{tot}$	Overall mass flow-rate [ $\text{g min}^{-1}$ ]
$c_{p,i}$	Specific heat capacity at constant pressure of the specie i [ $\text{cal g}^{-1} \text{°C}^{-1}$ ]
$T_i$	Temperature of the fluid i [ $\text{°C}$ ]
$T_j$	Temperature of the jacket [ $\text{°C}$ ]
$T^{IN}$	Inlet temperature of the tubular reactor [ $\text{°C}$ ]
$T^{OUT}$	Outlet temperature of the tubular reactor [ $\text{°C}$ ]
$PM_i$	Molecular weight of the i-th compound [ $\text{g mol}^{-1}$ ]
q	Heat flow [ $\text{cal min}^{-1}$ ]
$\Delta H_i$	Enthalpy of the i-th reaction [ $\text{cal mol}^{-1}$ ]
$X_{DB}$	Double bonds conversion degree [-]

### Subscripts and superscripts

H	Proton
FA	Formic Acid
PFA	Performic Acid
aq	Aqueous phase
org	Organic phase
J	Jacket
P	Process
r	Epoxidation reaction
ox	H <sub>2</sub> O <sub>2</sub> decomposition
deg	Ring Opening reaction (degradation)

IN	Inlet
OUT	Outlet

# Chapter 7

## *Alternatives to the Prileschajew type reaction in soybean oil epoxidation*

“Give me a place to stand, and I will move the Earth.”

**Archimedes**

(287 BC- 212 BC, Greek mathematician, physicist,  
engineer, inventor, and astronomer)

### 7.1 Introduction

As discussed in previous section, on industrial scale, the vegetable oils epoxidation is currently carried out with Prileschajew reaction, where the unsaturated oils react with percarboxylic acid, such as peracetic and performic, obtained through the acid catalyzed oxidation of the respective organic acid with hydrogen peroxide [1]. Water soluble mineral acids, commonly sulphuric acid, are used as catalysts for this reaction.

Main drawbacks of this technology are concerning to:

1. Environmental, related to the disposal of salts formed during the final neutralization of the mineral acid;
2. Technical, associated to the corrosion and difficult separation operations.
3. Chemical, related to the oxirane ring opening reaction with a decrease of the selectivity.

Thus, in recent years several papers have dealt with the setting up of the catalytic process aimed at overcoming such disadvantages, using more sustainable compounds and technology [2].

The most attractive possible answers to this challenge could be:

1. Heterogenization of Prileschajew reaction, in which the soluble mineral acid can be replaced by an acid solid, such as acid resins [3];
2. Substitution of Prileschajew type reaction by metal or no catalyzed epoxidation, using directly hydrogen peroxide or organic hydroperoxide as oxidant species.

A brief description of these alternative solutions is reported in the following sections.

#### 7.1.1 Heterogenization of Prileschajew type epoxidation reaction

Several attempts have been made in the past to replace the soluble mineral acid by solids one such as acid exchange resins [1,3]. With an acid ion exchange resin as catalyst, the porous structure of the solid and size of natural unsaturated triglycerides were found to minimize the side reactions and thus improved the selectivity [3].

Indeed, with functionalized microreticular ion exchange resins only the small carboxylic acid molecules can enter into their gel like structure, while the bulky epoxidized triglyceride molecules cannot. The oxirane ring can thence be protected from the attack of protons which are confined inside the gel matrix and, so a result, further ring degradation is prevented [4].

Also, catalysts recovery and regeneration is easier. Several strongly acid sulphonic (such as DOWEXx50, Amberlite IR-120) have been reported to contribute to minimize oxirane ring opening [5]. Mungroo et al [5] studied the epoxidation of the canola oil using peracetic acid generated in situ using Amberlite IR-120, at 65 °C with a hydrogen peroxide to double bonds molar ratio of 1.5:1, and catalyst loading of 22 wt% of oil used. In these conditions high conversion and selectivity (90%) were reported. However,

this process required a very large amount of resin with respect to the amount of olefin. Besides, there are some disadvantages such as the physical and chemical degradation of the resin, which must be often replaced. Other resins, such as Amberlyst 15, Dowex50x2 and Nafion were also tested with worst results. The best catalyst, Amberlite IR-120, has 8% of divinylbenzene as cross linking agent, while Amberlyst 15 has 20% of divinylbenzene and Dowex50x2 2% of divinylbenzene as cross linking agent. Attempts to describe the kinetic behavior of these tri-phase systems taking into account also the effect of the resin swelling and reagents absorption were published by two different authors [5,6].

Rios et al. [7] studied epoxidation of jatropha oil methyl esters using acidic resins of the sulfonated-polystyrene with different degree of cross-linking and acidic strength. They found that epoxide selectivity strongly depends on the resin cross-linking and morphology. The most crucial feature to prevent the formation of glycols was to minimize the exposure of the epoxide to the acid sites of the catalyst, which could be achieved using resins with a high cross-linking and with low external surface area. Activity could be increased by increasing the strength of the acid sites, as in the case of SAC13 (Nafion) but the selectivity decreased. They reported that with resins in gel form, i.e. 2% and 8% DVB, the selectivity to the epoxides decreased by lowering the cross-linking. Thus glycols were produced by adding water to the epoxides that were activated (protonated) on the acid sites, and the formation of these glycols was enhanced with low cross-linking. The resin with 20% DVB, which had the highest cross-linking, also showed a poor selectivity to epoxides due to the formation of glycols. This result could be attributed to the fact that this resin had a macro-reticular structure and therefore it had a high surface area on which epoxides could be protonated and opened by water to form glycols.

### 7.1.2 Metal-Catalyzed Epoxidation

In homogenous phase the most catalysts are soluble compounds of the early transition elements Ti(IV), V(IV), Mo(VI) and W(IV) [5]. With organic hydroperoxide  $\text{Mo(VI)} > \text{Ti(IV)} > \text{V(V)} > \text{W(IV)}$ , but with hydrogen peroxide W(IV) catalysts than others [9]. Some compounds of these metals have been successfully heterogenized.

The metal ions which catalyze oxygen transfer in epoxidation reactions with  $\text{H}_2\text{O}_2$  or  $\text{RO}_2\text{H}$  can be divided into in two types based on the active intermediate : a peroxometal or an oxometal complex [10].

Peroxometal pathways usually involve early transition elements with  $d^0$  configuration, e.g. Mo(IV), W(IV), V(V), Ti(IV). Late or first row transition elements, e.g. Cr(IV), V(V), Mn(V), Ru(VI), Ru(VIII), Os(VIII), generally employ oxometal pathways. Some elements, for example vanadium, can employs oxometal or peroxometal pathway depending on

the substrate. An important difference is that peroxometal pathways do not involve any change in oxidation state of the metal, i.e. the metal acts as Lewis acid and activity is not restricted to variable valence elements [10].

The epoxidation of olefins with  $R_2OH$  catalyzed by early transition metals involves a peroxometal mechanism, in which the rate limiting step is oxygen transfer from an electrophilic peroxometal species to the nucleophilic olefins.

The metal centre does not undergo any change in oxidation state during the catalytic cycle. It functions as a Lewis acid by withdrawing electrons from the O-O bond and thus increasing the electrophilic character of the coordinated peroxide. Therefore, active catalysts are metals which are strong Lewis acids and relatively weak oxidants /to avoid one electron oxidation of the peroxide in their highest oxidation state [10].

A description of metal catalysts for epoxidation of oil is presented below.

#### 7.1.2.1 Titanium catalysts

The catalysts based on  $TiO_2/SiO_2$  (consisting of 0.5-5 wt%  $TiO_2$  on  $SiO_2$ , developed by Shell [11]) are the first truly heterogeneous epoxidation catalysts useful for continuous operation in liquid phase. They are used for the commercial epoxidation of propene with Ethyl benzene hydroperoxide delivering 93-94 % yield and 96% hydroperoxide selectivity. These hydrophilic materials are active only with alkyl hydroperoxides as oxidants and they are at least as selective as the best homogeneous molybdenum [12]. It is generally accepted that titanium is attached to the silica surface by at least three siloxoxy group. The catalytic activity of these solids was attributed to site isolation of Ti(IV) on the silica surface, preventing the formation of  $TiO_2$  domains and to enhanced Lewis acidity of Ti(IV) resulting from electron withdrawal by Si-O-ligands.

Santacesaria et al. [13] reported the grafting titanium alkoxide on silica surface as innovative method to prepare highly dispersed  $TiO_2/SiO_2$ , with superior properties relative to catalysts prepared by traditional methods.

However, similar to the homogeneous catalysts with Ti(IV),  $TiO_2$  on  $SiO_2$  is sensitive towards the deactivation by water, for this reason these catalysts do not work in epoxidation with hydrogen peroxide [12]. Moreover in presence of very polar molecules as hydrogen peroxide, the leaching of titanium occurred [10].

The latter problem was overcome with discovery by Taramasso et al. at Enichem [14] of TS-1 (titanium silicalite). It contains Ti(IV) distributed in the crystalline framework by isomorphous substitution of a part of the silicon atoms [ $Ti/(Ti+Si) \leq 0.04$ ] and can activate hydrogen peroxide as an oxidant, due to its hydrophobic nature [15-17].

A drawback of this excellent catalyst is the pore dimension  $5.6 \text{ \AA} \times 4.7 \text{ \AA}$ , providing access only to small substrates with kinetic diameter lower than  $5.6 \text{ \AA}$ . Vegetable oils are bulky

substrates that do not easily enter the pores of these materials; for instance, oleic acid methyl esters has a molecular size of  $5 \times 5 \times 25$  Å.

Extensive work has been done to incorporate Ti(IV) in large pore molecular sieves, leading to the materials Ti-Beta [18], Ti-MCMC-41 [1], and Ti-MCM-48 [19].

Ti-beta has a pore diameter of  $7.6 \times 6.4$  Å and is able to epoxidize substrates that enter into pores with organic hydroperoxide. Ti-MCM-41 was reported as a good catalyst for epoxidation of fatty esters [1, 20] with *tert*-butyl hydroperoxide: the later displayed in this case superior catalytic performance respect than to no ordered mesoporous titanosilicates.

However from economic point view, this type of approach can be used only in the case of very large epoxidation production (like the propylene oxide production). As a matter of fact in this case the co-products amount justifies their commercialization.

#### 7.1.2.2 Tungsten catalysts

System derived from tungstic acid ( $\text{H}_2\text{WO}_4$ ) phosphate and amorphous or phosphonium counterions, that act as phase transfer agents, were found to be catalysts for olefins epoxidation with hydrogen peroxide [21]. They were always formed in situ, but catalytically active complexes such as  $(\text{R}_4\text{N})_3\{\text{PO}_4(\text{W}(\text{O})(\text{O}_2)_2)_4\}$  were isolated and characterized crystallographically by Venturello [22]. Since its discovery in 1983 this system was extensively studied in particular with regard to exact nature of the active phosphotungstate [23]. Noyori [24] reported a significant improvement of the original system. The choice of tetralkylammonium cation and bisulphate ( $\text{HSO}_4^-$ ) anion as phase transfer catalyst, in combination with  $\text{H}_2\text{NCH}_2\text{PO}_3\text{H}_2$  and sodium tungstate produced a system for epoxidation with  $\text{H}_2\text{O}_2$  in toluene/water, in absence of an organic solvent. However, problems of effluent catalyst separation were often associated with these homogenous reactions. To overcome these problems many attempts were realized to heterogenize latter systems.

At least two general strategies have proven successful for the immobilization of W epoxidation catalysts [25].

First electrostatic interactions could be used, whether in an ion exchanger or in a precipitated ionic compound. Secondly, peroxotungstates formed heteronuclear associations with As, S or P oxyanions and especially P-O-W associations are sufficiently stable in catalytic conditions to permit immobilization. Sels et al [25] reported the use of  $\text{WO}_4^{2-}$  exchanged layered double bonds hydroxides,  $\text{WO}_4^{2-}$  LDH, as a truly heterogeneous catalyst for the epoxidation of allylic alcohols, and non functionalized olefins with hydrogen peroxide in alcohol/water media.

Recently Poli et al. [26] reported a selective epoxidation of methyl oleate using a tungsten containing catalyst called Tetrakis.

### 7.1.2.3 Molybdenum catalysts

There are few examples in literature of heterogeneous molybdenum catalysts due to the inability to be incorporated in tetrahedral positions of molecular sieves. Poly-peroxo molybdates has been heterogenized on layer double hydroxide [27] which work in epoxidation of olefins with hydrogen peroxide. However, leaching of molybdenum was not demonstrated.

### 7.1.2.4 Niobium catalysts

Mesoporous niobiosilicalites were found to be effective catalysts for cyclooctene and cyclohexene [28-30] epoxidation and their catalytic activity was found to be influenced by niobium dispersion in  $\text{SiO}_2$  matrix and by the synthesis conditions. Acid properties of these materials [29] and the niobium coordination [30] were hypothesized to play an important role in this reaction [30].

$\text{Nb}_2\text{O}_5\text{-SiO}_2$  catalysts can be synthesized by different procedure, besides the traditional impregnation [31], such as hydrothermal synthesis, eventually in the presence of cationic surfactants or expanders [29,30] or sol-gel [28,32,33].  $\text{Nb}_2\text{O}_5\text{-SiO}_2$  aerogel catalyst were obtained by Somma et al [28,33] by evaporation of the solvent under hypercritical conditions ( $P_c=48$  atm,  $T_c=235^\circ\text{C}$ ). These systems were active for olefins epoxidations and showed no leaching of the active phase, however the niobium content was limited to 6 wt% [33].

$\text{Nb}_2\text{O}_5\text{-SiO}_2$  solids have recently been synthesized by an innovative sol-gel method that is simpler and less expensive than other synthesis methods, because, it is carried out almost completely in air at room temperature starting from economic precursor of Niobium [34]. This method allows to obtain chemical gels in a wide compositional range (7-37 wt%), characterized by a very high dispersion of Niobium in the matrix, that is an nanometric scale for the content of Nb [34]. These catalysts were active and stable catalyst for the epoxidation of cyclooctene [35].

Nowak et al. [36] synthesized organosilicas containing Niobium (Nb-PMO), which consist of a hybrid material with ethane and octane in niobium- silica framework, where organic and inorganic moieties are distributed homogeneously at molecular level in the framework. These material showed a good activity and selectivity for epoxidation of Fame of sunflower oil.

### 7.1.3 Non-Transition metal-catalyzed epoxidation using hydrogen peroxide

Although the majority of catalytic system for epoxidation with hydrogen peroxide is based on transition metals, main group elements and organic compounds are also known to activate hydrogen peroxide [23]. The latter could be more commercially attractive because no expensive precious metals are required.



### 7.1.3.1 Alumina

The term “Alumina” refers to a series of ionic solids which have the formula  $\text{Al}_2\text{O}_3 \cdot (\text{H}_2\text{O})_n$  where  $n=0$  to 3 [37]. They are derived by heating naturally occurring or synthetic, crystalline and amorphous  $\text{Al}(\text{OH})_3[\text{Al}_2\text{O}_3(\text{H}_2\text{O})_3]$  and  $\text{AlO}(\text{OH})[\text{Al}_2\text{O}_3(\text{H}_2\text{O})]$ . Gibbsite and bohemite, for example, are crystalline  $\text{Al}(\text{OH})_3$  (monoclin) and  $\text{AlO}(\text{OH})$ (ortho-tombic), respectively. The end point in the synthesis, which occurs by heating the materials above  $1100^\circ\text{C}$ , is corundum, one of the hardest substance known and thermodynamically most stable form  $\text{Al}_2\text{O}_3$ . At temperatures below of  $1100^\circ\text{C}$ , a series of transition aluminas can be generated whose structures are dependent on the precursor final temperature and mode of heating. Heating to  $600^\circ\text{C}$ , for example, yields the  $\gamma$  series of aluminas, which contains  $\rho$ ,  $\chi$ ,  $\eta$  and  $\gamma$  types [38].

Usually for catalytic applications, it is necessary to activate the alumina, which is done by thermal dehydration of alumina hydroxide or oxyhydroxide in a temperature of the range of  $250$ – $600^\circ\text{C}$ ,  $\gamma$  series of aluminas are obtained, which include  $\rho$ ,  $\chi$ ,  $\eta$  and  $\gamma$  types [39].

Their principal characteristics are lower crystallinities and more extensive porous structure of the aluminum oxide with large surface area. In alumina activation many factors, such as precursors type, structural properties (crystallinity, crystallite size, and impurities), mode of heating and final temperature, affect the structural properties of the transition aluminas and modify their reactivity in organic reactions.

In 1977, Leffer and Miller [40] showed that different kinds of  $\text{Al}_2\text{O}_3$  react with organic peroxides, yielding  $\text{Al}-\text{OOH}$  surface species, which decompose to  $\text{Al}-\text{OH}$ ,  $\text{O}_2$  and carboxylic acids. The authors also showed that  $\text{H}_2\text{O}_2$  reacts in a similar way, forming water instead of carboxylic acids. About two years later, Rebek and McReady [41] showed that  $\text{Al}_2\text{O}_3$  can be employed in epoxidation however, a large excess of alumina and oxidant were used (molar ratio  $\text{alken}/\text{H}_2\text{O}_2/\text{Al}_2\text{O}_3 \approx 1/10/50$ ). Regarding catalytic epoxidation, alumina showed to be an efficient catalyst for a wide variety of nucleophilic olefins, such as linear, cyclic, substituted and terpenes.

Among the advantages of using alumina as an epoxidation catalyst is that it is non polluting compound and that it is possible use the environmentally friendly oxidant hydrogen peroxide.

However, the properties which the alumina requires to have good catalytic activity are not yet well understood.

Investigations on the alumina system clearly indicate that the reaction takes place at the surface [42, 43]. The reactivity observed for the different substrates are consistent with a “normal” electrophilic mechanism. Apparently the Lewis acid aluminum centre activates the hydroperoxide oxo-group ( $\text{AlOOH}$ ) for electrophilic epoxidation of the alkenes. Sepulveda et al reported good performance for two commercial aluminas and

one produced by the sol-gel method in epoxidations of unsaturated fatty esters using anhydrous or aqueous hydrogen peroxide as oxidant and ethyl acetate as solvent [44]. The aluminas showed a good catalytic activity and selectivity towards the epoxides (conversion of 95% and selectivity 97% obtained after 24h). These results show clearly that alumina is an alternative catalysts for epoxidation of vegetable oil.

Based on this information, and keeping in mind the aim of the intensification of oil epoxidation process with more clean and efficient routes, it was decided to investigate the activity of the following solids in epoxidation reaction with hydrogen peroxide:

1.  $\text{Nb}_2\text{O}_5\text{-SiO}_2$
2. Alumina

## 7.2 Evaluation of $\text{Nb}_2\text{O}_5\text{-SiO}_2$ catalysts in Soybean Oil Epoxidation

### 7.2.1 Introduction

The catalytic activity of  $\text{Nb}_2\text{O}_5\text{-SiO}_2$  solids obtained as described in [34, 35] is tested in soybean oil epoxidation with hydrogen peroxide (60 wt%). Moreover, the acid properties of the catalysts have been evaluated in reaction types such as esterification and transesterification of acid oils.

### 7.2.2 Experimental Section

#### 7.2.2.1 Synthesis of catalysts

The synthesis procedure of the investigated materials is reported in detail elsewhere [34]. Niobium–silicon mixed oxide nanocomposites, whose nominal molar composition can be expressed by the formula  $x\text{Nb}_2\text{O}_5\cdot(1-x)\text{SiO}_2$  with  $x = 0.025, 0.050$  and  $0.10$  were prepared by sol–gel using niobium chloride,  $\text{NbCl}_5$  (99%, Gelest), and tetraethoxysilane,  $\text{Si}(\text{OC}_2\text{H}_5)_4$  (TEOS) (99%, Gelest), as starting materials. Transparent and amorphous hardened dry gels were obtained for all the compositions [34, 35]. The catalysts were obtained by finely grounding the hardened dry gels and then calcining at  $400^\circ\text{C}$  for 3 h. For all samples it was shown that the actual composition was very close to the nominal one [34], therefore hereafter the gel-derived catalysts will be referred to according to their nominal  $\text{Nb}_2\text{O}_5$  content: 2.5Nb (7.12 wt.% Nb), 5Nb (13.2 wt.% Nb), and 10Nb (23.0 wt.% Nb), respectively.

For comparative purpose,  $\text{SiO}_2$  xerogels were prepared under the same conditions.

#### 7.2.2.2 Structural Characterization

The surface structures of the catalysts were studied by diffuse reflectance infrared Fourier transform (DRIFT) spectroscopy. DRIFT spectra were recorded at room temperature using a Perkin Elmer Spectrum One FT-IR Spectrometer (U.S.A) equipped with a diffuse reflectance unit. 0.20 mg of each sample was mixed with 200 mg of KBr (FTIR grade, Aldrich, Chemical, Co., Milwaukee, WI, USA). The mixture was finely ground in an agate mortar and transferred to a sample holder. Its surface was smoothed with a microscope glass slide. In all spectra determinations, 10 scans were collected with a resolution of  $1\text{ cm}^{-1}$ . All spectra, corrected for KBr, are reported in Kubelka-Munk units.

#### 7.2.2.3 Epoxidation Tests

The catalytic performance of the material in epoxidation was tested with soybean oil. Soybean oil, with Iodine Number of 128 ( $\text{g}_{\text{I}_2}/\text{g}_{\text{sample}}$ ) was purchased in a local food-store (the fatty acid composition of this oil, determined by gas-chromatographic analysis, was (% w/w): palmitic = 11, stearic = 4, oleic = 23, linoleic = 56, linolenic = 5, others = 1).

Epoxidation reactions were carried out in a round-bottom three-necked flask equipped with a condenser and thermometer. In a typical experiments 600 mg of catalyst,  $20\text{ cm}^3$  of ethyl acetate, 5 g soybean oil (25 mmol of double bonds), 6.9 g of hydrogen peroxide 60 wt% (12 mmol) was heated under reflux with magnetic stirring.

The final solution was separated from catalyst by decantation and was analyzed to evaluate the double bonds conversion, through the determination of the Iodine Number, and the epoxide yield, through the evaluation of the Oxirane Number, according to the analytical methods reported in Appendix.

#### 7.2.2.4 Transesterification/Esterification Tests

The Transesterification/Esterification reactions have been performed by using a series of vial reactors.

The vials were of stainless steel because the high pressure of methanol (12 bar) achieved in the vials at the high reaction temperature ( $180\text{ }^\circ\text{C}$ ).

2.0 g of soybean oil (containing a known amount of free oleic acid, 10-20% by weight) 0.88 g of methanol and a defined amount of the catalyst (0.1 g) were introduced in each reactor.

All the reactors were fixed at a rotating bar inside a ventilated oven to assure the mixing of the reaction mixture. The temperature of the oven was initially fixed at  $50\text{ }^\circ\text{C}$  for 14 min and then increased at a rate of  $20\text{ }^\circ\text{C}/\text{min}$  up the reaction temperature ( $180\text{ }^\circ\text{C}$ ), the samples have been kept at this temperature for 1 h. At the end of the reaction, the samples were quenched by putting the vials in a cold bath and were analyzed by a

standard acid–base titration procedure for the evaluation of the free residual acidity, as reported in appendix.

The FAME (fatty acid methyl esters) yields ( $Y_{FAME}$ ) were determined with H-NMR technique (Bruker 200 MHz) as reported in Appendix.

### 7.2.3 Discussion and results

The based on niobium solids, whose catalytic activity studied in epoxidation reaction, are resumed in table 7.1 together some data of morphological characterization.

**Table 7.1:** Surface area and pore volume of Nb<sub>2</sub>O<sub>5</sub>–SiO<sub>2</sub> catalysts [34,35].

Catalyst	Nb <sub>2</sub> O <sub>5</sub> (mol%)	SiO <sub>2</sub> (mol%)	Surface Area (m <sup>2</sup> g <sup>-1</sup> )	Pore Volume (cm <sup>3</sup> g <sup>-1</sup> )
2.5Nb	2.5	97.5	369	0.190
5Nb	5	95	159	0.107
10Nb	10	90	164	0.091

#### 7.2.3.1 Soybean Oil Epoxidation

The results of soybean oil epoxidation are reported in Figure 7.2. The obtained double bond conversions are in agreement with that reported previously for cyclooctene epoxidation [35]: the 2.5Nb shows the highest activity and the difference with 5Nb and 10Nb depends on the nature of catalytic sites on the surface.

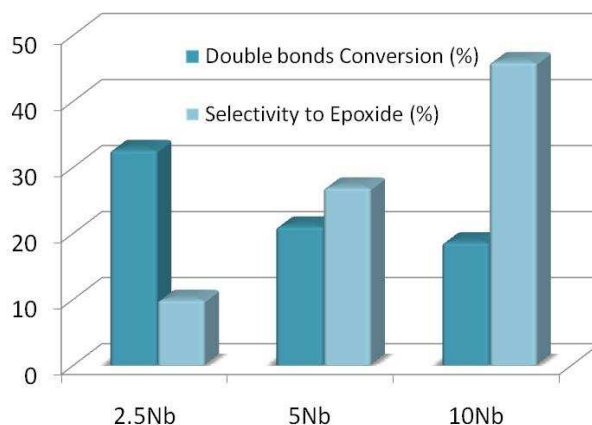


**Figure 7.2:** Soybean oil Epoxidation with hydrogen peroxide catalyzed by different niobium containing catalysts  
Experimental Conditions: catalyst, 600mg; soybean oil, 5g (25mmol double bonds); 40 mmol; H<sub>2</sub>O<sub>2</sub>, 60 mmol; Ethyl Acetate, 20 ml; T=80°C; reaction time=300min

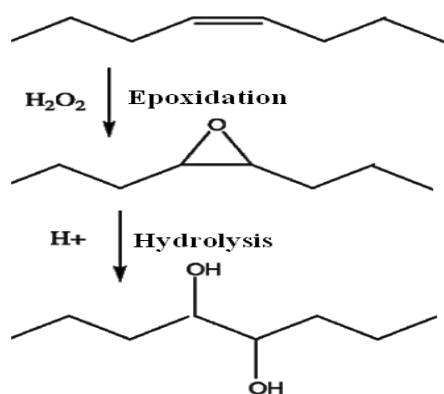
The decrease of catalytic activity in epoxidation with Nb content agrees with the decrease of the concentration of Lewis acid sites of moderate strength (see the previous paragraph) [35]. As a reported previously Lewis acid sites of moderate strength are involved in the mechanism of epoxidation of alkenes with H<sub>2</sub>O<sub>2</sub> [35] and references

therein], while strong Lewis acidity activates the  $\text{H}_2\text{O}_2$  decomposition reaction [42, and references therein].

However, in Figure 7.2 an increase in the selectivity to epoxide with the increase of Nb content can be observed.

The lowering of selectivity to epoxide is due to reaction of epoxide ring with water present in the reaction environment giving place to diol, as displayed in Scheme 7.3.

As this reaction is catalyzed by Brønsted acids [45], the obtained results suggest that on 2.5Nb there are present Brønsted acid sites stronger than those present on 5Nb and 10Nb.



Scheme 7.3

This result can be supported by the analysis of the DRIFT spectra shown in Figure 7.3, where the spectrum of the gel-derived  $\text{SiO}_2$  heat treated in the same conditions of the catalysts (3h at  $400^\circ\text{C}$ ) is also reported.

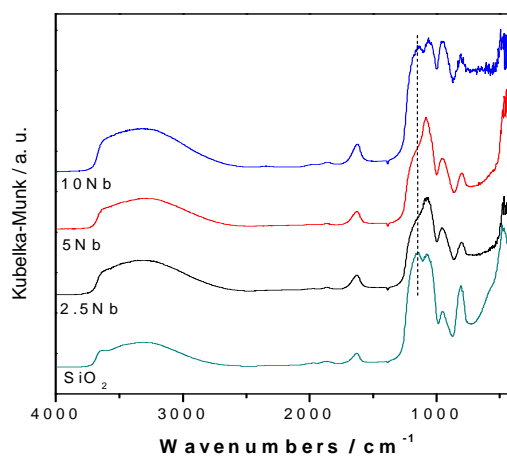


Figure 7.3 : DRIFT spectra of gel-derived  $\text{SiO}_2$  and catalysts heated 3h at  $400^\circ\text{C}$ .

This spectrum exhibits the typical IR bands detected in a  $\text{SiO}_2$  reflectance spectrum. The siloxane network bands at 1147, 1077, 806, 480-430  $\text{cm}^{-1}$  that are related to the longitudinal-optical ( $\nu_{\text{asyLO}}$  Si-O-Si) and the transverse-optical ( $\nu_{\text{asyTO}}$  Si-O-Si) components of the asymmetric stretching of Si-O-Si bridges, the symmetrical stretching of Si-O-Si ( $\nu_{\text{sym}}$  Si-O-Si) and network bending modes ( $\nu_{\text{Si-O-Si}}$ ), respectively [46, 47].

The broad band related to OH groups occurs at about 3300  $\text{cm}^{-1}$  ( $\nu_{\text{O-H}}$ ) and exhibits a shoulder at about 3640  $\text{cm}^{-1}$  indicating the presence of different type of silanols involved in hydrogen bonding of different strength [16]. The corresponding Si-OH stretching modes are seen at 950  $\text{cm}^{-1}$  ( $\nu_{\text{Si-OH}}$ ) and the deformation modes of O-H bonds of molecularly adsorbed water are seen at 1627  $\text{cm}^{-1}$  ( $\nu_{\text{O-H}}$ ) [34].

The comparison with the catalyst DRIFT spectra shows some differences, the most notable of which concern the  $\nu_{\text{asyLO}}$  Si-O-Si and  $\nu_{\text{O-H}}$  modes. The band at about 1147  $\text{cm}^{-1}$  (dashed line in Figure 7.3) almost disappears in the 2.5Nb DRIFT spectrum, is as a shoulder in the 5Nb spectrum and then reappears as a clear peak in the 10Nb DRIFT spectrum (Figure 7.3).

Moreover, in the spectra of the catalysts the high frequency bands of OH groups is wider than that of  $\text{SiO}_2$ , mainly in the low frequency side, and a new component of the band related to  $\nu_{\text{Si-OH}}$  appear at about 960  $\text{cm}^{-1}$ .

These differences mirror the different distribution of structural units on the surface of the catalysts with respect to the  $\text{SiO}_2$ , mainly due to the presence of Nb-OH groups besides the Si-OH ones. This interpretation well agrees with the previous structural characterization of the catalysts performed by Raman and FTIR spectroscopy [34]. It was shown that niobium is uniformly distributed into the siloxane framework of the 2.5Nb and 5Nb while it appears insulated in nanodomains for the 10Nb.  $\text{NbO}_4$  or  $\text{NbO}_6$  isolated species prevail at low Nb content (2.5Nb and 5Nb), while clustering of  $\text{NbO}_6$  octahedra with the disappearance of  $\text{NbO}_4$  tetrahedra occur at higher Nb content [34].

Consequently, the kind of surface acid sites and their distribution change with the niobium content. It was shown, by  $\text{NH}_3$  TPD and FTIR of acetonitrile as adsorbed basic probe, that the catalysts exhibit both Brønsted and Lewis acid sites, whose strength and distribution depend on the niobium content [35]. Particularly, Lewis acid sites with medium, medium-strong strength are seen for all catalysts even if in 2.5Nb there is a slightly higher amount of weaker acid sites than stronger ones. On the contrary, the 2.5Nb catalyst exhibits Brønsted acid sites stronger than the Si-OH ones, while increasing the Nb amount the relative amount of weaker Brønsted acid sites, with a similar acidity to that observed over pure silica, increases.

### 7.2.3.2 Transesterification and Esterification reactions

In order to further investigate the catalytic mechanism, the catalysts were also used in the production of biodiesel (a mixture of fatty acid methyl esters, FAME) starting from soybean oil containing a high concentration of free fatty acids (FFA) and methanol. In this reactive system soybean oil is transesterified by methanol to produce FAME and glycerin, while FFA are esterified by methanol to give again FAME and water. The system is interesting from industrial point of view (as a matter of fact, it is a model of waste oils [48]) but it could also be useful to discriminate the type and the strength of acid sites on a heterogeneous catalyst. In fact, it is well known that the Brønsted acid sites mainly catalyze the esterification reaction, while the Lewis acid sites mainly catalyze the transesterification reaction [48]. In Figure 7.4 the glycerides conversion (related to the activity in transesterification reaction) and the FFA conversion (related to the activity in esterification reaction) are reported.

As can be seen, 2.5Nb does not show activity in transesterification (the correspondent conversion is similar to that of the uncatalyzed run), while this activity increases with the amount of Nb. Instead, the esterification activity is the highest for 2.5Nb catalysts and decreases with the amount of Nb (10Nb shows the same FFA conversion of the uncatalyzed run).

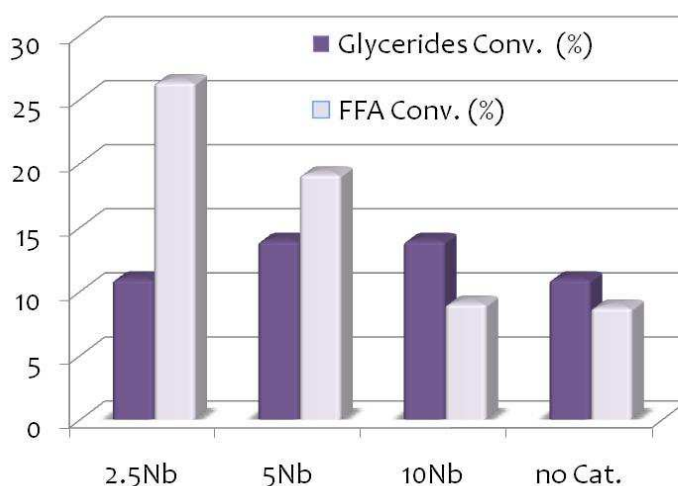


**Figure 7.4:** Activity in Esterification and Transesterification reaction. Experimental Conditions: molar ratio MeOH/Acid Oil (10 wt % Oleic Acid) =12; weight ratio catalyst/oil=0.05 Temperature programme:  $T_i=50^\circ\text{C}$  for 10 min, increase with  $20^\circ\text{C}/\text{min}$  to  $180^\circ\text{C}$ , finally  $T=180^\circ\text{C}$  for 1 h.

These results are in agreement with the catalysts surface characterization. Actually, increasing the Nb content the concentration of stronger Lewis acid sites, which are absent on 2.5Nb, increases. So the Lewis acid sites of moderate strength, which are active in the epoxidation reaction, are not active (in the adopted reaction condition) in

the transesterification reaction. On the other hand, the 2.5Nb catalyst, in which the niobium is highly dispersed into the siloxane framework, has the stronger Brønsted acid sites that can be considered the catalytic sites for the esterification and also for the epoxide ring opening reaction.

#### 7.2.4 Conclusions

The Nb<sub>2</sub>O<sub>5</sub>-SiO<sub>2</sub> catalysts prepared by sol-gel technique confirmed their activity also in the epoxidation with hydrogen peroxide of soybean oil. The trend in the activity with the niobium content was the same observed previously in the case of the epoxidation of cyclooctene [35], being the catalyst with the lowest niobium content (2.5Nb) the most active. However the trend of selectivity to epoxide is inverse. This behavior has been justified by the individuation with FT-IR on the 2.5Nb catalysts surface of hydroxyls with a Brønsted acid strength higher than the one present on the silica surface. By increasing niobium content the concentration of these sites decreases. The Brønsted acid sites can catalyze the reaction of epoxide ring with water forming the diol group.

The presence of strong Brønsted acid sites on 2.5Nb has been confirmed by the esterification runs, being the 2.5Nb also the more active in this reaction.

### 7.3. Alumina as Heterogeneous Catalysts of Soybean Oil Epoxidation

#### 7.3.1 Introduction

As it was shown previously,  $\gamma$ -alumina was found to be an inexpensive and efficient catalyst for the epoxidation of different olefins and that the activity is highly affected by the acidity of the catalyst [42,43]. Good performances were obtained also with methyl oleate and methyl esters of soybean oil [44]. However, no detailed work was conducted with bulkier substrate such as oil.

For this purpose, in present work a comparison of two different alumina in epoxidation of soybean oil with hydrogen peroxide is reported, investigating the influence of chemical - physical properties of the catalysts and of the used solvent on the activity and selectivity.

#### 7.3.2 Experimental

##### 7.3.2.1 Catalysts Characterization

Power x-ray diffraction (XRD) patterns were determined with a Philips 1887 diffractometer, using Cu K $\alpha$  radiation, with a step sizes of 0.02° and counting time of 1 s. Specific surface area of aluminas were determined by BET method using nitrogen adsorption isotherms in Sorptomatic 1990 instrument, using a N<sub>2</sub> adsorption isotherm at 77 K.



### 7.3.2.2 Epoxidation / Solvent Effect Tests

All reactions were carried out in a round-bottom three-necked flask equipped with a condenser and thermometer. In a typical experiments 600 mg of alumina, 20 cm<sup>3</sup> of solvent, 5 g soybean oil (25 mmol of double bonds), 6.9 g of hydrogen peroxide 60 wt% (12 mmol) was heated under reflux with magnetic stirring.

The final solution was separated from catalyst by decantation and was analyzed for determining the iodine number, the oxirane number and the residual unreacted hydrogen peroxide, according to the analytical methods reported in Appendix.

## 7.3.3 Discussion and Results

### 7.3.3.1 Soybean Oil Epoxidation

The pattern XRD of aluminas used for epoxidation reaction confirmed that for all the  $\gamma$ -phase is present. These patterns show very broad peaks indicating small crystallites and amorphous material [49]. Two types of commercial  $\gamma$ -aluminas have been tested in soybean oil epoxidation reaction, which are listed in Table 7.4 together some data of morphologic characterization.

**Table 7.4:** Surface area and pore volume of Aluminas.

Solids	Surface area (m <sup>2</sup> g <sup>-1</sup> )	Pore volume (cm <sup>3</sup> g <sup>-1</sup> )
Al <sub>2</sub> O <sub>3</sub> Enghelard	162	0.461
Al <sub>2</sub> O <sub>3</sub> Enghelard 300°C 3h	159	0.451
Al <sub>2</sub> O <sub>3</sub> Fluka	115	0.312
Al <sub>2</sub> O <sub>3</sub> Fluka 600°C 4h	143	0.267

The results of Soybean oil Epoxidation are reported in Table 7.5 and Figure 7.5. It is interesting to observe that in the case of using alumina, as catalyst, differently from Niobium based catalysts, higher values of activities and selectivities have been reached.

**Table 7.5:** Activities and selectivities of Al<sub>2</sub>O<sub>3</sub> catalysts on the soybean oil epoxidation, for different reaction times. H<sub>2</sub>O<sub>2</sub>/Substrate= 4 (mol/mol); Substrate/Catalyst= (8 g/g). temperature 80°C.

Solids	Time (h)	Conversion (%)	Yield (%)	Selectivity (%)
Al <sub>2</sub> O <sub>3</sub> Enghelard	5	38	23	62
Al <sub>2</sub> O <sub>3</sub> Enghelard 300°C 3h	5	49	47	96
Al <sub>2</sub> O <sub>3</sub> Enghelard 300°C 3h	8	57	49	86
Al <sub>2</sub> O <sub>3</sub> Fluka	5	56	33	59
Al <sub>2</sub> O <sub>3</sub> Fluka	10	73	46	64
Al <sub>2</sub> O <sub>3</sub> Fluka 600°C 4h	5	43	9	20

The Engelhard alumina calcined at 300°C for 3 hours was the most selective (>90%), even if that Fluka seems the most active with a selectivity about 60%.

However the alumina tested for this work seems poor active for epoxidation oil, in fact the results obtained for this reaction, both in terms of conversion and selectivity, are lower than those reported by Sepulveda [44], concerning fatty acid esters epoxidation reaction (conversion = 60% selectivity = 98% after five hours of reaction). These results can be explained considering the use of a different substrate (oil instead of fatty acid esters) and lower specific surface area for the proven alumina (see table, values about 115-162 m<sup>2</sup>g<sup>-1</sup>) than those used by Sepulveda (values between 200-300 m<sup>2</sup>g<sup>-1</sup>). In fact, in most works of literature [42-44] it was confirmed that the catalytic activity of alumina in the epoxidation reaction with hydrogen peroxide is highly dependent on surface properties of the solid. The higher yields were obtained with catalysts with acidity similar but higher specific surface area. It is interesting to note that the yield values found for Engelhard and Fluka aluminas (47, 33 % respectively) are similar to those reported by Suarez [50] for methyl oleate epoxidation reaction (33, 21 %) in presence of alumina with similar specific areas.(162 m<sup>2</sup>g<sup>-1</sup>, 11 m<sup>2</sup>g<sup>-1</sup> for Engelhard and Fluka; 167m<sup>2</sup>g<sup>-1</sup> and 120 m<sup>2</sup>g<sup>-1</sup> for those of Suarez).

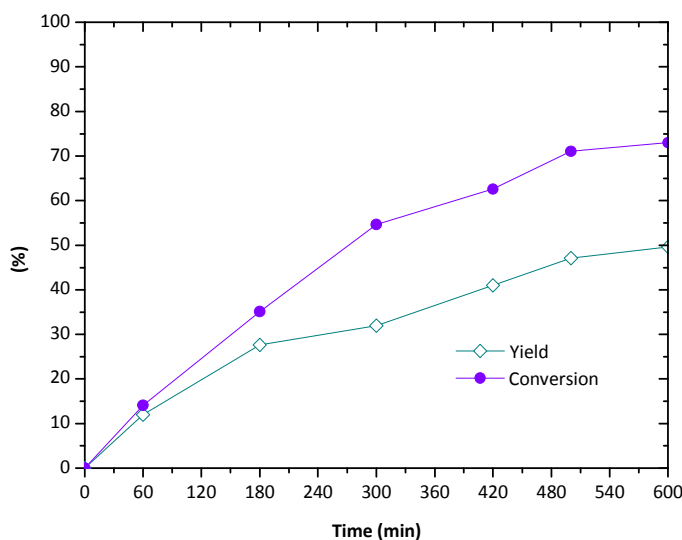
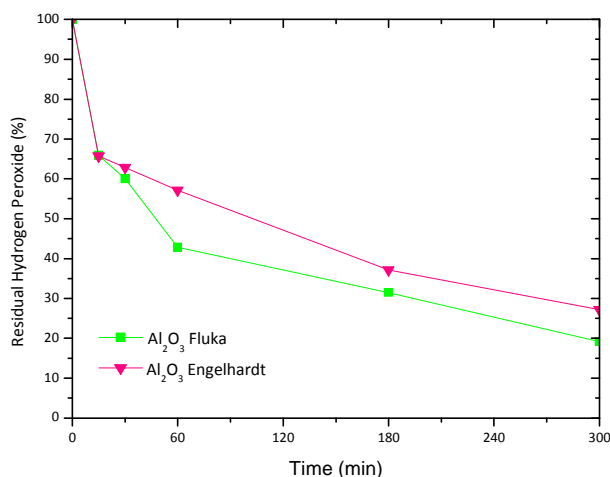


Figure 7.5: Performance of the  $\gamma$ -alumina (FLUKA) catalyst in the epoxidation of soybean oil.

From Figure 7.5 it is evident that the reaction rate decreased probably due to the decrease in hydrogen peroxide concentration, latter decomposed by alumina too.

Regarding this aspect, a test has also been performed to evaluate the H<sub>2</sub>O<sub>2</sub> decomposition during the runs in the presence of Al<sub>2</sub>O<sub>3</sub>. The obtained results are reported in Figure 7.6. As it can be seen, H<sub>2</sub>O<sub>2</sub> gradually decomposed and this explains the loss of activity during the time.



**Figure 7.6:** Hydrogen peroxide decomposition in the presence of alumina

Most of literature works concerning the application of  $\gamma$ -alumina as epoxidation catalyst reported the use of reaction solvent such as ethyl acetate. Only in [43] lower reaction yields in the presence of acetonitrile as solvent are reported. The detection of the characteristic odor of acetic acid in the final product epoxidation reaction in the presence of ethyl acetate as solvent, led to the hypothesis that at the reaction temperature (80 °C) and in the presence of water from the hydrogen peroxide, alumina could promote the hydrolysis of ethyl acetate to acetic acid. Given the highly oxidizing environment, it was assumed that the latter could form peracetic acid, which could then react with the double bonds in the oil. This assumption is agree with the observation that on the surface of the alumina are three different types of sites, only some of which promote the reaction of epoxidation, others can favor the decomposition of hydrogen peroxide and absorb the ethyl acetate promoting in this way the hydrolysis to acetic acid [42].

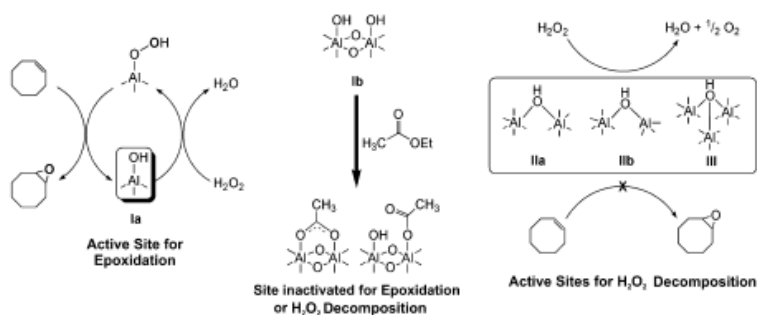


**Figure 7.7:** Scheme of active sites present on the alumina surface and their role in epoxidation reaction with hydrogen peroxide [42].

### 7.3.3.2 Solvent Effect

Based on these considerations have been carried out tests aimed to verify the presence of acetic acid in the epoxidation system in the presence of  $\gamma$ -alumina and ethyl acetate, so that it could support the hypothesis of the dual function of the alumina in the reaction epoxidation, such as:

- 1) epoxidation catalyst
- 2) hydrolysis of ethyl acetate catalyst.

For this purpose several test have been conducted by adopting the same conditions used for epoxidation reactions but in presence of different solvents such as acetonitril and tetrahydrofuran, as listed in table 7.6.

**Table 7.6:** Operative conditions adopted for epoxidation of soybean oil in the presence of alumina catalyst. In any case 20 cm<sup>3</sup> of solvent were used.

Run	T (°C)	Solvent	H <sub>2</sub> O <sub>2</sub> 60wt% (g)	Oil (g)	Alumina (Fluka) (g)
1	77.0	Ethyl acetate	6.9	5.0	0.6
2	77.0	Ethyl acetate	6.9	No oil	0.6
3	77.0	Ethyl acetate	6.9	5.0	No catalyst
4	77.0	Ethyl acetate	6.9	5.0	0.6
5	82.0	Acetonitril	6.9	5.0	0.6
6	66.0	Tetrahydrofuran	6.9	5.0	0.6

Run 1 was taken as reference point, while Run 2, performed in absence of catalyst, showed any activity. Run 3 was carried out in order to verify the acetic acid presence in reaction system. For this purpose, this run was performed in absence of oil and the acidity was evaluated at end of the test trough acid-base titration with KOH (0.00813 N in water). The results clearly indicated that the reaction medium was acid (pH=2.5 and mg<sub>KOH</sub>/mg<sub>campione</sub>=2.8).

To evaluate the formation of peracetic acid by reaction of acetic acid and hydrogen peroxide, hence to react with unsaturated oil the run 4 was performed in two steps: first, the hydrogen peroxide and ethyl acetate were been reacted for 2.5 hours in presence of alumina without oil; secondly, after removal of alumina, the oil was added and the reaction was proceeded for other 2.5 hours. The results obtained at end of the second step (conversion 11% and yield 4.5%) demonstrated that the formation of peracid was occurred, only specie could react with oil.

Further evidences of “no-innocent” role of ethyl acetate in epoxidation with hydrogen peroxide and in presence of alumina as catalyst are reported in Figure 6.8. Latter refers

to the comparison between the results obtained for epoxidation tests in presence of ethyl acetate, acetonitrile and tetrahydrofuran as solvents.

Acetonitrile and tetrahydrofuran were chosen due to their different polarity characteristics (dielectric constant of Acetonitrile=37, dielectric constant of Tetrahydrofuran =7), regarding that the Ethyl acetate was an partial polar solvent with dielectric constant of 6.0.

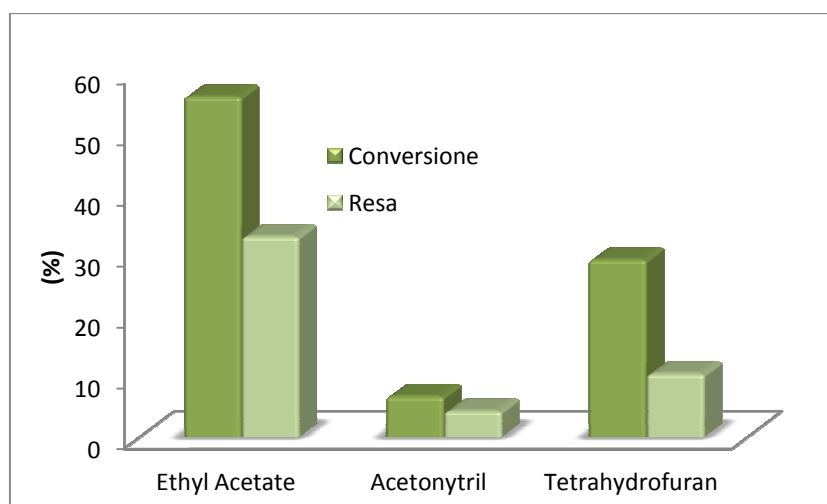


**Figure 7.8:** The comparison between the results obtained for epoxidation tests in presence of ethyl acetate, acetonitrile and tetrahydrofuran as solvents.

The check, through KOH titration, at end of the reaction indicated that in presence of acetonitrile and tetrahydrofuran as solvent the reaction medium was not acid.

### 7.3.4 Conclusions

In this work it is shown that common commercial alumina is active in epoxidation of soybean oil with aqueous hydrogen peroxide as oxidant. However, the selectivities to epoxide are lower than that industrial.

A no innocent role of solvent, like ethylacetate, for epoxidation reaction, it is supposed and demonstrated. As matter of fact, the hydrolysis reaction of ethyl acetate can be possible with formation of acid acetic and successively peracetic acid derived by reaction with hydrogen peroxide. Peracetic acid can react with double bonds of oil according to Prileschajew mechanism.

## References

- [1] A. Rios, P. Weclles, M. Schutter, W.F. Hoeldrerich, *J. Catal.*, 232 (2005) 19.
- [2] 2A. Campanella, M.A. Baltanas, M.C. Capel-Saichez, J.M. Campos-Martin and J.L.G. Fierro, *Green. Chem.*, 6 (2004) 330-334.
- [3] V.V. Gound, A. Patwardhan, S.Dinda, N.C. Pradhan, *Chem. Eng. Sci.*, 62 (2007) 4065.
- [4] R.L. Musante, R.J. Grau, M.A. Baltanas, *App. Catal. A: Gen.*, 197 (2000) 165.
- [5] R. Mungroo, N.C. Pradhan, V.V. Goud, A.K. Dalai, *J. Am. Oil Chem. Soc.*, 85 (2008) 887.
- [6] S.S. Fiser, M. Jankovic, Z.S. Petrovic, *J. Am. Oil Chem. Soc.*, 78 (2001) 725.
- [7] L.A. Rios, D.A. Echeverri, A. Franco, *App. Catal. A: Gen.*, 394 (2011) 132.
- [8] S.T. Oyama, "Mechanisms in Homogeneous and Heterogeneous Epoxidation Catalysis", (2008, ed. Elsevier Science, pp 16.
- [9] K.A. Jorgensen, *Chem. Reviews*, 89 (1989) 431.
- [10] I.W.C.E. Arends, R.A. Sheldon, *App. Catal. A: Gen.*, 212 (2001) 175.
- [11] F. Wattimena, H.P. Wulff, British Patent 1,249,079 (1971) (to Shell).
- [12] R.A. Sheldon, J.A. Vand Doorn, C.W.A. Schran, A.J. De Jang, *J. Catal.*, 31 (1973) 438.
- [13] M. Cozzolino, M. Di serio, R. Tesser, E. Santacesaria, *App. Catal. A: Gen.* 325 (2007) 256-262.
- [14] M. Taramasso, G. Perego, B. Notari, U.S Patent 4,410,501 (1983) (to Enichem).
- [15] B. Notari, *Adv. Catal.*, 41, (1996), 253
- [16] B. Notari, *Catal. Today*, 18, (1993), 163
- [17] U. Romano, A. Esposito, F. Maspero, C. Neri, M.G. Clerici, *Chim. Ind. Milan*, 72, (1990), 610
- [18] M.A. camblor, A. Corma, A. Martinez, J. Perez-Pariente, *J. Chem. Soc. Chem. Commun.*, (1992), 589.
- [19] K.A. Koyano, T. Tatsumi, *Chem. Commun.* (1996) 145-146.
- [20] M. Guidotti, N. Ravasio, R. Psaro, E. Gianotti, S. Coluccia, L. Marchese, *J. Mol. Catal. A: Chem.*, 250 (2006) 218.
- [21] B.S. Lane, K. Burgess, *Chem. Rev.*, 103(7) (2007) 2457.
- [22] G. Venturello, E. Almeri, M. Ricci, *J. Org. Chem.* 48 (1983) 3831.
- [23] I.W.G.E. Arends, R.A. Sheldon, *Top. Catal.*, 19(1) (2002) 133.
- [24] K. sato, A. Aoki, M. Ogawa, T. Hashimoto, R. Noyori, *J. Org. Chem.*, 61 (1996) 8310.
- [25] D.E. De Vos, B.F. Sels, P.A. Jacobs, *Ad. Synth. Catal.*, 345(4) (2003) 457.
- [26] E.J.M. Poli, C.J. Barramet, Y. Ponillox, *Catal. Today*, 140 (2009) 19.
- [27] F. van Laar, D.E. de Vos, B.F. de Sels, P.A. Jacobs, F. Pierard, A. del Guerzo, A. Kirsch-de Mesmaecker, *Chem. Commun.*, (1998) 267.
- [28] F. Somma, P. Canton, G. Strukul, *J. Catal.*, 229 (2005) 490.
- [29] I. Nowak, B. Kilos, M. Ziolek, A. Lewandowska, *Catal. Today*, 78 (2003) 487.
- [30] J.M.R. Gallo, H.O. Pastore, U. Schuschardt, *J. NonCryst. Solids*, 354 (2008) 1648.
- [31] J.E. Wachs, J.M. Jehng, G. Deo, H. Hu, N. Arora, *Catal. Today*, 128 (1996) 199.
- [32] L. dragone, P. moggi, G. Predieri, R. Zanoni, *App. Surf. Sci.* 187 (2002) 82.
- [33] F. Somma, G. Strukul, *Catal. Lett.*, 107 (2006) 73.
- [34] A. Aronne, E. Marennna, V. Califano, E. Fanelli, P. Pernice, M. Trifuoggi, A. Vergara, *J. Sol-gel Sci. Technol.*, 43 (2007) 193.
- [35] A. Aronne, M. Turco, G. Bagnasco, G. Ramis, E. Santacesaria, M. Di Serio, E. Marennna, M. Bevilacqua, C. Cammarano, E. Fanelli, *App. Catal. A: General*, 347 (2008) 179..
- [36] A. Feliczak, K. Walczak, A. Wawrzynczak, I. Nowak, *Catal. Today*, 140 (2009) 23.
- [37] C. Misra, *Amer. Chem. Soc. Washington*, (1986).
- [38] G.W. Kabalka, R.M. Pagni, *Tetrahedron*, 53(24), (1997) 7999.
- [39] J.B. Peri, *J. Phys. Chem.*, 69 (1965) 211.
- [40] J.E. Leffler, D.W. Miller, *J. Am. Chem. Soc.*, 99, (1977), 480.
- [41] J. Rebek, R. McCready, *Tetrahedron Lett.* 45, (1979), 4337.
- [42] R. Rinaldi, F. Y. Fujiwara, W. Holderich, U. Schuchardt, *J. Of Catal.*, 244 (2006), 92.
- [43] R. Rinaldi, J. Sepulveda, U. Schuchardt, *Adv. Synth. Catal.*, 346, (2004), 281.
- [44] J.S. Sepulveda, Texeira, U. Schuschardt, *App. Catal. A: Gen.* 318 (2007) 213.
- [45] F. A. Long, J. G. Pritchard, F. E. Stafford, *J. Am. Chem. Soc.*, 79 (1957) 2362.

- [46] E. L. Lee, I. E. Wachs, *J. Phys. Chem. C*, 111 (2007) 14410..
- [47] E.I Kamitsos, A.P. Patsis, G. Kordas, *Phys. Rev. B*, 48 (1993) 12499.
- [48] M. Di Serio, R. Tesser, L. Pengmei, E. Santacesaria, *Energy & Fuels*, 22 (2008) 207.
- [49] G. Paglia, PhD Thesis, (2004), Curtin University of Tecnology, Perth, Australia (published on line at <http://library.curtin.edu.au/theses/find.html>).
- [50] P. A. Z. Suarez, M. S. C. Percira, K. M. Doll, B. K. Sharma, S. Z. Erhan, *Ind. Eng. Chem. Res.* 48 (2009) 3268.

# Chapter 8

## *Vegetable Oils Transesterification Reaction for Biodiesel Production: General Aspects*

*“Without continual growth and progress, such words as improvement,  
achievement, and success have no meaning.”*

**Benjamin Franklin**

(1706-1790, American Scientist)



### 8.1 Background

The advancing and developing economies are strongly dependent on fossil fuel transportation. It is estimated that within the EU countries around 90% of CO<sub>2</sub> emission between 1990-2010 are attributed to the transport sector [1]. For this reason the European Union and other countries have established specific action plans for the promotion of biofuels in their market, such as the 2003 EU (2003/30/EU) and 2009/28/CE directives, which suggested that all Member States should blend biofuels in conventional fuels at 2% ratio in 2005, which will gradual rise up to 5.75 % in 2010. Biodiesel production and market continually grown in world, especially in Europe. [2]

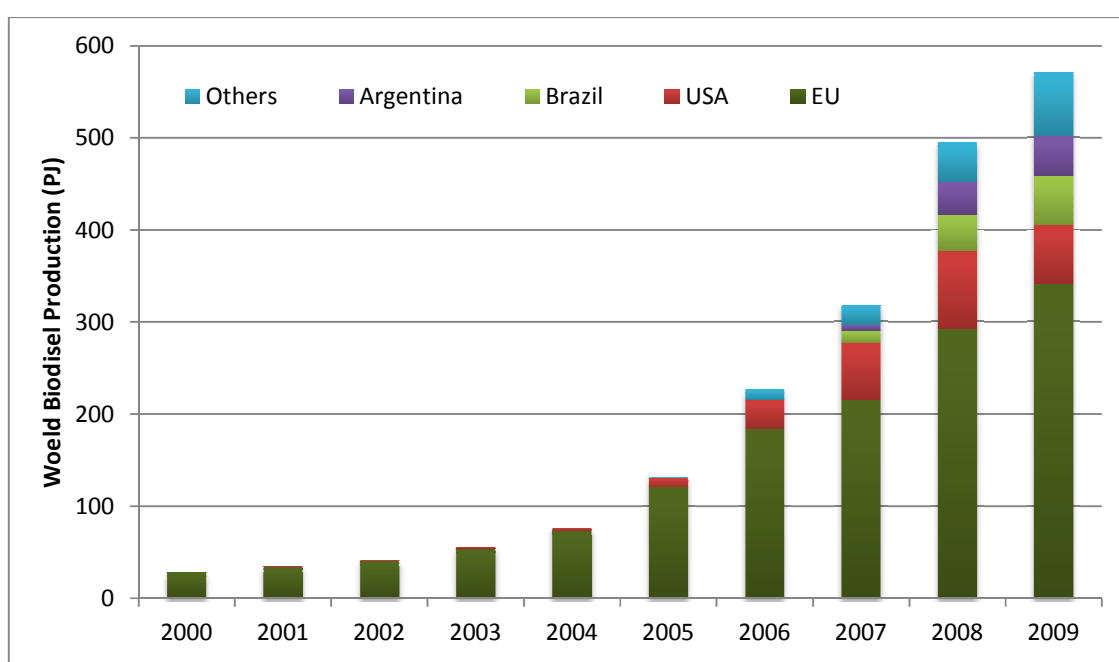


Figure 8.1: Worldwide biodiesel Production, data supplied by EUROSTAT 2009, [2].

Biodiesel is defined, in technical terms, by ASTM as “a fuel comprised of mono-alkylesters of long chain fatty chain acids derived from vegetable oils or animal designated as B100” [3].

However, the term biodiesel is often used to describe blends of biodiesel with petroleum diesel, that are generally referred to as “B2,” “B5,” “B20,” etc., where the number indicates the percent of biodiesel used. Technical properties of biodiesel are given in Table 8.1, while Table 8.2 shows the fuel ASTM standards of biodiesel and petroleum diesel fuels.

Biodiesel has several advantages over fossil fuel. Firstly, the Cetane Number of biodiesel is generally higher than that of the conventional diesel [4], which up to a certain extreme may improve its auto-ignition ability. Also, the biodiesel viscosity is normally

twice as high as that of conventional diesel fuel [5], which is important for lubricity engine.

**Table 8.1:** Technical properties of biodiesel

<b>Common name</b>	Biodiesel (bio-diesel)
<b>Common chemical name</b>	Fatty acid (m)ethyl ester
<b>Chemical formula range</b>	C <sub>14</sub> –C <sub>24</sub> methyl esters or C <sub>15-25</sub> H <sub>28-48</sub> O <sub>2</sub>
<b>Kinematic viscosity range (mm<sup>2</sup>/s, at 313 K)</b>	3.3–5.2
<b>Density range (kg/m<sup>3</sup>, at 288 K)</b>	860–894
<b>Boiling point range (K)</b>	>475
<b>Flash point range (K)</b>	420–450
<b>Distillation range (K)</b>	470–600
<b>Vapor pressure (mm Hg, at 295 K)</b>	<5
<b>Solubility in water</b>	Insoluble
<b>Physical appearance</b>	Light to dark yellow, clear liquid
<b>Odor</b>	Light musty/soapy odor

**Table 8.2:** ASTM standards of biodiesel and petro-diesel fuels

Properties	Test Method	ASTM D975 (petrodiesel)	ASTM D6751 (biodiesel, B100)
Flash point	D93	325 K min	403 K
Water and Sediment	D2709	0.05 max %vol	0.05 max% vol
Kinematic viscosity (at 313K)	D445	1.3–4.1 mm <sup>2</sup> /s	1.9–6.0 mm <sup>2</sup> /s
Sulfated ash	D874	-	0.02 max %wt
Ash	D482	0.01 max %wt	-
Sulfur	D5453	0.05 max %	-
Sulfur	D2622/129	-	0.05 max %
Copper Strip Corrosion	D130	No. 3 max	No. 3 max
Cetane Number	D613	40 min	47 min
Aromaticity	D1319	35 max % vol	-
Carbon Residue	D4530	-	0.05 max %mass
Carbon residue	D524	0.35 max% mass	-
Distillation T (90% volume recycle)	D1160	555 K min–611 K max	-

Overall, the biodiesel is biodegradable, as well as free from sulfur and aromatics [6]. Regarding emissions, biodiesel significantly reduces PM exhaust emissions, which are particularly high in large cities, but slightly NO<sub>x</sub> emission [6]. Unlike fossil fuels, biodiesel, produced from biomass, have the potential to be “carbon–neutral” over their

life cycles, as the carbon dioxide, derived from the combustion and returned to the atmosphere, is absorbed by feedstock crops through photosynthesis [7]. There are some drawbacks for using biodiesel as alternative diesel type fuel. Due to its considerable oxygen content (typically about 11%), biodiesel has lower content of carbon and hydrogen contents compared to petroleum diesel. This results in a reduction in mass energy content of about 10%, causing power decrease and increased fuel consumption [6].

A significant problem of biodiesel is related to cold starts due to its long chains that increase cloud point, pour point, cold-flow plugging point (CFPP).

Clearly the biodiesel quality depends on the feedstock (raw material).

Biodiesel can be produced by transesterification of virtually any triglycerides feedstock. This includes oil-bearing crops, animal fats and algal lipids. The literature contains hundreds of references of biodiesel production from wide variety of feedstock. As shown, in Figure 8.2 [8], the raw material of biodiesel depends greatly on climate, local soil conditions and availability.



Figure 8.2: FAME around the world

Nowadays, however, the dominant feedstock are soybean oil in U.S., rapeseed in EU, and palm oil in Asia [9]. Beef and sheep tallow from animal sources and waste cooking oil are niche market for biodiesel in many regions. Other raw material having commercial interest are jatropha, karanja, corn, [10].

Feedstock acquisition currently accounts for over 75% of biodiesel production costs, which is a serious problems to the economic viability of the biodiesel industry as depicted in Figure 8.3 [8]. Accordingly, the final cost of the biodiesel mainly depends on

the price of feedstock. As vegetable oil price has been increased in recent years, the cost of producing biodiesel will keep raising. Biodiesel will lose its competitive advantage due to high price. Furthermore, problems associated with the impacts on food security and land change have also arisen. It is believed that large-scale production of biodiesel from edible oils may bring about a global imbalance in the food supply-and-demand market.

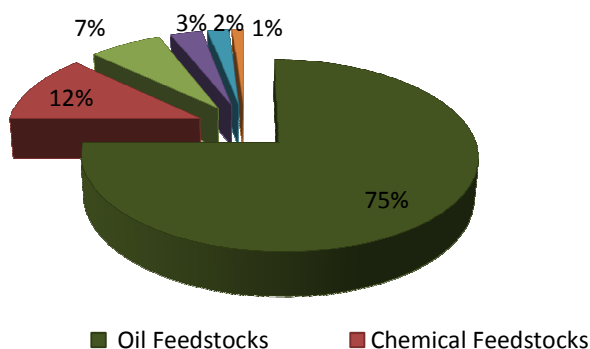


Figure 8.3: Biodiesel production costs

One potential solution to this problem is employment of alternative feedstocks of varying type, quality, and cost. These feedstocks may include acid oils, tall oils, waste cooking oils, various animal fats, non-food vegetable oils, and oils obtained from trees and microorganisms such as algae.

## 8.2 Transesterification Reaction

Most biodiesel is produced today by transesterification of vegetable oils and animal fats with methanol or ethanol in the presence of base or acids catalysts [11]. One molecule of triglyceride reacts with three molecules of alcohols and produces three molecules of esters and one of glycerol, as shown in following figure.

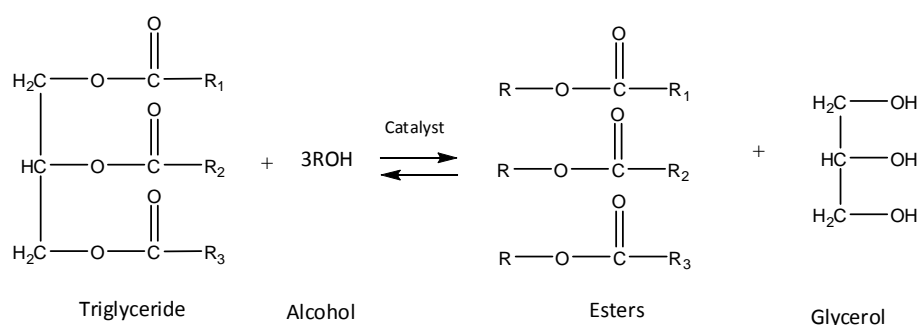


Figure 8.4: Overall transesterification reaction of triglycerides with alcohol, where R-OH-alcohol; R<sub>1</sub>, R<sub>2</sub>, and R<sub>3</sub>-long chain alkyl groups

The mechanism is described below.

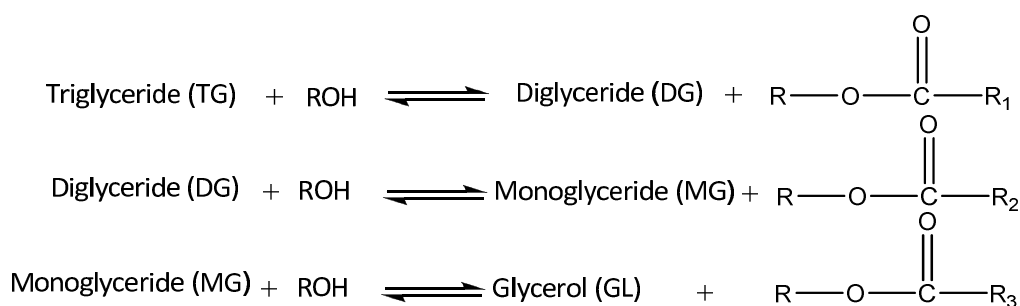


Figure 8.5: Stepwise transesterification reactions of triglycerides with alcohol [12]

The stepwise of the reaction are reversible and a little excess of alcohol is used to shift the equilibrium towards the formation of esters.

Freedman *et al.* [12] first investigated the kinetics of the transesterification of soybean oil (SBO). They determined how some variables including type of alcohol, molar ratio of alcohol to SBO, catalyst type and reaction temperature affected reaction rates. Forward reactions appear to be pseudo-first order or second order depending upon conditions used. Reverse reactions appear to be second order. At a molar ratio of MeOH/SBO of 6:1, a shunt reaction was observed where 3 moles of MeOH directly attacked 1 mol TG resulting in rapid appearance of esters without the appearance of intermediate DG and MG. The values of energy activation ranged from 8 to 20 kcal/mol. Darnoko *et al.* [13] studied the kinetics of transesterification of palm oil with methanol in a batch reactor in the presence of potassium hydroxide. The rate of transesterification in a batch reactor increased with temperature up to 60°C. Higher temperatures did not reduce the time to reach maximal conversion. The conversion of TG, DG and MG appeared to be second order up to 30 mins of reaction time. Reaction rate constants for TG, DG and MG reactions were higher at higher temperatures and higher for the MG reaction than for the TG hydrolysis. Activation energies were: 14.7, 14.2 and 6.4 kcal/mol for the TG, DG and MG hydrolysis reactions, respectively. The optimal catalyst concentration was 1% KOH.

TG and alcohol phases are immiscible and form two liquid layers upon their initial introduction into the reactor. Mechanical mixing is normally applied to increase the contact between the reactants, resulting in an increase in mass transfer rate. Therefore, it is very important to study how the mixing intensity affects the kinetics of the transesterification reaction. Nouredini and Zhu [14] investigated the effects of variations in the mixing intensity and temperature on kinetics of transesterification of SBO with methanol. During the reaction, the molar ratio of methanol to triglycerol (6:1) and the concentration of catalyst (0.2wt% of SBO) were held constant. A reaction mechanism consisting of an initial mass transfer-controlled region followed by a kinetically controlled region was proposed.

### 8.3 Conventional Biodiesel production process

Most of the biodiesel produced today uses the base-catalyzed transesterification reaction, which needs low temperature and pressure, yields high. However, the vegetable oil and alcohol must be substantially anhydrous and have a low FFA content because the presence of FFA promotes soap formation. The soap formation partially consumes the catalyst, lowers the yield of esters and renders the downstream separation of the products difficult [15]. A conventional biodiesel production process is shown in Figure 8.6.

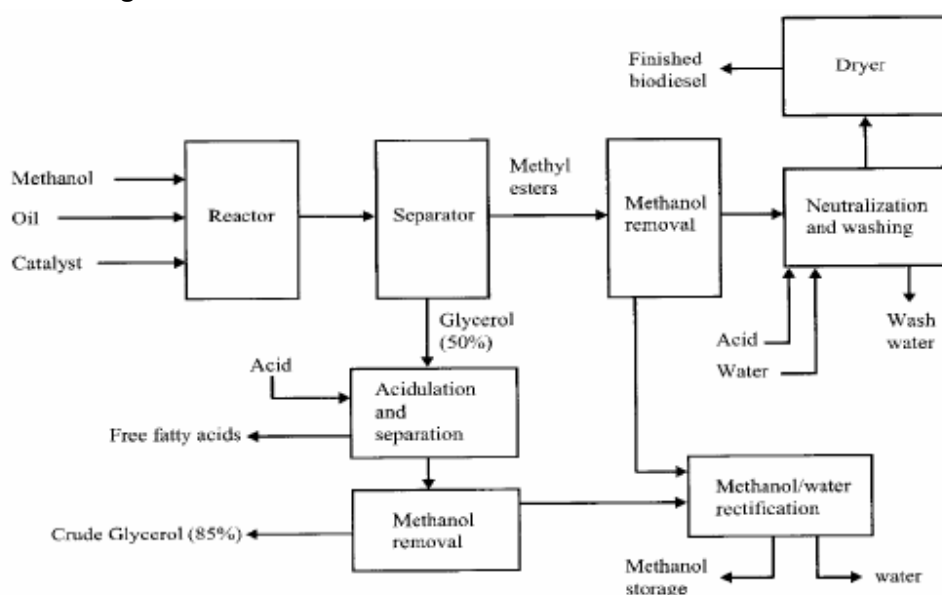


Figure 8.6: General process flow schematic for biodiesel production via base catalyzed transesterification .

The whole process consists of reaction followed by downstream processing. Reaction usually takes place in a continuous stirred tank reactor (CSTR) where the alcohol and catalysts are added into oil in a predetermined molar ratio and catalyst concentration. Following the reaction, the glycerol is removed from the methyl esters. Generally, this separation may be accomplished with either a settling tank or a centrifuge due to the low solubility of glycerol in the esters. Water may be added to the reaction mixture after the transesterification is complete to improve the separation of glycerol. Then, the excess methanol is recycled from methyl ester and glycerol phases for reactant by a vacuum flash process. In order to obtain the desired products, methyl ester and glycerol streams need additional processing procedures including neutralization and water washing in the end.

The current conventional techniques involve long residence time, high molar ratio of alcohol to oil and catalyst concentration, and most of them are run in a batch mode and thus do not gain some of the advantages of continuous operation. Long residence times

and downstream processing time incur low production efficiency. High cost and energy consumption are involved in order to recover excess amounts of alcohol and catalyst, and to deal with the resulting significant amounts of toxic waste water during downstream processing.

#### 8.4 Intensification of Biodiesel Production Process

For current biodiesel production process there are the following limits:

- a. Mass Transfer due to the presence of reactants ( oil and alcohol) in two immiscible phases;
- b. Transesterification itself is a reversible reaction and therefore there is an upper limit to conversion in the absence of product removal;
- c. Most commercial processes are run in a batch mode and thus do not gain some of the advantages of continuous operation.

To overcome these problems the intensification of the technologies involved in biodiesel synthesis is need. Process intensification technologies have significant potential for enhancement in transport processes and higher reaction rates provide the scope for continuous production. Hence higher conversion yields are possible, under milder conditions and involving reduced molar ratios of alcohol to oil, lower reaction temperature and catalyst concentration than conventional stirred reactors.

Some process intensification technologies have been developed and applied to improve mixing and mass/heat transfer between the two liquid phases in recent years. Main goal of those methods is to improve mixing and mass/heat transfer rate between two liquid phases and enhance reaction rate so residence time may be reduces. Some of process intensification technologies are presented in Table 8.3 together with their comparison.

The static mixers can accomplish effective radial mixing as fluids pass trough it. Their biggest advantage is low maintenance and operating cost and low space requirement because they have no moving parts [16]. However, the mixing process relies mainly on slow, unforced molecular diffusion in the laminar regime and therefore reactions in them are still slow. Microchannel reactors improve heat and mass transfer due to short diffusion distance and high volume/surface area so reaction rates achieved in them are rapid. Beside that, because of microreactor size, they offer reductions in construction and operating costs [17].

**Table 8.3:** Comparison of process intensification technologies for continuous biodiesel production with conventional stirred tank reactors.

	Residence Time	Energy Efficiency (g/J)	Operating and Capital Cost	Current Status
Static Mixer	~30 min	14.9-384 [30]	Low	Lab Scale
Micro-channel reactor	28 s-several minutes	0.018 [8]	Low	Lab Scale
Oscillatory flow reactor	30 min	N/A	Low	Pilot Plant
Cavitation reactor	Microseconds-several seconds	$1 \times 10^{-4}$ to $2 \times 10^{-4}$ (hydrodynamic cavitation) $5 \times 10^{-6}$ to $2 \times 10^{-5}$ (acoustic cavitation)	Low	Commercial Scale
Spinning reactor	<1min	N/A	Low	Lab Scale
Microwave reactor	Several Minutes	~0.038 L/kJ [24]	Lower	Pilot Plant
Reactive distillation	1-3h	~ $1 \times 10^{-4}$	Lower	Pilot Plant
Centrifugal Contactator	~1 min	N/A	Lower	Commercial Scale

Oscillatory reactors enhance radial mixing and transport processes by independent and controlled oscillatory motion [18]. In cavitation reactors, the collapse of cavity or bubbles produces high temperature and pressure turbulence locally resulting in rapid reaction rate. Rotating/spinning tube reactors take the advantage that two liquids are mixed instantaneously and moved through the annular gap between two tubes. Under those conditions a coherent thin liquid film is formed that leads to high mass transfer rate and very short mixing time [19]. Microwave reactors utilize microwave irradiation to transfer energy directly into reactants and thus accelerate the rate of chemical reaction [20]. Membrane reactors integrate reaction and membrane-based separation into single process. They achieve high reaction rate by selective removal of bound glycerin from products via a membrane [21]. Reactive distillation combines chemical reactions and product separation by distillation also in one unit. Combination and implementation of centrifugal separation of product and reaction is the main principle of the centrifugal contactor [22]. As the rotor in the contactor rapidly rotates within a stationary cylinder, intense mixing and good mass transfer are achieved together with quick phase separation by high centrifugal force.

In this work the feasibility of intensification of biodiesel production process will attempt through the use of :

- Corrugated Plates Heat Exchanger Reactor (Chapter 9)
- Microreactors (chapter 10)
- Mixer static reactors (chapter 10).



Regarding the particular geometries of selected devices, it is supposed that the mass transfer between the immiscible phases is improved, resulting in high productivity for the process.

**References**

- [1] BIOFRAC (2006) Biofuels in the Europe Union- A vision for 2030 and beyond- EU Biofuels Technological Platform, KI-NA-22066-EN-C.
- [2] EUROSTAT (2009), KS-GH-09-001-EN-C.
- [3] Report No. D6 751-ASTM2008
- [4] B.K. Bala, *Energy, Education, Sci. and Technol.*, 15 (2005) 1.
- [5] M. Balat, *Energy, Ed., Sci. Technol.*, 16 (2005) 45.
- [6] A. Dermibas, *Energy, Conversion, Management*, 50 (2009) 14
- [7] B. Wahlund, J. Yan J, M. Westermarck, *Biomass Bioenergy*, 26 (2004) 531.
- [8] X. Meng, J. Yang, X. Xu, L. Zhang, Q.J. Nie, M. Xian, *Renew Energy*, 34 (2009) 1.
- [9] Biodiesel 2020: global market survey, feedstock trend and forecast, 2<sup>nd</sup> ed. Houston, TX: Emerging Market online, (2008)
- [10] Altun S., *Energy Ed. Sci. Technol.* 26 (A) (2011) 165.
- [11] M. Di Serio, R. Tesser, L. Pengmei, E. Santacesaria, *Energy & Fuels*, 22(1) (2008) 207.
- [12] B. Freedman, R.O. Butterfield, E.H. Pryde, *J. Am. Oil Chem. Soc.*, 63 (1986) 1375.
- [13] D. Darnoko, M. Cheryan, *J. Am. Oil Chem. Soc.*, 77 (2000) 1263.
- [14] H. Nouredдини and D. Zhu, *J. Am. Oil Chem. Soc.*, 74 (1997) 1457.
- [15] B. Freedman, E.H. Pryde, T.L. Mounts, *J. Am. Oil Chem. Soc.*, 61 (1984) 1638.
- [16] J.C. Thompson, B.B. He, Bi, *Trans. ASABE*, 50 (2007) 161.
- [17] Z. Wen, X. Yu, S.-T. Tu, J. Yan, *Bioresour. Technol.*, 100 (2009) 3054.
- [18] A.P. Harvey, M.R. Mackley, T. Seliger, *J. Chem. Technol. Biotechnol.*, 78 (2003) 338.
- [19] [ P.R. Gogate, A.B. Pandit, *Rev. Chem. Eng.* 17 (2001) 1.
- [20] T.M. Barnard, N.E. Leadbeater, M.B. Boucher, L.M. Stencel, B.A. Wilhite, *Energy & Fuels*, 21 (2007) 1777.
- [21] M.A. Dube, A.Y. Tremblay, J. Liu, *Bioresour. Technol.*, 98 (2007) 639.
- [22] [G.J. Harmsen, *Chem. Eng. Process.*, 46 (2007) 774.

# Chapter 9

## *Use of Corrugated Plates Heat Exchanger Reactor for Biodiesel Production*

*"He who is fixed to a star does not change his mind"*

**Leonardo da Vinci**

(1452-1519-1832, Italian Renaissance polymath)

### 9.1 Introduction

As described in previous section, in microreactors, mass and heat transfer are greatly increased due to the small dimensions and large surface area to-volume ratio. Moreover, higher conversion and selectivity are obtained within a shorter reaction time when compared with a batch stirred reactor. Application microchannel reactor to mass-transfer-limited reactions with two-phase systems of immiscible liquid reagents has been reported [1-3]. It has been found that mass transfer across the boundary of immiscible liquids in a microchannel could be significantly enhanced by internal circulation in segmented liquids [2 -5]. Malsch et al.[6] suggested that internal circulation in the segments is induced by the shear force between the two immiscible liquids as well as by liquid/wall friction. Tice et al. [7] found that rapid mixing in droplet-based microfluidic devices could be achieved using internal circulation flow in aqueous droplets separated by oil. Burns and Ramshaw [3, 4] nitrated benzene using immiscible liquid-liquid flow inside a microchannel reactor and found that industrially competitive reaction rates could be realized. Therefore, two-phase flow of immiscible fluids in microchannels shows potential for high-yield processing in chemical engineering.

The transesterification reaction for biodiesel production is a typical two-phase reaction due to the immiscibility of oil and methanol. The rate of transesterification is primarily controlled by the rate of mass transfer between the methanol and oil phases. Stirred batch reactors are used commercially due to their operation flexibility. However, development of a continuous process that will reduce production costs and increase product uniformity for large-scale production would be desirable.

Recently, some works related to the continuous process of Biodiesel production using a microreactor system appeared in literature [8-11]. Canter et al. [8, 9] reported biodiesel yields higher than 90% with a residence time of 4 min in a microchannel reactor, but the operating conditions were not described in detail.

Sun et al. [10] designed a microreactor system for the continuous production of biodiesel and reported that the required residence time was remarkably reduced when a microtube reactor was used instead of a laboratory-scale batch reactor. Similar results were also reported in our previous study. Sun et al. [10] investigated the effects of the methanol to oil molar ratio, residence time, catalyst concentration, reaction temperature, and microtube dimensions on biodiesel yield in detail. However, in the study by Sun et al., the methanol and oil were mixed with catalysts in a stirred batch reactor and the mixture was then injected into the microtube reactor. Therefore, the reaction yield reached approximately 81% before the mixed solution was injected into the microtube.

Recently, thanks to a collaboration between NICL (Naples Industrial Chemistry Laboratories of the University FEDERICO II) and Mythen SpA Co. (a biodiesel producer) a

new continuous reactor having very high performances in terms of productivity and conversion has been developed and patented [12]. The reactor consisted in a corrugated plates heat exchanger reactor (CP-HEX), characterized by a very active local micromixing to enhanced the biodiesel production. The reactor can also be used for other liquid-liquid reactions and more advantageously for very exothermic or endothermic reactions. The reactor can easily be adapted then also for liquid-liquid reaction promoted by solid catalyst and is very flexible for other types of reactions.

The use of CP-HEX reactors, and more generally of heat exchangers reactors, is not a novelty, as can be seen in a review devoted to this topic [13] and represents another example of PI innovation.

The improved heat transfer and mixing performance of the CP-HEX reactors, see Figure 9.1, means that these devices can replace larger conventional reactors, thus reducing plant size and investment costs [14].

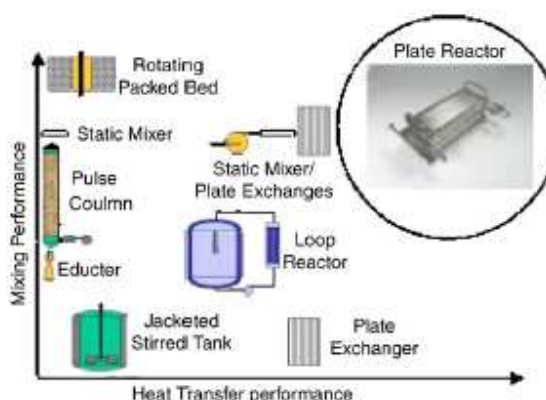


**Figure 9.1:** Heat transfer performance and mixing performance for the OPR and other kinds of chemical reactors [14].

Plate heat exchangers, were introduced in the 1930s and were almost exclusively used as liquid/liquid heat exchangers in the food industries because of their ease of cleaning [15]. Over the years, the development of the Plate Heat Exchangers has generally continued towards larger capacity, as well as higher working temperature and pressure. Successively, a gasket sealing was replaced by a brazed material, and each thermal plate was formed with a series of corrugations (herringbone or chevron). These greatly increased the pressure and the temperature capabilities. The corrugated pattern on the thermal plate induces a highly turbulent fluid flow. The high turbulence in the PHE leads to an enhanced heat transfer, to a low fouling rate, and to a reduced heat transfer area[15].

Clearly, these devices have been mainly proposed for their efficiency in heat exchange. Therefore, heat exchange reactors [14] have mainly been used for highly exothermic

single phase reactions and also characterized for the aspects related to micromixing always related to single phase system. In particular, in the review of Anxionnaz et al. [13] in the section devoted to the corrugated plates exchangers reactors, it is mentioned the necessity to do experiments in the presence of two phase reactions that have never been investigated. Therefore, the element of novelty of our paper is the observation of the micromixing role in promoting a fast liquid-liquid reaction in a CP-HEX reactor. Three simple concepts are the basis of our investigation: (i) increase the temperature as much as possible to obtain a very high reaction rate; (ii) increase the local turbulence (micromixing intensity), favouring mass transfer as much as possible, thereby avoiding the reaction rate limit; and (iii) promote as much as possible the heat exchange. All these conditions can be achieved by using a corrugated plates heat exchanger of opportune geometry and choosing suitable temperatures and pressures sufficiently high to complete the reaction in the short residence time that must be adopted for obtaining a satisfactory micromixing effect inside the plates. A heating/cooling fluid is fed in the plates that are adjacent to the reacting system assuring, as much as possible, a constant temperature to the reaction interspaces. In this work the developed reactor is described in detail, and the obtained performances in biodiesel production will be reported and compared with those obtained with both a conventional well mixed reactor[16, 17] and a microchannel type reactor [18]

## 9.2.Experimental Section

### 9.2.1 Apparatus

The employed reactor was a brazed plate heat exchanger composed of 20 plates opportunely corrugated, as reported in Figure 9.2.

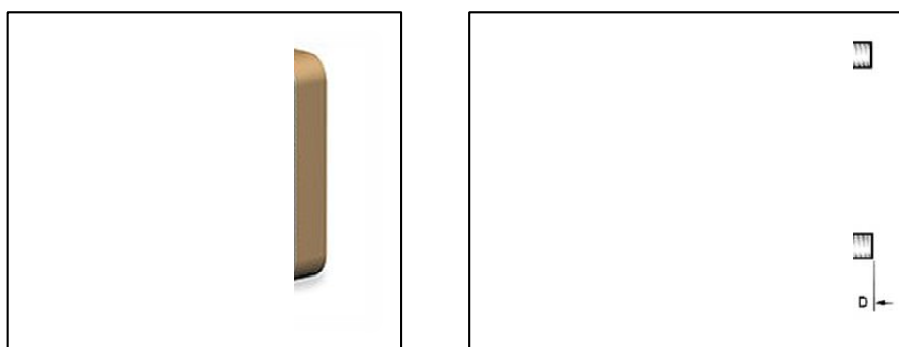


**Figure 9.2 :** Scheme of the brazed plate heat exchanger used for the intensification of biodiesel production. The sizes on the figure are: A= 203 mm; B= 73 mm; C= 200 mm; D= 22mm.

The distance between the plates was about 1.5-2 mm. The interspaces were used with geometrical alternation for flowing respectively the liquid reactants and the thermostating fluid through independent fluid pathways. The main sizes of the device are reported on Figure 9.2. The volume available as reactor is 200 cm<sup>3</sup>, while, the volume in which flowed the thermostating fluid was 250 cm<sup>3</sup>.

### 9.2.2 Reactor Fluid Dynamic Characterization Runs

The reactor has been subjected, first of all, to fluid dynamic characterisation with a step test by using a known concentration of Methylene Blue as tracer to evaluate the minimum flow rate to be used in order to have liquid turbulence between the plates. The concentration of Methylene Blue at the reactor outlet for different flow rates has been determined by a spectrophotometric determination at 664nm of wave length. The initial concentration of the tracer was 12 mg/L.

### 9.2.3 Soybean Oil Transesterification Runs

Soybean Oil transesterification runs have been made by feeding to the described reactor independently, methanol containing the dissolved catalyst (KOH wt 1% with respect to the oil or, in one case sodium methoxide, with the same concentration) and a refined soybean oil. The oil was preheated at the reaction temperature, while, methanol was fed at room temperature. For temperature greater than 60°C and pressure higher than the atmospheric one a tubular pre-heater filled with glass spheres of 4 mm of diameter has been used. A scheme of the plant used is reported in Figures 9.3, 9.4, while, in Table 9.1 all the runs performed are reported together with the experimental conditions adopted in each case.

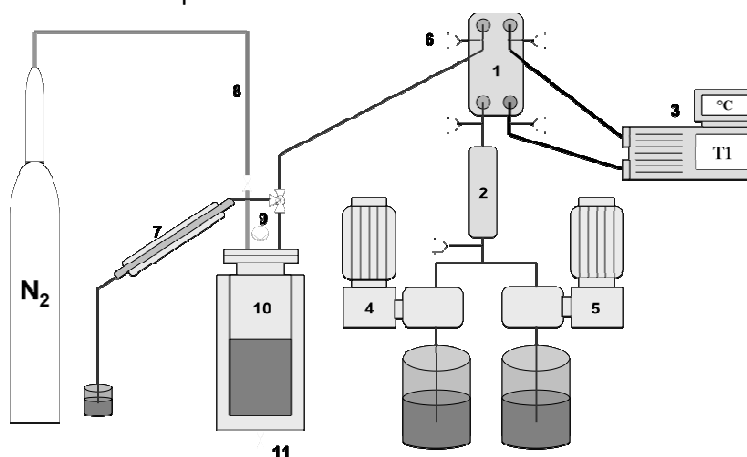


**Figure 9.3 :** Scheme of the plant used. (1) Reactor; (2) Pre-heater (used only for  $T > 60^{\circ}\text{C}$ ); (3)Thermostat; (4) Pump for the soybean oil;(5) Pump for methanol+catalyst; (6) Thermocouples; (7) Condenser; (8) Nitrogen line; (9)Purge; (10) Reservoir; (11) Samples withdrawing



Figure 9.4: Picture of the plant used.

Table 9.1: List of the runs performed and related experimental conditions

Run	T(°C)/ P (bars)	Oil flow rate (cm <sup>3</sup> /min)	Methanol flow rate (cm <sup>3</sup> /min)	Residence time (min)	Methanol/Oil ratio (mol/mol)	Catalyst/ concentration (g/g oil)
1	60/1	31.8	8.2	5	6	KOH / 0.01
2	60/1	79.5	20.5	2	6	KOH / 0.01
3	60/1	159	41	1	6	KOH / 0.01
4	90/3	159	41	1	6	KOH / 0.01
5	90/3	318	82	0.5	6	KOH / 0.01
6	90/3 (second stage)	318	82	0.5	6	KOH / 0.01
7	60/1	318	82	0.5	6	NaOMe/ 0.01
8	25/1	318	82	0.5	6	KOH / 0.01



The FAME (fatty acid methyl esters) yields, were determined by using  $^1\text{H-NMR}$  technique (GEMINI 200 Mz), [19] as reported in Appendix. In some particular cases the conversion values were confirmed by gas-chromatographic analysis[ UNI 10946:2001], (Appendix).

## 9.3 Results and discussion

### 9.3.1 Reactor fluid dynamic characterization

The reactor, before use, was submitted to a fluid dynamic characterization. The results of this characterization are summarized in Figure 9.5, where the dimensionless tracer concentrations ( $C/C^0$ , where  $C^0$  is the inlet concentration and  $C$  is the outlet measured concentration) are reported as a function of the dimensionless time ( $t/t_R$ , where  $t_R$  is the residence time) for three different volumetric flow rates.

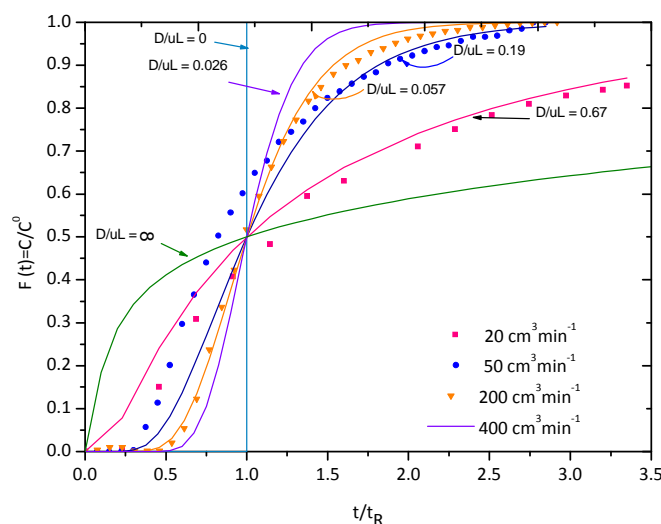


**Figure 9.5:** Dimensionless concentrations of the tracer at the reactor outlet for different flow rates.

An additional curve, obtained by extrapolation, corresponding to  $400 \text{ cm}^3/\text{min}$  is reported. This flow rate has been considered because it is experimentally used as the overall flow rate in the transesterification runs. In the same plot is also reported, for a useful comparison, the ideal behaviors of plug flow ( $D/uL=0$ , where:  $D/uL$ =intensity of axial dispersion,  $u$ =linear fluid velocity,  $L$ =reactor length,  $D$ =axial dispersion coefficient). An approximate estimation of the axial dispersion intensity number, which reciprocal is often called the Peclet number, can be evaluated by considering, for the curves of Figure 8.5, the slopes at  $t/t_R=1$ , according to the relation 2 from [20]:

$$\left[ \frac{dF(t)}{d(t/t_R)} \right]_{t/t_R} = \frac{1}{2} \sqrt{\frac{uL}{\pi D}} \quad (1)$$

where  $F(t)=C/C^0$ . The estimated values for  $uL/D$  at 20, 50, and 200  $\text{cm}^3/\text{min}$  were about 1.8, 5.2, and 18, respectively. A more accurate evaluation can be made by solving the equation [20]:

$$F(t) = \frac{1}{2} \left\{ 1 - \operatorname{erf} \left[ \frac{1}{2} \sqrt{\frac{uL}{D}} \left( \frac{1-t/t_R}{\sqrt{t/t_R}} \right) \right] \right\} \quad (2)$$

Where erf is the standard error function corresponding

$$\operatorname{erf}(x) = \frac{2}{\sqrt{\pi}} \int_0^x e^{-y^2} dy \quad (3)$$

In Figure 9.5, we can appreciate the obtained fitting for the three dynamic tests performed. The best fitting has been obtained for the highest flow rate because the curve becomes symmetrical. The  $D/uL$  numbers evaluated with the simulation are 0.67, 0.19, and 0.057, respectively, in correspondence of 20, 50, and 200  $\text{cm}^3/\text{min}$ . It was not possible to increase further the flow rate for the experimental difficulty of withdrawing many samples to be analyzed in a very short time. However, starting from the obtained  $uL/D$  values, it is possible to evaluate the dispersion factor  $D$  for each case.

We obtained a value that is nearly constant in the experimented range, varying from 13 to 15  $\text{cm}^2/\text{min}$ . It is, therefore, possible to extrapolate the  $F(t)-t/t_R$  plot for higher flow rates. For example, as some kinetic runs of transesterification have been performed, as it will be seen, at an overall flow rate of 400  $\text{cm}^3/\text{minute}$ , an extrapolated curve at this flow rate is always reported on Figure 9.5. As it can be seen, in this case  $D/uL=0.026$  approaching more and more the ideal plug flow behavior. Then, it is interesting to point out that the Reynolds numbers ( $Re$ ) for the highest flow rates of 200 and 400  $\text{cm}^3/\text{min}$  resulted to be about 9 and 17, respectively. This means that a high intensity micromixing is operative in the tested CP-HEX (see Figure 9.6) with formation of many eddies between the plates.

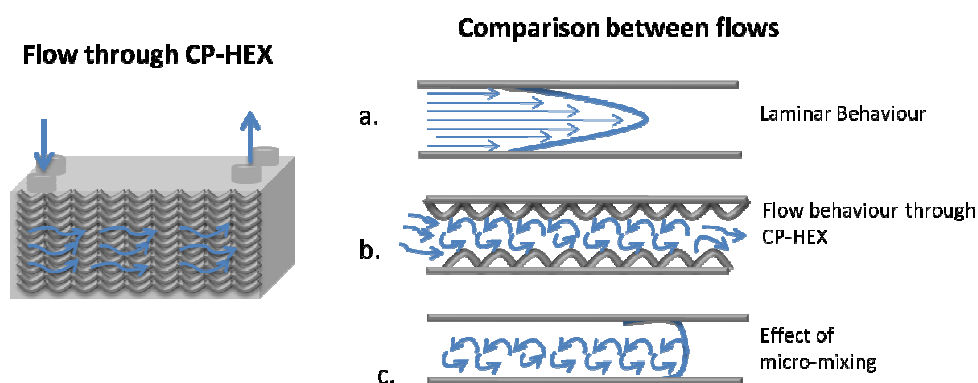


Figure 9.6: Micromixing effect between two corrugated plates.

A passive mixing occurs at a microscale with the formation of small droplets of a phase dispersed in the other one. As it will be seen, the micromixing effect will be evident also in the presence of two immiscible reacting liquids such as methanol and soybean oil, because the reaction rates obtained in the CP-HEX reactors are very high if compared with the well mixed batch reactors.

Although, some papers have been published on the micromixing occurring for a single liquid phase in a corrugated heat exchanger [21, 22] no paper has been published considering this aspect for the immiscible liquids [13], since the problem is very complex.

### 9.3.2 Reactor Performances

Kinetic runs of transesterification have been made, first of all, at different residence times of 5, 2, and 1 min by setting the temperature at 60 °C and the pressure at 1 bar. All the experimental conditions are summarized in Table 9.1. The obtained results are reported in Tables 9.2-9.4.

**Table 9.2:** Results obtained for an overall flow rate of 40 cm<sup>3</sup>/minute, mean residence time 5 minutes. Other conditions 60°C and atmospheric pressure.

Run	Time (minutes)	Yields in methylesters (%)
1	15	54.5
1	30	54.5
1	45	54.5
1	60	54.5

**Table 9.3 :** Results obtained for an overall flow rate of 100 cm<sup>3</sup>/minute, mean residence time 2 minutes. Other conditions 60°C and atmospheric pressure.

Run	Time (minutes)	Yields in methylesters (%)
2	5	50.3
2	10	54.5
2	15	57
2	30	61.5

**Table 9.4 :** Results obtained for an overall flow rate of 200 cm<sup>3</sup>/minute, mean residence time 1 minutes. Other conditions 60°C and atmospheric pressure.

Run	Time (minutes)	Yields in methylesters (%)
3	5	64
3	10	69
3	15	72
3	30	78

Data reported for each run correspond to the yields obtained at different working time. As it can be seen, in some cases (runs 2 and 3) a transient behavior is initially observed before reaching the steady state conditions, occurring after more than 30 min, while, in the case of run 1 (Table 9.2) steady state has been promptly reached after 15 min and the conversion remained constant after this time. It is then surprising that by strongly decreasing the residence time the yields in methylesters significantly increases, as it can be appreciated in Figure 9.7.

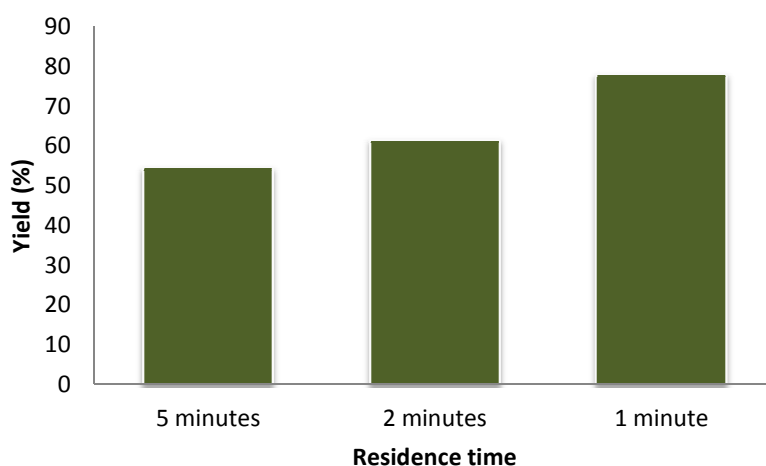


**Figure 9.7:** A comparison of the performances obtained by the CP-HEX for different mean residence times.

Other kinetic runs have then been performed, at higher temperatures and pressures, in the hope to further improve the reactor performances. At this purpose, runs have been made at 90 °C and 3 bar with residence times of 0.5 and 1 min. The other operative conditions are also reported in Table 9.1. The obtained results confirmed our expectation, as it can be appreciated in Table 9.5.

**Table 9.5** : Results obtained for overall flow rates of 200 and 400 cm<sup>3</sup>/minute, mean residence time 1 or 0.5 minutes. Other conditions 90°C and pressure 3 bars.

Run	Time (minutes)	Yields in methylesters (%)
4	60	85
5	30	88

Again by increasing the flow rates the yields in methylester increases, too. This can be explained by assuming that a high local turbulence allows to operate in chemical regime without mass transfer limitation between the two immiscible liquid phases. Moreover, by increasing the temperature from 60 to 90 °C the reaction rate strongly increases and the obtained performances are consequently greater.

The biodiesel obtained in the run 5 has been submitted to a second stage of reaction (run6), in the same conditions, after the separation of glycerol, by using fresh methanol and catalyst obtaining a yield of 96%.

As it has been seen, despite the high reaction rates observed the yields remains in the first stage under 90%. This is probably due to the use of KOH as catalyst that undergoes to the formation of the corresponding methoxide and water giving then hydrolysis and saponification reaction. As a matter of fact, by performing the same reaction, at 60°C, in the presence of sodium methoxide (run 7) with a residence time of 30 seconds a conversion of 98% was obtained. By performing the gas-chromatographic analysis the following composition the biodiesel produced has been obtained: methylesters 98.34%, monoglycerides 1.11 %, diglycerides 0.2%, triglycerides 0.3%.

### 9.3.3 The kinetic approach and the comparison with other reactors

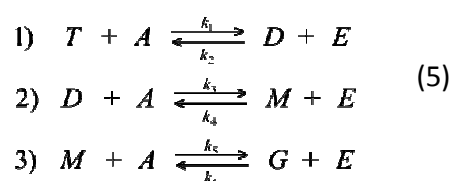
To have the possibility to compare the performances of the previously described CP-HEX with the ones of a microchannels reactor, reported in the literature, a run has been performed at room temperature, corresponding to 25 °C. The operative conditions are also reported in Table 9.1 (run 8). The obtained methylesters yield was about 50% for a residence time of 30 s. A microchannels reactor, operating in the same conditions, reported a comparable conversion of about 30% [18]. This means that a simpler and cheaper device like a CP-HEX, with a suitable fluid dynamic regime, gives performances comparable with those of microchannels reactors. However, the microchannel reactors

have a completely different fluid-dynamic behavior, where the two liquids flows are segmented [10]. The comparison with a well mixed traditional reactor can be made by considering the papers that have been published on the literature related to the kinetics of the reaction [17, 23-28]. Some of these papers report data that are clearly affected by mass transfer limitation, because the reaction occurs in a range of 20-30 min. More realistic data have been collected in the most recently published papers where the reaction occurs in a time range of 2-3 min [24-27].

All the data have been collected in batch well mixed reactors using different types of oils and NaOH or KOH as catalyst, in the temperature range between 20 and 65 °C. In particular, Stamenkovic et al. [17] have shown the role of methanol drop size in the mass transfer limitation, in particular in the initial part of the run when the reaction rate is very high. At last, very recently Mahamuni et al. [29] have shown that with the use of a multi frequency ultrasonic reactor higher yields in biodiesel production can be achieved. As it is well-known that high intensity ultrasound improves emulsification and micromixing of two immiscible liquids such as methanol and oil; this finding supports our suggestion that the micromixing is the main responsible of the high performances obtained in the described CP-HEX reactor. This means that it is not easy, for a well mixed batch reactor, to reach the condition of chemical regime, especially in the initial part of the run, when the reaction rate is relatively high, and also at low temperature for the high viscosity of the oil. To give a more quantitative approach to the behavior of the CP-HEX reactor we have elaborated the following plug flow kinetic model:

$$\begin{aligned} r_1 &= k_1 C_{\text{cat}} C_T C_A - k_2 C_{\text{cat}} C_D C_E \\ r_2 &= k_3 C_{\text{cat}} C_D C_A - k_4 C_{\text{cat}} C_M C_E \\ r_3 &= k_5 C_{\text{cat}} C_M C_A - k_6 C_{\text{cat}} C_G C_E \end{aligned} \quad (4)$$

where  $r_1$ ,  $r_2$ , and  $r_3$  represent, respectively, the rate of reactions



with T=triglycerides, D=diglycerides, M=monoglycerides, G=glycerol, E=methyl ester, and A=methyl alcohol.  $C_{\text{cat}}$  is the catalyst concentration estimated to be 0.129 M, considering 1% of KOH in methanol. The mass balance, related to each component, performed on infinitesimal volume, are reported in the following equations:

$$\begin{aligned}
Q \frac{dC_T}{dV} &= -r_1 \\
Q \frac{dC_D}{dV} &= r_1 - r_2 \\
Q \frac{dC_M}{dV} &= r_2 - r_3 \\
Q \frac{dC_G}{dV} &= r_3 \\
Q \frac{dC_E}{dV} &= r_1 + r_2 + r_3 \\
Q \frac{dC_A}{dV} &= -r_1 - r_2 - r_3
\end{aligned} \tag{6}$$

where  $Q$  is the volumetric flow rate.

By assuming, as a first approximation, the absence of any mass transfer limitation and by adopting the kinetic constants derived from the papers published by Vicente et al. [16, 25] opportunely re-elaborated, we have made calculations to simulate, with this model, the behavior of the CP-HEX reactor in different conditions. Data from Vicente et al. [16] collected in batch reactors, are the best found in the literature, because, as a consequence of the high stirring rates of the impeller (600 rpm), high reaction rates have been obtained. The authors correctly calculated a list of apparent rate constants for runs performed at different temperatures and catalyst concentrations. Unfortunately, the elaboration of these constants to obtain activation energies and preexponential factors of the different involved reactions is wrong, and we have recalculated these parameters for both sunflower and Brassica carinata oils. The correct parameters are reported in Table 9.6.

**Table 9.6:** Kinetic Parameters Related to the Three Reactions (4)<sup>a</sup>

Constant	Sunflower Oil		Brassicata carinata Oil	
	$E_A$ (J/mol)	$K_0$ ( $L^2 mol^{-2} min^{-1}$ )	$E_A$ (J/mol)	$K_0$ ( $L^2 mol^{-2} min^{-1}$ )
$k_1$	67888	$7.16 \times 10^{11}$	68846	$1.06 \times 10^{12}$
$K_2$	81232	$6.25 \times 10^{14}$	81463	$7.22 \times 10^{14}$
$K_3$	98887	$8.03 \times 10^{17}$	95578	$2.17 \times 10^{17}$
$K_4$	110294	$7.00 \times 10^{19}$	106228	$1.61 \times 10^{19}$
$K_5$	14707	1020	14268	848

<sup>a</sup> Kinetic constant  $k_6$  of the reverse reaction has not been considered. These parameters have been calculated from data by Vicente et al [16, 25] related to transesterification of sunflower and Brassica carinata oils.

As it can be seen, the obtained parameters, as expected, are very similar for the two types of oils, since they are the same reaction and catalysts and because the chemical oil compositions are not very different. The parameters of Table 9.6 have been used to

simulate the conversions of our reactor and the obtained results are reported, for three different temperatures, in Table 9.7 in comparison with the experimental data. The numerical method used for integrating the balance eqs 6 was the fourth-order Runge-Kutta method implemented by Berkeley- Madonna software [32]. The conversions obtained by calculations, related to 90 °C, have been obtained by extrapolating the kinetic constants of Table 9.6 at that temperature, that is, out of the field of experimentation (25-65 °C).

**Table 9.7:** A Comparison between Experimental and Calculated Data with a Plug Flow Model and the Kinetic Constant Derived from Vicente et al.[16, 25]

run	Temperature (°C)	Residence time (s)	Experimental yields (%)	Calculated yields (%) [11]	Calculated yields (%) [11]
8	25	30	50	13	20
3	60	90	78	65	64
5	90	60	88	56	54

As it can be seen, in all the considered cases the kinetic constants seem underestimated. This means that despite the high stirring rates used in the batch stirred reactors, a diffusional limitation is always operative at least in the initial part of the runs in batch conditions. However, the greatest differences between experimental and simulated conversions have been observed at low temperature. We attribute this large difference to the very low interface area that can be developed in the batch reactors at low temperature as a consequence of the high oil viscosity that does not favor the two phases mixing. On the other hand, the observation that the experimental conversions, obtained by using a CP-HEX, are always higher than the corresponding values obtained by simulation using the kinetic constants derived from runs performed in batch reactors, means that our system approaches much more the chemical regime. Another important observation is that mixing is clearly more active in CP-HEX than in a well stirred batch reactor. This confirms a very efficient micromixing inside the corrugated plates. This last phenomenon merits to be further deepened, and it will be the object of our further investigations. Until now, micromixing effects in this type of reactors have been studied by few authors,[13, 30, 31] but only on a single-phase system. This is the first work considering the performances of a CP-HEX reactor with immiscible liquid-liquid reactants. At last, it would be interesting to explore the behavior of the CP-HEX reactor for a wider range of residence times, obviously increasing the overall flow rates, but this is difficult to do on a laboratory scale due to the large amounts of reactants that are necessary.



#### 9.4 Possibilities of a More General Use of the CP-HEX Reactors for Other Reactions

As it has been seen, by using a plates heat exchanger with corrugated plates, it is possible to increase very much the productivity of biodiesel. A simple calculation for the case in which sodium methoxide (run 7) has been used as catalyst shows a productivity of 420 kg/day of biodiesel with a reactor of 450 cm<sup>3</sup> of total volume and 200 cm<sup>3</sup> of working volume. By increasing the temperature and optimizing the flow rate, a greater productivity can probably be achieved. Transesterification is an optimal test reaction for a plates reactor, because is an athermic reaction, so we can isolate the effect of micromixing from that of heat transfer. However, many other liquid-liquid reactions can be performed in a similar device. In particular, there are many advantages in using corrugated plates heat exchangers when the reactions are highly exothermic or endothermic, because in these cases we have both a high heat and mass transfer rates [12]. There is also the possibility of using an heterogeneous catalyst by depositing it on the walls or by introducing the catalyst in the form of small pellets or spheres in the reaction interspaces [12]. The presence of pellets or sphere between the plates can further favor the local turbulence and allows the use of lower flow rates for reaching the ideal plug flow conditions. The filling material can also be an inert material having only the scope of positively modify the fluid dynamic characteristic of the reactor [12]. Obviously, in these cases heat exchangers with removable plates must be used instead of brazed plates.

## References

- [1] K. Morgenschweis, *Catal. Today*, 433 (2003) 79.
- [2] M.N. Kashid, I. Gerlach, I. S. Goetz, J. Franzke, J.F. Acker, F. Platte, D.W. Agar, S. Turek, *Ind. Eng. Chem. Res.* 44 (2005) 5003.
- [3] J.R. Burns, J. R.; Ramshaw, C. *Lab Chip*, 1 (2001) 15.
- [4] J. R.; Burns, C. Ramshaw, *Trans. IChemE* 77 (A) (1999) 206.
- [5] S.A. Khan, A. Guñther, M.A. Schmidt, K.F. Jensen, *Langmuir*, 20 (2004) 8604.
- [6] D. Malsch, M. Kielpinski, R. Merthan, J. Albert, G. Mayer, J.M. Kohler, H. Susse, M. Stahl, T. Henkel, *Chem. Eng. J.*, 135S, 2008, S166.
- [7] J.D. Tice, H. Song, A.D. Lyon, R.F. Ismagilov, *Langmuir*, 19 (2003) 9127.
- [8] N. Cater, *Tribol. Lubr. Technol.*, 60 (2004) 16
- [9] , N. Cater. *Tribol. Lubr. Technol.*, 62 (2006) 15.
- [10] J. Sun, J. Ju, L. Ji, L. Zhang, N. Xu, *Ind. Eng. Chem. Res.*, 47 (2008) 1398.
- [11] G. Guan, K. Kusakabe, N. Sakurai, K. Moriyama, *Ind. Eng. Chem. Res.*, 48 (2009) 357.
- [12] E. Santacesaria, M. Di Serio, R. Tesser, R. Turco, D. Verde, L. Casale Italian Patent assigned to MYTHEN SpA Co. N. MI2008A002302, Dec. 2008.
- [13] Z. Anxionnaz, M. Cabassud, C. Gourdon, P. Tochon, *Chem. Eng. Process.*, 47 (2008,) 2029..
- [14] S. Haugwitz, P. Hagander, T. Nore'n, *Control Engineering Practice*, 15 (2007) 779..
- [15] D. Han, K.J. Lee, Y.H. Kim J. Korean, *Phys. Soc.*, 43(1) (2003) 66..
- [16] G. Vicente, M. Martinez, J. Aracil, *Energy Fuels*, 20 (2006) 1722.
- [17] O.S. Stamenkovic, Z.B Todorovic, M.L. Lazic, V.B. Veljkovic, D.U. Skal, *Bioresourc. Technol.* 99 (2008) 1131.
- [18] G.N. Jovanic , B. K. Paul, J.Parker, A. Al-Dhubabian, PCT No. WO2007142983, Dec. 13, 2007.
- [19] G. Gelbard, O. Bres, R.M. Vargas, F. Vielfaure and U.F. Schuchardt, *J. Am. Oil Chem. Soc.*, 72 (1995) 1239.
- [20] Hill, C. G. An Introduction to Chemical Engineering Kinetic and Reactor Design; John Wiley & Sons: 1977, p 404.
- [21] J. Nilsson, F. Sveider, [www.chemeng.lth.se/exjobb/002.pdf](http://www.chemeng.lth.se/exjobb/002.pdf), (2002).
- [22] S. Ferrouillat, P. Tochon, H. Peerhossaini, *Chem. Eng. Process.*, 45 (2006) 633.
- [23] H. Nouredini, D.J. Zhu, *Am. Oil Chem. Soc.*, 74 (1997) 1457.
- [24] D. Darnoko, M. Cheryan, *J. Am. Oil Chem. Soc.* 77 (2000) 1263.
- [25] G. Vicente, M. Martinez, J. Aracil, A. Esteban, *Ind. Eng. Chem. Res.*, 44 (2005) 5447.
- [26] T. Leevijit, W. Wisutmethangoon, G. Prateepchaikul, C. Tongurai, M. Allen, The Joint International Conference on Sustainable Energy and Environment (SEE) 2004.
- [27] M.E. Bambase, N. Nakamura, J. Tanaka, M. Matsumura, J. *Chem. Technol. Biotechnol.*, 82 (2007) 273.
- [28] P.C. Narvaez, S.M. Rincon, F.J. Sanchez, *J. Am. Oil. Chem. Soc.*, 84 (2007) 971.
- [29] N. Mahamuni, Y.G. Adewuyi, *Energy Fuels*, 23 (2009) 2757.
- [30] J. Nilsson, F. Sveider, [www.chemeng.lth.se/exjobb/002.pdf](http://www.chemeng.lth.se/exjobb/002.pdf), 2002
- [31] S. Ferrouillat, P. Tochon, H. Peerhossaini, *Chem. Eng. Process.*, 45 (2006) 633.
- [32] Berkeley Madonna, Modelling and Analysis of Dynamical Systems.  
<http://www.berkeleymadonna.com/> [Accessed: Sept. 2009].

**Nomenclature**

$t$ =time (min)

$t_R$ =average residence time (min)

$F$ =dimensionless concentration  $C/C^0$  (-)

$E$ =derivative of  $F$  curve ( $dF/dt$ ) ( $\text{min}^{-1}$ )

$u$ =linear fluid velocity ( $\text{cm min}^{-1}$ )

$L$ =reactor length (cm)

$D$ =axial dispersion coefficient ( $\text{cm}^2 \text{min}^{-1}$ )

$r_i$ =reaction rate for  $i$ -th reaction ( $\text{moles cm}^{-3} \text{min}^{-1}$ )

$k_i$ =kinetic constant for  $i$ -th reaction ( $\text{cm}^6 \text{mol}^{-2} \text{min}^{-1}$ )

$C_j$ =concentration of the  $j$ -th component ( $\text{mol cm}^{-3}$ )

$C_{\text{cat}}$ =catalyst concentration ( $\text{g}_{\text{cat}} \text{cm}^{-3}$ )

$V$ =reactor volume ( $\text{cm}^3$ )

$Q$ =overall flow rate ( $\text{cm}^3 \text{min}^{-1}$ )

Component symbols

$T$ =triglyceride

$M$ =monoglyceride

$D$ =diglyceride

$A$ =methanol

$G$ =glycerol

$\text{cat}$ =catalyst

# Chapter 10

## *Biodiesel Process Intensification using Static Mixer Tubular Reactors*

“If I have seen further than others,  
it is by standing upon the shoulders of giants.”

**Isaac Newton**

(1643-1727, English physicist, natural philosopher)

### 10.1 Introduction

Static mixers, also known as motionless mixers, have become standard equipment in the process industries. They are employed inline in a once-through process or in a recycle loop, as supplement or even in substitution of a conventional agitator.

The potential benefits of static mixers over conventionally agitated vessels are resumed in Table 10.1 [1].

**Table 10.1:** Potential advantages of static mixer compared to mechanically agitated vessels.

Static Mixer	CSTR
Small space requirement	Large space requirement
Low equipment cost	High equipment cost
No power required except pumping	High power consumption
No moving parts except pump	Agitator drive and seals
Small Flanges to seal	Small flanges plus one large flange to seal
Short Residence Times	Long Residence Times
Approaches Plug Flow	Exponential distribution of residence times
Good Mixing at low shear rates	Locally high shear rates can damage sensitive materials
Fast product grade changes	Product grade changes may generate waste
Self-cleaning, interchangeable mixers or disposal mixers	Large vessels to be cleaned

The prototypical design of a static mixer is a series of identical, motionless inserts that are called *elements* and that can be installed in pipes, columns or reactors. The purpose of the elements is to redistribute fluid in the directions transverse to the main flow, i.e. in the radial and tangential directions.

Commercial static mixers have a wide variety of basic geometries and many adjustable parameters that can be optimized for specific applications.

Figure 10.1 shows commercial designs, and Table 10.2 lists manufacturers.

Mixing operations are very important in the industrial industries. They include the classical mixing of miscible fluids in single phase flow as well as heat transfer enhancement, dispersion of gas into a liquid continuous liquid phase, dispersion of an immiscible organic phase as drops in a continuous aqueous phase, three-phase contacting and mixing of solids. Static mixers have been applied to all these applications, including liquid–liquid systems (e.g. liquid–liquid extraction), gas–liquid systems (e.g. absorption), solid–liquid systems (e.g. pulp slurries) and solid–solid systems (e.g. solids blending). They are currently used in the chemical and petrochemical industries to perform continuous operations. They have also found applications in the pharmaceutical, food engineering and pulp and paper industries.

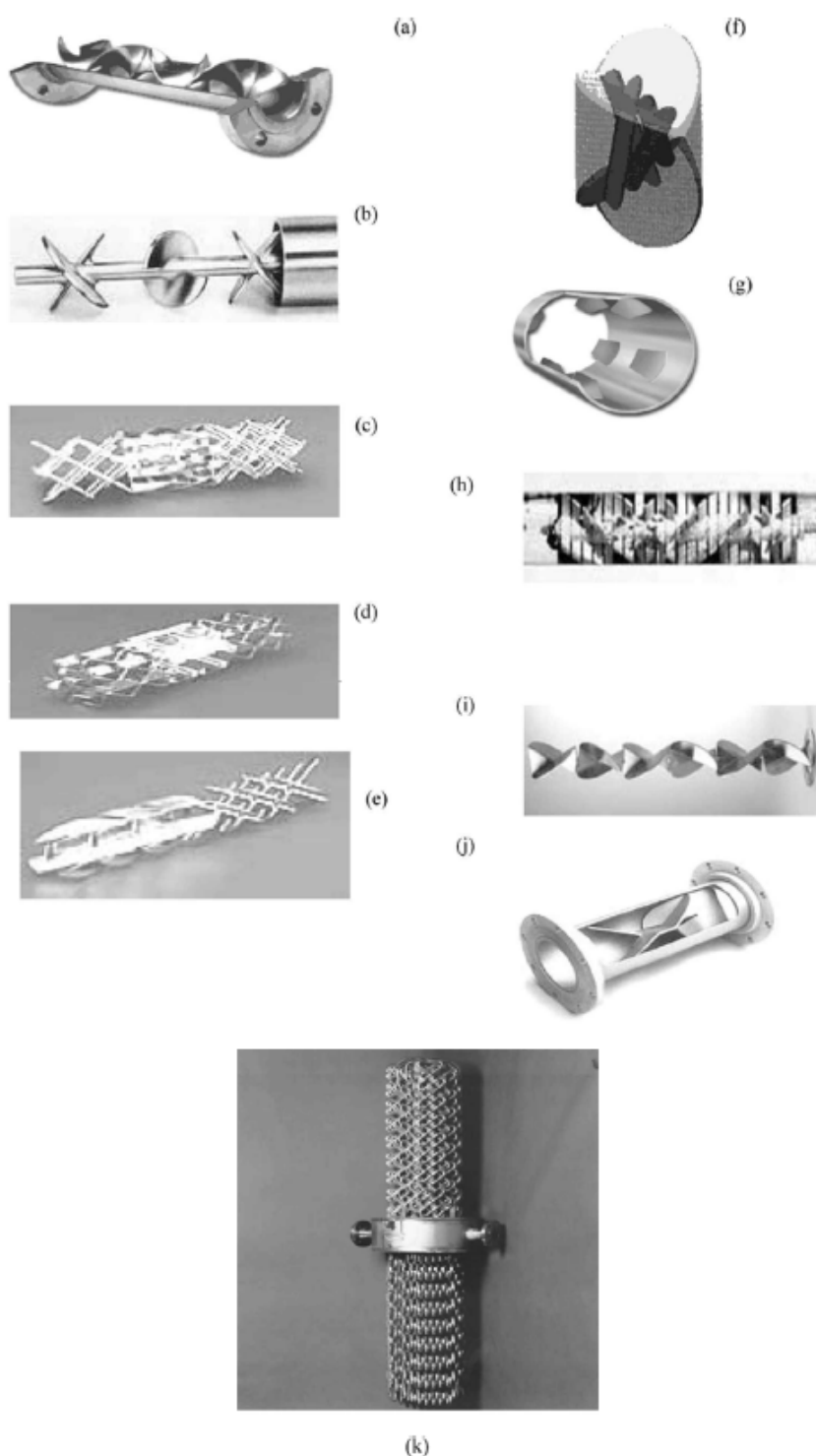


**Figure 10.1:** Elements of different commercial static mixers: (a) Kenics (Chemineer Inc.); (b) low pressure drop (Ross Engineering Inc.); (c) SMV (Koch-Glitsch Inc.); (d) SMX (Koch-Glitsch Inc.); (e) SMXL (Koch-Glitsch Inc.); (f) Interfacial Surface Generator-ISG (Ross Engineering Inc.); (g) HEV (Chemineer Inc.); (h) Inliner series 50 (Lightnin Inc.); (i) Inliner series 45 (Lightnin Inc.); (j) Custody transfer mixer (Komax systems Inc.); (k) SMR (Koch-Glitsch, Inc.).

**Table 10.2:** Commercially available static mixers

Company	Mixers
Chemineer-Kenics	Kenics mixer (KM), HEV (high efficiency vortex mixer)
Koch-Sulzer	Sulzer mixer SMF, SMN, SMR, SMRX, SMV, SMX, SMXIL.
Charles Ross&Son	ISG (interfacial surface generator) LPD (low pressure drop), LLPD
Wymbs Engineering	HV (high viscosity), LV (Low viscosity)
Lightnim	Inliner Series 45, Inliner Series 50
EMI	Cleveland
Komax	Komax
Brann and Lubbe	N-form
Toray	Hi-Toray Mixer
Prematechnik	PMR (pulsating mixer reactor)
UET	Heliflo (Series, I, II, and III)

Different types of static mixers behave quite differently, and they are usually classified based on the geometry of the mixing elements [2, 3]. As matter of the fact the commercial static mixers can be divided into five main groups:

1. open designs with helices (Figure 10.1a),
2. open designs with blades (Figure 10.1b, g–j),
3. corrugated-plates (Figure 10.1c), multi-layers designs (Figure 10.1d and 10.1e)
4. closed designs with channels or holes (Figure 10.1f).

Moreover, the applications of these designs can be classified in four groups:

- group 1: mixing of miscible fluids;
- group 2: interface generation between non-miscible phases;
- group 3: heat transfer operation and thermal homogenization;
- group 4: axial mixing.

Group 1 includes applications to homogeneous reactions, while Group 2 includes multiphase reactions coupled with separation processes, such as reactive absorption.

Group 3 includes traditional thermal homogenization and heat transfer in heat exchangers involving viscous fluids in the laminar regime, such as polymer solutions, and they are generally used for highly exothermic chemical reactions.

Group 4 mixers are an entirely new type with the design intention of promoting mixing and specifically to approximate the residence time behavior of a continuous flow stirred tank with moving parts.

Static mixers were initially designed to achieve good mixing in the cross-section of a circular tube for a fluid in laminar flow. Suppose an empty pipe has two feed streams, a black liquid and a white liquid, each liquid occupying a semicircular section of the tube as shown in Figure 10.2(a). In laminar flow, the streamlines are straight and the two

liquids will emerge from the tube exactly as they entered except for a graying at the interface, where they mixed by molecular diffusion. There is no convective mixing in either the tangential or radial directions. Thus, a similar situation arises when the two fluids are separated in the radial direction as illustrated in Figure 10.2(b).

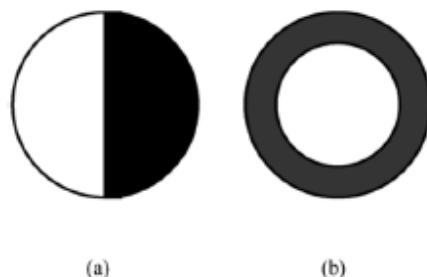


**Figure 10.2:** Spatial inhomogeneities: (a) tangential variations; (b) radial variations

Conventional static mixers are designed to homogenize the fluid by redistributing it in the radial and tangential directions. Undisturbed laminar flow also gives temporal inhomogeneities in the sense that molecules leaving the tube at some instant will have entered at different times. The same redistribution of fluid that gives spatial mixing also gives temporal mixing. In the ideal case of plug flow, which is also known as piston flow, the black and white liquids will be uniformly gray when they leave the tube, and all the molecules leaving together will have entered together. The extent to which actual static mixers approach is ideal can be characterized using the residence time distribution for temporal variations. Figure 10.3 shows response curves for several flow geometries to a sudden, step input of an inert tracer.

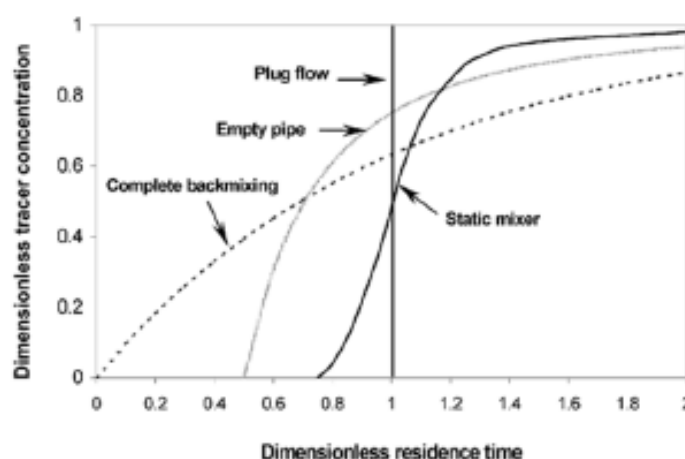


**Figure 10.3:** Cumulative residence time distributions for various flow systems.



The resulting, monotonically increasing curve is the cumulative distribution function of residence times,  $F(t)$ . The reference case is an empty pipe under laminar flow (Poiseuille flow) in the absence of diffusion. The broad distribution of residence times for this case is due to the parabolic velocity profile, and the redistribution caused by the static mixing elements gives a residence time distribution that more closely approaches the sharp distribution of plug flow.

With the static mixers good mixing in the cross-section is possible, thanks to blades or corrugated plates induce, present in these mixers, which changes the fluid streamlines. Inserts with holes, channels, helical elements and oblique blades cause local acceleration. They split the incoming fluid into layers and then recombine the layers in a new sequence (Figure 10.4). These various mixing actions cause distributive mixing. It is mixing caused by convection rather than diffusion, although to the extent that distributive mixing is high, diffusion is better able to achieve homogeneity on a molecular scale.

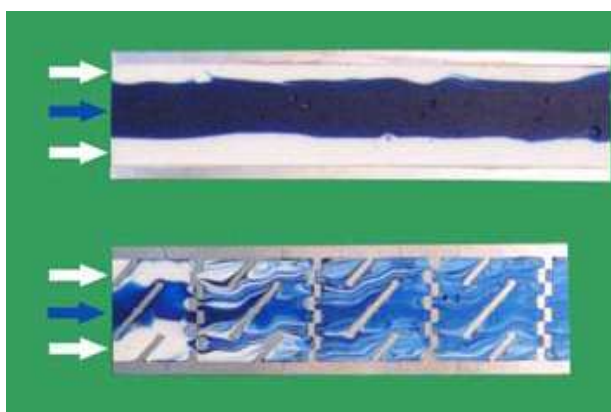


Figure 10.4: Laminar flow in an empty tube (top) and through a static mixer (bottom).

Static mixers can also be used for reactive fluids obtaining in this way the static mixer reactors.

As discussed in previous chapters, one of the difficulties faced in the current technology for biodiesel production is the requirement for rigorous mixing of methanol with the oil in the reactor. Utilization of blade mixer has limitations due to the immiscible state of those substances. Long reaction time as caused by the low reaction rate is directly related to low collision frequency among reactants. This collision frequency can be enhanced by a better mixing mechanism during the process. Most of industrial biodiesel reactors use blade agitators for mixing, which create a main flow in the reaction tank with circulation on axial and tangential directions, and with little turbulence [4].

Thompson [5] has studied the possibilities of using static mixers as a continuous-flow reactor for biodiesel production in laboratory scale. Biodiesel (canola methyl ester) was

produced under varying conditions using a closed-loop static mixer system. Sodium methoxide was used as the catalyst. Process parameters of flow rate or mixing intensity, catalyst concentration, reaction temperature, and reaction time were studied. The most favorable conditions for completeness of reaction were at 60° C and 1.5% catalyst for 30 min of transesterification reaction time.

In this work, the KOH transesterification reaction of oil with methanol has been studied in stainless steel tubular reactor with different filling, that could promote the reaction between the immiscible phase through the micromixing.

The behavior of these device is the same to commercial static mixer reactors, described above, hence they could be useful as laboratory reactors for orienting on the choice of the best static mixer or for modeling microreactors but are not useful for industrial purposes being the productivity, for reactor volume unity, relatively low.

## 10.2 Experimental

### 10.2.1 Reactor Setup

Five different reactors have been tested starting from a stainless steel AISI 316 cylindrical tube of 20 cm length and 12.7 mm (1/2") of external diameter with an internal diameter of 10 mm. The internal void volume of the reactor was 15.7 cm<sup>3</sup>. This tube was filled by using different static mixer elements:

1. TRR, consisted in 8 stainless steel threaded rods, of the same length of the reactor, having 3 mm of diameter and 0.5 mm of thread, forced into the cylinder (the acronym for this reactor is TRR);
2. RP1, consisted a single size packing of stainless steel AISI spheres of 2.5 mm diameter;
3. RP21, consisted a dual size packing of spheres of two different diameters (2.5 and 1.0 mm respectively);
4. RP22, consisted in dual size packing (RP22) in which spheres of two different diameters (2.5 and 0.39 mm respectively);
5. RWTR, consisted in stainless steel ribbon wool.

The volume and void fractions of the used reactors are reported for comparison in Table 10.3.

**Table 10.3** :Volume of all the used reactors. The void fractions are referred to an empty tubular reactor of 15.7 cm<sup>3</sup>.

Reactors	Volumes (cm <sup>3</sup> )	Void Fractions
RP1	7.15	0.45
RP21	6.05	0.38
RP22	3.50	0.22
RWTR	13.9	0.89
TRR	6.00	0.38

The three different packing configurations (RP1, RP21 and RP22) are reported in Figure 10.5.

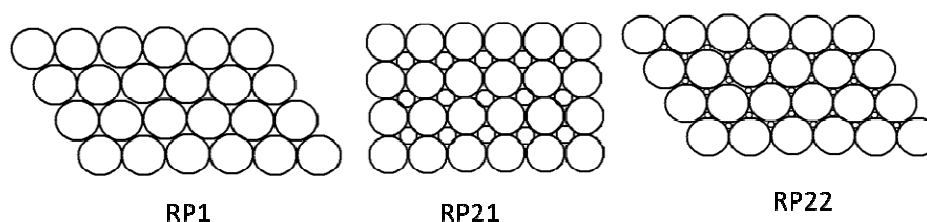


**Figure 10.5:** Three different geometrical ensembles of spheres filling.

A theoretical hexagonal packing of the bigger spheres RP1 leads to two different kind of cavities called octahedral (the bigger ones) and tetrahedral (the smaller ones). If the ratio between the radius of the spheres is  $r/R=0.414$ , the smaller spheres occupy the octahedral cavities, while, the tetrahedral cavities are filled just if  $r/R=0.227$ . In our case, we have chosen first of all a  $r/R=0.156$  in order to occupy both the cavities; this value has been obtained choosing a diameter for the smaller spheres of 0.39 mm. Therefore, the RP1 packing structure allows the introduction of the smaller spheres of 0.39 mm of diameter without altering the geometrical framework created by the bigger spheres. In the case of the RP22 structure the introduction of spheres of 1.0 mm of diameter forces the bigger spheres to assume a geometrical cubic framework as the corresponding structure reported in Figure 10.5.

An estimation of the size of the microchannels has been made considering an ideal packing, so obtaining an average value of about 1000  $\mu\text{m}$  for the structure RP1, 500  $\mu\text{m}$  for the RP22 and 300  $\mu\text{m}$  for the RP21. For filling the reactor 1050 spheres of 2.5 mm diameter were used for the RP1 structure, 888 spheres of 2.5 mm diameter and 4560 of spheres of 1.0 mm for RP21 reactor, 1050 spheres of 2.5 mm diameter and 101800 spheres of 0.39 mm diameter for RP22.

The void fractions obviously changed in the three mentioned cases, as it can be appreciated in Table 10.3.

The estimated theoretical minimum value of the void fraction for RP21 corresponding to 0.39. This value is greater than the theoretical one of monodisperse RP1 system, because, the size of the smaller sphere has been chosen in a way to constrain the larger sphere to assume a different type of packing, as it can be seen in Figure 5. In the case of the bidisperse RP22 system, a minimum theoretical void fraction of 0.25 has been estimated. As it will be seen, these values have been determined also experimentally and the obtained results are in a reasonable agreement for RP22, considering a random loose packing, and in the other cases considering the minimum theoretical void fractions (Figure 8.6). The theory of monodisperse packing sphere is a very old problem faced for the first time by Kepler in 1611. Kepler estimated for spheres of the same diameter a

maximum packing density of 0.74 corresponding to a void fraction of 0.26. More later, different approaches have been formulated defining a “Random Close Packing” for mono-modal system, like the RX1 reactor, corresponding to a minimum void fraction of  $\epsilon = 0.36$  ( $\epsilon$  = void volume/total volume). However, there are in the literature numerous experiments showing that the loosest way of packing spheres (Random Loose Packing) gives a void fraction of 0.45 [6].

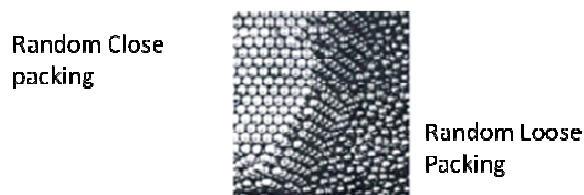


Figure 10.6: A picture of different types of packing

The described tubular reactors, filled in different ways, are useful as laboratory reactors to foresee the behaviour of the transesterification reaction in the presence of static mixers (intense local micro-mixing) or micro-reactors (presence of micro-channels) but cannot be considered the base for the development of an industrial size reactor, being the void fraction of the reactor too low as it can be appreciated always in Table 10.3. For this reason, a tubular reactor filled with a stainless steel ribbon wool (RWTR) (like the one reported in Figure 10.7) having a void fraction of 0.89 (see Table 10.3) was used.



Figure 10.7: Stainless steel ribbon wool employed for filling the reactor

### 10.2.2 Fluid dynamic characterization tests

All the described reactors have been subjected to a fluid dynamic characterization with a stimulus-response step test to evaluate the RTD (retention time distribution). Water has been used as flowing medium and cobalt nitrate (II) hexahydrate, having a characteristic pink color, has been used in the test as a tracer. A solution of known concentration ( $C_0$ ) of the tracer was sent to the reactor at time=0; from this time samples have been periodically withdrawn from the outgoing flow in order to record the step response. Then, the samples have been analyzed by an UV-visible

spectrophotometer, monitoring the absorbance of cobalt nitrate at 511 nm. The tests have been repeated at different flow rates. An HPLC pump was used for regulating the cobalt solution flow rate.

### 10.2.3 Methanol-soybean oil transesterification runs

The described reactors have then been used to perform transesterification reaction in a laboratory plant schemed in Figure 10.8.

Kinetics runs have been made by feeding to the reactor independently, methanol containing the dissolved catalyst (KOH, normally 1 wt% with respect to the oil) and a refined soybean oil. The oil was preheated at the reaction temperature, whereas methanol was fed at room temperature.

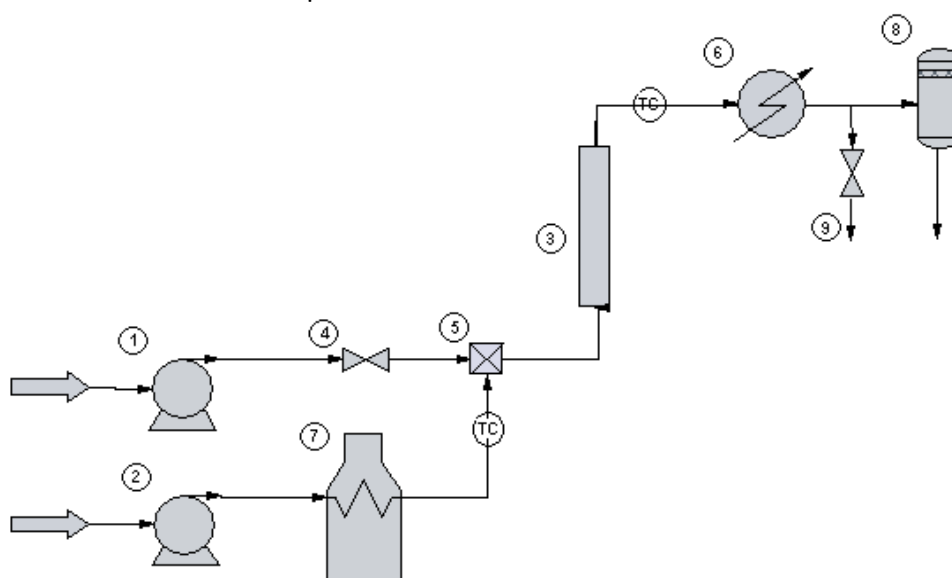


**Figure 10.8:** Scheme of the laboratory plants used for performing transesterification runs. (1)–(2) are HPLC pumps for respectively methanol and oil feeding, (3) tubular reactor with the electric resistance, (4) check valve for preventing the back flow of oil towards the methanol pump, (5) T mixer, (6) condenser filled with Rashig rings, (7) oil pre-heater, (8) collecting tank, (9) withdrawing samples. The reactor and the pre-heater are heated with an electric resistance and insulated with rock wool.

## 10.3 Results and discussion

### 10.3.1 Results of the fluid dynamic tests

In order to evaluate accurately the void volume of the systems under examination and to study the fluid dynamics of the three described reactors, some step tests have been performed. By reading the flex of the sigmoidal function that best fit the experimental data it was possible to determine the mean residence time and from these values, to estimate the empty volumes of the three packing filling the reactors (see Table 10.3)

The results of this characterization for the reactor TRR are shown in Figure 10.9, where the dimensionless tracer concentrations  $F (C/C_0)$ , are plotted as a function of the

dimensionless time  $\theta$  ( $t/t_m$ , where  $t_m$  is the mean residence time) for two different volumetric flow rates of respectively 5.6 and 8.3  $\text{cm}^3/\text{min}$ .  $C_0$  is the inlet solution concentration and  $C$  is the outlet measured concentration.

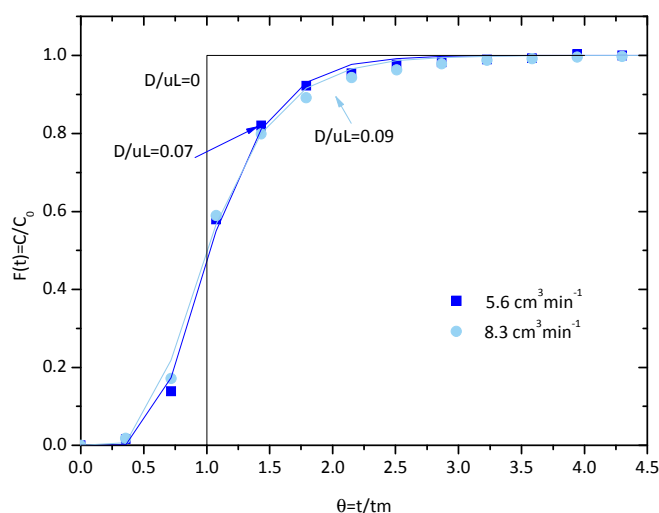


**Figure 10.9:** F function plot against the dimensionless time for the TRR fluid dynamic tests.

The results of fluid dynamic characterization for the reactor RP1, RP21, RP22 AND RWTR are shown in Figures 10.10, 10.11, 10.12, 10.13.

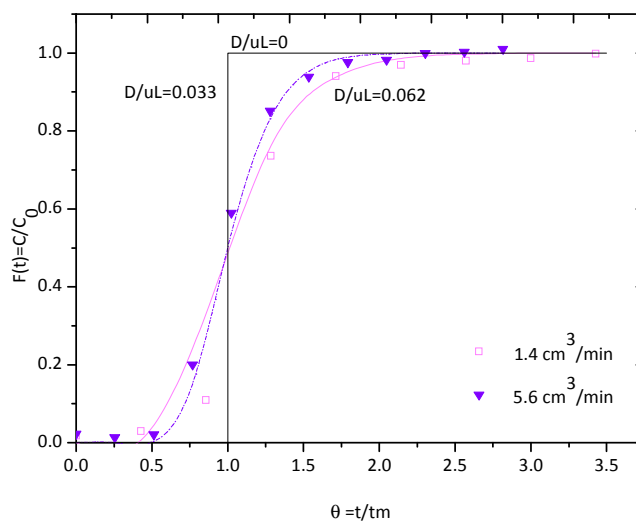


**Figure 10.10:** F function plot against the dimensionless time for the TPR1 fluid dynamic tests.

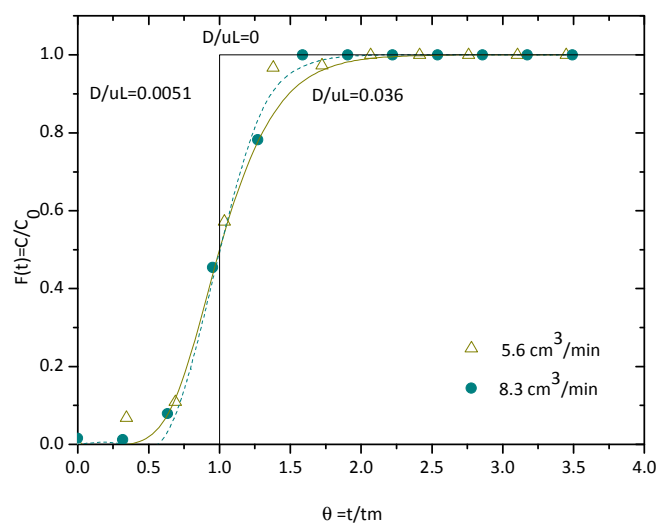


**Figure 10.11:** F function plot against the dimensionless time for the TPR21 fluid dynamic tests.

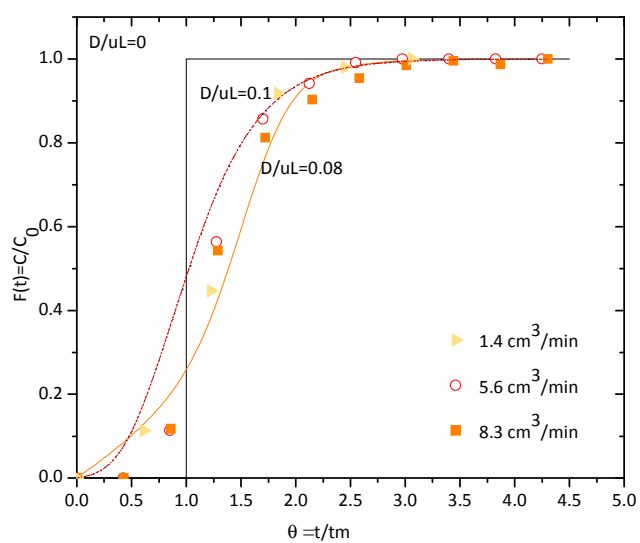


**Figure 10.12 :** F function plot against the dimensionless time for the TPR22 fluid dynamic tests.

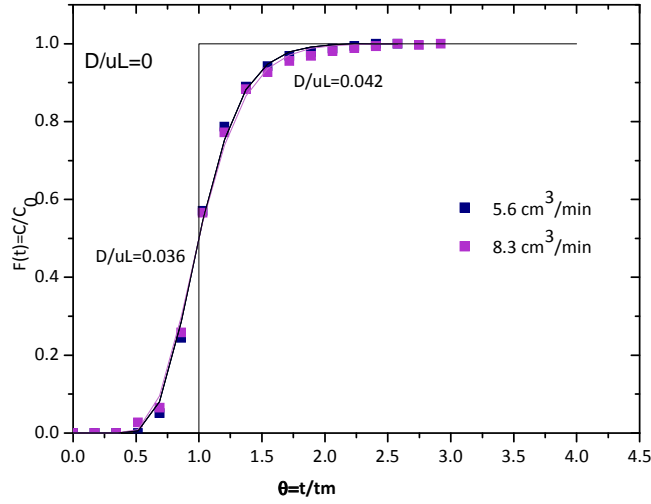


**Figure 10.13:** F function plot against the dimensionless time for the RWTR fluid dynamic tests.

Then, the fluid dynamic experimental data can be elaborated by mathematical regression analysis using a single parameter function; the parameter is known as the axial dispersion number ( $N_D$ ), normally indicated as the reciprocal of the Peclet number ( $Pe$ ), defined by the following expression.

$$N_D = \frac{1}{Pe} = \frac{D}{u \cdot L} \quad (1)$$

Where  $u$  is the fluid linear velocity (m/s) calculated from the volumetric flow rate and the section of the empty reactor,  $D$  is the axial dispersion coefficient ( $m^2/s$ ) and  $L$  the length of reactor (m). It is possible to estimate the  $N_D$  value from the slope of the curve  $F(t)$  for  $\theta = 1$ , according to the following relationship [6].

$$\left[ \frac{dF(t)}{d(t/t_m)} \right]_{t/t_m=1} = \frac{1}{2} \cdot \sqrt{\frac{uL}{\pi D}} \quad (2)$$

The integrated function  $F(t)$  is reported below.

$$F(t) = \frac{1}{2} \cdot \left\{ 1 - \operatorname{erf} \left[ \frac{1}{2} \cdot \sqrt{\frac{uL}{\pi D}} \cdot \left( \frac{1-t/t_m}{\sqrt{t/t_m}} \right) \right] \right\} \quad (3)$$



Where erf is the error function defined as following:

$$\text{erf}(x) = \frac{2}{\sqrt{\pi}} \cdot \int_0^x e^{-y^2} dy \quad (4)$$

The  $N_D$  numbers for all the tested reactors are reported in Table 10.4

**Table 10.4** :Dispersion Numbers obtained for all the different used reactors.

Reactor	Flow rates (cm <sup>3</sup> min <sup>-1</sup> )	1/Pe=D/uL
RP1	1.4-5.6	0.033-0.062
RP21	5.6-8.3	0.035-0.050
RP22	1.4-5.6-8.3	0.083-0.10
RWTR	5.6-8.3	0.036-0.042
TRR	5.6-8.3	0.07-0.091

The literature findings confirm that the  $N_D$  values estimated for the reactors are very close to the ones expected for the static mixers that are  $1/N_D = Pe = 70 \cdot L$  [7] (where  $L$  stands for the length of the reactor expressed in meters).

It is important to underline that for all the described systems the local turbulence is not given mainly by the flow-rate, but by the static mixer elements that warrants an intimate mixing between the two immiscible phases, because of the eddies formation. However, as these numbers are near to zero the flows, in all cases, can be approximated to a plug flow.

### 10.3.2 Methanol-soybean oil transesterification runs performed in the described packed bed reactors

The typical experimental conditions for many of the runs performed, are: molar ratio methanol/soybean oil = 6:1 considering for soybean oil an average molecular weight of 885 g mol<sup>-1</sup>, a KOH catalyst concentration of wt % referred to the oil and a temperature of 60 °C. To examine the effect of the presence of a packed bed, a first run was performed with the empty reactor using a total flow rate of 8.33 cm<sup>3</sup>/min. The esters yield obtained in this case was only 3%. This blank value can be compared with the much higher values obtained in the presence of a packed bed.

#### 10.3.2.1 Methanol-soybean oil transesterification runs performed TRR

The experimental runs were performed fixing the temperature (60°C) and the catalysts concentration (KOH 1 wt% referred to oil) changing the residence time, in order to evaluate the effect of the latter on the reaction rate.

A list of the runs performed and related results are reported in Table 10.5.

**Table 10.5:** Transesterification runs performed using the TRR reactor.

Run	$Q_{oil}$ (cm <sup>3</sup> /min)	$Q_{MeOH}$ (cm <sup>3</sup> /min)	$Q_{tot}$ (cm <sup>3</sup> /min)	T (°C)	$\tau$ (minutes)	KOH (%b.w.)	Yield (%)
1	9.80	2.53	12.33	60	0.58	1.00	72.87
2	6.60	1.73	8.33	60	0.86	1.00	75.59
3	5.50	1.40	6.90	60	1.04	1.00	70.44

It must be observed, first of all, that the presence of the packed bed gives place to a very strong increase of the conversion with respect to the empty reactor due to the static mixing effect.

The observed behaviors, appreciated in Table 8.5, are very singular, yields decrease very slightly by increasing the residence time.

### 10.3.2.2 Methanol-soybean oil transesterification runs performed RP1

Some experimental runs were performed fixing the temperature (60 °C) and the catalyst concentration (KOH 1 wt% referred to the oil) in order to study the effect of the residence time on the methylesters yield, while another test was performed varying the catalyst concentration at a fixed residence time. A list of the runs performed and related results are reported in Table 10.6.

**Table 10.6:** Transesterification runs performed using the RP1 configuration.

Run	$Q_{oil}$ (cm <sup>3</sup> /min)	$Q_{MeOH}$ (cm <sup>3</sup> /min)	$Q_{tot}$ (cm <sup>3</sup> /min)	T (°C)	$\tau$ (minutes)	KOH (%b.w.)	Yield (%)
4	9.80	2.53	12.33	60	0.58	1.00	62.52
5	6.60	1.73	8.33	60	0.86	1.00	79.31
6	5.50	1.40	6.90	60	1.04	1.00	80.70
7	4.40	1.15	5.55	60	1.29	1.00	81.76
8	1.10	0.29	1.39	60	5.16	1.00	73.30
9	2.40	0.61	3.02	60	2.37	1.00	73.30
10	0.58	0.15	0.73	60	9.79	1.00	43.63
11	6.60	1.73	8.33	60	0.86	0.50	55.39

Then, it must be pointed out that, by increasing the residence time, the yield in methylesters increases until a maximum is reached, a further increase of the residence time gives place to a decrease of the yield. This behavior can be better appreciated by plotting the yields as a function of the residence time, as reported in Figure 10.14.

The lowest yield of 44%, obtained at about 10 min of residence time, is very probably due to a less active micromixing giving place to a reduction of the interphase area and to the intervention of mass transfer limitation on the reaction rate. On the contrary, the

decrease of the yield observed, at the lowest residence time, would be the normal behavior of a plug flow reactor working in a chemical regime. Another observation is that by decreasing the catalyst concentration the activity consistently decreases (see entry 11).

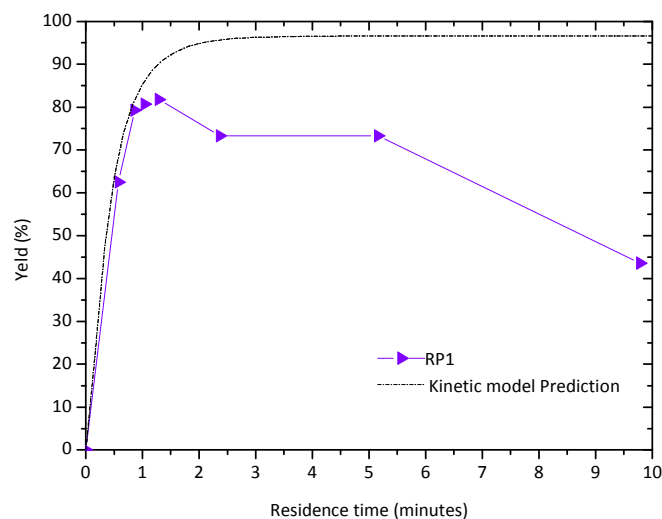


**Figure 10.14:** Methyl esters yields plot as a function of the residence time obtained using the RP1 reactor. In the same plot is reported for comparison also the simulation obtained with a kinetic model derived from kinetic runs. [8, 9].

### 10.3.2.3 Methanol-soybean oil transesterification runs performed RP21

Another set of experimental runs was performed in the reactor with the filling RP21 by imposing the following conditions: temperature of 60 °C and catalyst concentration of 1 or 2 wt % of KOH. The list of the run performed is shown in the Table 10.7.

In this case, the observed behaviors are very singular and can be better appreciated in Figure 10.15. The yields decrease very slightly by increasing the residence time for the runs performed with 1% of catalyst and the values, in particular at low residence time are greater than the ones obtained with the RP1 reactor.

On the contrary, for the runs performed with 2% of catalyst a small increase of the yield with the residence time is observed until reaching a maximum yield of 98.17% in correspondence of one minute of residence time. This probably is the yield equilibrium value. It is very interesting to note that the role of the catalyst concentration is determinant in this case. As a matter of fact, the yield goes from 82% to 98% by using respectively 1 wt % or 2 wt % of catalyst.

**Table 10.7:** Transesterification runs performed using the RP21 reactor.

Run	$Q_{oil}$ (cm <sup>3</sup> /min)	$Q_{MeOH}$ (cm <sup>3</sup> /min)	$Q_{tot}$ (cm <sup>3</sup> /min)	T (°C)	$\tau$ (min)	KOH (%wt.)	Yield (%)
12	28.62	7.38	36.00	60	0.17	1.00	83.57
13	19.24	4.96	24.20	60	0.25	1.00	81.15
14	9.62	2.48	12.10	60	0.50	1.00	80.33
15	4.85	1.25	6.10	60	0.99	1.00	81.91
16	2.38	0.61	3.00	60	2.02	1.00	78.69
17	28.62	7.38	36.00	60	0.17	2.00	93.63
18	19.24	4.96	24.20	60	0.25	2.00	93.76
19	9.62	2.48	12.10	60	0.50	2.00	94.68
20	4.85	1.25	6.10	60	0.99	2.00	98.17
21	2.38	0.62	3.00	60	2.02	2.00	97.06

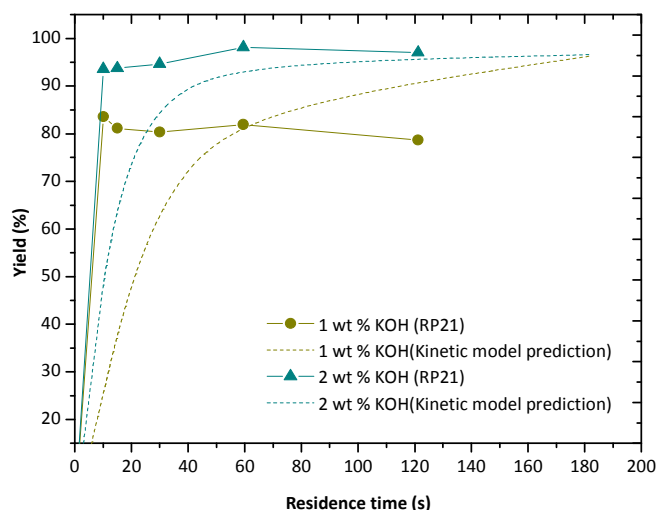


**Figure 10.15:** Methylesters yields plot as a function of the residence time obtained using the RP21 reactor by using different amounts of catalysts (1 and 2 wt%). In the same plot is reported for comparison also the simulation obtained with a kinetic model derived from kinetic runs. [8, 9].

#### 10.3.2.4 Methanol-soybean oil transesterification runs performed RP22

Another set of experimental runs was performed in the already described RP22 reactor, always by fixing the temperature, at 60 °C and KOH catalyst concentration, at 1 wt% of oil. The list of the runs performed with this reactor is reported in Table 10.8 together with the obtained results in terms of yields to methyl esters.

**Table 10.8:** Transesterification runs performed using the RP22 reactor.

run	$Q_{\text{olio}}$ (cm <sup>3</sup> /min)	$Q_{\text{MeOH}}$ (cm <sup>3</sup> /min)	$Q_{\text{tot}}$ (cm <sup>3</sup> /min)	T (°C)	$\tau$ (min)	KOH (%wt.)	Yield (%)
22	9.80	2.53	12.33	60	0.31	1.00	80.53
23	7.90	2.04	9.94	60	0.38	1.00	81.52
24	6.60	1.73	8.33	60	0.46	1.00	78.64
25	5.50	1.40	6.90	60	0.55	1.00	77.17
26	4.40	1.15	5.55	60	0.68	1.00	81.52
27	3.20	0.83	4.03	60	0.94	1.00	80.58
28	2.4	0.61	3.02	60	1.26	1.00	82.31
29	1.10	0.29	1.39	60	2.73	1.00	91.57
30	0.58	0.15	0.73	60	5.21	1.00	80.50
31	4.40	1.15	5.55	100	0.68	1.00	85.82

From the data reported in Table 10.8 it can be possible to observe, first of all, that the obtained yields are normally higher than the ones obtained with RP1 reactor and comparable with those of RP21 reactor, at the lowest residence time, but slightly higher at 2.02 min of residence time. This can tentatively be attributed to the development of a greater surface area at the liquid–liquid interphase due to both the effect of the intense local micromixing and of the presence of narrower micro-channels (300 $\mu$ m). Again, a maximum in methylesters yields is reached by increasing the residence time to a value of 2.73 min, as it can be appreciated in Figure 10.16.

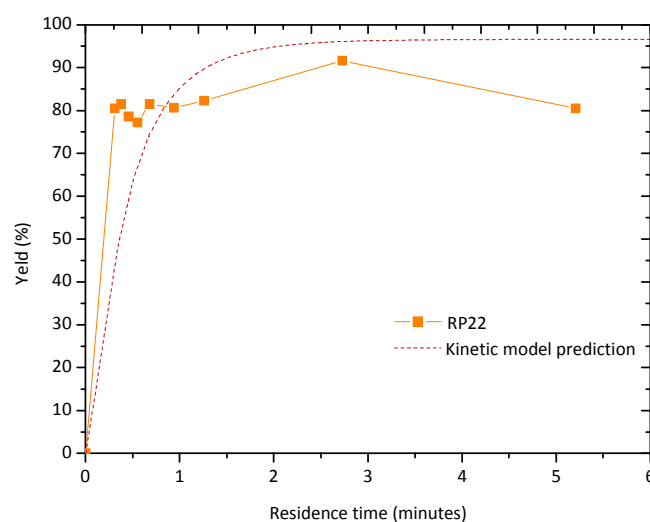


**Figure 10.16:** Methylesters yields plot as a function of the residence time obtained using the RP22. In the same plot is reported for comparison also the simulation obtained with a kinetic model derived from kinetic runs. [8, 9].

Also in this case, as observed for the RP21 reactor, the trend of the yield with the residence time is almost flat in the examined range. These behaviors, as before mentioned, are very singular and difficult to describe with a simple model based on a pseudo-monophasic assumption like the ones proposed by literature [8, 9]. In practice, in the range of residence time of 0.5–6 min the yields does not change very much. This means that operating at high volumetric flow-rates the productivity of the system becomes very high. At last, the effect of the temperature (see entry 24 and 29 of Table 8.8 for the comparison) in the described conditions, is consistent but not so important as the effects of both micromixing and catalyst concentration (see runs made with RP21 reactor). Some kinetic runs on RP1, RP21 and RP22 have been repeated different times, in the same conditions, in order to evaluate the reproducibility and an average experimental error of less than 1–2% has been found.

#### 10.3.2.5 Methanol-soybean oil transesterification runs performed RWTR

Some experimental runs were performed fixing the temperature (60 °C) and the catalyst concentration (KOH 1 wt %. referred to the oil) in order to study the effect of the residence time on the methylesters yield, while another test was performed varying the catalyst concentration at a fixed residence time. A list of the runs performed and related results is reported in Table 10.9.

**Table 10.9 :** Transesterification runs performed using the RWTR reactor.

Run	$Q_{oil}$ (cm <sup>3</sup> /min)	$Q_{MeOH}$ (cm <sup>3</sup> /min)	$Q_{tot}$ (cm <sup>3</sup> /min)	T (°C)	$\tau$ (min)	KOH (%wt.)	Yields (%)
32	35.77	9.23	45.00	60	0.31	1.00	39.80
33	31.00	8.00	39.00	60	0.36	1.00	57.08
34	25.04	6.46	31.50	60	0.44	1.00	81.88
35	14.31	3.69	18.00	60	0.77	1.00	80.31
36	9.80	2.53	12.33	60	1.13	1.00	76.83
37	6.60	1.73	8.33	60	1.67	1.00	83.24
38	5.50	1.40	6.90	60	2.02	1.00	80.43
39	4.40	1.15	5.55	60	2.51	1.00	83.82
40	2.40	0.62	3.02	60	4.62	1.00	84.08
41	3.69	0.95	4.64	60	3.00	1.00	76.90
42	2.77	0.71	3.48	60	4.00	1.00	74.91
43	2.21	0.57	2.78	60	5.01	1.00	73.64
44	1.10	0.29	1.39	60	10.04	1.00	67.10
45	11.07	2.86	13.93	60	1.00	2.00	81.02
46	5.54	1.43	6.97	60	2.00	2.00	88.63
47	3.70	0.95	4.65	60	3.00	2.00	97.05
48	2.77	0.71	3.48	60	4.00	2.00	93.71
49	2.21	0.57	2.78	60	5.01	2.00	85.21

It must be observed, first of all, that the presence of the packed bed gives place to a very strong increase of the conversion due to the static mixing effect. Then, it must be pointed out that, by increasing the residence time, the yield in methylesters increases until a maximum is reached, a further increase of the residence time gives place to a decrease of the yield. This behavior can be better appreciated by plotting the yields as a function of the residence time, as reported in Figure 10.17. The low value of the yield, obtained at the highest residence time, is very probably due to a less active micromixing having as a consequence the reduction of the interphase surface area and the intervention of the mass transfer limitation, while, the decrease of the yield observed at the lowest residence time seems the normal behavior of a system working in a chemical regime.

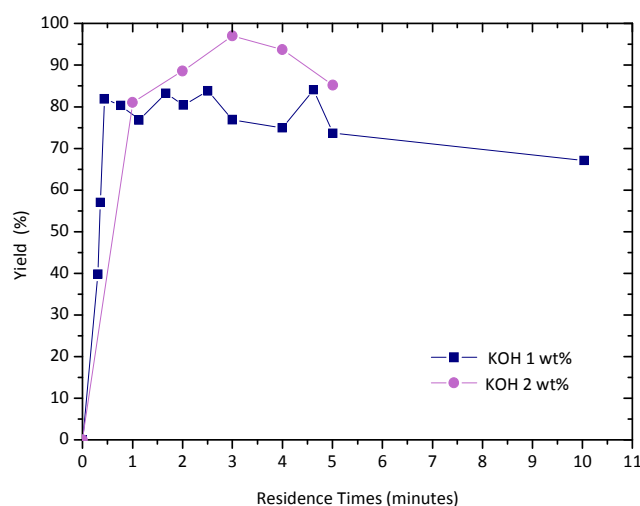


**Figure 10.17:** Methylesters yields plot as a function of the residence time obtained using the RWTR.

Several runs have then been performed by using 2% of KOH catalyst. It is interesting to observe that the increase of the catalyst amount gives place to a very high yield.

### 10.3.3 Methanol-soybean oil transesterification, a comparison of the runs performed in different packed bed tubular reactors (TRR, RP1, RP21, RP22, RWTR)

The yields obtained, as a function of residence time, with the different tested reactors are reported for comparison in Figure 10.18.

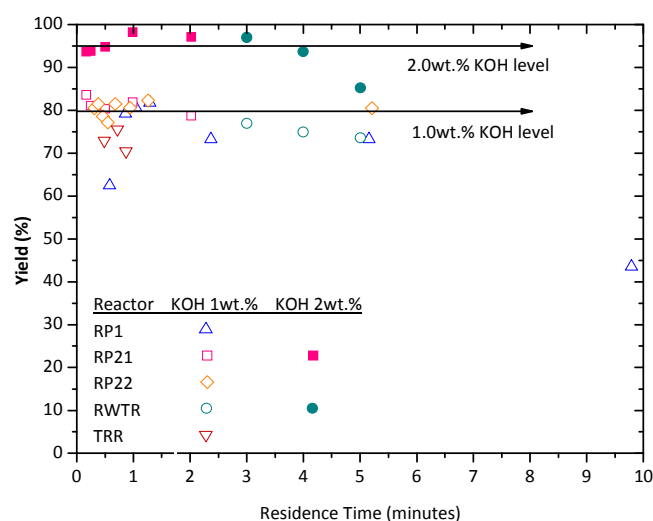


**Figure 10.18:** Comparison between the five reactors performances. In the same plot are also reported the simulation derived from kinetic runs performed in well-mixed batch reactors [8, 9].

First of all, it must be observed, that in any case the presence of a packed bed gives place to a very strong increase of the conversion due to the static mixing effect. Then, it must be pointed out that, in many cases, by decreasing the residence time, the yield in methylesters increases until reaching a maximum value. This behavior can be explained by considering that increasing the flow rate, in these systems, means to increase the liquid-liquid interface. Therefore, the lower values of the yield, obtained at the highest residence time, are probably due to a less active micro-mixing, having as a consequence the reduction of the interface area, while, the decrease of the yield observed at the lowest residence time seems the normal behavior of a reacting system in a kinetic regime requiring time to occur. At last, as it can be seen in Figure 10.18, several runs have been performed by using 2% of KOH catalyst. It is interesting to observe that the increase of the catalyst amount gives place to much higher yields. A so large increase in the yields, simply by increasing the amount of used catalyst, is unexpected and as it will be seen later, this behaviour cannot be described by using a monophasic pseudo-homogeneous kinetic model, normally, adopted in the literature for describing batch runs [8, 9].

A more reliable biphasic kinetic model would be useful to have a more detailed description of what effectively occurs in the studied system.



The development of such a biphasic model is the subject of the next chapter of this thesis.

#### 10.4 Conclusion

In this chapter, the effect of different types of static mixers on the intensification of the biodiesel synthesis has been deeply investigated.

It was shown that a tubular reactor filled with different elements of different sizes can usefully be used to simulate the behavior of both a “static mixer” and a “microreactor”. As a matter of fact, with this type of device it is possible to change opportunely the size of the microchannels, so simulating microreactors, or the intensity of local micromixing by changing feeding flow rates, so simulating static mixers.

On the basis of the experimental results obtained for transesterification of vegetable oil with methanol, promoted by KOH, it is possible to conclude that an intense local micromixing, favoring the development of a great interface area, gives place to very high yield in mild conditions (60 °C) and very short residence times (less than 1 minute). Another important experimental observation is that by increasing the catalyst concentration the yield increases very much in the same conditions of temperature and residence time. This means that the maximum yields obtained cannot correspond to equilibrium values depending on the catalyst concentration. On the other hand, in the literature are reported many runs, performed in batch conditions, in which the final conversion increases with the catalyst concentration. It is possible to conclude that the monophasic kinetic models, normally adopted in the literature, considering the transesterification steps as equilibrium reactions, are not adequate to describe in any detail biodiesel production.

**References**

- [1] R. K. Thakur, Ch. Vial, K. D. P. Nigam, E. B. Nauman, G. Djelveh, *Trans. Chem. E.*, 81(A) (2003) 787.
- [2] J.R. Baker, *Chem Eng Prog*, 87 (1991)32.
- [3] K.J.Myers, A. Bakker, D. Ryan, *Chem Eng Prog*, (1997) 28.
- [4] E. Paul, V.A.A. Obeng, S.M. dan Kresta, (2003). *Handbook of Industrial Mixing*. Wiley-Interscience, New York.
- [5] J.C. Thompson, J.C. B.B.He, *Transactions of the ASABE*, 50(1) (2007) 161.
- [6] C. Song, P. Wang, H.A. Makse, *Nature*, 453 (2008) 629.
- [7] C.G. Hill, *An Introduction to Chemical Engineering Kinetic and Reactor Design*, John Wiley & Sons, 1977, p. 404.
- [8] G. Vicente, M. Martinez, J. Aracil, A. Esteban, *Ind. Eng. Chem. Res.*, 44 (2005) 5447.
- [9] G. Vicente, M. Martinez, J. Aracil, *Energy Fuels*, 20 (2006) 1722.

# Chapter 11

## *A biphasic model describing vegetable oil transesterification with methanol in batch and continuous reactors*

*"Most of the fundamental ideas of science are essentially simple, and may, as a rule, be  
expressed in a language comprehensible to everyone."*

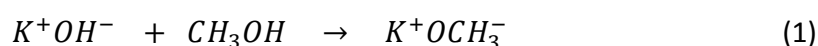
**Albert Einstein**

(1879-1955, German-born Swiss theoretical physicist)

### 11.1 Introduction

Biodiesel is usually produced in industry by reacting vegetable oils with methanol in the presence of a homogeneous catalyst such as NaOH, KOH, or related alkoxides, at 60 °C (the methanol boiling point) and atmospheric pressure, as it was discussed in previous sections. The reagents are immiscible liquids and the interphase plays a fundamental role, as it was. Many of the published works reporting kinetic data are related to batch reactors and are often affected by mass transfer limitation [1-7].

In previous chapter of this thesis (7) it was shown that a very high productivity (2000 kg/day L) can be obtained by performing the transesterification reaction in a continuous corrugated plates heat exchanger reactor (CP-HEX reactor) working in a range of temperatures between 60 and 100 °C. The high performances observed are due to a very active local micromixing, because, the conversion increases by increasing the overall liquid flow rate. Therefore, it derives that all the reactors favoring a local micromixing or more generally increasing the liquid-liquid interfacial area can give high performances in this reaction. This observation is confirmed by many results, reported in the literature, in which the transesterification reaction is performed in the following: reactors containing a static mixer, microwave irradiated reactors, ultrasonic irradiated reactors, centrifugal contactors, rotating packed bed reactors, and jet flow stirred reactors. It is then possible to increase the liquid-liquid interfacial area also by using microreactors. In other words, transesterification of triglycerides with methanol seems strongly promoted by the extension of the polar/apolar interface area. As the most commonly used catalyst KOH reacts in methanol giving place to KOCH<sub>3</sub> according to the reaction:



The high interface area initially occurs to give the possibility to the anion CH<sub>3</sub>O<sup>-</sup> to react with a molecule of triglyceride so transferring the anion charge in the oil phase in the form of diglycerolate [8]. Higher is the initial interface area faster is the CH<sub>3</sub>O<sup>-</sup> disappearance and the formation in situ of the true catalyst, that is, a mixture of di- and monoglycerolate [8]. Equilibrium (1) is clearly shifted to the right as a consequence of the methanolate disappearance. Then, the reaction rate abruptly declines, because of the ultimate formation of glycerolate anion. This anion migrates in the polar phase being insoluble in the oil phase and is poorly active in the reaction. It was supposed that this behavior is responsible also of a never explained experimental phenomenon observed in batch kinetic runs, that is, by using different amounts of catalyst a different plateau is observed in the conversion [5,6] not corresponding to the chemical equilibrium composition. This aspect, already observed in batch conditions, appeared dramatic in continuous reactors, as it was seen in chapter 10 of this thesis, passing from

1 to 2 wt% of catalyst, the conversion changes from 80-85 to 95-97% by using the same reactor and operative conditions of flow rate, temperature, and methanol/oil ratio. Moreover, as it was observed in previous chapter, the performance of static mixer reactor in transesterification reaction were so high that none of the pseudohomogeneous kinetic models proposed by the literature, derived from runs performed in batch conditions, is suitable to describe the observed kinetic behaviors. At this scope, a new biphasic model, based on a reliable catalytic mechanism, more adherent to the physical behavior of the system, has been developed and it will be described in this chapter.

### **11.2 Mechanism of the methanol-soybean oil transesterification reaction**

From the observation of the kinetic data collected and described in chapter 10, it is possible to conclude that the increase of the liquid-liquid interface area is beneficial for the reaction. Moreover, when the interface area is high the reaction consistently occurs also for very low residence time. The same observation can be derived also considering the data collected in the literature [9] with different techniques like: oscillatory flow reactors, microwave irradiated reactors, ultrasonic irradiated reactors, centrifugal contactors, rotating packed bed reactors and jet flow stirred reactors. The conclusion could be that methoxide anions, formed with the reaction (1), react at the liquid-liquid interface with triglycerides transferring the charge from the polar to the apolar phase. Greater is the initial interface area, greater is the methoxide disappearance rate. After this reaction, occurring at the interface, the transesterification takes place in the oil phase through three different consecutive steps, according to the scheme (2-4):



Where, T represents the triglycerides, D the diglycerides, M the monoglycerides, G glycerol and E the methylesters. These reactions are catalysed by di- and monoglyceroxide anions dissolved in the oil phase. Hence, together with the successive transesterification steps also the catalyst is subjected to change with the reaction starting from  $CH_3O^-$ , dissolved in the polar phase, that is transformed in three successive steps to digliceroxides, mono-gliceroxides and gliceroxides anions, that is, many different catalytic species are formed like the ones reported in Figure 11.1.

The existence of acylglycerolates anions is postulated by Dijkstra et al.[8] However, recently Kouzu et al.[10] have prepared pure calcium glycerolate.

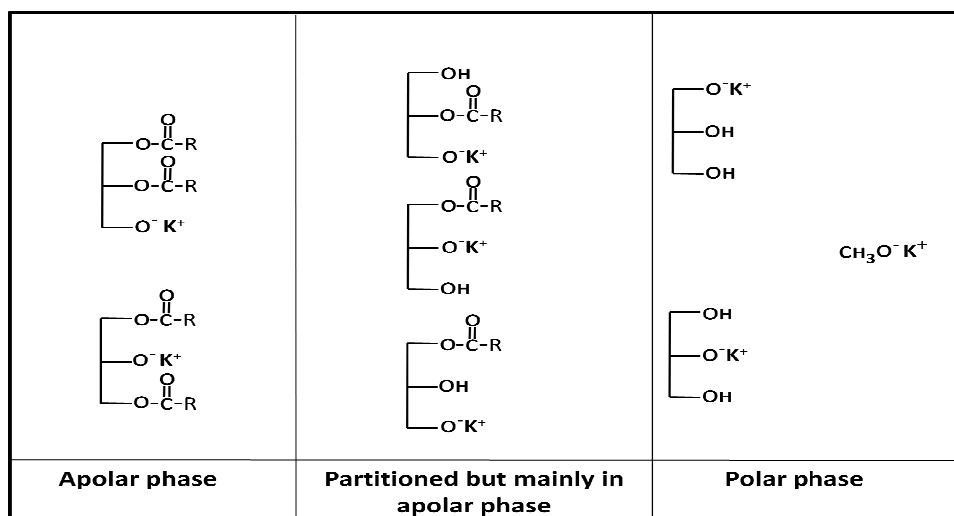


Figure 11.1: Anions population in agreement with the catalytic mechanism via enolates.

Glycerolates anions are not soluble in the oil phase and promptly migrate in the polar phase; consequently, the reaction rate rapidly slows down. A mechanism of this type suggests that it is very important to promote the formation of a high interface area in the initial reaction step (reaction 5) in order to consume methanolate anions as soon as possible, and then the reaction prosecutes in the oil phase in chemical regime until the catalytic species, soluble in oil, are present. Moreover, as the FAME yields change along the time from 0 to near 95-99%, the composition of the two phases greatly changes; in particular, as diacylglycerolates and monoacylglycerolates have tenside properties, a stable well dispersed methanol/oil emulsion can be formed, i.e., a great interfacial area is formed. Some other physical properties of the mixture change, too, and all these aspects can influence the reaction rate. However, as it is extremely difficult to take into account all the mentioned aspects on the reaction rates, we have neglected them in the model as a first approximation averaging the interface area for any adopted fluid dynamic condition. The reaction of methanolate with triglycerides, at the interface, can be schemed as follows:



(being  $\text{D}^-$  a digliceroxide anion). The rate of this reaction is reasonably proportional to the interface area, the catalyst concentration and the concentration of T at the interface (this last we assumed proportional to the bulk concentration). Therefore, we can write:

$$r_{\text{CH}_3\text{O}^-} = k_1 \cdot a \cdot [\text{CH}_3\text{O}^-] \cdot [\text{T}] \quad (6)$$

where  $a$  is the liquid-liquid interface area. The effect of reaction (5) is that of transferring the catalyst from the polar to the apolar phase where the transesterification reaction effectively occurs. As the rate of  $\text{CH}_3\text{O}^-$  disappearance depends on the interface area, the limit of this rate will be the one corresponding to the contact of two monomolecular films. This is in agreement with the following observations: (i) kinetic data, reported in the literature, are often in disagreement probably because the stirring rates and consequently the interface area of the reactors are different; (ii) none of the monophasic kinetic models published in the literature can simulate the very high conversions obtained in a few seconds in different efficient mixing devices, because, in those cases the obtainable interface areas are much higher. Another important observation is the dramatic change of the conversion in well mixed continuous reactors obtained when the amount of used catalyst is increased by a factor of 2. These differences are poorly dependent on the residence time, that is, the conversion reached does not increase further with time for reaching a chemical equilibrium. This behavior can be observed also for many experimental batch runs reported in the literature [5,6] where by increasing the catalyst concentration an increase of the reaction rate is observed but the final plateau changed with the amount of used catalyst. Therefore, the plateau is clearly a consequence of the catalyst deactivation not of the chemical equilibrium. The deactivation occurs, because the catalyst continues to change during the transesterification reaction according to the following simplified

Mechanism:



Being  $\text{M}^-$  = monoglyceroxides anions and  $\text{G}^-$  = glyceroxides anions.

The corresponding reaction rates are:

$$r_{\text{D}^-} = k_{\text{D}^-} \cdot [\text{D}^-] \cdot [\text{CH}_3\text{OH}]^{\text{oil}} \quad (9)$$

$$r_{\text{M}^-} = k_{\text{M}^-} \cdot [\text{M}^-] \cdot [\text{CH}_3\text{OH}]^{\text{oil}} \quad (10)$$

$\text{G}^-$  is not soluble in the oil phase and migrates in the polar phase.  $\text{G}^-$  is much less active than  $\text{D}^-$  and  $\text{M}^-$  that are the true catalysts formed in situ and soluble in the oil phase. Its catalytic action probably is due to the equilibrium:



$\text{CH}_3\text{O}^-$  formed for exchange with  $\text{G}^-$  reacts again, at the interface, with mono and diglycerides molecules according to the reactions:



Then, reactions 12 and 13 prosecute more slowly being the equilibrium (11) shifted to the left, according to the experimental observations. It cannot be excluded also the charge exchange between  $\text{CH}_3\text{OH}$  and  $\text{M}^-$  or  $\text{G}^-$ , but the extent of this reactions is probably negligible for the draining effect of the sequence of reactions bringing from methanolate to glycerolate anion.

To use more catalyst means to have a greater concentration of the active components in any step of the reaction in the oil phase and also the catalyst deactivation is slowed. The reaction occurs in the oil phase in the three consecutive steps reported in the schemes 4-6, and the related reaction rates can be described in a simplified way as

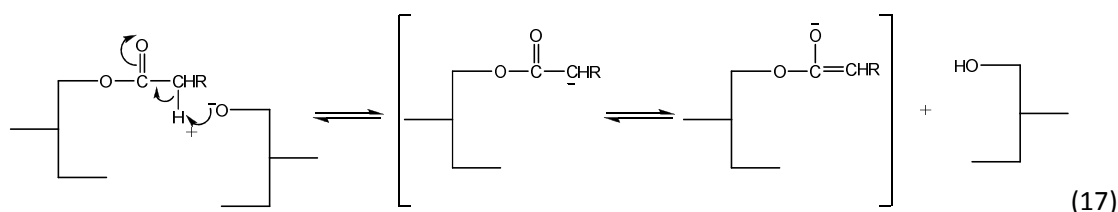
$$r_T = k_T \cdot [\text{D}^- + \text{M}^-] \cdot [\text{T}] \cdot [\text{CH}_3\text{OH}]^{\text{oil}} \quad (14)$$

$$r_D = k_D \cdot [\text{D}^- + \text{M}^-] \cdot [\text{D}] \cdot [\text{CH}_3\text{OH}]^{\text{oil}} \quad (15)$$

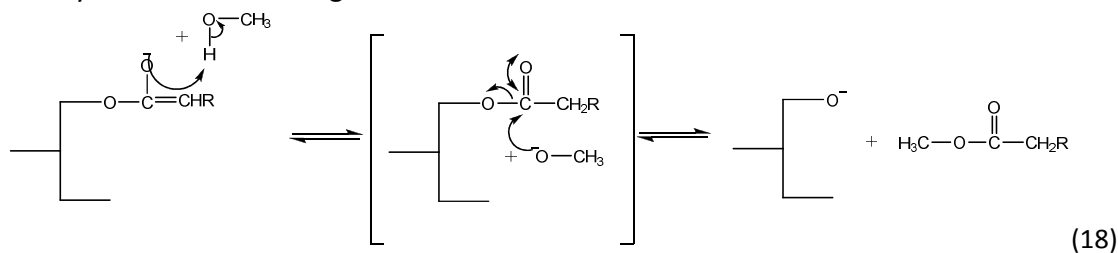
$$r_M = k_M \cdot [\text{D}^- + \text{M}^-] \cdot [\text{M}] \cdot [\text{CH}_3\text{OH}]^{\text{oil}} \quad (16)$$

Methanol is partitioned between the two liquid phases and obviously only methanol dissolved in the oil phase is involved in the reaction. In some conditions, this last aspect can further slow down the reaction rate as a consequence of mass transfer limitation.

The described mechanism is oversimplified, because, as recently reported by Dijkstra et al. [14], digliceroxide anion formed in the first catalytic reaction step (5) migrates in apolar phase and promotes further transesterification steps with the formation of enolates intermediates:



Then, the enolates react with methanol, dissolved in the apolar phase, to give methylester and a new digliceroxide anion:



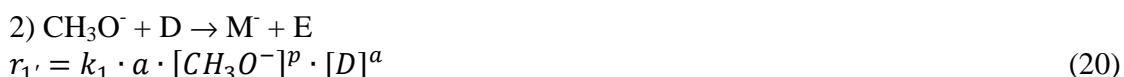


With the same mechanism, in successive steps are formed also monoglycerides and monoacylglycerolate anions, glycerol, and glycerolate anion. We have individuated at least 12 different anionic species (considering also enolates species) and 12 different reactions. These ionic species are predictable on the basis of the mechanism described in the literature proposed by Dijkstra et al. [8] in particular, they have not been experimentally observed, but their presence can be reasonable from a mechanistic point of view as intermediate or charged species. Clearly, the system needs to be simplified for the kinetic approach. Therefore, on the basis of the described mechanism, we have developed, as a first approximation, a lumped biphasic kinetic model.

### **11.3 Description of the biphasic kinetic model and application to batch runs taken by the literature**

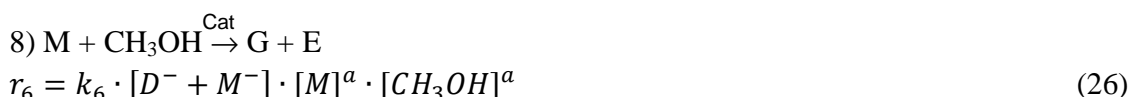
As before mentioned, kinetic data collected in well stirred batch reactors, reported in the literature, are often in disagreement. Moreover, these data are normally interpreted with a pseudomonophasic model. The most reliable and recently published kinetic data are the ones reported by Vicente et al. [5,6]. Therefore, we considered those data for testing the validity of the biphasic model developed by us and determining the corresponding kinetic parameters. Our biphasic kinetic approach considers the following: (i) all the reactions occurring in each phase, polar or apolar, and (ii) the partition of methanol and glycerol among the two phases. Although all the components are partitioned and we can evaluate the composition of the two phases as a function of the conversion [11] by using ChemCAD 6.3 software setting the UNIFAC LLE model, we neglected the partition of the components other than methanol and glycerol in order to simplify the model. (iii) The methanol and glycerol mass transfer have been determined by adopting the Whitman's two film theory [12]. Let us consider, first of all, the adopted reaction scheme and related kinetic equations

#### **Interface**

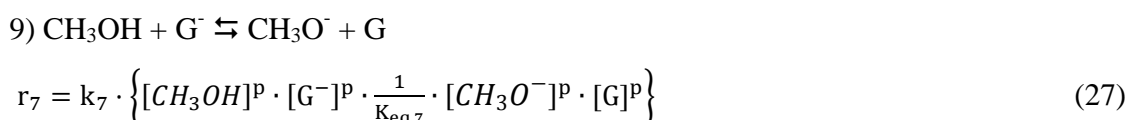


Being  $p$  and  $a$  respectively reference to polar and apolar phase. As it can be seen, the kinetic constants for these three reactions have been assumed the same as a reasonable first approximation.

#### Apolar phase



#### Polar phase



Here, the dependence between the kinetic constant with the temperature is expressed with a modified Arrhenius, whose expression is reported below:

$$k_i = k_i^{ref} \cdot \exp \left[ \frac{E_{a_i}}{R} \cdot \left( \frac{1}{T^{ref}} - \frac{1}{T} \right) \right] \quad (28)$$

With  $T$  expressed in Kelvin, and  $T^{ref}$  is the referring temperature at 298 K. In particular, we have imposed, as a first approximation, three activation energy values that are:

- $E_{a_1}$ : Activation energy for the reactions (19-21)
- $E_{a_2}$ : Activation energy for the reactions (22) and (23)
- $E_{a_3}$ : Activation energy for the reactions (24-26)

Reaction (27) is always near to the equilibrium.

The equations describing the mass transfer of methanol and glycerol from the two phases are:

### Polar phase

$$J_{CH_3OH}^p = k_{l,CH_3OH} \cdot a \cdot ([CH_3OH]^p - H_{CH_3OH} \cdot [CH_3OH]^{a,*}) \quad (29)$$

$$J_G^p = -k_{l,G} \cdot a \cdot ([G]^p - H_G \cdot [G]^{a,*}) \quad (30)$$

$$J_{G^-}^p = -k_{l,G^-} \cdot a \cdot ([G^-]^p - H_{G^-} \cdot [G^-]^{a,*}) \quad (31)$$

### Apolar phase

$$J_{CH_3OH}^a = k_{l,CH_3OH} \cdot a \cdot ([CH_3OH]^{a,*} - [CH_3OH]^a) \quad (32)$$

$$J_G^a = -k_{l,G} \cdot a \cdot ([G]^{a,*} - [G]^a) \quad (33)$$

$$J_{G^-}^a = -k_{l,G^-} \cdot a \cdot ([G^-]^{a,*} - [G^-]^a) \quad (34)$$

The interfacial concentration (\*) can be calculated solving the following balance that, considering a steady-state condition, is always valid for the J component.

$$J_J^p \cdot V^p = J_J^a \cdot V^a \quad (35)$$

By solving the previous equation it is possible to obtain:

$$[J]^{a,*} = \frac{V^p \cdot \beta_j \cdot [J]^p + \beta_j \cdot V^a \cdot [J]^a}{\beta_j \cdot V^a + V^p \cdot \beta_j \cdot H_A} \quad (36)$$

$$[J]^{p,*} = H_J \cdot [J]^{a,*} \quad (37)$$

Being  $\beta_j = k_{l,j} \cdot a$ .

For solving the mass transfer equations it is necessary to define also the solubility parameters  $H_j = [J]^a / [J]^p$  for both methanol and glycerol. By using ChemCAD V. 6.3 and the UNIFAC LLE model we can determine the evolution of the solubility parameters with the triglycerides conversion (x). The following optimised polynomial equations have been obtained:

$$1/H_{CH_3OH} = 25.85 - 23.00 \cdot x - 11.21 \cdot x^2 + 36.41 \cdot x^3 \quad (38)$$

$$1/H_G = 6304.75 - 15430.10 \cdot x - 1643.71 \cdot x^2 + 64912.73 \cdot x^3 - 92127.03 \cdot x^4 + 43103.45 \cdot x^5 \quad (39)$$

It is now possible to write the mass balances for both the polar and apolar phase:

### Polar phase

$$\frac{d[CH_3OH]^p}{dt} = -J_{CH_3OH}^p - r_7 \quad (40)$$

$$\frac{d[G]^p}{dt} = +J_G^p + r_7 \quad (41)$$

$$\frac{d[CH_3O^-]^p}{dt} = -(r_1 + r_{1'} + r_{1''}) \cdot \frac{V_a}{V_p} + r_7 \quad (42)$$

$$\frac{d[G^-]^p}{dt} = +J_{G^-}^p - r_7 \quad (43)$$

$$[CH_3O^-]^{p,0} = [KOH]^p \quad (44)$$

### Apolar phase

$$\frac{d[T]^a}{dt} = -r_1 - r_4 \quad (45)$$

$$\frac{d[D]^a}{dt} = +r_4 - r_5 - r_{1'} \quad (46)$$

$$\frac{d[M]^a}{dt} = +r_5 - r_6 - r_{1''} \quad (47)$$

$$\frac{d[G]^a}{dt} = +r_6 - J_G^a \quad (48)$$

$$\frac{d[E]^a}{dt} = +r_1 + r_{1'} + r_{1''} + r_2 + r_3 + r_4 + r_5 + r_6 \quad (49)$$

$$\frac{d[CH_3OH]^a}{dt} = -r_2 - r_3 - r_4 - r_5 - r_6 + -J_{CH_3OH}^a \quad (50)$$

$$\frac{d[D^-]^a}{dt} = +r_1 - r_2 \quad (51)$$

$$\frac{d[M^-]^a}{dt} = +r_2 - r_3 + r_{1'} \quad (52)$$

$$\frac{d[G^-]^a}{dt} = +r_3 - J_{G^-}^a + r_{1''} \quad (53)$$

This model has been applied, first of all, to interpret the kinetic runs performed by Vicente et al. [5,6] in a batch reactor. The considered experimental data are the ones of the runs listed in Table 11.1.

**Table 11.1:** List of the experimental runs reported in the literature [5,6], submitted to mathematical regression.

Run	Temperature (°C)	Stirring Rate (rpm)	KOH (wt.%)	MeOH/Oil (mol/mol)	Oil
1	25	600	1.0	6:1	Brassica
2	25	600	1.5	6:1	Sunflower
3	25	600	0.5	6:1	Brassica
4	25	600	1.5	6:1	Brassica
5	25	600	0.5	6:1	Sunflower
6	25	600	1.0	6:1	Sunflower
7	35	600	0.5	6:1	Sunflower

These data have been submitted to mathematical regression analysis and the kinetic parameters of the model giving the best fitting are reported in Table 11.2.

**Table 11.2:** List of the parameters obtained by mathematical regression analysis on the batch runs reported in the literature.

Parameters	Values	Units
$\gamma_1=k_1 a$	0.427	$L^p/(mol \cdot min)$
$k_2$	0.225	$L^a/(mol \cdot min)$
$k_3$	0.225	$L^a/(mol \cdot min)$
$k_4$	18.16	$L^{2,a}/(mol^2 \cdot min)$
$k_5$	4.61	$L^{2,a}/(mol^2 \cdot min)$
$k_6$	1.92	$L^{2,a}/(mol^2 \cdot min)$
$K_{eq,7}$	1.69 e-3	-
$\beta_{CH_3OH}$	1.52	$min^{-1}$
$Ea_1$	8.75e-5	kcal/mol
$Ea_2$	17.61	kcal/mol
$Ea_3$	26.62	kcal/mol

By observing the list of the runs, reported in Table 11.1, some of these runs have been performed with Sunflower oil, some others with Brassica oil. We have observed that the two oils have exactly the same kinetic behaviour as it can be seen in Figure 11.2. So, we have considered all the runs together not distinguishing one oil from the other.

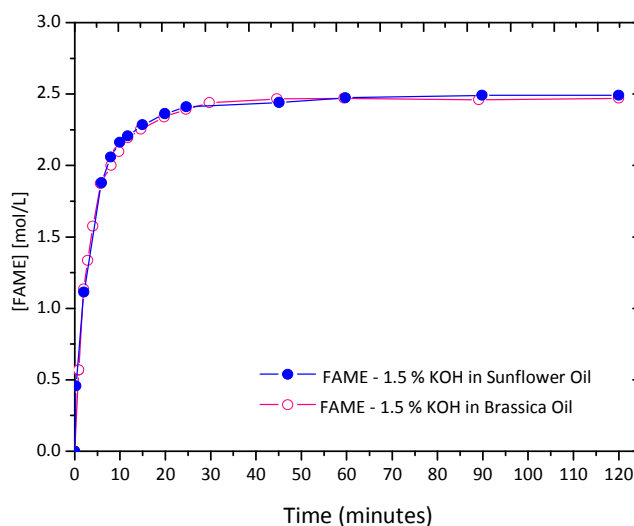


**Figure 11.2:** Comparison between the FAME concentration obtained in the same experimental conditions (25 °C and 1.5 wt.% KOH referred to the oil) but using two different oils, that are Brassica and Sunflower oil. Taken from Vicente et al [5,6]

In Figure 11.3 an example of simulations made with the biphasic model is reported.

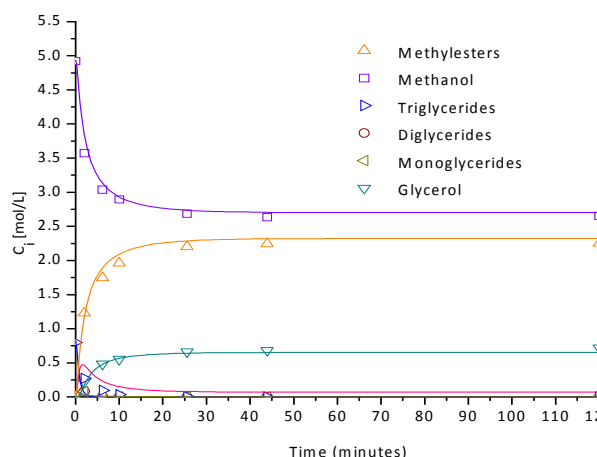


**Figure 11.3:** Simulations of an experimental run taken by the literature (Vicente et al. [5,6]) Run 1 of Table 11.1. Symbols represent the experimental points while lines the simulations.

As it can be seen, the obtained agreement is very good, but the most important agreement is the one obtained for the runs performed with different amounts of catalysts (Figure 11.4).

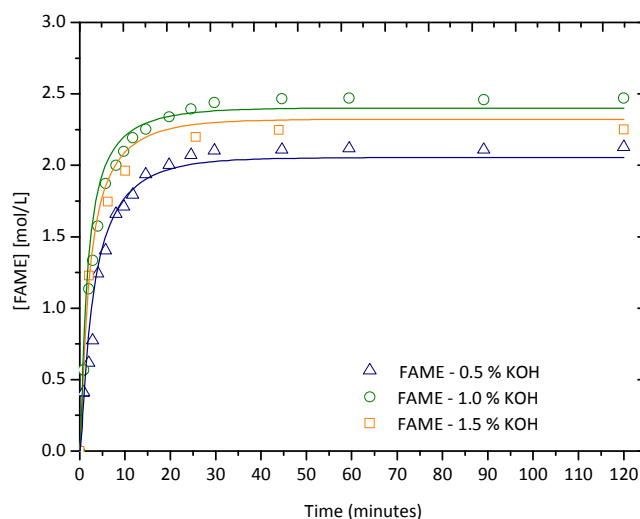


**Figure 11.4:** Simulations of three experimental runs taken by the literature at different catalyst concentration, that correspond to Runs 1, 3 and 4 of Table 11.1. Symbols represent the experimental points while lines the simulations

In this case the biphasic model is able to describe not only the difference in the initial reaction rates but also the final plateau, while, the pseudo-monophasic model cannot reproduce this behaviour giving the same plateau, corresponding to the chemical

equilibrium that is the same in all the cases because the runs have been performed at same temperature of 25°C.

The difference observed for the final plateau by using a different amount of catalyst are explained by the dynamic behaviour of the biphasic system: the initial rate is much higher and the concentration of the catalyst formed in the oil is greater. The plateau, therefore, is the consequence of the reaction rate leveling and not of the chemical equilibrium. The activation energy near to zero found for Ea1 can be accepted being reaction 5 a fast ionic exchange reaction, while reactions 7 and 8 are only apparently ionic exchange reactions, because we have lumped the kinetic model. In those cases the reactions pass through the formation of enolates and reaction with methanol (reactions 17 and 19), and the rate determining step is probably an activated intermediate reaction of the overall mechanism.

#### **11.4 Biphasic kinetic model applied to continuous runs**

By operating with continuous packed bed tubular reactors in chapter 10 it was observed two important phenomena: (i) the final conversion is strongly affected by the initial interface area; (ii) the conversion is strongly affected by the initial catalyst concentration. In some cases the conversion increases by decreasing the residence time until a maximum value is reached, in other cases the conversion remains relatively constant with the residence time. In order to simulate the continuous runs the following mass balance equations must be solved:

##### ***Polar phase***

$$\frac{d[CH_3OH]^p}{dV} = \frac{-J_{CH_3OH}^p - r_7}{Q} \quad (54)$$

$$\frac{d[G]^p}{dV} = \frac{+J_G^p + r_7}{Q} \quad (55)$$

$$\frac{d[CH_3O^-]^p}{dV} = \frac{-(r_1 + r_{1'} + r_{1''}) \frac{Q_a}{Q_p} + r_7}{Q} \quad (56)$$

$$\frac{d[G^-]^p}{dV} = \frac{+J_G^p - r_7}{Q} \quad (57)$$

##### ***Apolar phase***

$$\frac{d[T]^a}{dV} = \frac{-r_1 - r_4}{Q} \quad (58)$$

$$\frac{d[D]^a}{dV} = \frac{+r_4 - r_5 - r_{1'}}{Q} \quad (59)$$

$$\frac{d[M]^a}{dV} = \frac{+r_5 - r_6 - r_{1''}}{Q} \quad (60)$$

$$\frac{d[G]^a}{dV} = \frac{+r_6 - J_G^a}{Q} \quad (61)$$

$$\frac{d[E]^a}{dV} = \frac{+r_1 + r_{1'} + r_{1''} + r_2 + r_3 + r_4 + r_5 + r_6}{Q} \quad (62)$$

$$\frac{d[CH_3OH]^a}{dV} = \frac{-r_2 - r_3 - r_4 - r_5 - r_6 + -J_{CH_3OH}^a}{Q} \quad (63)$$

$$\frac{d[D^-]^a}{dV} = \frac{+r_1 - r_2}{Q} \quad (64)$$

$$\frac{d[M^-]^a}{dV} = \frac{+r_2 - r_3 + r_{1'}}{Q} \quad (65)$$

$$\frac{d[G^-]^a}{dV} = \frac{+r_3 - J_G^a + r_{1''}}{Q} \quad (66)$$

In order to simulate simultaneously experimental runs performed at different flow-rates, we have assumed that both  $\gamma_1 = k_1 a$  and  $\beta_{CH_3OH} = k_{i,CH_3OH}$  values depend linearly on the overall volumetric flow-rate, being these parameters both dependent on the interfacial area.

$$\gamma_1 = \gamma_1^0 \cdot Q/Q^{\text{ref}} \quad (67)$$

$$\beta_{CH_3OH} = \beta_{CH_3OH}^0 \cdot Q/Q^{\text{ref}} \quad (68)$$

With  $Q^{\text{ref}} = 1.0 \text{ cm}^3/\text{min}$ .

All the other equations, of mass transfer, partition, reaction rate laws and the equations of congruence are the same reported in paragraph 11.3. The agreements in simulating the continuous runs have been obtained by using the same kinetic parameters, derived from batch runs, reported in Table 11.2. For simulating all the continuous runs, it is necessary to adjust only two parameters, that are:  $\gamma_1^0$ , correlated with the interface area (relation 67), and eventually  $\beta_{CH_3OH}^0$  correlated with the mass transfer coefficient for methanol and again with the interface area (relation 70). In Table 11.3 are reported  $\gamma_1^0$  and  $\beta_{CH_3OH}^0$ .

**Table 11.3** : List of the parameters used for simulating the continuous runs.

Parameter	RP1	RP21	RP22	RWTR	TRR	Unit
$\gamma_1^0$	4.73	25.84	22.84	72.00	13.11	$\text{cm}^{3,p}/(\text{mol} \cdot \text{min})$
$\beta_{CH_3OH}^0$	39.93	2.09	0.29	3.57	6.44	$\text{min}^{-1}$

In Table 11.4, all the experimental conditions adopted and the comparison between the experimental and calculated yields are reported for the runs performed in the different reactors, at 60°C, by using 1% of catalyst.



**Table 11.4:** Experimental runs performed in the described continuous reactors, at 60 °C, by using 1.0 wt.% KOH catalyst.

Run	Reactor	$Q_{oil}$ (cm <sup>3</sup> min <sup>-1</sup> )	$Q_{MeOH}$ (cm <sup>3</sup> min <sup>-1</sup> )	$\tau$ (min)	$Y_{EXP}$ (%)	$Y_{SIM}$ (%)
1	RP1	9.80	2.530	0.58	62.50	84.87
2	RP1	6.60	1.730	0.86	79.30	81.88
3	RP1	5.50	1.400	1.04	80.70	80.61
4	RP1	4.40	1.150	1.29	81.80	78.61
5	RP1	1.10	0.287	5.16	73.30	64.73
6	RP1	2.40	0.615	2.37	73.30	73.21
7	RP1	0.58	0.150	9.79	43.60	56.96
8	RP21	28.62	7.382	0.17	83.60	83.50
9	RP21	19.24	4.962	0.25	81.10	81.00
10	RP21	9.62	2.480	0.50	80.30	80.20
11	RP21	4.85	1.251	0.99	81.90	81.80
12	RP21	2.38	0.615	2.02	78.70	78.60
13	RP22	9.80	2.530	0.31	80.50	85.10
14	RP22	7.90	2.040	0.38	81.50	85.20
15	RP22	6.60	1.730	0.46	78.60	84.08
16	RP22	5.50	1.400	0.55	77.20	83.22
17	RP22	4.40	1.150	0.68	81.50	81.60
18	RP22	3.20	0.830	0.94	80.60	80.08
19	RP22	2.40	0.615	1.26	82.30	78.55
20	RP22	0.58	0.150	5.21	80.50	71.80
21	RWTR	3.69	0.950	3.00	76.90	77.20
22	RWTR	2.77	0.710	4.00	74.90	74.90
23	RWTR	2.21	0.570	5.01	73.60	73.20
24	TRR	5.50	1.400	1.09	70.44	70.44
25	TRR	6.60	1.730	0.91	75.59	75.59
26	TRR	9.80	2.526	0.61	72.87	72.87

On the contrary, in Table 11.5, are reported all the experimental conditions adopted and the comparison between the experimental and calculated yields for the runs performed in the different reactors, at 60°C by using 2% of catalyst. As it can be seen the agreement found is satisfactory considering all the simplifications introduced in the model. In the continuous runs the difference in the conversions observed with respectively 1 or 2% of catalyst are much more pronounced than in the batch conditions, but the reason for this difference is the same. The obtained agreement can be better appreciated in Figure 11.5 reporting the trends of the yield with the residence time for the reactors RP1 and RP22 corresponding to the runs reported in Table 11.4.

**Table 11.5:** Experimental runs performed in the described continuous reactors, at 60 °C, by using 2.0 wt.% KOH catalyst.

Run	Reactor	$Q_{oil}$ (cm <sup>3</sup> min <sup>-1</sup> )	$Q_{MeOH}$ (cm <sup>3</sup> min <sup>-1</sup> )	$\tau$ (min)	$Y_{EXP}$ (%)	$Y_{SIM}$ (%)
27	RP21	28.62	7.382	0.17	93.60	91.30
28	RP21	19.24	4.962	0.25	93.80	90.70
29	RP21	9.62	2.480	0.50	94.70	90.90
30	RP21	4.85	1.251	0.99	98.20	92.10
31	RP21	2.38	0.615	2.02	97.10	90.10
32	RWTR	3.70	0.950	3.00	97.00	88.80
33	RWTR	2.77	0.710	4.00	93.70	87.00
34	RWTR	2.21	0.570	5.01	85.20	85.20

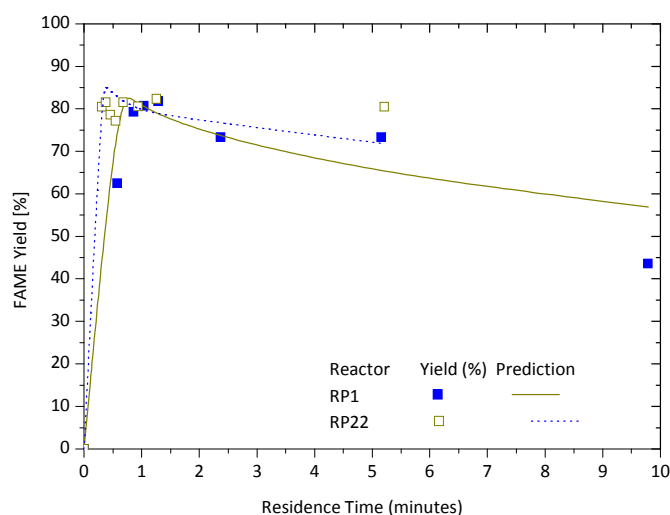


**Figure 11.5:** Runs performed with the reactors RP1 and RP22 by using 1% of KOH catalyst

At last, in Figure 11.6 a parity plot related to the experimental runs performed with the reactors RP21, RWTR, and TRR (see conditions in Tables 6 and 7). As it can be seen, the parity plot shows an error inferior to 10%. Moreover, it seems that a systematic error affects the simulations at the highest level of yield. This means that the model needs to be further improved.

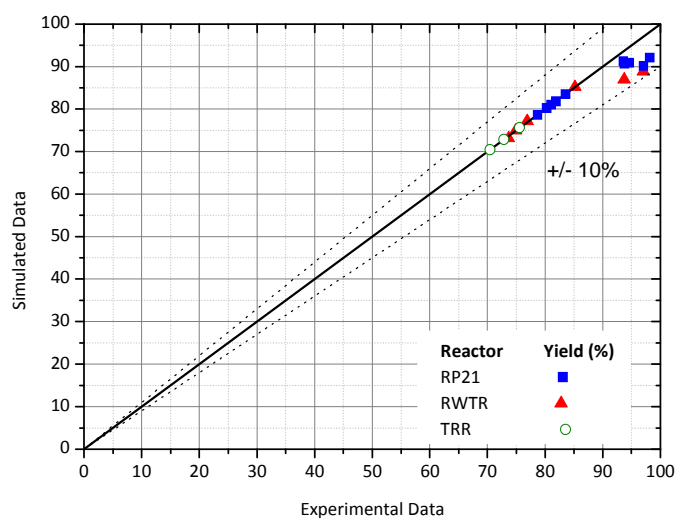


**Figure 11.6:** Parity plot obtained for the runs performed with the reactors RP21, RWTR and TRR.

### 10.5 Conclusions

A new biphasic model based on a more reliable reaction mechanism has been described in this work and successfully applied to both batch runs, taken from the literature, and continuous runs in tubular reactor filled with different static mixer elements.

### **References**

- [1] B. Freedman, R. O. Butterfield, E. H. Pryde, *J. Am. Oil Chem. Soc.*, 63 (1986) 1375.
- [2] H. Nouredдини, D. Zhu, *J. Am. Oil Chem. Soc.*, 74 (1997) 1457.
- [3] D. Darnoko, M. Cheryan, Kinetics, *J. Am. Oil Chem. Soc.* 77 (2000) 1263.
- [4] K. Komers, F. Skopal, R. Stloukal, J. Machek, *Eur. J. Lipid Sci. Technol.* 104 (2002) 728.
- [5] G. Vicente; M. Martinez, J. Aracil, A. Esteban, *Ind. Eng. Chem. Res.* 44 (2005) 5447..
- [6] G. Vicente, M. Martinez, J. Aracil, , *Energy Fuels* 20 (2006) 1722.
- [7] O. S. Stamenkovic, Z. B. Todorovic, M. L. Lazic, V. B. Veljkovic, D. U. Skal, *Bioresource Technol.* 99 (2008) 1131.
- [8] A.J. Dijkstra, E.R. Toke, P. Kolonits, K. Recseg, K. Kovar, L. Poppe, *Eur. J. Lipid Sci. Technol.*, 107 (2005) 912.
- [9] Z. Qiu, L. Zhao, L. Weatherley, *Chem. Eng. and Process.* 49 (2010) 323.
- [10] Kouzu, M.; Hidaka, J. S.; Wakabayashi, K.; Tsunomori, M. *Appl. Catal.*, A 2010, 390, 11.
- [11] Chemical Process Simulator ChemCAD 6.2 by Chemstations (2009).
- [12] W. G. Whitman, *Chem. Metall. Eng.*, 29 (1923) 146.

## Nomenclature

A1	Methoxylic groups single signal at $\delta=3.7$ ppm
A2	Methylenic groups triplet signal $\delta=2.3$ ppm
$N_D$	Dispersion number
Pe	Peclet number, defined as the reverse of the dispersion number
D	Axial dispersion coefficient ( $m^2/s$ )
u	Axial velocity (m/s)
L	Reactor's length (m)
F	Dimensionless tracer concentration ( $C/C_0$ ) where C and $C_0$ are respectively the actual and the initial concentrations
$\Theta$	Dimensionless time defined as $t/t_m$ , being $t_m$ the residence time
TRR	Reactor packed with 8 stainless steel threaded rods: length=20 cm, diameter=3 mm, thread= 0.5 mm
RP1	Single size packing filled with spheres of 2.5 mm diameter
RP21	Dual size packing filled with spheres of two different diameters: 2.5 and 1.0 mm
RP22	Dual size packing filled with spheres of two different diameters: 2.5 and 0.39 mm
RWTR	Reactor packed with stainless steel wool
T	Triglycerides
D	Diglycerides
M	Monoglycerides
G	Glycerol
E	Methylesters
$D^-$	Diglyceroxide anion
$M^-$	Monoglyceroxide anion
$G^-$	Glyceroxide anion
$r_i$	Reaction rate ( $mol\ L^{-1}\ min^{-1}$ )
$k_i$	Kinetic constant (units depend on the reaction)
Cat	Catalyst
a	Interfacial area ( $cm^2/cm^3$ )
$\gamma_1$	Kinetic parameter of reaction defined as $k_1 \cdot a$
$Ea_i$	Activation energy (kcal/mol)
$K_{eq,i}$	Equilibrium constant
$J_j^i$	Mass transfer rate for the j component in the phase i ( $mol\ L^{-1}\ min^{-1}$ )
$k_{l,j}$	Mass transfer coefficient of the j component (cm/min)
$\beta_j$	Mass transfer parameter of the j component defined as $k_{l,j} \cdot a$ ( $min^{-1}$ )
$H_j$	Partition coefficient of the j component ( $[j]^a/[j]^b$ )
x	Conversion degree (-)
Q	Overall volumetric flow rate ( $cm^3/min$ )
$\tau$	Residence time (minutes)
V	reactor's volume ( $cm^3$ )

## Subscripts and Superscripts

Oil	oil phase
P	polar phase
a	apolar phase

# Chapter 12

## *Conclusions*

“Humanity needs practical men, who get the most out of their work, and, without forgetting the general good, safeguard their own interests. But humanity also needs dreamers, for whom the disinterested development of an enterprise is so captivating that it becomes impossible for them to devote their care to their own material profit..”

**Marie Curie**

(1867-1932, physicist and chemist)

The aim of this work was the intensification of two interesting industrial process:

1. Biodiesel Production
2. Epoxidized Oils Production

In the first case the reaction in traditional industrial reactors is strongly limited by mass transfer, due to the presence of two immiscible liquid reactants phases, thus it requires very long residence times in order to create a high interfacial area to promote the reaction. For the vegetable oils epoxidation reaction, apart from the mass transfer limitations, there are limitations related to the heat transfer, due to the very exothermicity of the reaction.

It was shown that the intensification of the epoxidation process could be possible through the shift from the pulse fed batch reactors (current technology) to continuous ones able to mix the immiscible reagents and remove the heat released by the reaction. The use of microreactors represents the best solution in this case, taking account the high dispersion capability of these devices, that could enhance the mass and heat transfer. Such shift could be obtained only by acquiring sufficient insight on the reaction kinetics and by developing a reliable physical model able to describe the evolution of all the components involved, considering in particular the secondary reactions that decrease the selectivity. For this purpose, it was developed a kinetic model, that contains the main physico-chemical peculiarities of the considered reacting system: components partition between the two liquid phases, mass transfer limitation across liquid-liquid interface, heat transfer between the reacting mixture and reactor jacket, different reactivity in epoxidation and oxirane ring opening (degradation) of the different types of double bonds (trienic, dienic, monoenic).

The model was successfully applied, in a first step, to a set of experimental fed-batch runs performed in controlled isothermal conditions with the scope of evaluating the kinetic parameters at a reference temperature. Subsequently, a group of pulse fed-batch runs with variable temperature were used to evaluate activation energies and thermal parameters such as the global heat transfer coefficient. The very good agreement between the experimental data and the model prediction confirmed that the model was able to describe the behavior of the fed-batch reactor in different conditions. At last, with the aim to further validate the model, several experiments have been performed in a conventional continuous tubular reactor, filled with stainless steel spheres. Also for continuous runs the performances of the model resulted satisfactory and, in perspective, the model will be useful to design a continuous epoxidation operation in safe conditions and could be the basis for the process intensification in microreactors.

Moreover, the intensification of the epoxidation process could be possible through the use of only hydrogen peroxide as oxidant reactant, in presence of a heterogeneous catalyst. In this way, it would avoid the formation of byproducts, regarding that the only byproduct derived from oxidation with hydrogen peroxide is water, and the presence of a heterogeneous catalyst would get easier the final product separation and more selective the reaction.

For this purpose in this thesis, two different solid catalytic systems were studied:

1.  $\text{Nb}_2\text{O}_5/\text{SiO}_2$
2. Alumina

The first system, that was prepared by sol-gel technique, showed a low activity and selectivity in epoxidation reaction. In particular it was observed that the activity increased with the niobium content, whereas the trend of the selective was inverse. This behavior was justified by individuation on the catalyst surface of hydroxyl with a Bronsted acid strength, which could catalyze the ring opening reaction of the oxirane with water forming diol groups. The presence of strong Bronsted acid sites on the solid with lower content of niobium was confirmed by the esterification runs.

On the contrary, the second system, consisting in commercial  $\gamma$ -alumina, showed higher activity in epoxidation of vegetable oils with hydrogen peroxide. Moreover, it was supposed and demonstrated that the solvent used for the epoxidation runs, that corresponded to the most used in literature in this type of the studies, was not innocent. As matter of the fact, the hydrolysis reaction of ethyl acetate can be possible with the formation of acetic acid and successively peracetic acid derived by reaction with hydrogen peroxide. The peracetic acid could react with double bonds of oils according the Prileschajew mechanism, explaining in this way, the higher activity observed for the alumina.

Concerning to the biodiesel production process intensification, several reactors able to improve the mass transfer between the immiscible liquid reagents, through the creation a very high interfacial area and a very intensive local micromixing, were studied.

For this purpose a corrugated plates heat exchanger reactor (CP-HEX) was applied to promote the transesterification of soybean oil with methanol for the biodiesel production. A very high productivity (420 kg/day) was obtained with a very small device of 450 cm<sup>3</sup> of overall volume and 200 cm<sup>3</sup> of working volume. This was explained by assuming a very high intensity micromixing occurred in this type of the reactors through the formation of eddies between plates. This depends on both the distance between the plates (1.5-2mm) and the type of plate corrugations. Latter factors contribute to promote the locale turbulence and in presence of two immiscible reactants, favors a good mixing with a dispersion of one phase into the other.

Then, the effect of different types of static mixers on the intensification of the biodiesel synthesis were deeply investigated.

It was shown that a tubular reactor filled with different elements of different sizes and shapes can usefully be used to simulate the behavior of both a "static mixer" and a "microreactor". As a matter of fact, with this type of device it is possible to change opportunely the size of the microchannels, so simulating microreactors, or the intensity of local micromixing by changing feeding flow rates, so simulating static mixers.

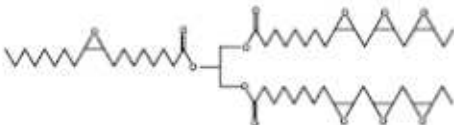


On the basis of the experimental results obtained for transesterification of vegetable oil with methanol, promoted by KOH, it is possible to conclude that an intense local micromixing, favoring the development of a great interface area, gave place to very high yield in mild conditions (60 °C) and very short residence times (less than 1 minute). At last, a new biphasic model based on a more reliable reaction mechanism was developed in this work and successfully applied to continuous runs in tubular reactor filled with different static mixer elements.

## Appendix

### A.1. Properties of Epoxidized Soybean oil and Soybean Oil

#### A.1.1 Epoxidized Soybean Oil

Product Identification	
Cas. No.	801307
Molecular Formula	CH <sub>3</sub> -CHOR-CH <sub>2</sub> OR, where R=fatty acids side chains unsaturated or saturated of varying carbon length (95% is C <sub>18</sub> )
Structural Formula	
Molecular weight (g/mol)	940-950
Toxicity (mg/Kg)	Oral Rat LD50: 224400
Synonyms	ESO; ESBO; Soy Epoxy Ester; Soybean Oil epoxidized
Classification	Plasticizer and stabilizer
Physical and Chemical Properties	
Physical State	Clear to yellow liquid
Melting Point (°C)	-2.2
Boiling Point	Decomposes
Relative density (g/cm <sup>3</sup> )	0.9875-0.9930 (25°C)
Vapour Pressure (Pa at 25 °C)	<0.001
Solubility in Water	Insoluble
Solvent Solubility	Miscible in aromatic hydrocarbons, butanol, ketones, plasticizers and partly soluble in aliphatic hydrocarbons and ethanol
viscosity	450 cps at 25 °C
Refractive Index	1.470-1.472
Flash Point (°C)	>280
Stability	Stable in ordinary conditions
Sales Specifications	
Appearance	Clear to yellow liquid
Oxirane Number (g <sub>O2</sub> /g <sub>sample</sub> )	6 (min)
Acid Value (mg <sub>KOH</sub> /g)	1.0 (max)
Water %	0.5% (max)
Iodine Number (g <sub>O2</sub> /g <sub>sample</sub> )	2-6

**A.1.2. Soybean Oil**

Product Identification	
Cas. No.	8001-22-7
Molecular Formula	
Structural Formula	
Molecular weight (g/mol)	
Toxicity (mg/Kg)	Oral Rat LD50: 224400
Synonyms	refined soybean oil; Soya oil; Soybean acidulated soap stock; Soybean deodorizer distillate; Soy Bean Oil; Soybean oil fatty acids, glycerol triester;
Classification	
Physical and Chemical Properties	
Physical State	clear liquid
Cloud Point (°C)	10
Boiling Point	Decomposes
Relative density (g/cm <sup>3</sup> )	0.915-0.925 (25°C)
Vapour Pressure (mPa at 25 °C)	50
Solubility in Water	Insoluble
Solvent Solubility	
viscosity	
Refractive Index	
Flash Point (°C)	280
Stability	Stable in ordinary conditions
Sales Specifications	
Appearance	Clear to yellow liquid
Acid Value (mg KOH/g)	2.0 (max)
Saponification Value (mg KOH/g)	1.0 (max)
Iodine Number (gO <sub>2</sub> /g <sub>sample</sub> )	128-134
Typical Carbon Length distribution	16:0 (10 - 15%) + C18:0 (3 - 5%) + C18:1 (20 - 25%) + C18:2 (45 - 55%) + C18:3 (8 - 10%) + C20:0 ( 1%)

## A.2 Analysis of epoxidation reaction mixtures

The quality of the epoxy products is evaluated according to certain specifications such as:

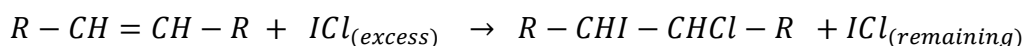
- Iodine Number
- Oxirane Number

Such values were determined for each epoxidized products, obtained in this research work, according to the procedures described below.

### A.2.1 Determination of Iodine Number [1]

The Iodine Number gives a measure of the average degree of unsaturation of oils and fats: the higher the iodine value, the greater the number of C=C double bonds. By definition, the Iodine Number is expressed in terms of centigrams of iodine per gram of sample (weight percent of absorbed iodine).

One of the most commonly used methods for determining the iodine value of oils and fats is "Wijs method". The sample to be analyzed is weighed and dissolved in a suitable organic solvent, to which a known excess of iodine chloride (Wijs solution) is added. Some of the ICl reacts with the double bonds in the unsaturated lipids, while the rest remains:



The amount of ICl that has reacted is determined by measuring the amount of ICl remaining after the reaction has gone to completion ( $ICl_{reacted} = ICl_{excess} - ICl_{remaining}$ ). The amount of ICl remaining is determined by adding excess potassium iodide to the solution to liberate iodine, and then titrating with a sodium thiosulfate ( $Na_2S_2O_3$ ) solution in the presence of starch to determine the concentration of iodine released.

#### Chemicals and Titrant

- 15 ml Chloroform
- 25 ml Wijs solution
- 20 ml 10% potassium iodide, KI
- 100 ml water
- Sodium Thiosulphate 0.1N
- 1 ml Starch

#### Procedure

The sample, weighed previously, is dissolved in Chloroform. Then 25 mL of Wijs solution are added to sample and final solution is kept in the dark for approximately 1 hour to complete the reaction.

After 1 hour, 20 mL of KI solution are added to liberate Iodine. Finally the excess iodine is titrated with sodium thiosulphate.

In order to calculate the number of iodine is necessary to perform the titration of Blank, that is to follow the same procedure without the sample.

The iodine number is determined by applying the following equation:

$$\text{Iodine Number} = \frac{(V^0 - V) \cdot C \cdot 12.69}{M}$$

where:

V = Titrant volume used for the sample

$V^0$  = Titrant volume used for blank

C = titrant normality

M = weight of sample

The conversion related to the double bonds reacted is calculated with the following:

$$\text{Conversion (\%)} = \frac{(\text{Iodine N.})_0 - (\text{Iodine N.})}{(\text{Iodine N.})_0} \cdot 100$$

where:

$(\text{Iodine N.})_0$  = Iodine Number of the blank.

### A.2.2 Determination of Oxirane Number [2]

The Oxirane Number defines the content of epoxy groups in a epoxidized oil. The method involves the determination of oxirane oxygen by potentiometric titration. It is based on the reaction between perchloric acid and bromide, with the transformation of latter in the hydrogen bromid, that by interaction with the oxirane group forms bromidrina. The equivalence point, determined by titration, is detected at an excess of perchloric acid.

#### Chemicals

- Glacial acetic acid
- Titrant : 0,1 N Perchloric acid in acetic
- Hexadecyltrimethylammonium bromide (CTAB) (0.1 N in acetic acid)

#### Procedure

10 ml of CTAB are added to 0.5 g of sample, dissolved in 50 ml of acetic acid.

The titration is performed to the equivalent point

The Oxirane Number is calculated as following:

$$\text{Oxirane Number} = \frac{V \cdot 1.6 \cdot N}{M}$$

Where:

V= volume (ml) of titrant

M= weight of sample

N= Normality titrant.

The yields to epoxide have been determined as:

$$\text{Yield} = \frac{\text{Oxirane Number} \cdot \text{PM}_{\text{I}_2}}{\text{Iodine Number} \cdot \text{PM}_\text{O}} \cdot 100$$

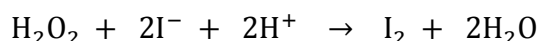
Where:

PM<sub>I<sub>2</sub></sub> = molar weight of I<sub>2</sub> [g/mol]

PM<sub>O</sub> = molar weight of Oil [g/mol]

### A.3 Determination of Residual Hydrogen Peroxide [3]

The residual concentration of H<sub>2</sub>O<sub>2</sub> was estimated by an iodometric analytical method [3]. Latter is based on the reaction of hydrogen peroxide with potassium iodide KI, in acid, with formation of iodine (I<sub>2</sub>):



The reaction is slow enough, thus is catalyzed by adding of ammonium molybdate

#### **Chemicals**

- 10 mL of H<sub>2</sub>SO<sub>4</sub> (2M)
- 1 g KI
- 25 mL water
- Starch
- Molybdate ammonium
- Sodium thiosulphate 0.1 N

#### **Procedure**

25 ml of water, 1 g of potassium iodide, 10 ml of sulphuric acid solution and few drops of molybdate are added to the weighted sample. Finally, the iodine is titrated with thiosulphate in presence of starch as indicator.

The results can be expressed in terms of grams of hydrogen peroxide, using the following relation:

$$g_{h2o2} = \frac{N \cdot V \cdot PM_{H2O2}}{2}$$

Where:

N= Titrant normality

V= Titrant volume

PM<sub>H2O2</sub> = molar weight of hydrogen peroxide [g/mol]

#### A.4 Analysis of transesterification reaction mixtures

##### A.4.1 NMR analysis [4]

The FAME (fatty acids methyl esters) yield were determined by using <sup>1</sup>H NMR technique, measuring the area of H NMR signal related to methoxylic (A1, single signal at δ=3.7 ppm) and methylenic groups (A2, triplet signal at δ=2.3 ppm) respectively.

The FAME yields can be calculated by using the following equation:

$$yield_{FAME} = \left( \frac{2 \cdot A1}{3 \cdot A2} \right) \cdot 100$$

The <sup>1</sup>H NMR spectra were obtained with Gemini-200 equipment in deuterated chloroform.

##### A.4.2 Gas-chromatographic analysis [5]

In all the cases the conversion values were confirmed by gas-chromatographic analysis [UNI 10946:2001], using a gas chromatograph (Perkin-Elmer model Clarus 500), equipped with a flame ionization detector (FID), an on-column injector, and employing a FS-HP5 column (10 m X 0.32 mm, I.D. 0.1 µm film). Before analysis, the samples were derivatized by BSTFA (N,O – bis (trimethylsilyl) trifluoroacetamide with trimethylchlorosilane). As internal standards, methyl-heptadecanoate was used for methyl ester and 1,2,4 butantriol was used for glycerol.

**References**

- [1] Method NGD C 32-1976
- [2] Paquot C., Hautfenne A., Commission on Oils Fats and Derivatives: Standard Methods for the Analysis of Oils, Fats and Derivatives, Blackwell Scientific Publications, IUPAC, Applied Chemistry Division, London, 1987.
- [3] Kolthoff I.M., Meehan S., Treatise on Analytical Chemistry, 2<sup>nd</sup> Ed.; Wiley: New York 1978; pp 888.
- [4] Gelbard G., Bres O., Vargas R.M., Vielfaure F., Schuchardt U.F., *J. Am. Oil Chem. Soc.*, 72 (1995) 1239.
- [5] UNI 10946:2001.



## Publications

Publications included in this PhD thesis

### Papers

1. E. Santacesaria, R. Turco, V. Russo, R. Tesser, M. Di Serio, *Soybean Oil Epoxidation: Kinetics of the Epoxide Ring Opening Reaction*, submitted for publication
2. E. Santacesaria, R. Turco, M. Tortorelli, V. Russo, M. Di Serio, R. Tesser, *Biodiesel process intensification: the role of the liquid-liquid interface area in the achievement of a complete conversion in few seconds*, submitted for publication
3. M. Di Serio, R. Turco, P. Pernice, A. Aronne, F. Sannino, E. Santacesaria, *Valuation of Nb<sub>2</sub>O<sub>5</sub>-SiO<sub>2</sub> catalysts in Soybean Oil Epoxidation*, submitted for publication.
4. E. Santacesaria, A. Renken, V. Russo, R. Turco, R. Tesser, M. Di Serio, *A Biphasic Model Describing Soybean Oil Epoxidation with H<sub>2</sub>O<sub>2</sub> in Continuous Reactors*, submitted for publication.
5. E. Santacesaria, R. Turco, M. Tortorelli, V. Russo, M. Di Serio, R. Tesser, *Biodiesel Process Intensification by Using Mixers Tubular Reactors*, Ind. Eng. Chem. Res., doi: 10.1021/ie201640w.
6. E. Santacesaria, M. Di Serio, R. Tesser, M. Tortorelli, R. Turco, V. Russo, *A simple device to test biodiesel process intensification*, Chemical Engineering and Processing: Process Intensification, doi:10.1016/j.cep.2011.05.023.
5. E. Santacesaria, R. Tesser, M. Di Serio, R. Turco, V. Russo, D. Verde, *A Biphasic Model Describing Soybean Oil Epoxidation with H<sub>2</sub>O<sub>2</sub> in a Fed-Batch Reactor*, Chemical Engineering Journal, 176 (2011) 198-209.
6. E. Santacesaria, M. Di Serio, R. Tesser, V. Russo, R. Turco, *A new Simple Microchannel Device to test Process Intensification*, Ind. Eng. Chem. Res., 50 (5) (2011) 2569–2575.
8. E. Santacesaria, M. Di Serio, R. Tesser, R. Turco, D. Verde, L. Casale. MYTHEN SPA, *Reactor for Immiscible Liquid Reagents*. PCT Int. Appl. (2010) WO 2010073216 (A1).
9. E. Santacesaria, M. Di Serio, R. Tesser, L. Casale, D. Verde, R. Turco, A. Bertola, *Use of a Corrugated Plates Heat Exchanger Reactor for Obtaining Biodiesel with Very High Productivity*. ENERGY & FUELS, 23 (2009), 5206-5212.

## Abstracts book

10. R. Turco, V. Russo, M. Di Serio, R. Tesser, E. Santacesaria, *Epoxidation of Soybeal oil: Kinetic study and modelling in fed-batch and continuos reactors*, Abstracts book of XXIV Congresso Nazionale della Società Chimica Italiana, Lecce, September 2011.
11. V. Russo, R. Turco, M. Di Serio, R. Tesser, E.Santacesaria, *A Biphasic Kinetic Approach to Biodiesel Production*, Abstracts book of XXIV Congresso Nazionale della Società Chimica Italiana, Lecce, September 2011.
12. E. Santacesaria, M. Di Serio, R. Tesser, R.Turco, V. Russo, Key factors in the process intensification of the soybean oil epoxidation, Abstracts book of European process intensification conference, Manchester UK , June 2011.
13. E. Santacesaria, M. Di Serio, R. Tesser, R.Turco, M. Tortorelli, V. Russo, *Biodiesel process intensification in a very simple microchannel device*, Abstracts book of European process intensification conference, Manchester UK , June 2011.
14. E. Santacesaria, R.Turco, M. Tortorelli, V. Russo, M. Di Serio, R. Tesser, *Biodiesel process intensification by using static mixers tubular reactors*, Abstracts book of Catalysis in Multiphase Reactors CAMURE-8 International Symposium on Multifunctional Reactors ISMR-7 , Naantali (Turku) May 2011.
15. R. Tesser, E. Santacesaria, R.Turco, V. Russo, M. Di Serio, *Epoxidation of soybean oil: kinetic study and modelling in fed-batch and continuous reactors*, Abstracts book of Catalysis in Multiphase Reactors CAMURE-8 International Symposium on Multifunctional Reactors ISMR-7 , Naantali (Turku) May 2011.
16. R. Turco, M. Di Serio, R. Tesser, A. Aronne, P. Pernice E. Santacesaria, *Valuation of Nb<sub>2</sub>O<sub>5</sub>-SiO<sub>2</sub> catalysts in Soybean Oil epoxidation*, Abstracts book of 7th International Symposium on Five Group Element, Riccione, May 2011.
17. E. Santacesaria, M. Di Serio, R. Tesser, R. Turco, V. Russo, *Epoxidation of soybean oil, a study on the possibilities of process intensification*, Abstracts book of 19th International Congress of Chemical and Process Engineering CHISA 2010 and the 7th European Congress of Chemical Engineering ECCE-7, Prague, September 2010.
18. E. Santacesaria, M. Di Serio, R. Tesser, V. Russo, R. Turco, M. Tortorelli, *A new Simple microchannel device for intensifying biodiesel production*, Abstracts book of Chemical reactors and Technologies for Emerging Application (CHEMREACTOR-19), Vienna, September 2010.